A platform for genome editing insect vectors of leishmaniasis (*Lutzomyia longipalpis* and *Phlebotomus papatasi*) and Chagas disease (*Rhodnius prolixus*) via CRISPR-Cas9 based approaches.

Luke John Brandner-Garrod

Thesis submitted in accordance with the requirements for the degree of

Doctor of Philosophy of the University of London

January 2024

Department of Infection Biology
Faculty of Infectious and tropical disease
LONDON SCHOOL OF HYGIENE & TROPICAL MEDICINE

No funding received

Research group affiliation(s):

Dr Matthew Yeo

Dr Thomas Walker

0. 1. Declaration of own work

I, Luke John Brandner-Garrod, confirm that the work presented in this thesis is my own. Where information has been derived from other sources, I confirm that this has been indicated in the thesis.

0. 2. Abstract

Chagas disease and leishmaniasis currently infect an estimated 11 million people, causing mortality in the thousands and close to 1 million disability-adjusted life years lost. Control efforts, in the context of vector management have had mixed success and new intervention approaches are needed.

Research into the genetic modification of insect vectors has been revolutionised by the application of new gene editing approaches such as CRISPR-Cas9. They allow for the precise manipulation of gene targets within multiple eukaryotic species. Utilising techniques such as gene drives it is possible to achieve successful integration of exogenous DNA within the germline, spreading inherited traits through a population at a rate higher than Mendelian inheritance. Recent approaches in the context of medically important insect vectors have focused on the integration and expression of effector molecules, and the targeting of genes affecting reproductive fitness. Both approaches have the capacity to interrupt disease transmission. To date there is a dearth of published information regarding genetic modification of the insect vectors of Chagas disease or leishmaniasis. The research outlined in this thesis has contributed towards the development of CRISPR-Cas9 methodologies applied to the insect vectors of Chagas disease (triatomine bugs) and leishmaniasis (phlebotomine sand flies).

We focused on the successful validation of CRISPR-Cas9 systems within the sand flies *Lutzomyia longipalpis* and *Phlebotomus papatasi* and the triatomine bug species *Rhodnius prolixus*. A number of gene targets were identified, which when functionally lost could elicit a phenotypic response in the insects. gRNAs targeting these phenotypic genes were incorporated into CRISPR-Cas9 DNA constructs, which were then transfected into sand fly and triatomine bug embryos. We observed phenotypic changes when targeting cuticle tanning and wing phenotype genes in sand flies. In *R. prolixus* bugs we utilized CRISPR-Cas9 homology directed repair approaches, potentially integrating exogenous DNA into the genome of embryos as confirmed by PCR. The integration of exogenous DNA via homology directed repair has not previously been achieved in these insects. The gene editing platform we developed here has the potential to contribute the understanding and development of novel control methods for Chagas disease and leishmaniasis, alleviating an enormous burden of human suffering.

0. 3. Acknowledgements

Firstly, I would like to thank my primary supervisor Dr Matthew Yeo, for without him this research would not have occurred. His support has been invaluable, especially in the early days, when we stood side by side trialling novel techniques. Thank you to my secondary supervisor, Dr Thomas Walker, for his support through the writing process and for always being available for a chat when I needed it.

I would like to give a special thanks to my research partner Dr Rhodri Edwards. We started this journey together with very little to go on and managed to achieve so much. Thank you for the many half-day conversations we had in the office, and for the alarmingly large amount of caffeine we consumed together.

I would like to thank our collaborators at Charles University in Prague, Prof Petr Volf and Dr Erich Telleria, who opened up their lab and supported us without hesitation. I would also like to highlight Barbora Kykalová, I have no doubt she will be running her own lab in a few years, which she may have built brick by brick with her own hands.

There have been a number of colleagues I have met throughout this journey who have inspired me with their dedication to science and the kindness that they show to others. Pat and Shahida who supported me with the insectaries, I hope to continue our coffee chats for years to come. Cheryl thank you for all of your entomological knowledge and for putting up with my constant intrusions. Tapan and Martin for my random queries about molecular biology. Mojca, for being so supportive with my research and writing, even though you never stop being busy.

Throughout my PhD I have been supported by a number of friends. I will now rank them based on their contributions to my mental health and research: Richard, Ieuan, Dan, Dave, Alex M, Archie, Lydia, Shannan, Lucy, Niamh, Rich, Syreen, Sophia, Jack, Amy, Harry, Laura, Saba.

To my parents, who have supported me in every aspect of life, always telling me I can do anything I put my mind to. My partner Meg, whom I love, for always being there for me. Thank you for the many joyous distractions. Finally, I would be remiss if I did not mention my cat, Ebi. He has brought me such joy in recent years, whether it's him biting me awake whilst my morning alarm goes off, or the slightest crumb of attention he gives me each evening before I go to sleep.

0. 4. Impact of COVID-19 statement

The COVID-19 global pandemic significantly limited the potential outputs and capacity of this research. The London School of Hygiene and Tropical medicine put in place protective rules for working within the building from March 2020 to September 2021, these affected this research in several ways. From March 2020 to May 2020, I was not able to access the LSHTM building forcing a hiatus on my laboratory work. When the building reopened, laboratories and offices were to be used at a low occupancy, with many of those used in this research being designated as single occupancy. This forced research to be conducted on a rota system, impacting capacity and efficiency of experiments. This continued until March 2021. During this period England had two further lockdowns for which I had to take leave of absences for personal reasons. Once normal working conditions had returned to the LSHTM, our research was limited by restrictions on travel to Charles University, Prague, Czech Republic, where the sand fly colonies used in this research were performed (Section 3. 3.). We were able to first visit Charles University in October of 2021.

To overcome these restrictions, we focused our research on *in vitro* experiments utilizing the *Lutzomyia longipalpis* based cell lines LLE/LULS40 and 45. There were a number of limitations we observed within these lines (Section 2. 4.), in the context of COVID-19, the lines took 3-6 months to recover from cryopreservation. This left large periods of time after lockdowns, where *in vitro* experiments could not be performed. During these periods, gene targets were identified (Section 3. 2. 1.), and plasmids were developed (Section 3. 2. 2.) ready for transfections when cells became available. If travel restrictions had not limited our time collaborating with Charles University, we would have utilised more of these plasmids *in vivo* (Section 3. 3.) and potentially derived a line of Cas9 expressing sand flies utilizing the UbiqCas9.874W plasmid (Section 2. 2. 2.). Further details on the adjustments to our research aims can be found in Section 6. 1. 1.

Ultimately, the work we achieved despite these setbacks is novel and lays a foundation for further genome engineering within the insect vectors of Chagas disease and Leishmaniasis.

0. 5. Table of contents

0. 6. List of figures

0. 7. List of tables

0. 8. List of appendices

0. 9. Abbreviations

a.u.	Arbitrary Units
aaNAT	Arylalkylamine-N-Acetyltransferase
ABC	ATP-Binding Cassette
ADA	Algorithmic Deconvolution Analysis
AMP	Anti-Microbial Peptides
Cas9	CRISPR Associated Endonuclease
casp	Caspar
CC9-RNP	CRISPR-Cas9 Ribonucleoprotein Complex
CH	Cuticular Hydrocarbons
CL	Cutaneous Leishmaniasis
cn	Cinnabar
CRISPR-Cas9	Clustered Regularly Interspaced Short Palindromic Repeats- CRISPR Associated Sequences 9
daisy drives	Daisy Chain Gene Drives
DALYs	Disability Adjusted Life Years
Dmel	Drosophila melanogaster
DSB	Double-Stranded Break
dsDNA	Double-Stranded DNA
e	Ebony
EC	Ethanol-Chemotransfection
ey	Eyeless
FACS	Fluorescence-Activated Cell Sorting
FP	Few-Polyhedra
GFP	Green Fluorescent Protein

GM	Genetic Modification
gRNA	Guide RNA
HA	Homology Arms
HDR	Homology Directed Repair
HSC	CRISPR-Cas9 HDR Single Central gRNA Approach
HUTR	CRISPR-Cas9 HDR Multiplexed gRNA Approach
IC	Inhibitory Concentration
IDP	Internally Displaced Person
indel	Insertion/Deletion Mutations
IRS	Indoor Residual Spraying
ITR	Inverted Terminal Repeats
kr	Krüppel
LHA	Left Homology Arm
Llon	*Lutzomyia longipalpis*
MCL	Mucocutaneous Leishmaniasis
MGA	Mean Grey Scale Analysis
MGV	Mean Grey Scale Value
NADA	N-Acetyl Dopamine
NASC	Nucleic Acid Squaramide Carriers
NBAD	N-B-Alanyl Dopamine
NHEJ	Non-Homologous End Joining
PAM	Protospacer Adjacent Motif
PBS	Phosphate-Buffered Saline
PDL	Poly-D-Lysine

PEI	Polyethyleneimine
PFA	Paraformaldehyde
pgSIT	Precision Guided SIT
Ppap	Phlebotomus Papatasi
PSEA	Pol III Proximal Sequence Element A
r	Rudimentary
ReMOT	Receptor-Mediated Ovary Transduction Of Cargo
RFP	Red Fluorescent Protein
RHA	Right Homology Arm
RNP	Ribonucleoprotein
ROI	Region Of Interest
Rpro	*Rhodnius prolixus*
SCI	Southern Cone Initiative
SEM	Standard Error Of The Mean
sgRNA	Single Guide RNA
SIT	Sterile Insect Techniques
st	Scarlet
T7EI assay	T7 Endonuclease I Heteroduplex Assay
TALE	Transcription Activator-Like Effectors
TALEN	Transcription Activator-Like Effector Nucleases
toy	Twin Of Eyeless
UTR	Untranslated Regions
vg	Vestigial
VL	Visceral Leishmaniasis

w	White
WT	Wild-Type
y	Yellow
ZFN	Zinc Finger Nuclease
ZFP	Zinc-Finger Proteins

1. General introduction

1. 1. Epidemiology of Chagas disease and leishmaniasis

Trypanosoma cruzi (the causative agent of Chagas disease) and *Leishmania spp.* (the causative agents of leishmaniasis), are protozoan parasites (Trypanosomatida) transmitted by triatomine bugs (Order Hemiptera, subfamily Triatominae) and female phlebotomine sand flies (Order Diptera, subfamily Phlebotominae) respectively. Together they are responsible for an enormous health burden, spanning six continents, and affecting millions (1,2).

Both Chagas disease and leishmaniasis are regarded as neglected tropical diseases and principally impact disadvantaged communities. Chagas disease, currently affects an estimated 6.5 million people, leading to an average loss of ~275,000 Disability Adjusted Life Years (DALYs) and an associated mortality of ~9,500 people annually (1,2). Leishmaniasis, caused by various different *Leishmania spp*. affects roughly 4.6 million people globally, leading to ~5,700 deaths and an average loss of ~700,000 DALYs annually (1,2).

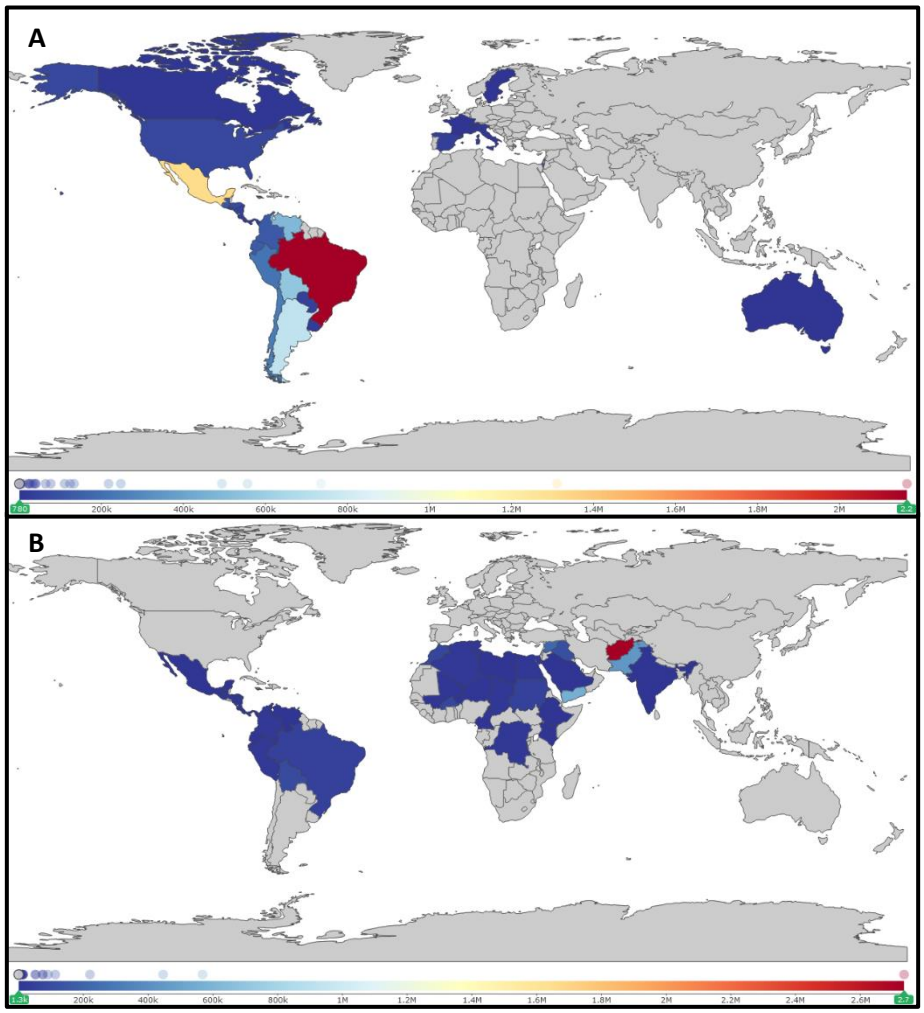

Figure 1. Global prevalence of Chagas disease and leishmaniasis in 2019.
Data from the Institute for Health Metrics and Evaluation (1,2). A) global prevalence of Chagas disease. B) global prevalence of leishmaniasis.

Chagas disease and leishmaniasis are both endemic to large areas of Latin America, but leishmaniasis is also endemic in North and Central Africa, Southern Europe as well as East Asia (1,2). Leishmaniasis presents as three principle forms of pathology depending on the *Leishmania* species (3,4). Broadly these are cutaneous leishmaniasis (CL) presenting skin lesions, mucocutaneous leishmaniasis (MCL) which presents inflammation of the mucosal membranes of the nasopharyngeal region leading to extensive tissue damage if untreated, and visceral leishmaniasis (VL) the systemic form which leads to ~95% mortality without treatment. Each form has a different geographical epidemiology with 90% of CL found in Afghanistan, Algeria, Brazil, Iran, Peru, Saudi Arabia, and Sudan, 90% of MCL cases occur in Bolivia, Brazil, Ethiopia and Peru and, 90% of VL is found in Bangladesh, Brazil, India, Nepal, and Sudan (5). Mass migration due to conflicts in endemic regions, political instability, or general migration is spreading these parasites to previously non-endemic countries (6). In Chagas disease, 60-80% of the infected population are asymptomatic, which has led to thousands of cases in non-endemic countries in Europe, North America and Asia, as shown in Figure 1A (1,2,7).

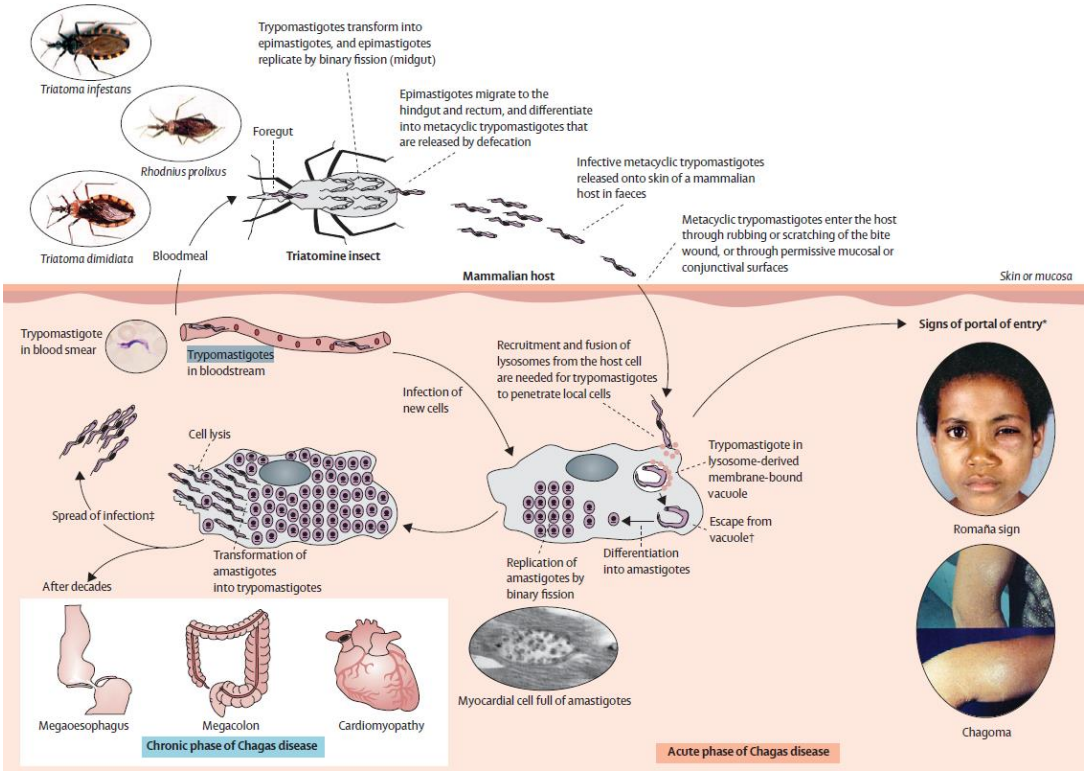

Figure 2. Vectoral transmission and life cycle of the parasite Trypanosoma cruzi.
Figure from Rassi *et al.,* 2010 (8).

The main transmission pathway for *T. cruzi* is by exposure to infected faeces from hematophagous insects of the subfamily Triatominae (8). Metacyclic trypanosomes within infected faeces enter the host through open wounds (such as the bite site) or through mucosal membranes. Infection can also occur by infected blood transfusion, organ transplantation, congenital transmission and by oral ingestion of contaminated foodstuff (8–11). Upon entering the host, infective trypomastigotes have

the capacity to infect a variety of host cells, where they differentiate into amastigotes and begin replication by binary fission to form pseudocysts. Prior to rupture of the pseudocyst, amastigotes differentiate to infective trypomastigotes. These spread throughout the circulatory system to infect distant tissues (mainly muscle cells) and carry out further replication (12). Infective trypomastigotes may also be ingested by triatomine bugs during blood feeding. In the bug's midgut, the parasites differentiate into epimastigotes and replicate via binary fission. Epimastigotes then migrate to the hindgut and rectum to differentiate into infective metacyclic trypomastigotes continuing the cycle (Figure 2) (12).

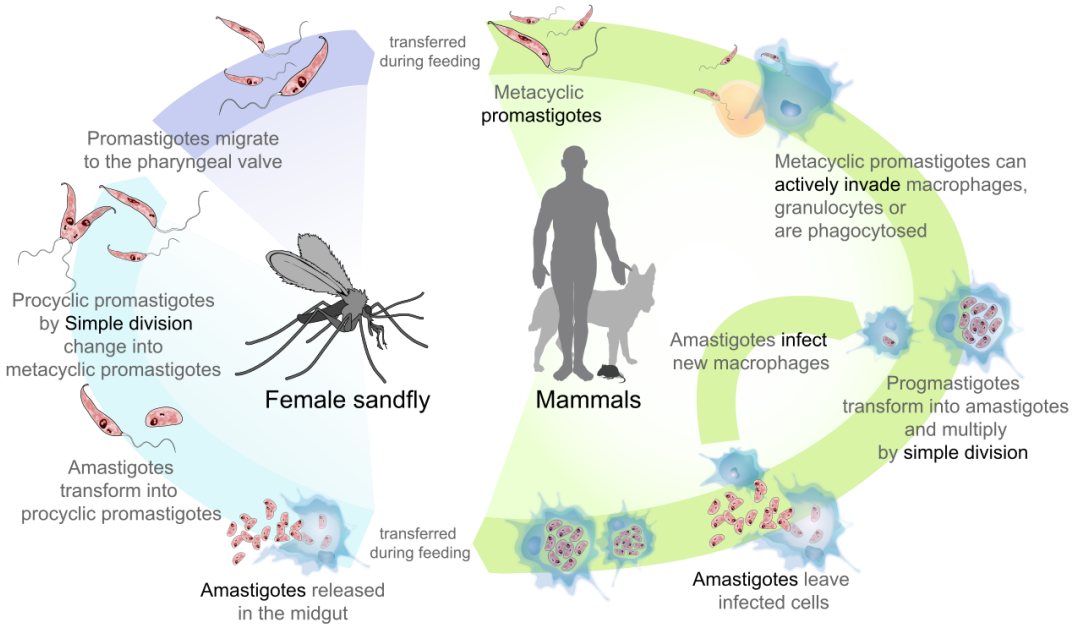

Figure 3. Vectoral transmission and life cycle of the parasites under the genus *Leishmania.*
Figure from Villarreal (13).

Transmission of leishmaniasis occurs via the bite from an infected phlebotomine sand fly vector, to mainly mammalian hosts (14). There are over 900 phlebotomine species but only around 50 are known to transmit leishmaniasis (Section 1. 3.)(13,15). Amastigote infected macrophages are ingested by the female sand fly during blood feeding, these differentiate in the sand fly gut through different promastigote forms (16). These promastigote forms are the procyclic promastigote which is found within the blood meal; the nectomonad promastigote responsible for breaking the peritrophic matrix and migrating to the foregut; the leptomonad promastigote forms within the foregut before differentiation into the metacyclic promastigote, the highly motile infective stage of *Leishmania*. Metacyclic promastigotes infiltrate the stomodaeal valve, contaminating the foregut and mouthparts of the sand fly and are transmitted to the host during the next blood feed (Figure 3) (13,15,17).

Within the host, following phagocytosis by neutrophils, promastigotes trigger cell apoptosis activating phagocytosis by macrophages (18). *Leishmania* is able to survive in the phagosomes by inhibiting maturation of lysosomal properties which would cause their degradation (19). Macrophages and dendritic cells are the main initial host cells (particularly in CL species), once immune cells are overwhelmed at the initial infection site, infected monocytes will migrate the infection or increase the area of the initial immune response (20,21). The cycle is completed by infection of blood-feeding female sand flies.

1. 2. Diagnosis, prevention, and treatment

Chagas disease comprises of two clinical stages, the acute phase, and the chronic phase. The acute phase typically lasts 4-8 weeks with symptoms including fever, inflammation at the inoculation site, unilateral periorbital swelling (Romaña sign), lymphadenopathy and hepatosplenomegaly, with 1-5% of patients developing the severe symptoms of myocarditis, pericardial effusion and meningoencephalitis (22). If left untreated, the chronic stage of infection can develop over 10-30 years, leading to symptoms of cardiomyopathy, megaviscera, megaesophagus and, megacolon in 30-40% of patients (22). Diagnosis of Chagas disease in the acute phase is carried out by either visualisation of trypomastigotes in peripheral blood via direct microscopy or PCR (23). Chronic infections are also diagnosed by serological tests detecting the presence of IgG antibodies against *T. cruzi* (23,24).

Chagas disease is treated with anti-trypanosomal drugs in both the acute and chronic stages with varying dosages based on age and pregnancy (23). Chemotherapeutics, benznidazole and nifurtimox are currently the only licensed treatments. However, in the late chronic stage, the efficacy of benznidazole is low and often the benefit is marginal over no treatment due to adverse effects (25).

The three major clinical forms of leishmaniasis all present varying symptoms. Cutaneous leishmaniasis will produce localised skin lesions at the inoculation site or wider dissemination causing large areas of tissue destruction (26). Mucocutaneous leishmaniasis forms highly damaging lesions, although they are localised to the nasal, pharyngeal and laryngeal mucosa (26). Visceral leishmaniasis, the systemic form of the disease, manifests itself in the form of anaemia, anorexia, cutaneous pigmentation, splenomegaly, lymphadenopathy, hepatomegaly, and weight loss. In the absence of VL treatment multisystem failure, haemorrhaging and thrombocytopenia can occur leading to death (26). Diagnosis is obtained via a biopsy of the cutaneous lesions, antibody detection or PCR (26).

Treatment of leishmaniasis currently comprises of intravenous pentavalent antimonials for all forms of the disease, in addition to Benzoxaborole based topical treatments for cutaneous leishmaniasis (26,27). The current first-line antimonial treatments are sodium stibogluconate, meglumine antimoniate and liposomal amphotericin B (26). Resistance to current anti-leishmanial drugs is increasing, to counter this a number of novel chemotherapeutics are currently in development (28).

There are currently no vaccines or prophylaxis for Chagas disease or leishmaniasis. However, development of multiple leishmaniasis vaccine targets are currently being assessed, including sand fly saliva antigens and whole-killed parasites (29). Until these are commonly available, prevention of transmission is key to a possible eradication.

Figure 4. Vector control programs for Chagas disease and leishmaniasis.
A) a traditional house in which triatomine bugs inhabit crevices between mud bricks and loose tiles (30). B) improved housing reducing colony establishment of triatomine bugs by providing smoothed walls, tight-fitting tiles, and windows slats (30). C) pyrethroid IRS against Chagas disease in Paraguayan Chaco (31). D) DDT spraying for reducing phlebotomine fly populations of IDP camps in Iraq 2015 (32).

The Southern cone initiative (SCI) a government ran strategy targeting Chagas disease has been the most successful large-scale public health intervention of a parasitic disease. The SCI has reduced the prevalence of Chagas disease by 95% in large areas of Argentina, Bolivia, Brazil, Chile, Paraguay, Peru and Uruguay (33). The SCI focused on blood donor serology screening, insecticide programs and research into the main mechanisms of transmission, whilst simultaneously introducing policies on a multinational level (33,34). Alternative control programs, to date, have not achieved the same success as the SCI. When indoor residual spraying (IRS) was introduced it was predicted to reduce the number of insects indoors by 70-90%, but this reduction was not achieved, and widespread resistance to insecticides was seen which is still persistent currently (35–40). Improvements to housing (Figure 4A & B) reduced seroprevalence and in most cases halted domiciliation of insects (30,41). However, housing improvements are highly expensive, must be well organised, and have the whole community's interests in mind (30,42).

IRS is the primary intervention to reduce leishmaniasis prevalence, along with insecticide-treated nets, clothing and bedsheets (43). Insecticide spraying of houses and peridomestic areas can reduce sand fly populations (Figure 4D). Resistance to carbiamates, pyrethrouds, Organochlorines (DDT),

and organophosphate insecticides has emerged in the Indian Subcontinent, Iran and Sudan, as well as pyrethroid resistance in South America (44–47). This shows the importance of novel insecticide development or alternative strategies for vector control.

Paratransgenesis is a potential transmission control methodology which facilitates the expression of antimicrobial compounds within insect digestive tracts via the ingestion of transgenic symbiotic bacteria (48). This technique was originally developed in the triatomine bugs, *Rhodnius prolixus*, due to *T. cruzi* parasites developing through multiple life stages within the insect's midgut and hindgut (49). Previous research was able to produce a 65% reduction in *T. cruzi* infection rates of *R. prolixus* insects by ingestion of *Rhodococcus rhodnii* bacteria expressing the antimicrobial peptide cecropin A (50). To develop a competent immune system 1st instar triatomine nymphs must ingest the faeces of older bugs, using this knowledge researchers were able to develop a method of dispersing transgenic bacteria by spraying of tainted faeces on surfaces where triatomines reside (51). In semi-field experiments, transgenic *R. rhodnii* were detected in 50% of F1 adult triatomine bugs 9 months after contact with tainted faeces (50). This methodology has also been adapted to phlebotomine sand flies, with initial experiments showing strong expression of GFP from transgenic *Bacilus subtilis* in adult *Phlebotomus argentipes,* following feeding of tainted rabbit faeces to larvae (52). Furthering this, semi-field experiments have shown dispersal to adult *Phlebotomus papatasi* of *Serratia AS1* bacteria can be achieved by feeding tainted food bait to native rodents which pass the transgenic bacteria in their faeces, where roughly 12% of emerged adults in field cages were infected with the bacteria (53). Paratransgenesis is still a developing methodology for transmission control and will need to pass major ethical and regulatory considerations before it can be implemented in disease control strategies (48).

In summary, control of Chagas disease and leishmaniasis can be effective with appropriate use of diagnosis, chemotherapeutics, insecticides, barrier methods, and control of blood transfusions (Chagas disease). However, the resources required are substantial and are often not available to those in need. New approaches to interrupt transmission are needed.

1. 3. Vectors of *T. cruzi* and *Leishmania spp.*

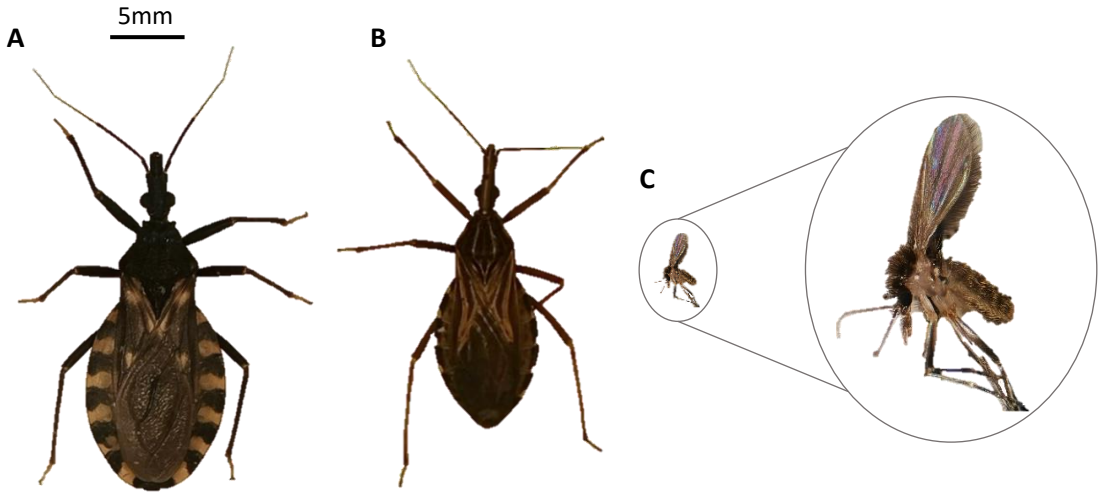

Figure 5. Insect vectors of Chagas disease and leishmaniasis.
A) an adult *Triatoma infestans* bug, the primary vector for Chagas disease in Southern cone countries. B) an adult *Rhodnius prolixus* bug, the principal vector for Chagas disease in Central America. C) an adult *Lutzomyia longipalpis* sand fly, one of the main vectors of leishmaniasis. The enlarged image of C is at a 6x magnification.

Chagas disease is transmitted by Hemipteran vectors of the Reduviidae subfamily Triatominae, commonly referred to as triatomine bugs or kissing bugs. There are over 130 species of triatomine bugs known, around 120 of these blood feed on mammals and approximately 80% of those are capable of transmitting *T. cruzi* (54,55). *Triatoma infestans* (Figure 5A) is the most important vector of Chagas disease in the southern cone region of South America (Figure 6) (56–59). *Rhodnius prolixus* (Figure 5B) is the primary vector across most of Central America and northern South America (Figure 6) (56,59). Medically important species possess the capacity to invade domestic environments and also tend to defecate when feeding. *Triatoma dimidiata,* which is far more widespread than *R. prolixus* (Figure 6)*,* colonises dwellings less frequently, reducing the risk for transmission (56,57,59). *Triatoma spp.* frequent terrestrial habitats including rocky crevices or rodent burrows, exploiting similar niches within households residing under roof tiles and wall cracks in poorly maintained housing (57,60). *Rhodnius spp*. typically inhabits palm trees in the sylvatic environment. They are eclectic feeders of avians and mammals and have adapted well to rural housing with thatched palm frond roofing (60). Chagas disease is split into six distinct genotypes (TcI-VI), these genotypes have been linked to potential pathologies (61,62). In mouse models, TcI infections developed to severe cardiomyopathy in 88% of cases whilst no cardiomyopathy develops in TcVI infected mice (63). The development of genotype pathologies is important as specific vector species have been identified as only competent to limited genotypes, reducing the capacity for specific lineages to spread within large geographical regions (64). Previous studies have found *Rhodnius spp.* favour TcI genotypes whilst *Triatoma spp.* have been found to transmit all genotypes except for TcIV (65).

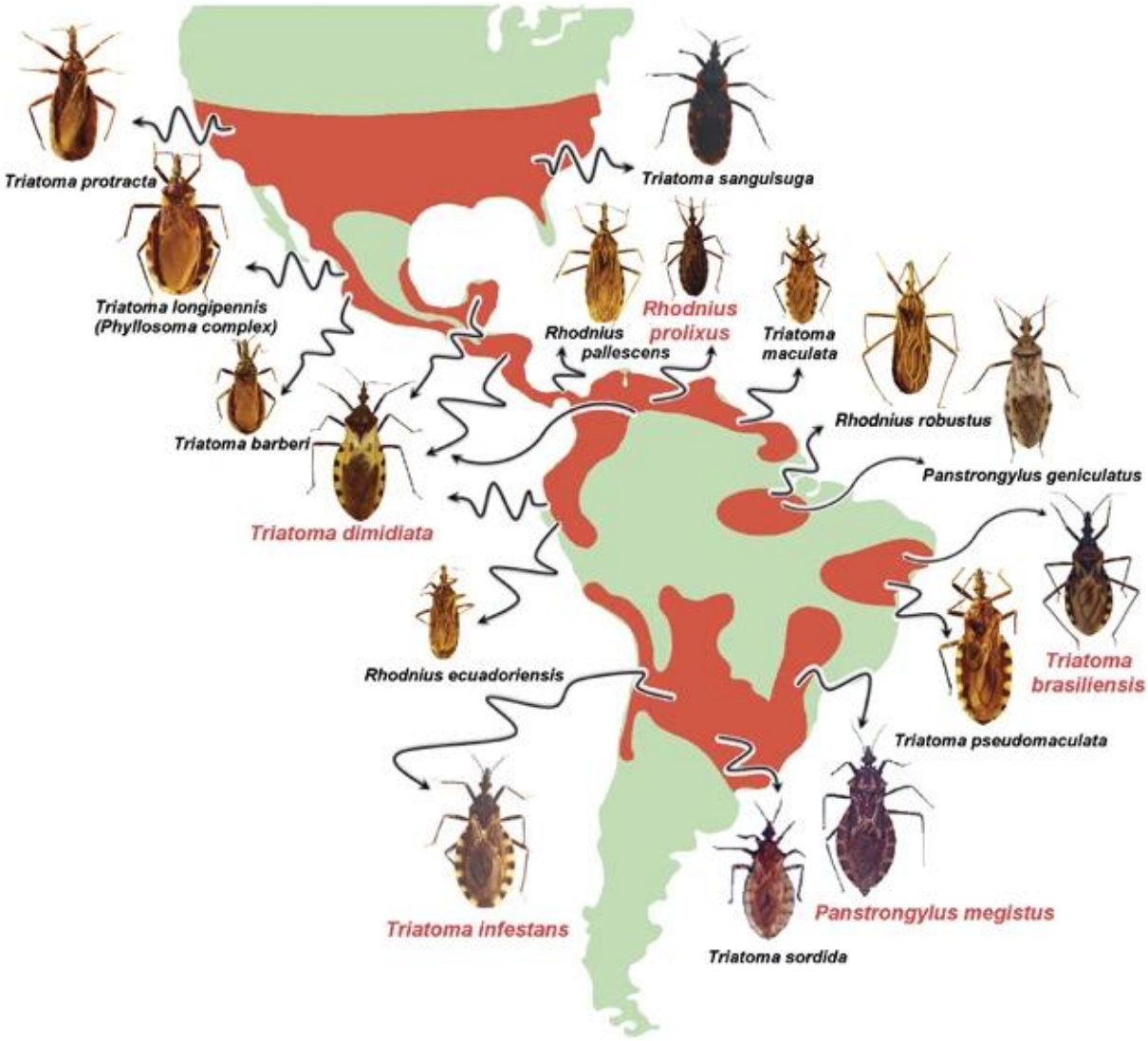

Figure 6. Distribution of the major epidemiologically relevant triatomine species.
The approximate geographical distribution of each species is highlighted in red. Species highlighted with red text are those seen as the most medically important due to Chagas disease transmission. Figure from (59).

Dipteran insects of the subfamily Phlebotominae, sand flies, are the vectors for leishmaniasis. 988 species of Phlebotominae have been identified and split into six genera (66). Representatives of two genera, *Phlebotomus* and *Lutzomyia* comprise of the major medically important species. *Phlebotomus spp.* are restricted to Afro-Eurasia countries and *Lutzomyia spp*. in the Americas (Figure 7) (66,67). *Lutzomyia longipalpis* (Figure 5C) is the most prominent vector in the Americas and the primary vector of VL (*L. infantum*), which is responsible for over 5,000 deaths per year (1,68,69). *Phlebotomus argentipes* is the only known vector of *L. donovani* in the Indian subcontinent, leading to 90% of global VL cases (70). Whilst *Phlebotomus papatasi,* an anthropophilic sand fly, is the primary vector for cutaneous leishmaniasis (*L. major*) across most of Afro-Eurasia (71). Poor sanitation, climate change and encroachment of humans into sylvatic habitats have been implicated in the increasing ecological range of sand flies (68,72). Sand flies are often opportunistic in their

feeding habits and are seldom exclusively anthropophilic, therefore, chicken coops/lifestock in peridomestic areas or pets such as dogs may help support vector populations (73,74).

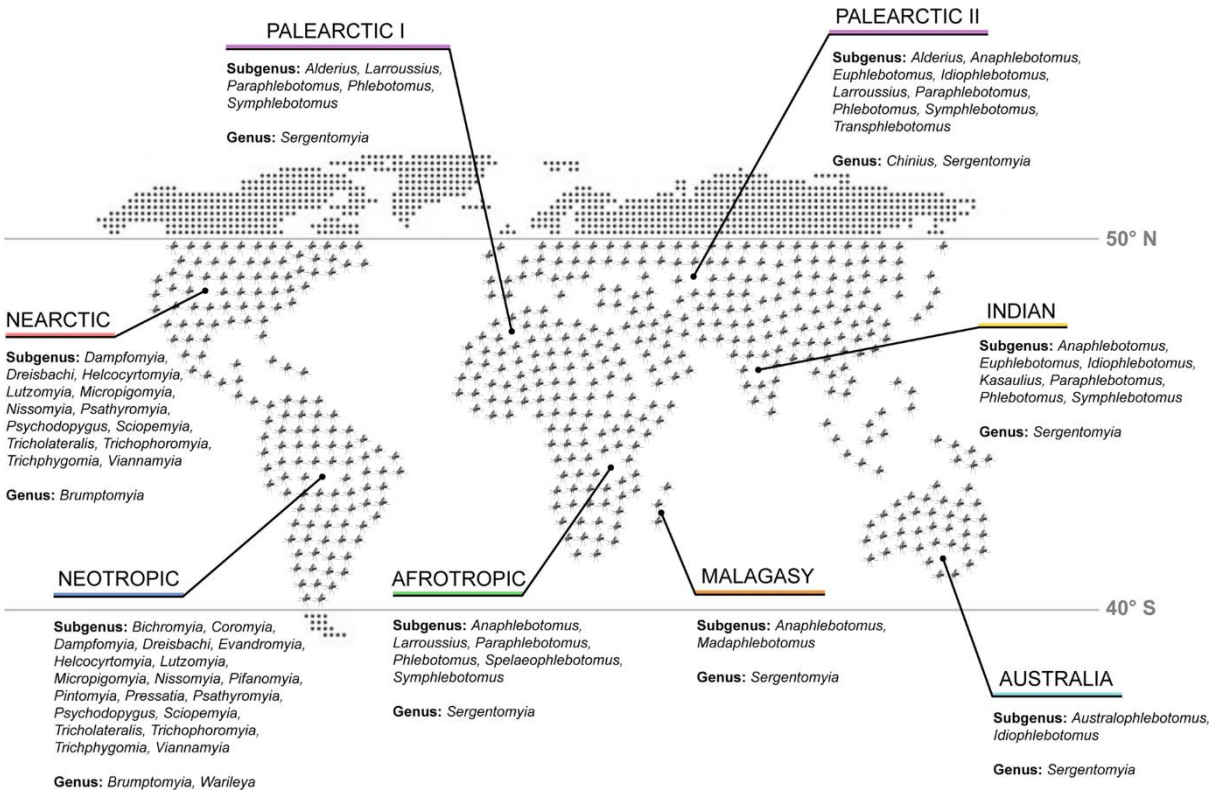

Figure 7. Global distribution of phlebotomine sand flies.
The map lists epidemiologically relevant sand fly genera based on eight zoogeographical regions. Sand flies are estimated to be distributed between latitudes of 50°N and 40°S as marked with the grey lines. Figure from (67).

T. cruzi has been observed in over 180 mammal species spanning domestic and sylvatic environments (75). The most medically important animal reservoirs include species from the rodent, opossum and primate groups (75,76). For leishmaniasis mammals from Orders Marsupialia, Cingulata, Pilosa, Rodentia, Primata, Carnivora, and Chiroptera have been implicated as animal reservoirs for human disease (77). Dogs are important reservoirs in the Americas, livestock and sylvatic reservoirs are implicated in transmission in Afro-Eurasia (77,78). Animal reservoirs, along with the presence of asymptomatic carriers make eradication via chemotherapeutic treatment alone unlikely.

1. 4. Genetic modification of insects

The use of genetic modification (GM) techniques in insects has been of wide interest to the scientific community. This is mostly due to its ability to elucidate gene functions and as a potential route to interrupt pathogen transmission (Section 1. 5.). The most commonly used method for delivering genome editing components to cells is DNA construct vectors. These deliver genome editing systems (Sections 1. 4. 1- 3) by the expression of a DNA cassette containing the coding regions of RNA

molecules or proteins, which are expressed in the ribosomes of cells without being present in chromosomal DNA. This expression is referred to as transient expression as it is often temporary and is unable to multiply with cell replication. The genome editing systems coded in these DNA constructs can migrate to the nucleus post-expression, to edit genomic DNA (79). Random integration of exogenous DNA can occur during genome replication or repair, when exogenous DNA binds with complimentary genomic DNA, often due to small regions of homology (Figure 9) (80,81). This is often utilized *in vitro* to create stable clonal cell lines by randomly integrating DNA cassettes containing drug resistance or fluorescent markers which can be selected by drug pressure or fluorescence-activated cell sorting (82,83).

The development of CRISPR-Cas9 based approaches have largely surpassed previous techniques such as piggyBac and zinc finger nucleases. The specific removal or replacement of a genes function has allowed for a deep understanding of vector-pathogen interactions and vector control strategies (84–87). Whilst CRISPR-Cas9 has become the main approach for GM in insects, multiple other approaches have been validated and optimised and with each one comes a suite of advantages. These techniques have the potential to be used by researchers to silence/overexpress/introduce genes of interests which can be used to understand the functional basis of gene pathways. This understanding of functional genomics allows researchers to further understand insect biology or pathogen-vector interactions. Which can be used to produce novel chemotherapies targeting parasite pathways involved in transmission or to develop vector control strategies affecting insect fecundity or immunity to pathogens.

1. 4. 1. *PiggyBac* transposable elements

PiggyBac transposable elements are one of the most widely used genetic modification techniques in insects. They were first identified in the cabbage looper (*Trichoplusia ni)* when it was observed that nuclear polyhedrosis viruses began incorporating genomic sequences from *T. ni* cells following infection (88). These mutations termed FPs (Few-Polyhedra) were characterized by their inverted terminal repeats (ITRs) located asymmetrically on either end of the inserted DNA (89). They were found to insert only at a TTAA sequence within the genome. A particular FP sequence (IFP2) encodes a transposase enzyme, which causes a double stranded break of genomic DNA at the TTAA sites (89). Using IFP2, a system of DNA construct vectors were developed, one incorporating ITRs flanking exogenous DNA for insertion, and a further vector containing the *piggyBac* helper transposase based on the IFP2 sequence (90). Once expressed the transposases bind to the ITRs in a DNA vector and locate a TTAA region in genomic DNA, the transposase then catalyses the integration of the exogenous DNA into the genome (Figure 88A) (91). If desired, the exogenous DNA can then be

excised from the genome without leaving insertion/deletion (indel) mutations by the use of an excision only *piggyBac* transposase (Figure 88B) (92).

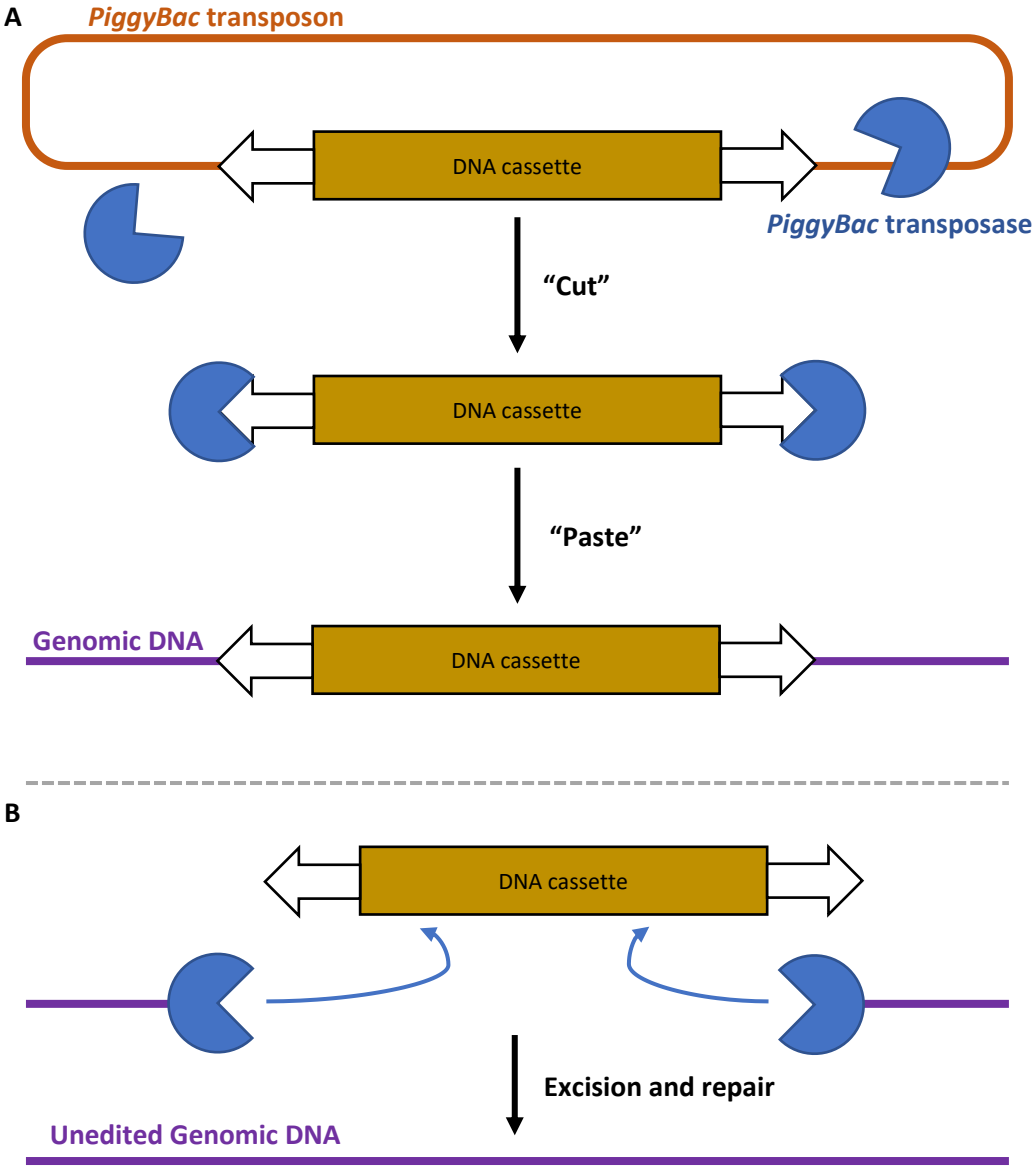

Figure 8. Integration and excision of a DNA cassette using the *piggyBac* transposon system.
A) a DNA cassette is integrated into the target genome at a TTAA site by *piggyBac* transposases. The *piggyBac* transposases bind to inverted terminal repeats (ITR) in a vector containing a *piggyBac* transposon. The transposon is then "cut" out of the vector and "pasted" into the genome at a TTAA site. B) DNA previously integrated via *piggyBac* is excised from the genome using *piggyBac* transposases. This excision leaves no scarring in the genome sequence.

Although *piggyBac* was developed from *T. ni,* its efficiency within mammalian cells was much greater than other transposable elements identified at the time (93–95). Altering the original *piggyBac* transposase's coding sequence to optimise codon usage for mammalian cells, transposition efficiencies increased by 20 fold in mammalian cells (96). Following this, screening of a range of transposase mutants found in *Saccharomyces cerevisiae* against mouse ES cells, a mutant referred to as *^{m}hyPBase* was discovered to produce a 17 fold increase in transposition efficiencies (97). Another

mutant was found to contain the same 7aa mutation as *^{m}hyPBase* but with the codon arrangement from the insect *piggyBac* transposase. This was referred to as *^{i}hyPBase* and was found to significantly increase transposition rates in *Drosophila melanogaster* over the *^{m}hyPBase* (98). This insect focused hyperactive transposase is now considered the gold-standard for insect *piggyBac* transfections.

The *piggyBac* system has shown high transfection efficiencies across multiple orders of insects, with species examples such as the Asian tiger mosquito (*Aedes albopictus),* African malaria mosquito *(Anopheles gambiae),* turnip sawfly *(Athalia rosae),* Queensland fruit fly *(Bactrocera tryoni),* two-formed bumble bee (*Bombus bifarius),* silk moth *(Bombyx mori),* New World screw-worm fly *(Cochliomyia hominivorax),* Asian lady beetle *(Harmonia axyridis),* and Red flour beetle *(Tribolium castaneum)* (99–107). However, to date there are no reports of successful application of PiggyBac applied to sand flies or triatomine bugs, a major omission. The semi random nature of *piggyBac* makes for easy integration into the genome but lacks the ability to target specific genes, which is necessary in some functional studies. However, the semi-random nature of insertion is a major advantage in non-model insects, especially those lacking a full genome assembly. In recent years, the inclusion of CRISPR-Cas9 elements (Section 1. 4. 3.) into piggyBac cassettes has allowed the targeting of specific genes for functional studies and even the production of high efficiency gene-drives (Section 1. 5. 1.) (108,109). This technology has the potential to create lasting vector control methods such as sterile insect techniques, which are introduced to populations with relative ease (110).

1. 4. 2. Zinc finger nucleases and transcription activator-like effector nucleases

Type IIS restriction enzymes are now widely used to cut genomic DNA allowing for targeted mutations to occur. Initially these enzymes were discovered to defend bacteria from exogenous DNA such as T7 phages (111). With this knowledge the *FokI* endonuclease from *Flavobacterium okeanokoites* was found to show efficient but non-specific cleavage of eukaryotic double stranded genomic DNA (112). Two GM systems were developed by attaching DNA binding proteins to the *FokI* endonuclease, with this adaptation, specific genome sequences could be targeted (113,114). These

two systems were known as zinc finger nucleases (ZFN) and transcription activator-like effector nucleases (TALEN).

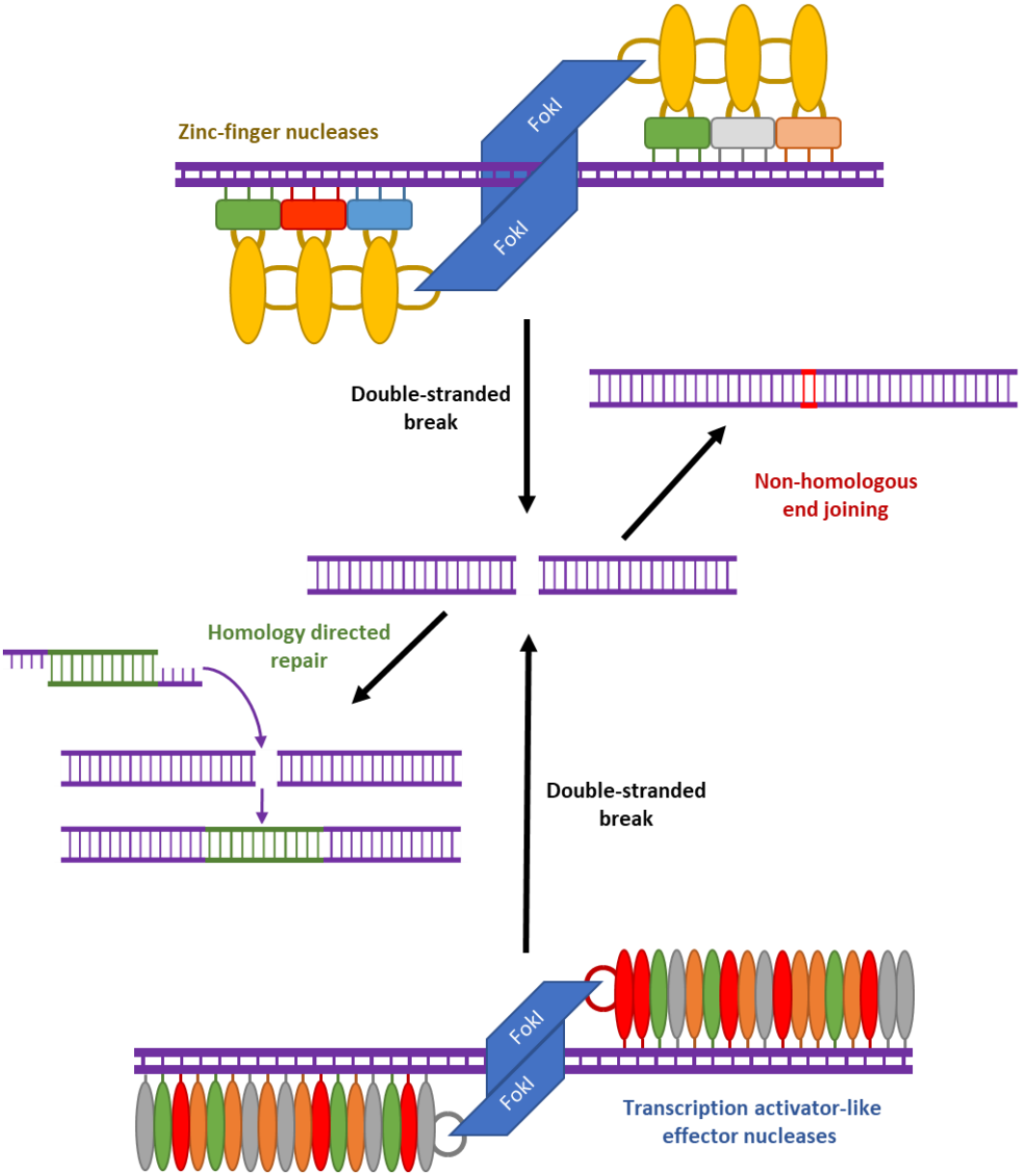

Figure 9. Genome engineering via zinc finger nuclease (ZFN) or transcription activator-like effector nuclease (TALEN) approaches.
ZFN uses zinc finger proteins to bind to a 3bp region of a target genome sequence. These proteins are attached in an array of 3-6 proteins and bound to a *FokI* endonuclease. This complex is known as a zinc finger nuclease. Another ZFN is designed for the complimentary strand directly upstream of the first ZFN. When these bind to the genome the FokI endonucleases dimerize causing a double-stranded break in the genomic DNA. This can be repaired by non-homologous end joining which can create insert/deletion mutations. Alternatively, if DNA with complimentary sequences to the region surrounding the cut site is present, homology directed repair may occur inserting the exogenous DNA into the genome. TALENs utilise transcription activator-like effectors instead of zinc finger proteins. These are capable of binding to a single nucleotide allowing for more accurate targeting of a genomic sequence.

The process of gene editing via the ZFN system goes as follows, Cys_2-His_2 zinc-finger proteins (ZFP) recognise and bind to a 3bp DNA sequence within the genome, allowing identification of a target region (115). 3-6 ZFPs are attached to create an array allowing for the targeting of an 18-36bp

region. The array is bound to a *FokI* restriction enzyme. Another array is formed to bind to the complimentary strand of the genome directly upstream and includes a *FokI* endonuclease. Following ZFNs binding to the genome the *FokI* enzymes dimerize and cleave the genomic DNA causing a double-stranded break (DSB) (Figure 99). This DSB can be used for non-homologous end joining (NHEJ) and homology directed repair (HDR) genome editing techniques. NHEJ is highly error-prone in attempting to repair the DSB, usually resulting in small indels and subsequently gene loss caused by a frameshift (Figure 99). HDR incorporates exogenous DNA with flanking arms complementary to the region surrounding the DSB, allowing for insertion of template DNA (Figure 99) (79).

The initial ZFPs were found in *Xenopus laevis* oocysts, and following *FokI* injections into oocysts, highly efficient cleavage of plasmid DNA was observed (116,117). Whilst initial studies used only three ZFPs to an array (identification of 18bp), a six ZFP system was developed allowing for more accurate target binding, by permitting mismatched nucleotides in the array (118). Optimizations of ZFP arrangements are still being created with recent papers showing the ability to skip nucleotides between ZFP binding sites (119). ZFNs have been applied to a wide range of eukaryote organisms including amphibians, fish, insects, and mammals (120–123). In the context of this thesis, their use in insects is most relevant. ZFNs were utilised for inheritable gene loss studies in model organisms such as *B. mori* and *D. melanogaster* (121,124). The function of the phenotypic *Laccase2* gene was removed in two-spotted cricket (*Gryllus bimaculatus)* offspring, showing ZFNs potential in non-model insect species (125). However, the complexity of producing ZFNs made it both expensive and time consuming and the approach was quickly dropped for insect transgenics in favour of other techniques such as *piggyBac*, CRISPR-Cas9 and TALENs (126).

Using transcription activator-like effectors (TALE) from the plant pathogenic bacteria *Xanthomonas,* Boch *et al.,* was able to develop a novel DNA binding array using proteins which bind to single nucleotides and attach to type IIS restriction enzymes for DNA cleavage (113,127). The biding arrays can be 12-28 proteins in length giving a potential 24-56 bp binding site. Similar to ZFNs, researchers create an array of TALEs which bind with one strand of double stranded DNA attached to a *FokI* endonuclease on the C-terminal end forming a transcription activator-like effector nuclease (TALEN). When the *FokI* endonucleases dimerize, they will cause a DSB which can lead to NHEJ or HDR repair (Figure 99). The main difference between ZFN and TALENs is the level of accuracy that can be selected due to TALEs binding to a single nucleotide. This gives much greater control in selecting a target site over ZFNs, as ZFNs were dependant on a select number of 3bp combinations (127).

TALENs are still widely used today for genetic modification of organisms. The system is often favoured for human gene therapies over tools such as CRISPR-Cas9 due to its ability to be location-

tagged for editing of specific DNA types such as mitochondrial DNA (128). TALENs are used for the creation of transgenic insect lines, with successful manipulation in a number of dipteran and lepidopteran insects (84,129–131). These approaches have been far more focused on functional genomics over those trialled with ZFN. Within *B. mori* the *fibroin heavy chain* gene was replaced with the *major ampullate spidroin-1* gene from the golden silk orb-weaver (*Nephila clavipes)* creating moths capable of producing spider-like silk (130). To halt malaria parasite development in the Asian Malaria Mosquito (*Anopheles stephensi)* the *kynurenine 3-monooxygenase* gene was removed, which reduced xanthurenic acid levels, a necessary acid for plasmodium exflagellation (84). Research using the TALENs technique still shows potential, however, due to the protein array production being more complex and expensive than that of gRNAs used in CRISPR-Cas9, its adoption in insect based research has been limited.

1. 4. 3. CRISPR-Cas9

First identified in *Escherichia coli* in 1987, CRISPR-Cas9 (Clustered Regularly Interspaced Short Palindromic Repeats- CRISPR Associated Sequences 9) is a bacterial defence mechanism against bacteriophages and viral transposable elements (132). DNA can be cleaved using CRISPR associated recognition sequences and an associated endonuclease (Cas9) causing a DSB at the site of palindromic repeats, allowing for targeted mutagenesis (133). The repeats, known as protospacer regions, do not naturally occur within bacterial genomes. Cas nucleases will cleave DNA following a protospacer adjacent motif (PAM) often the 3-6bp following a protospacer region (79).

The CRISPR-Cas9 mechanism has been translated for use in eukaryotic organisms to precisely manipulate genes in an efficient low-cost manner compared to approaches such as TALENs. The type IIA system originally translated from *Streptococcus pyogenes* is widely used for manipulation of eukaryotes, due to its homologous nature and use of the Cas9 endonuclease (134). Cas9 identifies a target cleavage site by associating with a short RNA sequence known as a single guide RNA (sgRNA) (Figure 1010B). A sgRNA comprises of a 20bp sequence homologous to the target region directly upstream of a PAM sequence (5'-NGG) and a 75bp scaffold sequence complementary to the Cas9 endonuclease. The sgRNA and Cas9 endonuclease bind together to form a ribonucleoprotein (RNP). Once the RNP is formed, the Cas9 endonuclease facilitates cleavage of the nucleotide following the

PAM sequence (Figure 10C) (79). Following DNA cleavage by Cas9 endonucleases, cells will invoke one of two repair mechanisms, NHEJ or HDR (Figure 10D).

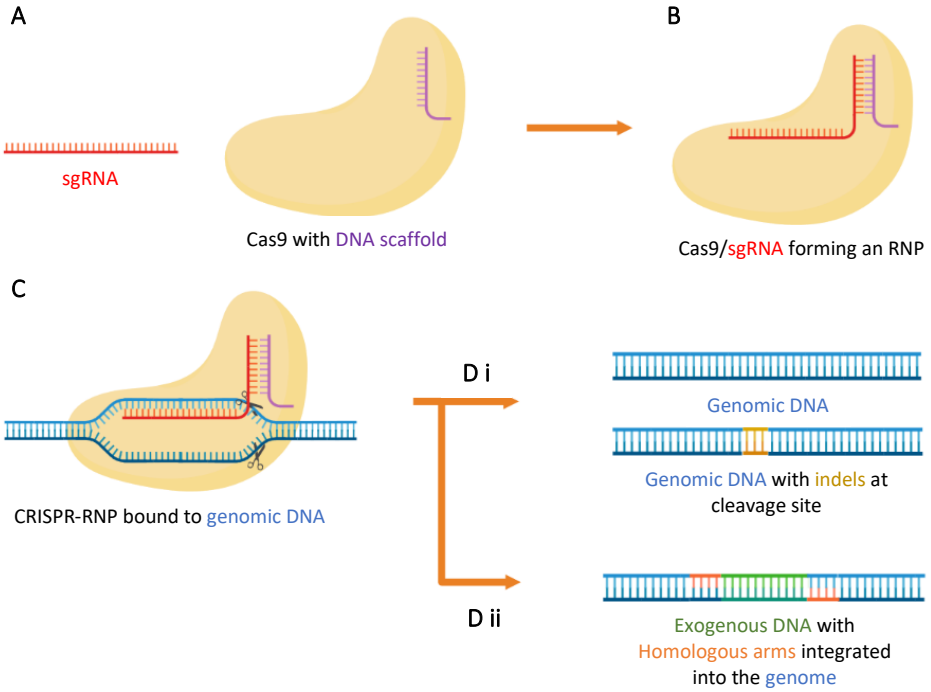

Figure 10. CRISPR-Cas9 cleavage of genomic DNA for Non-Homologous End Joining and Homology Directed Repair.
A) the Cas9 and sgRNA are expressed in or introduced to the target cell. B) the Cas9 endonuclease binds to the complementary scaffold and forms a ribonucleoprotein (RNP). C) the cas9 separates double stranded genomic DNA at the site complementary to the gRNA. The Cas9 then cleaves the genomic DNA 3bp upstream of the gRNA's terminal end causing a double stranded break. Di) NHEJ repairs the cleavage site potentially introducing indel mutations in the genomic DNA strands. Dii) HDR occurs if exogenous DNA with homologous arms complimentary to the region surrounding the cleavage site are present. This figure was created using the BioRender webtool.

This system has a number of advantages over that of type IIS restriction enzymes systems, most importantly, it is easier to produce target recognition via RNA over the chaining of specific peptides which are expensive and labour intensive. The relative simplicity has led to the mass adoption of CRISPR-Cas9 for GM over approaches such as ZFN and TALENs. *D. melanogaster* was the first published insect to be edited by the CRISPR-Cas9 system targeting eye phenotype genes *white* and *yellow* (135). Since then, the system has been applied to the insect orders Coleoptera, Diptera, Hemiptera, Hymenoptera, Lepidoptera, Orthoptera, and Zygentoma (136–142). Most of these early approaches were simple validations of the system using phenotypic genes as markers of successful loss of function mutations. Using the CRISPR-Cas9 system Awata *et al*, was able to validate the *dop1* gene as a neurotransmitter mediating aversive reinforcement when feeding salt or sugar water to *G. bimaculatus* (143). This revealed important insights in the understanding of learning and memory for insects. In locating and targeting relevant effector domains within a gene, researchers are able to repress or activate genes for functional studies. These targeted approaches are known as CRISPRi

(gene repression) or CRISPRa (gene activation). This has been used in *B. mori* to activate the silk production gene *Fibroin Heavy Chain*, which resulted in increased cell stress responses and silk secretion disorders (144). These approaches have also been shown to reduce the mortality associated with Cas9 over expression in *Drosophila* allowing for more detailed gene function studies without trait loss (145). Whilst the applications of CRISPR-Cas9 for the study of gene functions is important, other groups have been using the system to implement insect control strategies for crop pests and disease vectors (Sections 2. 1. 1. & 5. 1. 1.).

1. 5. Genetic modification strategies for vector control

Currently Chagas disease and leishmania vector control strategies rely on insecticides and housing improvements. These techniques can be effective but are limited by the emerging resistance to insecticides and they require significant funding and infrastructure to remain viable (30,46,146). The genetic modification of insect populations brings the opportunity to pass traits through inheritance, which are self-sustaining post release. The genetic control of insects has taken two main approaches, population suppression, and population replacement. These approaches are often driven through populations by the use of a gene drive system (Figure 11).

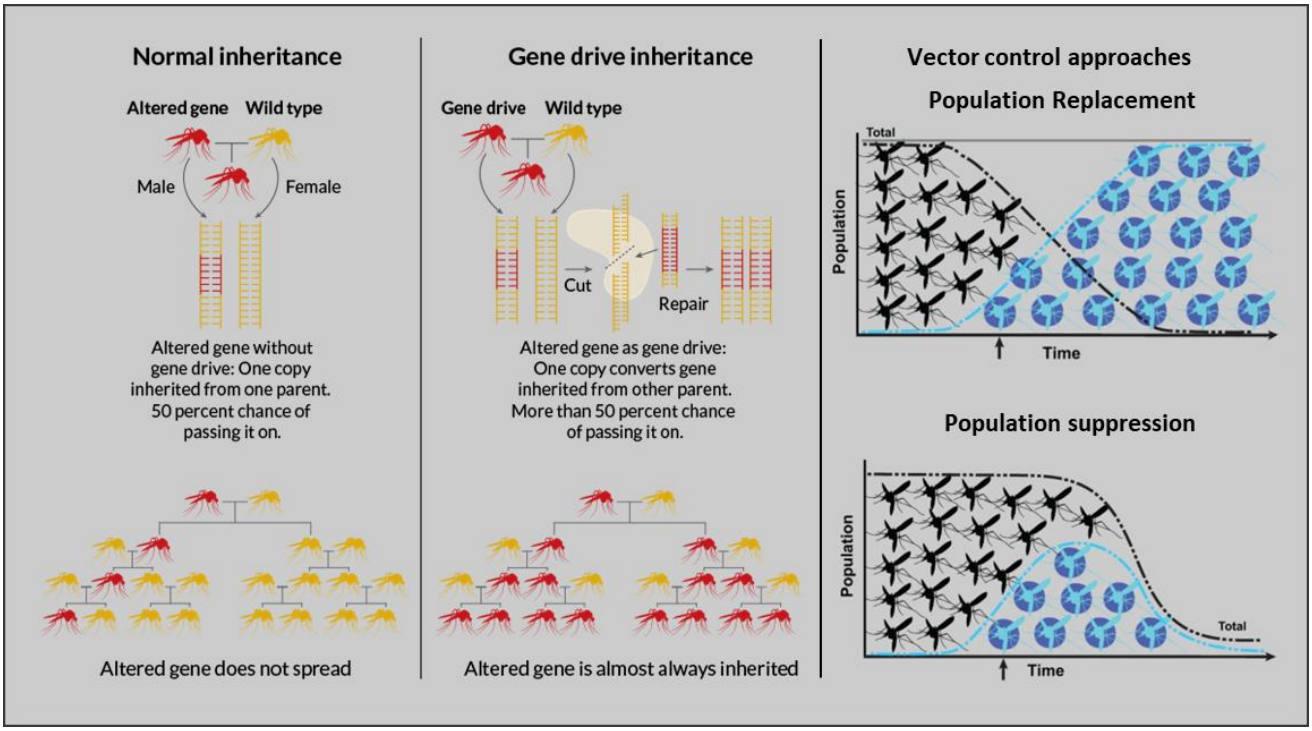

Figure 11. Insect genetic modification vector control strategies.
Gene drives facilitate the inheritance of introduced traits above that of Mendelian inheritance. They work by the integration of a CRISPR-Cas9 system into the genome expressed by a germline specific promoter. This expression results in the trait being incorporated into both target chromosomes, increasing the chance of an offspring inheriting the trait above 50%. Gene drives can be applied to population control strategies either replacing the population with a stable line exhibiting a desired trait (population replacement), or the

suppression of a population by introducing traits which reduce viability or reproductive fitness (population suppression). Figures from (147,148).

To ensure these traits are inherited by populations, any approach for genetically engineering insects (Section 1. 4) must be delivered to pre-blastoderm pole cells. During the embryogenesis of insects, the pre-blastoderm period is when the fertilised egg cell separates into two cell types, diploid germline derived cells which migrate to the posterior pole to form the embryo (pole cells), and a multinuclear coenocyte, which replicates clonally to create several thousand daughter cells (149). These daughter cells will migrate to the periplasm of the yolk forming a single cell layer, the blastoderm, which protects both the yolk and pole cells, allowing them to divide and differentiate into the insect embryo. Delivery to the pole cells prior to blastoderm formation, increases the efficiency of transfection as a low number of cell replications have occurred. This ensures the desired trait will be present in the majority of the embryonic cells, increasing the likelihood of gamete precursor cells carrying the desired trait and thus inheritance to the next generation. The blastoderm is thought to develop in the first 36-60 hours post oviposition for sand flies and 12 hours for triatomine bugs (150,151). Although, sand flies often oviposit fully melanised eggs, potentially inferring these eggs have already developed past blastoderm formation before being oviposited (152). The further the pole cells replicate, the lower the efficiency of integrating the desired traits into the majority of embryonic cells. This leads to mosaic expression of the trait in G0 tissues, and ubiquitous expression in further generations as these will have at least one chromosome expressing the trait. The integration of this trait in the second parental chromosome, so all germline cells possess the trait, is the basis of gene drive systems (153).

1. 5. 1. Gene drives

Gene drives are selfish genetic elements capable of spreading a desired trait, that has no benefit to an organism, through populations at levels above Mendelian inheritance (Figure 11) (147,148,154). A gene drive system typically incorporates three components, a sgRNA, the Cas9 endonuclease gene, and an insertional template incorporating homologous flanking arms targeting the desired insertional site leading to autocatalytic incorporation of an exogenous DNA template in the second wild- type allele resulting in homozygosity (154–156). This can be applied to a HDR CRISPR-Cas9 construct by incorporating germline-specific promoters such as *nanos, vasa* or *zpg*, this will allow desired traits to be inherited by entire populations within 5-15 generations (157,158).

Although gene drive approaches hold great promise, there are technical hurdles which need to be overcome before gene drive populations can be released. A key limitation to current strategies is the rise of resistance alleles. These are mutations surrounding the target site which when amplified in a

population reduce the ability for gene drives to function, therefore, removing the desired trait within a few generations (155). One solution which has been widely adopted is the use of multiplexed gRNA, this would require multiple resistance alleles to form before the trait is removed (159). Alternatively, by selecting a highly conserved target site in an essential gene, such as the *doublesex* gene, where mutations would elicit a viability loss within population, reducing the risk of resistance alleles over multiple generations (157).

A further limitation of gene drives is the spread of the trait across wider populations without end. If an insect carrying a hazardous trait is introduced to wild populations this trait would be carried across vast geographical areas. To combat this, two approaches are currently being developed, these are reverse gene drives and daisy chain gene drives (AKA daisy drives or local drives) (160,161). Reverse drives introduce a gene drive to a transgenic population which directly targets the initial gene drive elements halting its function in later generations (160). Although, modelling of the reverse drive strategy seems to suggest that the reverse drives would fail to reach every transgenic insect and the hazardous traits would migrate to new geographical areas away from reverse drive populations (162). Daisy drives introduce gene drive elements into multiple sections of the genome, with all elements being required for the trait to function (161). As resistance alleles form in future generations some elements cease to function. This limits the inherited trait to only a few generations, reducing its ability to spread across a large geographical area. Therefore, self-limiting approaches such as daisy chain drives are suggested for driving any trait that does not present a fitness cost (163).

The field of gene drives is still relatively early in development but the approaches being assessed in laboratory conditions are high impact and have the capacity to revolutionise vector control.

1. 5. 2. Population suppression approaches

Population suppression involves the inheritance of transgenes which cause a reduction in viability or reproductive fitness. Potential targets within this approach involve genes which alter sex ratios, produce sterile offspring, and limit mate seeking behaviours (110,131,157,164–170).

One target for the control of insects via population suppression is sex-determining factors. Potential genes implicated in sex determination have been discovered across multiple insect orders (171). For use in the textile industry, the *filial 1* gene in *B. mori* causes lethal mutations in developing females, leading to male only populations which produce higher quality silk cocoons (172). For vector control, male determining factors such as the *Nix* gene can be used to force male sex determination via upregulation by CRISPRa or female determination via CRISPR-Cas9 NHEJ (161,164,173). By targeting

the *I-PpoI* gene specifically in the X chromosome of *An. gambiae,* a high male bias developed in their offspring (165). Furthering this, a gene drive system targeting the *I-PpoI* gene, integrated into the *doublesex* locus, resulted in a male bias with females exhibiting male genitalia, resulting in a 100% male population within 10-14 generations from an allelic frequency of 2.5% (166).

Key genes relating to fecundity have been identified in a number of Diptera, the most important of which for vector control include *β2-tubulin, doublesex* and *intersex* (157,167,174). The *β2-tubulin* gene functions to produce tubulin in the testes and sperm of insects, a key structural component vital for sperm formation (175). Loss of the *β2-tubulin* gene in *Ae. aegypti,* created complete male sterility within 3 generations without the associated fitness costs found in sterile irradiated mosquitos (167). The *doublesex* gene regulates sex determination mRNAs, the regulation of each mRNA is carried out by either the *transformer* or *transformer 2* loci (176). By targeting specific exons of the *doublesex* gene with CRISPR-Cas9, a loss of transcription in either of the mRNAs can initiate the development of the gendered genitalia (157). When the female coding *doublesex* exon of *An. gambiae* was targeted in a CRISPR-Cas9 gene drive system, male genitalia was exhibited in all female offspring within 7-11 generations (157). The *intersex* gene was found to be a regulator of the female specific *doublesex* pathway, as it is required for sex differentiation creating the female genitalia of insects (174).

A number of genes have been targeted to affect mate seeking behaviours, leading to a reduction in mating and a population crash. Examples include olfactory targets such as *fruitless* and *odorant receptor co-receptor* (*orco*) or flight muscle genes such as *actin-4* and *myosin heavy chain* (*myo-fem*) (131,168–170,177). The *fruitless* gene is a female specific broad-complex tramtrack zinc finger transcription factor gene, which is linked to host seeking behaviours in females (178,179). When loss of function occurs in male insects, they lose their mate seeking behaviours making this gene a potential target for population suppression (177,179). Multiple *orco* genes have been discovered in insects relating to olfactory responses, especially host seeking behaviours in disease transmission (180,181). When targeted via TALENs in the Asian corn borer moth (*Ostrinia furnacalis),* a specific *orco* gene was found to drastically reduce attraction to sex pheromones, which could lead to a lack of mating in a controlled release (131). The *actin-4* gene is involved in the formation of muscle fibres within female wing muscles of mosquitos such as *Ae. aegypti* and the southern house mosquito (*Culex quinquefasciatus)* (169,170). The *myosin heavy chain* gene, *myo-fem,* is responsible for ATP conversion to mechanical energy with female flight muscles (168,170). Both genes have been targeted in CRISPR-Cas9 studies on *Ae. aegypti* and *Cx. quinquefasciatus* creating insect lines with female offspring unable to control their wings (168–170). Reducing mobility limits their contact with

potential male mates and reduces their ability to create the wingbeat frequency needed to attract mates within swarms.

The targeting of population suppression genes could replace classic methods of vector control such as sterile insect techniques (SIT) via chemicals or irradiation (182). The creation of sterile transgenic lines incorporating gene drives allows for a self-sustaining control strategy with little input post release. A self-limiting system for GM SIT has been developed, referred to as precision guided SIT (pgSIT) functions by introducing Cas9 to a single line of insects and target gRNAs into another line. When these lines mate their offspring contain the full machinery to induce the intended CRISPR-Cas9 trait. This system has been applied to insects targeting genes relating to fecundity, sex differentiation and mate seeking behaviours (168,183,184). A pgSIT system targeting the *doublessex*, *intersex*, and *β-Tubulin 85D* genes in *Ae. aegypti*, was able to create a 99% sterile male population with a lethal mutation to female offspring, leading to a rapid population decline (110). Similarly, this system has been applied to the crop pests *Drosophila suzukii,* and observed 100% of viable G1 offspring were sterile males (184). This approach has the potential to rapidly reduce disease transmission in localised areas without risking sylvatic population decline.

1. 5. 3. Population replacement approaches

Whilst population suppression has been heavily investigated as a leading vector control strategy, many ethical concerns have been raised around the eradication of a species. With the main ethical concern being the effect of a species loss on the surrounding ecosystem, in particular predators and plant species which rely on them for pollination (185). These concerns could be partially alleviated by the use of population replacement strategies, which alter the target population to reduce disease transmission without harming their ecosystem. Researchers have developed multiple strategies to induce refractoriness to disease agents including the loss of vector competency genes, the expression of vaccine candidates in insect saliva, and expression of effector molecules. These approaches have the potential to reduce the disease transmission from insect vectors without supressing populations.

Many genes related to vector competency in insects have been identified, and with the emergence of GM vector control strategies these genes can be targeted to reduce or eliminate transmission. One such target is the eye-phenotype gene *cardinal*, which has been assessed in a field-ready gene drive system for *An. gambiae,* which was able to drive the trait within 6-10 generations (186). The cardinal gene catalyses the synthesis of xanthurenic acid, which is required by malaria to activate gametogenesis, if the gene's function is lost, malaria parasites are unable to develop to oocysts

within mosquitos (186,187). Multiple potential targets have been identified for interrupting *Leishmania spp.* transmission in sand flies and *T. cruzi* in triatomine bugs. For leishmaniasis control, sand fly glycan genes could be targeted due to their role in parasite attachment to the midgut, which is essential for early differentiation (188,189). In *Phlebotomus papatasi* a galectin similar in form to β-galactosides 1-3, was required for attachment of *Leishmania major* to the midgut wall, whilst N-acetyl-D-galactosamine in *L. longipalpis* has been implicated in the binding of *Leishmania mexicana* promastigotes (188,189). In triatomines, gut epithelial cell glycoproteins found on the surface of their perimicrovillar membrane have been identified as responsible for *T. cruzi* attachment to the gut (190,191). If the glycoprotein genes were lost, parasite attachment would be inhibited leading to their excretion before they could develop to infective stages. The *caspar* gene in *L. longipalpis* has also been shown to increase immune responses and clear *Leishmania* infections following loss of function (192). All of these targets have the potential to reduce disease transmission with traditional loss of function gene-drive strategies.

A novel approach to combat transmission is the expression of vaccine candidates within insect populations. Yamamoto *et al*., successfully expressed the SP15 *Leishmania* antigen in *An. stephensi* salivary glands, which following multiple bites to mice raised anti-SP15 antibodies (193). The potential antigen would be transferred to humans post bite and induce an immune response, which could combat infection when it occurs. In principle, this concept could be applied to many infectious disease antigens or mRNA vaccine elements within multiple insect populations. There are concerns about vaccine consent and potential side effects, which has limited the application of this approach (185,193).

The final approach for population replacement is the expression of effector molecules. These molecules include antibodies, anti-microbial peptides (AMP), DNA/RNA strands, and proteins. Effector molecules have shown to be especially effective against arboviruses with multiple approaches being taken in *Ae. aegypti* mosquitos (194–196). One approach is the expression of targeted hammerhead ribozymes, which can cleave structural protein genes in viral RNA genomes such as chikungunya (194). Similarly transgenic *Ae. aegypti* expressing small-interfering dsRNA molecules targeting the NS3/4A region of the Zika genome were able to cleave essential sequences and create near complete inhibition of the virus (195). Another approach was the expression of microRNAs targeting viral pathways of dengue and chikungunya in transgenic *Ae. aegypti*, these inhibited the transcription of viral mRNA reducing transmission efficiencies (196). In malaria, multiple single-chain antibodies such as m1C3, m4B7, or m2A10 were identified to bind to parasites, inhibiting sporozoite formation in mosquitos and affecting release from oocysts (197). These single-

chain antibodies amongst others have been expressed from multiple gene-drive approaches, showing a reduction in transmission as well as reduced resistance alleles and population replacement within 5-11 generations (198,199). The expression of glycoinositolphospholipids in triatomines has also been theorised to reduce T. cruzi attachment to the midgut, limiting parasite development (191,200). AMPs are short peptide molecules usually derived from natural origins such as animal or insect genomes. AMPs have been expressed into mosquitos to target malaria via gene drives, this approach used magainin 2 and melittin in *An. gambiae,* limiting oocyst formation and creating a line of mosquitoes refractory to malaria (201). This expression was localised to the gut to reduce toxicity and increase contact with ingested parasites.

Table 1. Anti-microbial peptides active against *Leishmania spp.*

Rows highlighted in green are peptides which have known active concentrations against both *Leishmania spp.* and *Trypanosoma cruzi*. Active concentrations marked with a * represent IC90s, a ** is an IC20 value, and *** is a IC100 value.

Parasite targeted	Peptide name	Origin species	Active concentration (μM)	Mammalian cell toxicity	CDS length (bp)	References
Le. amazonensis	Phylloseptin 1	Waxy monkey tree frog *(Phyllomedusa sauvagei)*	3.93*	98	309bp	(202,203)
	Gomesin	Tarantula spider (Acanthoscurria gomesiana)	40*	5.3	548bp	(204)
Le. braziliensis	Tachyplesin	Chinese horseshoe crab *(Tachypleus tridentatus)*	12.5***	Not known	524bp	(205)
Le. chagasi	Dermaseptin 1 analogue	Waxy monkey tree frog *(Phyllomedusa sauvagei)*	18.5***	50**	358bp	(206)
Le. donovani	Cathelicidin-4	Domestic cow *(Bos taurus)*	0.000035	Not known	550bp	(207)
	Seminalplasmin	Domestic cow *(Bos taurus)*	0.00038	Not known	2156bp	(207)
	Thionins	Common wheat *(Triticum aestivum)*	1*	40	567bp	(208)
Le. mexicana	Scorpine	Emperor scorpion *(Pandinus imperator)*	27***	150	538bp	(209)
Le. tarentolae	REDLK	*Pseudomonas aeruginosa*	75.83*	75	n/a	(210)
Le. tropica	Halictine-2	Six-banded furrow bee *(Halictus sexcinctus)*	64***	65**	n/a	(211)

Table 2. Anti-microbial peptides active against *T. cruzi.*

Rows highlighted in green are peptides which have known active concentrations against both *Leishmania spp.* and *Trypanosoma cruzi*. Active concentrations marked with a * represent IC90s, a ** is an IC20 value, and *** is a IC100 value.

Parasite targeted	Peptide name	Origin species	Active concentration (μM)	Mammalian cell toxicity	CDS length (bp)	References
T. cruzi	Cathelicidin-6	Domestic cow *(Bos taurus)*	2*	Not known	477bp	(212)
	Scorpine	Emperor scorpion *(Pandinus imperator)*	2.5*	150	538bp	(213)
	Melittin	Honey bee *(Apis mellifera)*	2.5	Not known	229bp	(214)
	M-PONTX-Dq3a	South American giant ant (*Dinoponera quadriceps)*	4.7	25.7	N/A	(215)
	Hemocyanin 364-382	Asian tiger shrimp *(Penaeus monodon)*	4.79	200	2174bp	(216)
	NK-lysin	Wild boar (*Sus scrofa)*	5	50	780bp	(214)
	[Arg]7-VmCT1	Mexican scorpion (*Vaejovis mexicanus)*	5.37	66.47	412bp	(217,218)
	Dermaseptin 1 analogue	Waxy monkey tree frog *(Phyllomedusa sauvagei)*	6	50**	358bp	(206)
	Gomesin	Tarantula spider (Acanthoscurria gomesiana)	6.5	5.3	548bp	(204)
	Attacin	Tetse fly (*Glossina Morsitans)*	10	Not known	555bp	(219)
	Figainin 1	Chaco tree frog *(Boana raniceps)*	15.9	10	298bp	(220)
	Tachyplesin	Chinese horseshoe crab *(Tachypleus tridentatus)*	87.8	Not known	524bp	(205)

A suite of AMPs have been assessed in published literature, relating to the development of chemotherapies for Chagas disease and leishmaniasis. AMP candidates could potentially be adapted to expression cassettes for gene drives in sand flies and triatomine bugs. Tables Table ***1*** and Table ***2***, highlight some of the most promising AMPs previously assessed against *Leishmania spp.* and *T. cruzi.* These AMPs were selected based on efficacy at low active concentrations against the parasites and high concentrations for mammalian cell toxicity. The mammalian toxicity concentrations provide an estimate to the insect toxicity, which would need to be assessed prior to AMP integration within a gene drive construct. The AMPs with the lowest active concentration for *Leishmania* are cathelicidin-4 and seminalplasmin, which showed LD50 concentrations 100-1,000 times lower than the gold standard drug liposomal amphotericin B (0.008 µM against *Le. donovani*) (207,221). Potential AMPs for targeting *T. cruzi* were cathelicidin-6 and scorpine (212,213). Scorpine in particular demonstrates a low active concentration (2.5µM IC90 compared to 384µM IC20 for benznidalzole) and a low toxicity to a range of mammalian cell lines, limiting potential side effects which are common in Chagas disease chemotherapy (213).

The main limitation of effector molecule expression is the potential toxicity of these molecules to the surrounding ecosystems. For example, the expression of insect venoms such as melittin or scorpine could prove toxic to predators ingesting transgenic insects or humans who have contact with mosquitos. To alleviate this, each potential effector molecule would need to be assessed against a wide range of sylvatic animals, insect vectors and humans. A potential marker of this is the mammalian cell toxicity shown in Tables Table ***1*** and Table ***2***.

In summary, vector control via genetic modification has the potential to drastically reduce disease transmission. With a range of approaches previously assessed in insects, the main bottleneck currently is the development of gene editing systems in non-model organisms. In particular sand flies and triatomine bugs, for which limited approaches have been attempted (Sections 3. 1. 4. & 5. 1. 2.), which is a considerable omission considering their potential (222). These approaches could revolutionise Chagas disease and leishmaniasis control if the CRISPR-Cas9 system was readily available to edit the genomes of triatomine bugs and sand flies. This thesis focused on the development of a CRISPR-Cas9 platform for vector control via genome editing to be applied to Chagas disease and leishmaniasis.

1. 6. Research aim and objectives

1. 6. 1. Aim

This research project aims to develop a genome editing platform for the insect vectors of Chagas disease (*Rhodnius prolixus*) and leishmaniasis (*Lutzomyia longipalpis* and *Phlebotomus papatasi*). The genome editing platform comprises of mutagenesis to the target insects via piggyBac semi-random integration and CRISPR-Cas9 target approaches. Successful implementation of these systems would be novel for triatomine bugs (*Rhodnius prolixus*) and sand flies (*Lutzomyia longipalpis* and *Phlebotomus papatasi*) and provide a basis for potential vector control strategies such as the development of a gene drive system.

1. 6. 2. Objectives

1. 6. 2. 1. The assessment of two sand fly cell lines for use as an in vitro model for genetic modification systems

The validation of a novel *in vitro* model for the genetic modification of sand flies via transient expression of DNA constructs and genome integration using the piggyBac system. The model would be assessed to achieve transient expression via a suite of expression promoters and semi-random piggyBac integrations of fluorescent markers. The assessed elements would be applied to a CRISPR-Cas9 system in Chapter 3.

1. 6. 2. 2. Development of a CRISPR-Cas9 system in phlebotomine sand flies (Lutzomyia longipalpis and Phlebotomus papatasi)

Demonstration of CRISPR-Cas9 mutagenesis resulting in the targeted loss of gene function and the integration of exogenous DNA in *in vitro* and *in vivo* sand fly models.

1. 6. 2. 3. A novel chemotransfection methodology for the delivery of genome editing DNA constructs to Rhodnius prolixus embryos

Due to the robust morphological structure of triatomine eggs conventional transfection methodologies (microinjection) are not suitable. A novel methodology for the delivery of DNA constructs and the expression of exogenous DNA via piggyBac integrations will be developed.

1. 6. 2. 4. Application of the CRISPR-Cas9 system to triatomine bugs (Rhodnius prolixus)

To demonstrate evidence of transgenic triatomine bugs with exogenous DNA integrated at desired genomic sites via the CRISPR-Cas9 homology directed repair system. Exogenous DNA would be integrated within non-lethal genes which when lost would elicit a phenotypic change.

2. The assessment of two sand fly cell lines for use as an *in vitro* model for genetic modification systems

2. 1. Introduction

Genomic transfection methodologies in phlebotomine sand flies are still inefficient, time consuming and under-researched (152). *In vivo* approaches require complex transfection methodologies, densely populated insectary colonies and lengthy multigenerational assessments of targets (223). Validation and optimisation of molecular methodologies and gene targets can be performed *in vitro* to increase efficiencies prior to *in vivo* assessments. This chapter provides the primary validation of promoter expression and transfection of exogenous DNA within two *Lutzomyia longipalpis* cell lines, which can be adapted to the CRISPR-Cas9 system *in vivo*.

2. 1. 1. Insect cell lines as a model for molecular research

Insect cell lines have been utilized for the study of insect development, vector-parasite interactions, gene expression, and the production of recombinant proteins (224–226). In more recent years the introduction of CRISPR-Cas9 genetic manipulation has allowed efficient targeting of individual insect genes for loss of function and insertion of exogenous DNA. This system has been optimised in multiple commercial insect cell lines (Sf9, High Five™, and S2) to provide rapid screening of gene targets and expression systems (135,227,228).

In the context of medically important insects, multiple cell lines have been derived from whole insect stages such as embryos (Aag2 from the yellow fever mosquito, *Aedes aegypti*) or larvae (4a-3B cells from the African malaria mosquito, *Anopheles gambiae*) and from specific tissues (Hsu from the Southern house mosquito, *Culex quinquefasciatus* ovarian tissue) (229–231). Creating cell lines for these insects provides researchers with an *in vitro* model for the understanding of pathogen development, or the identification of potential disease control targets. Examples of this include the loss of the *Dcr2* gene in Aag2 (*Ae. aegypti*) cells via CRISPR-Cas9 reducing function of the *Piwi4* pathways and increasing viral infection, highlighting a key insect immunity pathway, which could be exploited in a CRISPRa system (Section 1. 4. 3) (225). The first use of a CRISPR-Cas9 HDR system in mosquito cell lines focused on the *AGO1* gene function in the U4.4 (The Asian tiger mosquito, *Aedes albopictus*) and Aag2 cell lines, which was mutated by NHEJ cleavage then restored using CRISPR-Cas9 HDR approaches to replace the damaged gene section (232). The *AGO1* gene was targeted as it is responsible for the microRNA immune pathway in mosquitos, by removing or modifying the gene researchers could regulate the infection pathways for pathogens. Utilizing bioinformatic pathways and mosquito cell lines Sau-5B (the African malaria mosquito, *Anopheles coluzzii*) and Hsu a high

throughput pooled CRISPR gene target screening platform was created (233). This approach allows researchers to rapidly test potential vector control targets before taking them forward to *in vivo* methodologies saving time and resources. Examples such as these illustrate the value of insect cell lines for the understanding and control of infectious diseases.

Insect cell lines have been developed and assessed for many species. However, few stable cell lines have been developed for phlebotomine sand flies, with a single published study having assessed molecular expression systems *in vitro* (234). Until recently, only two *L. longipalpis* (LL-5 and Lulo) and one *Phlebotomus papatasi* (PP-9) cell lines had been developed (234–236). The Lulo line has been used to show parasite attachment with the potential for further vector-parasite interaction studies to use this line (237,238). The LL-5 and Lulo lines were also assessed for parasite attachment following *Wolbachia* establishment, they showed no significant reduction in *Leishmania* attachment in the presence of *Wolbachia* (239). Both the LL-5 and PP-9 cell lines have been assessed for potential promoter expression. Expression of luciferase was achieved under the human cytomegalovirus (*CMV*), the fruit fly (*Drosophila melanogaster)* heat shock protein 70 (*hsp70*), simian virus 40 (*SV40*) and the buckeye butterfly (*Junonia coenia)* densovirus (*P9*) promoters (234). Whilst these lines were shown to be highly useful for leishmaniasis vector-parasite interactions and disease control, little further research has been carried out with them. The lines are not commercially available making them difficult to obtain and due to this have reduced their viability as an *in vitro* model. Bell-Sakyi *et al*, at the Tick Cell Biobank has produced four novel sand fly cell lines (240,241). These cell lines are yet to be assessed for molecular approaches such as the transfection of plasmid DNA or transgenic approaches such as piggyBac or CRISPR-Cas9. This chapter aims to address this gap and create an *in vitro* system for gene editing validation in sand fly cells.

2. 1. 2. Assessment of insect promoters

The identification of viable expression promoters in sand flies is key to the success of molecular methodologies such as CRISPR-Cas9 gene editing. In particular, population control strategies including gene drives (Section 1. 5. 1.), which require germline specific expression of *Streptococcus pyogenes* Cas9 endonuclease (SpCas9) and transcription of gRNAs from DNA integrated within their genomes. The assessment of promoters in a target organism is carried out by analysing the expression of reporter sequences from transient DNA constructs or the integration of sequences into the genome. These reporter sequences code RNAs and proteins which can be easily measured such as fluorescent proteins which can be visualised and measured by a light intensity analysis (242).

Research into insect promoters via fluorescent protein expression has been carried out in multiple model insect cell lines, including promoters based on *D. melanogaster (Ac5, Dm-hsp70*), the silk moth *(Bombyx mori)* (Bm-hsp90), and multiple mosquito species (*AgCP, hemolectin, ZPG*) being discovered (243–249). Some promoters such as, *actin5c, Dm-hsp70* and *ZPG*, carry conserved function across multiple insect orders, however, expression efficiencies can greatly differ between species (232,234,250). Previous *L. longipalpis* cell line research identified promoters *CMV, hsp70, P9,* and *SV40* as viable expressors of luciferase (234). Further promoters have been utilized to validate CRISPR-Cas9 system expression in insects, this includes *3xP3, Ac5,* and *PUb* (87,183,250). These are yet to be assessed for expression in sand flies.

The synthetic 3xP3 promoter drives expression localised in the ommatidia and ocelli of *D. melanogaster* (251). Due to the localised nature of this promoter it has commonly been used as an *in vivo* marker for fluorescent tag expression (252,253). When transfected into other insects such as the Caribbean fruit fly (*Anastrepha suspensa)* and *An. gambiae,* the promoter can also express ubiquitously or in organs other than the eye (87,252). Localised promoters such as 3xP3 are vital to proof of principle transgenic *in vivo* research and therefore are widely used. However, they are often not viable for *in vitro* experiments unless the cell line is clonal and characterised to express the localised promoter.

As the *L. longipalpis* lines used in this study are heterologous, the use of ubiquitous expression promoters is required to provide high expression. Two high-expression ubiquitous promoters are commonly used in insect cell lines, the *actin-5c* promoter (*Ac5*) and ubiquitin promoters. *Ac5* is taken from the *D. melanogaster actin-5c* gene, a cell cytoskeleton formation gene with functions involved in cell structure and mobility (254,255). As *actin* is an essential gene, the sequence and function is conserved across multiple orders of insects, and the *Ac5* promoter is found to function ubiquitously in a number of insects (227,243,250,256,257). Ubiquitin genes are found in all eukaryote cells and function to tag cellular proteins for degradation by their 26S proteosome (258). Ubiquitin in particular regulates chromatin formation, therefore, they are essential and highly conserved across all eukaryote species. Slight variations in ubiquitin gene sequences and function have led to multiple ubiquitin promoters being found to ubiquitously express in insects. These include polyubiquitin (*PUb* from *Ae. aegypti*), ubiquitin-63E (*Ubi-63E* from *D. melanogaster*), *SfPub* (from the fall army worm, *Spodoptera frugiperda*) (259–261).

Expression of these promoters in the sand fly cell lines designed by Bell-Sakyi *et al.,* via transient (expression plasmids) and integrated (piggyBac) approaches will validate their use for future CRISPR-Cas9 approaches.

2. 1. 3. Cell transfection methodologies

To assess potential promoters and ultimately CRISPR-Cas9 approaches in the *Bell-Sakyi* sand fly cell lines, transfection of DNA constructs must be achieved. Transfection of insect cells via plasmid DNA requires delivery across cell membranes by physical or chemical-based approaches. Examples of commonly used physical approaches include electroporation, sonoporation and laser-based transfection (262,263). Electroporation, is the most commonly used physical approach in insect cell lines, and is able to transfect cells which are resistant to chemical approaches (264,265). Briefly, electroporation increases the permeability of cell membranes by the passing of an electrical current (266,267). The main limitation of physical approaches is the damage to the membrane pores caused after long exposure, high voltage, heat or vibrations (262,268). Chemical transfection methodologies began to be favoured due to their reduced damage to cells.

Chemical transfections (AKA chemotransfection) utilise varied methods based on the formulation of their packaging reagent (262). These include lipid-based compounds and charged chemical elements. Lipofectamine™ is a lipid-based transfection reagent comprising of positively charged 2,3-dioleoyloxy-N- [2(sperminecarboxamido)ethyl]-N,N-dimethyl-1-propaniminium trifluoroacetate and 1,2-Dioleoyl-sn-glycerophosphoethanolamine molecules which bind to negatively charged plasmid DNA and overcome electrostatic repulsion of membrane pores (269). This has been assessed in multiple insect cell lines (c6/36, sf9 and S2) with high efficiencies and significantly less cell apoptosis than electroporation (270–272). Other chemotransfection reagents include but are not limited to Cellfectin® II, FlyFectin™, Effectene®, and FuGENE® (273,274). Unfortunately, the companies producing these reagents are secretive about the chemical formulas and transfection pathways of these compounds. Transfection efficiencies can vary greatly depending on the cell line, therefore, optimisation and the trial of multiple reagents is often needed to reach viable transfection efficiencies (273). Due to their ease of use and low cell mortality rates chemotransfection reagents remain the primary choice for insect cell line transfections.

2. 1. 4. Aims

The validation of an *in vitro* model for phlebotomine sand flies would provide a critical resource in the screening of genetic tools, due to the reduced cost, time and effort required for transfections over i*n vivo* methodologies. To create an *in vitro* model for molecular methodologies, multiple aims must be validated. This chapter focuses on two main approaches for validating the *Bell-Sakyi L. longipalpis* cell lines for future genetic modifications via CRISPR-Cas9 DNA constructs. The successful transfection of transient expressing DNA plasmids; and the transfection of piggyBac plasmids capable of genomic integration and expression. In achieving these aims multiple expression promoters will also be identified for *L. longipalpis* that have not been validated in previous research. Which can be utilized in CRISPR-Cas9 constructs. The successful transfection of piggyBac constructs could confirm successful integration of exogenous DNA via genetic engineering techniques. The results of this work would provide significant developments for genetic modification methodologies in sand flies.

2. 2. Methods

2. 2. 1. Insect cell cultures

2. 2. 1. 1. Cell line morphology

The cell lines LLE/LULS40 and LLE/LULS45 were produced by Bell-Sakyi *et al.,* utilizing *L. longipalpis* embryos 5-8 days post oviposition (240,241). Embryos were surface sterilised in 0.1% benzalkonium chloride and 70% ethanol before being homogenised in cell medium containing 50µg/ml amphotericin B, penicillin/streptomycin, and 5µg/ml tetracycline hydrochloride. Remaining eggshells and large embryonic tissue were removed by centrifugation and cultures were incubated in a reduced antibiotic medium for 45 days before passages began (240,241). With further passages cell lines began to form adherent cells.

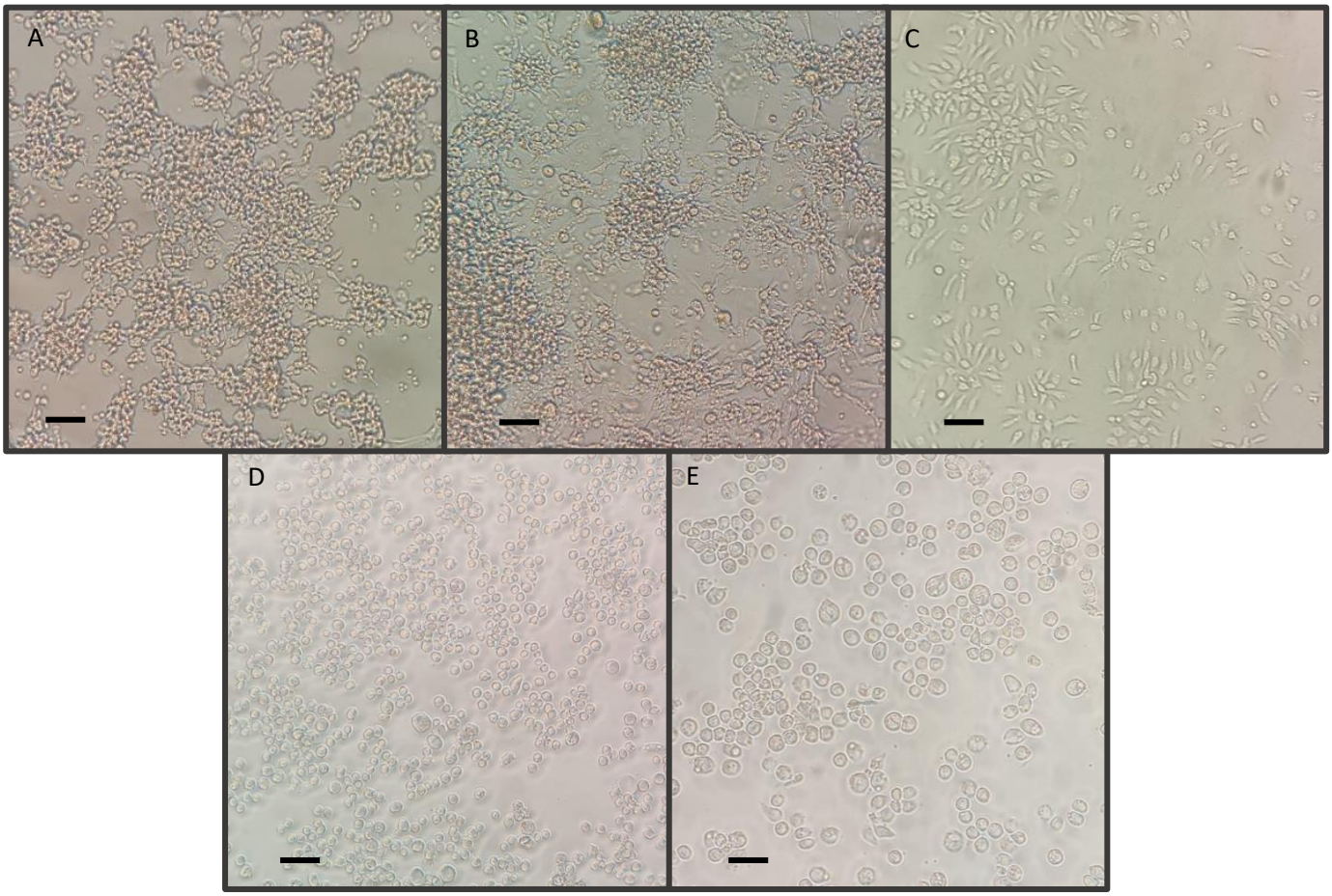

Figure 12. Various insect cell lines.
A) LLE/LULS40 cells derived from *Lutzomyia longipalpis* Campo Grande strain (240). B) LLE/LULS45 derived from *Lutzomyia longipalpis* Jacobina strain (241). C) 4a-3B cells derived from *Anopheles gambiae* strain 4a r/r (230). D) S2 cells derived from *Drosophila melanogaster* strain Oregan-R (275). E) Sf21 cells derived from *Spodoptera frugiperda* (J. E. Smith) (276). Images taken on a Nikon TMS-F microscope (Nikon, Japan) at a magnification of 200x. Scale bars represent 100µm in length. Maintenance conditions found in Section 2.2.1.2.

The LLE/LULS40 & 45 lines differ in morphology to each other as well as other insect lines. As seen in Figure 12A, LLE/LULS40 favours dense clumps over monolayers and does not coat the entire flask surface. These clumps will continue to grow away from the flask surface until they detach from the adherent cells and float freely in the culture media. In contrast, LLE/LULS45 produce fibroblast-like cells (Figure 12B) that coat the flask surface before forming clumps that often do not detach from the adherent cells. Both cultures form bubble-like vesicles that once excreted from cells will float within the culture media, though these are more common in LLE/LULS40. Both cultures are heterologous which explains their unusual cell morphology. In contrast, the clonal 4a-3B, S2 and Sf21 cell lines seen in Figure 12, show single cell types with uniform morphology.

2. 2 .1. 2. Culture maintenance

Each insect cell line used has unique media and incubation conditions. Cell lines were incubated at 28°C in a LEEC Culture Safe Precision 190D incubator (LEEC, UK) without CO_2 in Nunclon Delta T25 flasks (ThermoFisher, USA). Further conditions such as media components; flask type; and time between passages are found in Table 3.

Passages were carried out at the time points mentioned in **Table *3***. To passage cells, T25 flasks were positioned vertically and left to settle for 2-3 minutes. 6.5ml of the media was removed and replaced with 7ml of the corresponding media for the cell type (Table 3). Using a stripette™ (Corning, USA) cells and the cell media were washed from the flask surface to create a cell suspension. 20µl of this cell suspension was added to a new sterile flask which is then topped up with 6.5 ml of the required media (Table 3). Parent cultures and passages were then returned to the incubator until needed.

For cryopreservation, 1 x 10^6 cells were suspended in 900µl of fresh media with 10% DMSO in a 1.2ml cryovial (Simport, Canada). The cryovial was gradually frozen to -70°C in a Nalgene® Mr. Frosty freezing container (Sigma, USA) over 24-48 hours. After this period vials were transferred to liquid nitrogen until needed.

To revive cells from cryostasis, an appropriate T25 flask was filled with 7ml of prewarmed media according to Table 3. The cells were then removed from liquid nitrogen and immediately thawed in a 37°C water bath for 1 minute. The cell suspension was added directly to the T25 flask and incubated for 2-3 days at 28°C or until cells become adherent to the flask surface. After incubation, all the media was removed and replaced with fresh prewarmed media with an additional 10% of FBS and left to incubate for 2 weeks at 28°C. Following the 2-week incubation, cells returned to their normal passage rate.

Table 3. Insect cells culture conditions

Insect species	Insect strain	Cell line name	Media contents	Flask type	Time between passages
Lutzomyia longipalpis	Campo Grande	LLE/LULS40	L-15 medium + 2.05mM L-Glutamine (Cytiva, USA) with 10% heated inactivated FBS (Sigma, USA) and 1% Penicillin/Streptomycin (10,000units/10,000µg) (Gibco, USA)	Closed	1-2 weeks
Lutzomyia longipalpis	Jacobina	LLE/LULS45	L-15 medium + 2.05mM L-Glutamine (Cytiva, USA) with 10% heated inactivated FBS (Sigma, USA) and 1% Penicillin/Streptomycin (10,000units/10,000µg) (Gibco, USA)	Closed	1-2 weeks
Anopheles gambiae	4a r/r	4a-3B	Schneider's insect medium (Sigma, USA) with 10% heated inactivated FBS (Sigma, USA) and 1% Penicillin/Streptomycin (10,000units/10,000µg) (Gibco, USA)	Closed	2-3 days
Drosophila melanogaster	Oregan-R	S2	Schneider's insect medium (Sigma, USA) with 10% heated inactivated FBS (Sigma, USA) and 1% Penicillin/Streptomycin (10,000units/10,000µg) (Gibco, USA)	Vented	2-3 days
Spodoptera frugiperda	J. E. Smith	Sf21	Insect-XPRESS™ medium with 2% heated inactivated FBS (Sigma, USA) and 1% Penicillin/Streptomycin (10,000units/10,000µg) (Gibco, USA)	Vented	4-5 days

2. 2. 2. DNA constructs

To develop an *in vitro* model for sand fly genome editing we assessed several potential expression promoters as well as semi-random genomic integration via piggyBac. The piggyBac genomic integration system has been validated in multiple other insects and was chosen for its simplicity (Section 1. 4. 1.) (183,277). The plasmids selected for this study are Ac5-STABLE1-Neo (addgene #32425), pmaxGFP™ (Lonza, Switzerland), Ubiq-Cas9.874W (addgene #112686), and [i]hyPBase (183,277,278). The Ac5-STABLE-Neo plasmid was a gift from Rosa Barrio & James Sutherland. Ubiq-Cas9.874W was a gift from Omar Akbari. [i]hyPBase was a gift from Ernst Wimmer.

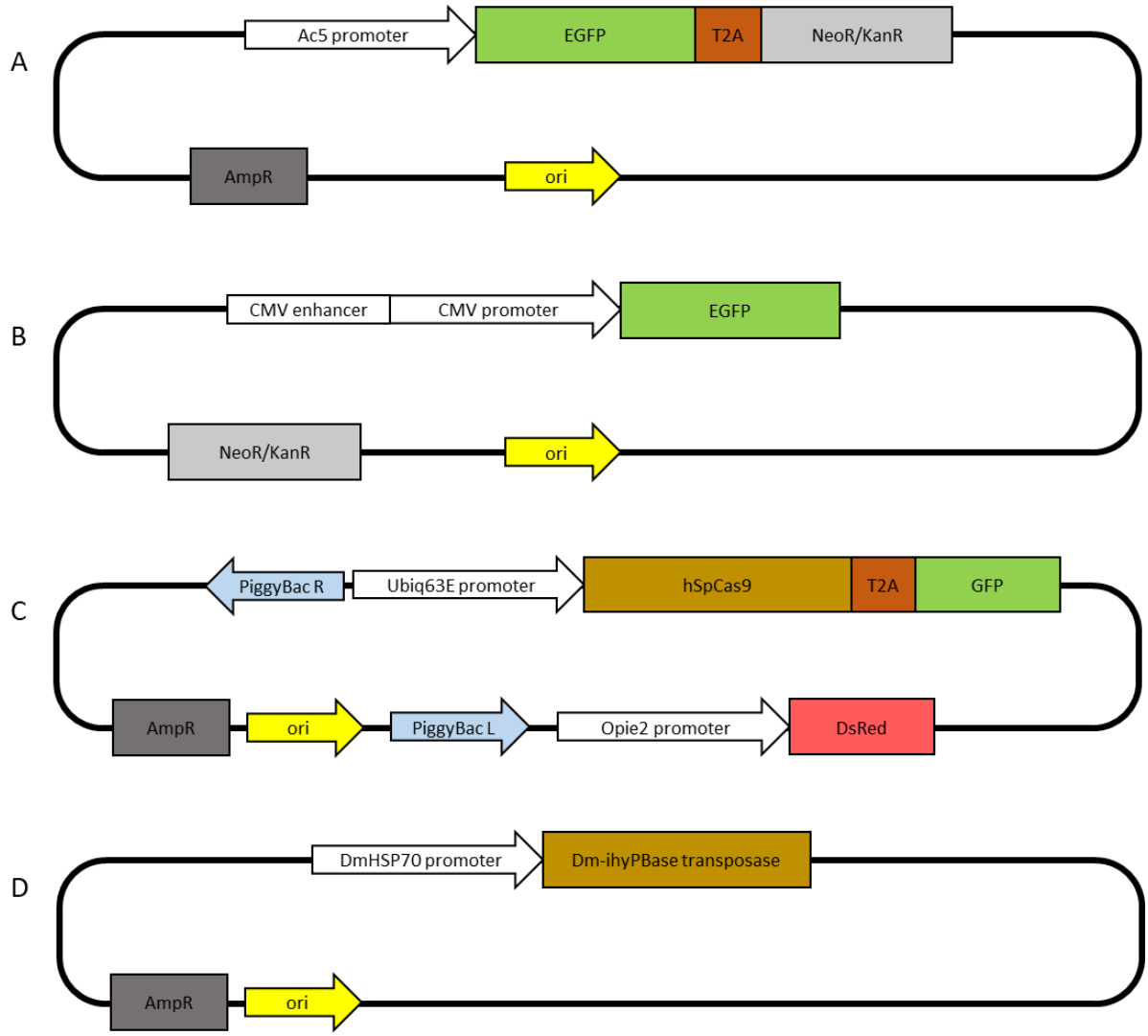

Figure 13. DNA constructs used for validating promoter expression with insect cell lines.
A) Ac5-STABLE1-Neo (addgene #32425) 6,762bp in length (278). B) pmaxGFP™ Vector (Lonza) 3,486bp. C) Ubiq-Cas9.874W (addgene #112686) 14,636bp in length (183). D) [i]hyPBase 5,918bp in length (277).

Ac5-STABLE-Neo and pmaxGFP were chosen to validate cytoplasmic expression of a green fluorescent protein (GFP) via known promoters *Ac5* and *CMV* as seen in their structure (Figure 13). Ubiq-Cas9.874W is a piggyBac genomic integration plasmid containing the *Ubi-63E* promoter which

drives expression of hSpCas9 attached to a GFP via a T2A self-cleaving peptide. Ubiq-Cas9.874W has a further fluorescent marker DsRed1, which should be expressed under control of the *OpIE2* promoter. piggyBac integration requires a source of transposase, this is provided by a helper plasmid [i]hyPBase. [i]hyPBase expresses *Drosophila* based hyperactive transposase by a *hsp70* promoter, both of which have been shown to have increased efficiency in insects over mammalian based transposases (98,277).

2. 2. 3. Transfection conditions

DNA constructs were delivered to insect cell lines via chemotransfection reagents. Three Chemotransfection reagents were used in the current and following chapter. These were Cellfectin® II (Gibco, USA), FlyFectin™ reagent (OZ Biosciences, France), and Lipofectamine™ 3000 reagent (Invitrogen, USA). The chemotransfection methodologies for these reagents were adapted from the manufacturer's protocols and optimised with efficiencies recorded by flow cytometry. Optimisations and flow cytometry for all reagents were performed by Dr Rhodri Edwards within 4a-3B, LLE/LULS45, S2 and Sf21 cell lines. Flow cytometry measures fluorescent light intensity as objects are passed through a photometer, if fluorescence is measured above a control threshold (created by wild-type controls) and the size/shape of the object matches the expected cell type then an event is recorded. The output relating to comparing transfection conditions in this chapter is Odds Ratios (OR) which relate to the odds of a transfected population expressing fluorescence over the odds of a wild-type population. This result reported by an OR is the number of magnitudes higher than the transfected cells are compared to control cells in terms of events e. g. and odds ratio of 3.5 would mean 3.5x more events occurred in a transfected population over a wild-type. Using this data, the optimised protocols found below were created:

2. 2. 3. 2. Cellfectin® II

$5x10^5$ cells were seeded on to a 24 well Nunclon Delta plate (ThermoFisher, USA) and maintained in complete media until they reach 70% confluency. Wells were then washed twice with Opti-MEM reduced serum medium (ThermoFisher, UK) and a final 400µl of Opti-MEM medium was added to each well. 3µl of Cellfectin® II reagent was diluted in 100µl of Opti-MEM and incubated at room temperature for 15-30 minutes. Whilst in tandem, a solution of 1µg of plasmid DNA and 2µl of PLUS™ reagent in 100µl of Opti-MEM medium was made and left to incubate at room temperature for 5 minutes. The two solutions were combined and incubated at room temperature for a further 5-15 minutes, before being added dropwise to the required well. After adding the DNA/Cellfectin® II solution to the cells, the plate was incubated at 28°C without CO_2 for 4-6 hours before replacing the

cell medium with complete cell media (Table 3) and incubating cells at 28°C without CO_2 for 48 hours before downstream processing was carried out.

2. 2. 3. 3. FlyFectin™

$5x10^5$ cells were seeded on to a 24 well Nunclon Delta plate and maintained in complete media until they reach 60-80% confluency. Wells were then washed twice with L-15 medium + 2.05mM L-Glutamine medium without serum or antibiotics and a final 250µl of L-15 medium was added to each well. 2µl of FlyFectin™ reagent was diluted in 100µl of L-15 medium and incubated at room temperature for 5 minutes. Whilst in tandem, a solution of 1µg of plasmid DNA and 100µl of L-15 medium was made and left to incubate at room temperature for 5 minutes. The two solutions were combined and incubated at room temperature for a further 15-30 minutes, before being added dropwise to the required well. After adding the DNA/ FlyFectin™ solution to the cells, the plate was incubated at 28°C without CO_2 for 4-6 hours before replacing the cell medium with complete cell media (Table 3) and incubating cells at 28°C without CO_2 for 48 hours before downstream processing was carried out.

2. 2. 3. 4. Lipofectamine™ 3000

$5x10^5$ cells were seeded on to a 24 well Nunclon Delta plate and maintained in complete media until they reach 70-90% confluency. Wells were then washed twice with Opti-MEM reduced serum medium and a final 450µl of Opti-MEM medium was added to each well. Transfection solutions of 50µl of Opti-MEM medium, 500ng of plasmid DNA, 1µl of P3000, and 0.9µl of Lipofectamine™ 3000 reagent was prepared as outline in the manufacturer's protocol (Invitrogen, USA). After incubating solutions for 10-15 minutes at room temperature, the entire solution volume was added to the corresponding well. The plate was incubated at 28°C without CO_2 overnight (12-16 hours) before replacing the Opti-MEM medium with complete cell media (Table 3) and incubating cells at 28°C without CO_2 for 48 hours before downstream processing was carried out.

2. 2. 4. Fluorescent imaging

Fluorescent imaging of insect cell lines was performed on both fixed and live cells. Live cell imaging was taken on a Nikon Eclipse Ti2 inverted fluorescent microscope within 24 well Nunclon Delta plates. Fixed cell imaging was taken on either a Nikon Eclipse Ti2 inverted fluorescent microscope (Nikon, Japan) or a Zeiss LSM880 with Airyscan (Zeiss, Germany) on glass slides through a 0.17mm thick coverslip. Images were captured and processed using the NIS-Elements software (Nikon, Japan) or Zen microscopy software (Zeiss, Germany). With excitation of the fluorescent proteins at wavelengths of 460nm (blue light), 530nm (green light), and 600nm (red light).

Live cells were prepared for imaging by DNA staining with Hoechst 33342 (ThermoFisher, USA). Following transfection (Section 2. 2. 3.), Hoechst 33342 was added to cell solutions within treatment wells to a concentration of 10µg/ml and incubated at 28°C for 1 hour. Cells were imaged immediately after incubation and returned to the incubator after imaging had concluded for potential downstream processing (Section 3. 2. 5. 1. 2.).

Cells were fixed for fluorescent imaging by removing the media and washing from the plate surface with sterile PBS via pipetting. Cells suspended in PBS were removed from the well and pelleted in a microcentrifuge at 1,000 xg. The cell pellet was washed twice more in PBS before being resuspended in 100µl of 4% paraformaldehyde and incubated at room temperature for 30 minutes. After incubation the cells were washed once more in PBS and the pellet was resuspended in 20µl of PBS. The 20µl cell suspension was added to a glass microscope slide and left to air dry at 30°C. Once the cell solution had almost evaporated, 15µl of VECTASHIELD with DAPI (Vector Laboratories, USA) was added to coat the fixed cells and a 0.17mm thick coverslip was placed over them and sealed with clear nail varnish. After the sealant dried the cells were imaged under the conditions outlined above. When not being imaged they were stored in a container absent of light at -20°C till required.

2. 3. Results

2. 3. 1. Transfection of sand fly cells with transient expressing fluorescent marker plasmids

The genetic modification of sand flies requires the delivery of nucleic acids to cells. We have provided evidence of the successful delivery of DNA constructs to the recently established LLE/LULS40 and LLE/LULS45 cell lines via chemotransfection reagents. In tandem, we have also validated expression of fluorescent proteins with the *AC5* and *CMV* promoters. These successes demonstrate the LLE/LULS40 and LLE/LULS45 cell lines as a viable *in vitro* model for transfection methodologies, which could be applied to approaches such as CRISPR-Cas9.

Sand fly cells were successfully transfected with the transient expressing pmaxGFP. The plasmid pmaxGFP contains an eGFP fluorescence marker expressed by the *CMV* promoter, which has previously been shown to express in multiple insect cell lines including sand fly cells (250,257,278,279). Transfection and promoter function were assessed by expression of eGFP, which is observed by fluorescent microscopy at an excitation wavelength of 530nm (Figure 14Aii- Cii). Transfection was achieved using the Lipofectamine™ 3000 reagent. *CMV* expression of eGFP provided evidence of the lipofectamine™ 3000 chemotransfection reagent delivering DNA to the sand fly cell lines. This result was qualitative only recording the expression of eGFP or lack thereof.

Following successful expression from the *CMV* promoter, we assessed the *AC5* promoter, as this has been used to drive Cas9 expression in several CRISPR-Cas9 insect transfections (250,257,278). The plasmid Ac5-STABLE-Neo transiently expresses eGFP under the *AC5* promoter. Expression of the eGFP from Ac5-STABLE-Neo was observed in both sand fly cell lines (Figure 14Aiii- Ciii). The *AC5* promoter had not previously been shown to promote expression in sand flies. This result validated the *AC5* promoter for expression of proteins such as Cas9 in CRISPR-Cas9 constructs.

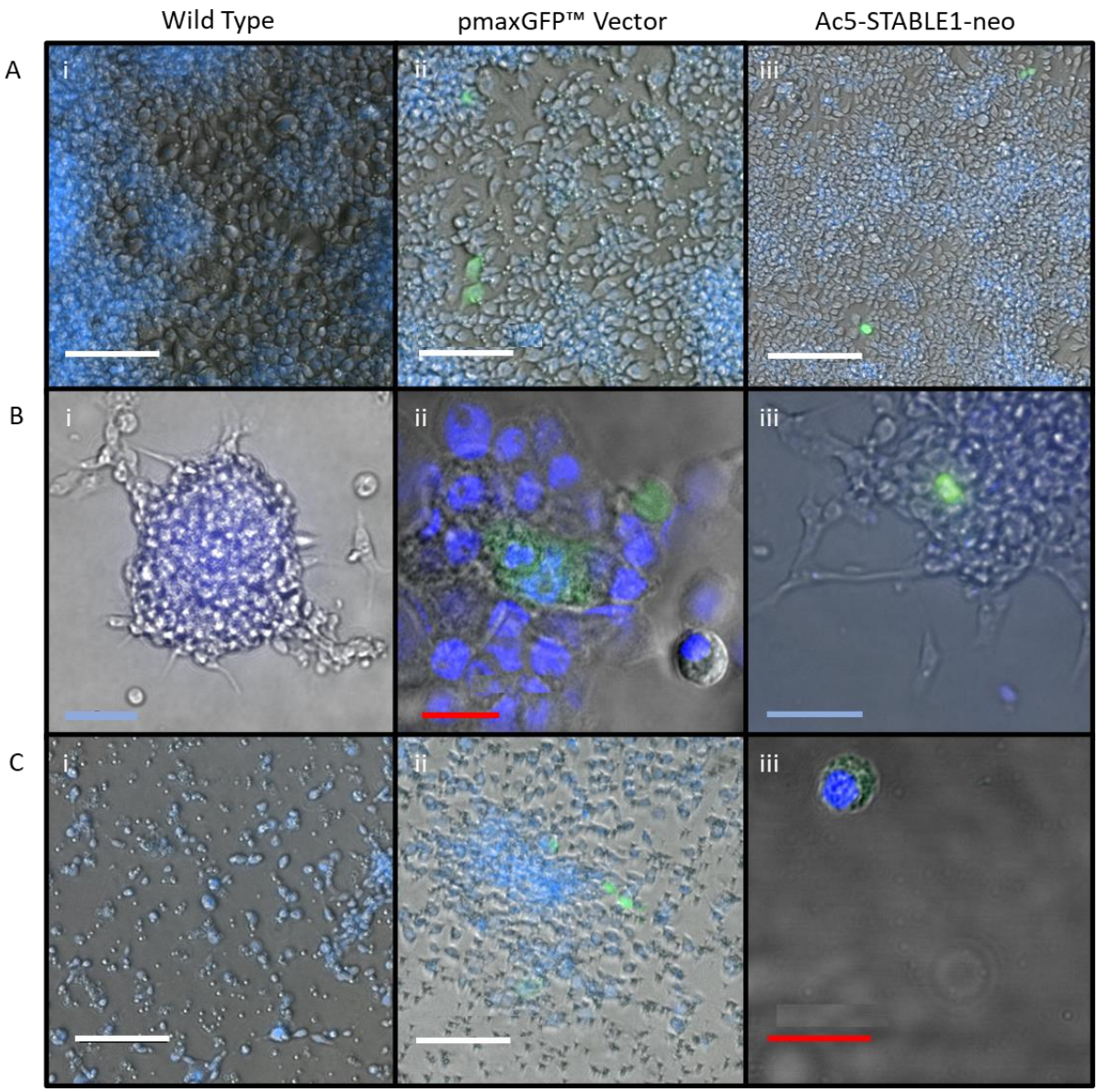

Figure 14. Insect cell lines expressing GFP under either the *actin-5c* or *cytomegalovirus* promoter.
A) 4a-3B cells, B) LLE/LULS40 cells, C) LLE/LULS45 cells. All micrographs are composite images of fluorescence in blue, green, red and phase channels. Blue colour represents Hoescht 33342 DNA stain excited at a wavelength of 460nm. Green colour represents excitation of eGFP at a wavelength of 530nm. Red colour represents artifact fluorescence excited at a wavelength of 600nm. Images Ai-iii; Bi & iii; and Ci & ii were imaged at a magnification of 200x on a Nikon Eclipse Ti2 inverted fluorescent microscope. Images Bii and Ciii were imaged at a magnification of 630x, imaged on a Zeiss LSM880 with Airyscan. The white scale bars represent 100µm; blue scale bars represent 50µm; red scale bars represent 10µm.

Visual expression of eGFP within the sand fly cell lines was often localised to single cells within clusters (Figure 14Biii) and we found reduced cell replication after transfection. In comparison, other literature on insect cell lines regularly reports close to 100% of cells showing protein expression following a Lipofectamine™ 3000 transfection (270–272). Potential toxicity of Lipofectamine™ 3000 was ruled out by WT controls, which also entered a death-like phase after nutrient starvation during the serum free media stages (Section 2. 2. 3.). The death-like phase presented as a constant release of small vesicles from cells until apoptosis (Figure 14Ci-ii). Transfections of the Ac5-STABLE-Neo plasmid were repeated with serum rich media for 4a-3B, LLE/LULS40, LLE/LULS45, S2 and Sf21 cell lines. Unfortunately, transfection wells containing serum rich media became contaminated on all attempts. High contamination levels found in S2 and Sf21 cells, which was potentially due to their aerobic culture conditions and therefore they were not used for any further experiments.

After this multiple other transfection reagents (Cellfectin® II and FlyFectin™) and methodologies were assessed to find an optimised protocol for cell transfections. Optimisation was carried out by altering the following conditions: DNA concentration; transfection reagent concentration; and initial number of cell seeded in the treatment well. Conditions which showed an increase in number of fluorescent cells over non-transfected wild-type controls via flow cytometry (carried out by Dr Rhodri Edwards) were selected for the optimised methods found in Section 2. 2. 3. Following optimisation transfection efficiencies remained low for the sand fly cell lines with flow cytometry ORs of 1.32 to 3.86 for Ac5-STABLE-Neo eGFP expression over WT controls. In comparison the ORs for S2 cell lines ranged from 1.07 to 348.91 using the same range of transfection methodologies (Cellfectin® II and FlyFectin™). The differences in transfection efficiencies for sand fly cell lines between the varying reagents were not statistically significant. Therefore, Lipofectamine™ 3000 was selected for further experiments.

2. 3. 2. Transfection of sandfly cells with integrative piggyBac plasmids

Following successful transfection of transient expressing plasmids into the sand fly cell lines, the next aim was the potential integration of exogenous DNA within the genome and expression of fluorescent marker proteins. This was achieved by the transfection of piggyBac semi-random integrative elements (Section 1. 4. 1.) in the plasmid Ubiq-Cas9.874W (Figure 13). Expression of these fluorescent markers provided putative evidence of DNA cassette integration which would need to be validated using sequencing techniques.

Transfection was attempted with the plasmid pHome-T and a helper plasmid expressing mammalian transposase under the hsp70 promoter (plasmids were a gift from Dr Tony Nolan, LSTM, UK).

pHome-T expresses GFP under the synthetic promoter *3xP3* and RFP under the *Ac5* promoter (252). After transfection using Lipofectamine™ 3000 (Section 2. 2. 3. 4.), expression was not observed in 4a-3B, LLE/LULS 40 or 45 cells. Using the insect coded hyperactive transposase found in the [i]hyPBase plasmid expression was not observed for either fluorescent protein in pHome-T. It was theorised that the pHome-T plasmid was not expressing as expected, as expression was observed in Ac5-STABLE1-neo transfections which utilise the same *AC5* promoter was able to drive expression of eGFP. Due to this we decided to assess the Ubiq-Cas9.874W piggyBac based construct.

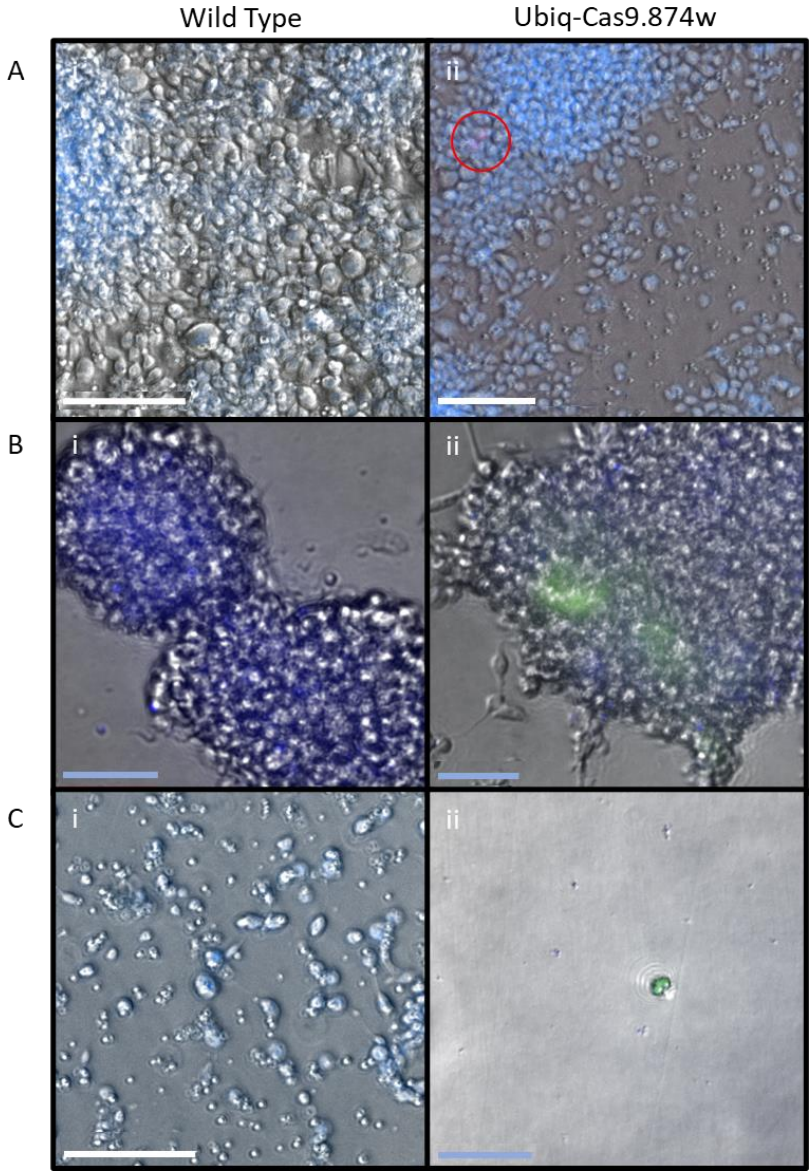

Figure 15. Insect cell lines validating transfection of Ubiq-Cas9.874W.
A) 4a-3B cells, B) LLE/LULS40 cells, C) LLE/LULS45 cells. All micrographs are composite images of fluorescence in blue, green, red and phase channels. Blue colour represents Hoescht 33342 DNA stain excited at a wavelength of 460nm. Green colour represents excitation of eGFP at a wavelength of 530nm. Red colour represents DsRed1 expression excited at a wavelength of 600nm. The red ring in image A ii highlights the DsRed1 excitation in the red-light field. Images Ai-ii, and Ci were imaged at a magnification of 200x. Images Bi-ii, and Cii were imaged at a magnification of 400x. All images were captured using a Nikon Eclipse Ti2 inverted fluorescent microscope. The white scale bars represent 100µm, and blue scale bars represent 50µm.

The plasmid Ubiq-Cas9.874W was assessed to replace pHome-T and for its *Ubi-63E* promoter. The *Ubi-63E* promoter is a ubiquitous ubiquitin-based promoter, which has been found to strongly express in *Drosophila spp*. We believed this would promote expression within our heterogenous cell line at higher efficiencies than the eye specific *3xP3* promoter (183,260,280). *Ubi-63E* drives expression of both hSpCas9 and an eGFP attached to the hSpCas9 via a T2A self-cleaving peptide. Ubiq-Ca9.874W also expresses DsRed1 under the *OpIE2* promoter, which has been shown to provide high expression in a number of insect cell lines (281,282). Transfection of Ubiq-Cas9.874W via Lipofectamine™ 3000 showed both eGRP and DsRed1 expression in 4a-3B cells, and eGFP expression in LLE/LULS40 and LLE/LULS45 cells (Figure 15). eGFP expression was not observed in every well for LLE/LULS cells and green fluorescence in the positive wells was only observed in ~30% of the field of visions. This is significantly less than with the transient expressing plasmids where fluorescence was visible in almost every field of vision. Expression of DsRed1 was only observed faintly in a small number of 4a-3b cells (Figure 15Aii) (less than 10 per treated reaction well) and was not visible in eGFP expressing cells. Expression of these fluorescent markers could be transient expression of the DNA construct and does not provide robust evidence of piggyBac cassette integration into the genome.

2. 4. Discussion

This chapter was successful in validating an *in vitro* model for DNA construct delivery and expression in *L. longipalpis* sand flies. This model is important for further research into genetic modifications via multiple transgenic approaches such as CRISPR-Cas9, allowing high-throughput assessment of these techniques without the costly labour-intensive rearing of insect populations. With further assessment the model could also be adapted for the screening of other methods such as insecticide treatments or vector-parasite interaction.

Transfection and expression of fluorescent protein tags were achieved with these cell lines. However, their heterologous nature and the fragility of cells in a low nutrient environment (Section 2. 3. 1.) infers that refinement of the cell lines would be needed before further *in vitro* work could be performed. Both *L. longipalpis* lines developed large tissue-like cell clusters which likely reduced transfection potentials due to reduced membrane contact with chemotransfection reagents. These cell clusters are potentially formed due to the cultures being produced from late-stage embryos with cells likely having already differentiated into tissues such as epidermis or muscle cells before being homogenised for cell line formation. The heterologous nature of the cell line could create biases in transfection efficiencies that would make modelling of any methods difficult (283). Potential approaches to overcome this bias could be the production of clonal cultures via drug selection or semi-solid agar approaches (278,284). Though, drug selection of insect cells has been proven to be difficult due to their high tolerance of common drug selection markers such as G418 (278). The use of serum free media in chemotransfection has previously been linked to reduced protein expression and loss of viability in cells (285). Once a clonal line is created further transfection methodologies such as electroporation or sonoporation could be viable options to remove the low nutrient medium stages of chemotransfection methodologies (263,265,286).

The potential promoters validated here provide valuable candidates for further transgenic research that could be incorporated into DNA constructs, driving expression of CRISPR-Cas9 components or proteins within exogenous DNA cassettes. These promoters included *Ac5, CMV, hsp70, OpIE2,* and *Ubi-63E*. Expression levels of these promoters were visually assessed showing that *CMV* and *Ac5* gave high intensities of fluorescent light in both insect cell lines. *Ubi-63E*'s low green fluorescence levels could be due to the T2A self-cleaving peptide in the Ubiq-Cas9.874W plasmid. T2A has been shown to reduce expression of downstream proteins by 70-95% (287). However, in other insects *Ubi-63E* has shown high expression making it a viable option for sand fly transgenics (183,288,289). Expression of eGFP and hSpCas9 has been shown within sand fly cells. These are vital for future transgenic approaches as both required endonucleases and fluorescent markers. Further approaches

could be taken to validate hSpCas9 expression following genome integration with the piggyBac system, by utilizing southern blotting and CRISPR-Cas9 cleavage assays.

In providing evidence of expression of piggyBac constructs in *L. longipalpis* cell lines, we have shown the potential of *in vitro* modelling for genome engineering of sand flies above that of any previous research (234). Due to the semi-random nature of piggyBac approaches confirmation of exogenous DNA integration by PCR and sequencing is limited. This is due to plasmids remaining in the media and cytoplasm of cells, which would be amplified by PCR giving false positives in Sanger sequencing. Without knowledge of integration sites amplifying from flanking regions of the genome is difficult. Techniques such as inverse PCR have previously been used to confirm piggyBac genome integrations and should be used in future experiment to rule out transient expression (290). To solve this future research would focus on targeted genome integration approaches such as CRISPR-Cas9.

Transgenic modification of sand flies *in vivo* is difficult, labour intensive and low yielding. Therefore, the demonstration of an *in vitro* model as shown here, is important for the rationalisation of transgenic approaches and gene targets before *in vivo* research can be caried out.

3. Development of a CRISPR-Cas9 system in phlebotomine sand flies (*Lutzomyia longipalpis* and *Phlebotomus papatasi*).

3. 1. Introduction

In recent years, the genetic modification of insects for vector control has become an achievable approach for multiple species that transmit disease. Whilst other genome editing techniques were initially assessed, CRISPR-Cas9 has become more widely adopted due to its highly specific gene targeting and relative ease of use. For the control of diseases spread by mosquitoes within the *Aedes*, *Anopheles,* and *Culex* genera, CRISPR-Cas9 has previously been assessed to supress or replace populations with mosquitoes that are refractory to pathogens (157,201,291–293). To date, there has been a lack of validation for CRISPR-Cas9 approaches for vector control of phlebotomine sand flies, the vectors of *Leishmania* parasites.

3. 1. 1. CRISPR-Cas9 genetic modification methodologies

Previous genetic modification methodologies in insects included *piggyBac* transposable elements, TALENs and ZFNs (Section 1. 4. 1. & 1. 4. 2.). These approaches were technically challenging, time consuming or targeted non-specific genomic regions (128,294,295). Since CRISPR-Cas9 approaches were adapted to insects, research into precise genomic editing has become widespread across multiple insect orders (Section 1. 4. 3.). This has allowed us to observe the precise functions of essential genes and gain insight into disease-vector interactions using infection models (84,157,198).

Briefly, CRISPR-Cas9 gene editing occurs by a CRISPR associated endonuclease (Cas9) forming a ribonucleoprotein complex (CC9-RNP) with a specific guide RNA which is complimentary in sequence to the genome target site (296). The CC9-RNP is able to binds to a single strand of genomic DNA and cleaves both strands just downstream of a specific protospacer adjacent motive (PAM) site (Figure 10A). The cell's repair mechanisms will repair the double stranded break via two methods that we can utilize for gene editing. The first, Non-Homologous End Joining (NHEJ) attempts to repair the break by blunt end ligation, which can be error prone introducing insertion/deletion mutations (indels) at the repair site (Figure 10B). These indels when targeted in the coding region of a gene can cause loss of function. Alternatively, homology directed repair (HDR) functions by cells repairing the break site using sequences complementary to the genomic DNA surrounding the cut site as a guide (Figure 10C). Using these complimentary regions exogenous sequences can be inserted by flanking a DNA cassette with homology arms (HAs).

Gene-drives are able to increase the inheritance of CRISPR-Cas9 induced traits in a transgenic organism's offspring above that of Mendelian inheritance (Section 1. 5. 1.). Gene-drives insert a cassette into the genome containing the coding regions for target gRNAs and a Cas9 endonuclease. The Cas9 must be expressed by a germline specific promoter (*vasa*, *nanos*, *zpg*), expressing the

entire CRISPR-Cas9 editing components into the pre-blastoderm era of embryonic cells copying the mutation to unmutated chromosomes, which leads to all offspring inheriting the desired trait (155). The use of gene-drives to spread mutations through populations has created a viable way to control disease vectors by population suppression or replacement (Sections 1. 5. 2. & 1. 5. 3.). The most promising examples of gene drives have been proved possible in lab strains of African malaria mosquitoes (*Anopheles gambiae)*. Gene-drives have been used to reduce their reductive capacity by knocking out the *doublesex* gene, creating intersex females that are unable to reproduce (157). Expression of anti-malarial peptides within *An. gambiae* guts has been achieved via integration of a gene-drive into the *gambicin* gene (201). Whilst technical hurdles still exist for gene-drives, such as resistance alleles, their ability to control malaria transmission with little human involvement post insect release is preferable to the resource exhaustive vector control methods currently used (155).

3. 1. 2. CRISPR-Cas9 component delivery methods for *in vivo* transfection of insects

For mutations to occur via CRISPR-Cas9 delivery of the CC9-RNP must be achieved, ideally into the pre-blastoderm cells. Delivery of the CC9-RNP has been performed in insects in multiple ways, such as the delivery of purified CC9-RNPs; delivery of gRNAs into Cas9 expressing insect lines; or DNA constructs containing the coding regions of the CC9-RNP components. These approaches have been successfully assessed in multiple insect orders such as Diptera, Coleoptera, Hemiptera and Lepidoptera (136,232,292,297–300). The development of Cas9 expressing mosquito lines has been well established and provides the highest mutation efficiencies for both CRISPR-Cas9 NHEJ and HDR, due to only gRNAs needing to be delivered to embryos (137,291,292). However, in non-model or longer living insects, creating lines such as these is difficult and the direct delivery of CC9-RNPs or DNA constructs has become mandatory. These approaches have very low efficiencies but can still achieve mutations that can be amplified through multiple generations (136,294,301).

Delivery of CRISPR-Cas9 components *in vivo* is usually carried out via microinjection of embryos in the pre-blastoderm stage or the ovaries of adults. Although the microinjection of embryos is the most common approached used, it results in significant mortality with survivorship for mosquitoes around 4-19% (155,186). Survivorship in other insects varies significantly due to the high skill barrier required for successful microinjection and morphology of other insect embryos not being well suited to injection (152,302). Alternative delivery methods have been attempted for insects but due to low uptake are underutilised in transfections. These alternatives include biolistic bombardment, chemotransfection and electroporation. Biolistic bombardment is the projection of DNA constructs coated on metal particles at high speeds into embryos (303,304). Chemotransfection and electroporation are able to deliver packaged DNA or proteins by altering porosity in cell membranes

using either chemical reagents or an electrical current (305–307). For insects, waxy layers on the egg shell or the melanised chorion, must be removed to allow CRISPR-component solutions to make contact with the embryonic cell membranes (306). These delivery methods and CRISPR-Cas9 approaches have revolutionised gene editing in insects and are likely to evolve further as they are adapted to new insect species, such as sand flies.

3. 1. 3. Insect phenotypic markers for *in vivo* gene knockout

Utilising the techniques outlined above, researchers have targeted non-lethal phenotypic markers as a validation method for CRISPR-Cas9. The main phenotypic gene groups targeted in insects are cuticle tanning, eye phenotypes and wing phenotypes (Figure 16), these can elicit distinct phenotypic changes that would visually confirm genetic modifications in target organisms.

Multiple cuticle tanning genes have been identified in insects. These include but are not limited to *black*, *ebony*, *pale*, *straw*, *tan*, and *yellow* (Figure 16). They are often important regulators of melanin synthesis, regulation, or transport, and therefore loss of function has a dramatic effect on body colour in insects (308,309). These genes have been used as markers of CRISPR-Cas9 function in insects such as the yellow fever mosquito (*Aedes aegypti),* Asian swallowtail *(Papilio xuthus)* and tobacco cutworm *(Spodoptera litura)* (310–312).

Genes involved in ommochrome synthesis and transport are known to elicit an eye colour phenotype when function is lost. Examples of these genes in insects are *brown, cinnabar, rosy, scarlet, vermillion* and *white*. These genes have been knocked out by CRISPR-Cas9 in a number of insects including the silk moth *(Bombyx mori),* cotton bollworm (*Helicoverpa armigera),* glassy-winged sharpshooter *(Homalodisca vitripennis),* and red flour beetle *(Tribolium castaneum)* (300,313,314). Further eye phenotypes such as the *eyeless* gene effect eye development (315).

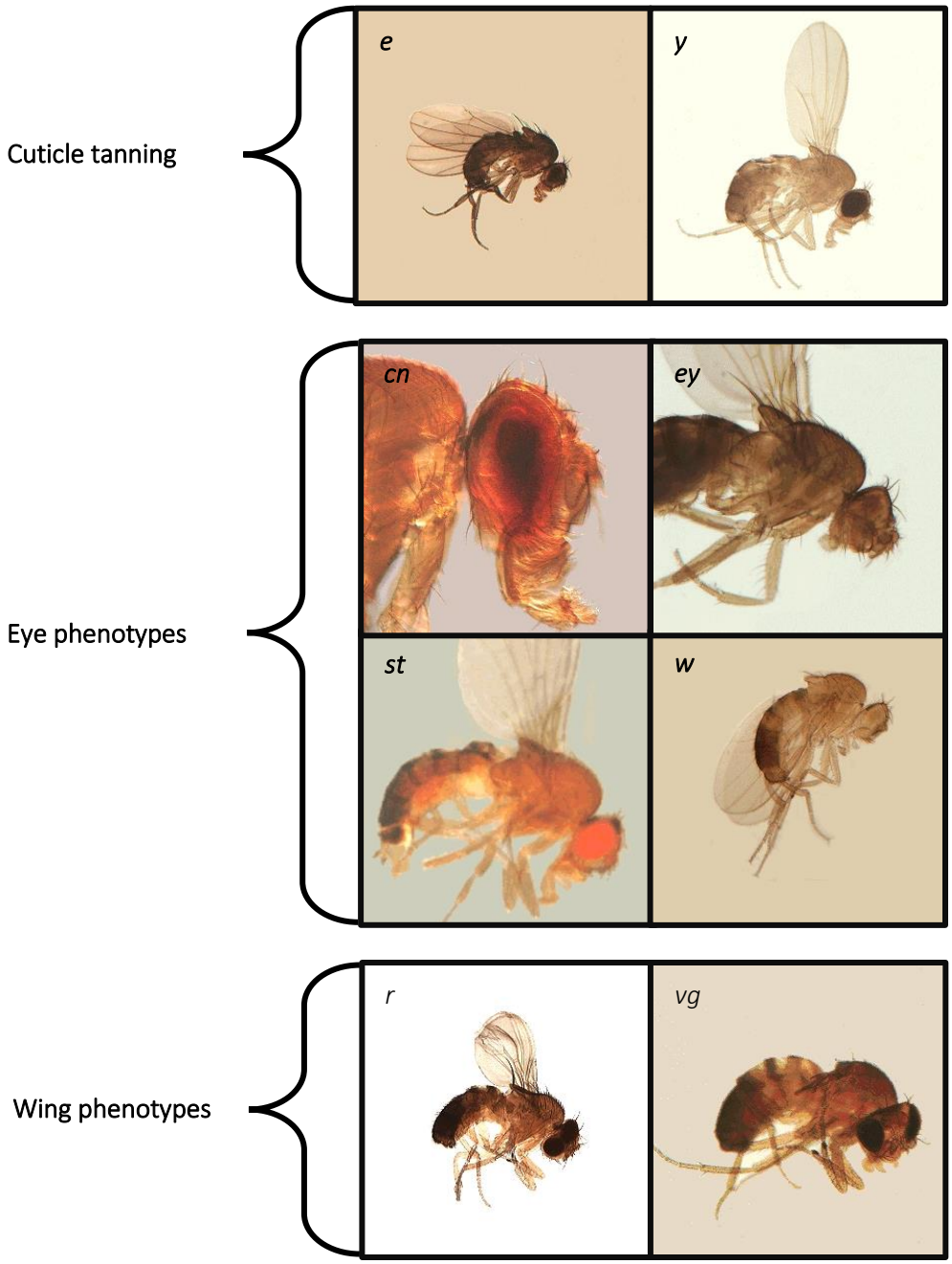

Figure 16. *Drosophila melanogaster* examples of phenotypic marker genes.
Gene abbreviations are as follows: *e* represents the *ebony* gene; *y* represents the *yellow* gene; *cn* represents the *cinnabar* gene; *ey* represents the *eyeless* gene; *st* represents the *scarlet* gene; *w* represents the *white* gene; *r* represents the *rudimentary* gene; and *vg* represents the *vestigial* gene. All images were taken from Otto 2000 (316).

There are a number of wing developmental genes known, which when targeted cause a non-lethal phenotypic change, examples include *crumpled, curly, rudimentary, vestigial,* and *wavy*. Most of which have been characterised in *D. melanogaster*, several have been assessed in other insects such as *Ae. aegypti, B. mori,* and the brown stink bug *(Euschistus heros)* (311,317,318).

These phenotypic markers are helpful to rapidly screen genome mutations via visual confirmation. Visual markers such as these are particularly beneficial when considering a target gene for HDR DNA cassette insertion not expressing a visible marker.

3. 1. 4. CRISPR-cas9 genomic modification of sand flies

Previous research into the genetic modification of sand flies has shown that molecular approaches are possible, but only one group , to my knowledge, has transfected sand flies (*Phlebotomus papatasi*) via CRISPR-Cas9 (222).

Initial molecular sand fly research focused on the adaptation of microinjection methodologies to sand flies. Creating a standardised protocol was important, as compared to mosquitos, sand fly embryos are smaller and more fragile, with the process of producing eggs via leking being more complicated. Two groups attempted this, Jeffries *et al.,* (LSHTM, UK) and Martin-Martin et al., (NIH, USA) (152,319). Jeffries *et al.,* focused on the microinjection of *Wolbachia* bacteria (*w*Mel strain) into *L. longipalpis* embryos. They were able to achieve an adult survivorship rate of 0.33% in the G0 (6/1815 embryos), which they refer to as similar to their *Ae. aegypti* microinjection survivorship rate (0.51% survivorship). From this 50% of G1 offspring were positive for *Wolbachia*. In contrast, Martin-Martin et al, injected *L. longipalpis* embryos with CC9-RNP targeting the *yellow* gene. Their larval hatch rates ranged from 11.9-14.22% with an adult survivorship rate of 9.95%. Unfortunately, no G0 were confirmed to be mutated by the CC9-RNPs injected and breeding of the G1 is not mentioned. These methodologies showed the potential of microinjection to deliver CRISPR-Cas9 components to sand flies.

Following this, Louradour et al., (NIH, USA) were able to genetically modify *P. papatasi* using CRISPR-Cas9 NHEJ to target the *relish* gene (222). They achieved this using the Martin-Martin *et al.,* methodology injecting CC9-RNPs. The *relish* gene is involved in a transcription factor of the insect's immune deficiency pathway, this led to sand flies that were more susceptible to *Leishmania major* infection. G0 adult survivorship for this study was 2.04% (11/540 embryos), however 72.73% of these showed mutagenesis. These mutations were also passed to the G1 offspring, although potentially due to the loss of key immune pathway functions the line was soon lost.

These research studies show the potential of CRISPR-Cas9 methodologies in sand flies. However, to this date no further research into the genetic modification of sand flies has been achieved. Genome editing has not been achieved in any further sand fly species and the HDR approach is yet to be assessed in published literature. This is an important omission in Leishmaniasis research and something that we aimed to change with this chapter.

3. 1. 5. Aims

Vector control via CRISPR-Cas9 is being applied to disease spreading insects but is yet to be fully optimised in phlebotomine sand flies. The research described here aims to validate CRISPR-Cas9 protocols applied to sand flies via *in vitro* and *in vivo* methodologies. To achieve this both CRISPR-Cas9 NHEJ and HDR approaches are pursued to demonstrate targeted mutations to the selected sand fly genomes. Achieving this would create novel methodologies for future development of vector control based CRISPR-Cas9 gene-drive technologies in phlebotomine sand flies.

3. 2. Methods

3. 2. 1. Identification and rationalisation of phenotypic targets for gene editing

3. 2. 1. 1. Sand fly genome assemblies

The genome assemblies of *L. longipalpis* and *P. papatasi* used for this research were hosted on VectorBase, a bioinformatics resource webtool focusing on invertebrate vectors of human disease, providing genome assemblies and bioinformatic tools for these organisms (320).

The *L. longipalpis* Jacobina strain genome was sequenced and assembled by the Baylor College of Medicine sand fly genome project (Houston, TX, USA) (321). This assembly consists of 22.6 million reads, with 38.9x coverage of the genome. The initial assembly was built using the Celera CABOG assembler (version 6.1), and longer superscaffolds were formed using Baylor's ATLAS-link program to fill discernible gaps. In 2020, Apollo annotations were integrated into the genome assembly leading to the most recent version, LlonJ1.6. This assembly is 154.23Mb, and consists of 11,532 scaffolds, and 10,458 protein coding genes. Genome versions LonJ1.5 and 1.6 were used for this chapter.

The *P. papatasi* Israel strain was sequenced and assembled at The Genome Institute, Washington University School of Medicine (St. Louis, MO, USA), with the DNA derived from Dr Mary Ann McDowell, Eck Institute for Global Health, University of Notre Dame (Notre Dame, IN, USA) (322). The assembly was built using the Newbler assembler (test release 2.6RC02) and screened for contamination and gaps using the PolyGraph Assembler. In 2020, Apollo annotations were integrated into the genome assembly forming the most recent version, PpapI1.6. This assembly shows ~22.5x coverage with 363.77Mb, 106,826 scaffolds and 11,405 protein coding genes. Genome versions PpapI1.5 and 1.6 were used for this chapter.

3. 2. 1. 2. Rationalisation of gene targets

Potential target genes were identified through a review of published literature across a large variety of insect species. Literature was searched via PubMed queries using key word searches such as "(((insect) OR (drosophila) AND (cuticle/eye/wing phenotype)) AND (gene)) AND (loss of function)". A shortlist of candidate genes was selected based on those implicated in exhibiting a non-lethal phenotypic change following knockdown of function. Candidate genes with conserved function across multiple insect orders were also used to rank candidates. Orthologues and paralogues within *L. longipalpis* and *P. papatasi* were identified using the bioinformatic web tools FlyBase and VectorBase (323). These orthologues were assessed via protein alignment by Clustal Omega (ver. 1. 2. 3.) against model organisms and gene function by searching on AmiGO 2 (ver. 2. 5. 17) (324,325).

3. 2. 1. 3. Identification of gRNAs

To identify potential gRNAs in candidate genes the webtool ChopChop (ver. 3) was used. ChopChop is a webtool capable of identifying gRNAs in a target sequence or genome based on a gene id or chromosome coordinates (326). gRNAs provided by ChopChop are displayed in a ranked order of estimated mutation efficiency based on potential off-target cleavage; GC-content; self-complimentary binding; and frameshift estimations, all of which have been shown to alter CRISPR-Cas9 efficiencies based on previous research (327–329). The tool can also provide primers flanking the gRNA for sequence confirmation and mutation confirmation in potentially transgenic organisms.

For this research certain settings were altered from ChopChop's default. For gRNA generation, after selecting the relevant genome, the setting "I intend to replace the leading nucleotides with GG" is selected. This is due to transcription of gRNAs from the pDCC6 plasmid requiring the gRNA to start with a GG in the 5' position. When designing gRNAs for the replacement of a gene's coding sequence in the multiplexed HDR approach the 5' or 3' UTR region is selected in the "Target specific region of gene" setting. For primer design, the product size is changed to 500-600bp as we use short read sanger sequencing for mutation confirmation; the primer size is changed to 18-22bp with the optimal at 20bp; and the distance to target site is changed to 200bp.

gRNAs were selected based on the rankings produced by the ChopChop webtool. Primers are selected by choosing the pair with the lowest off target binding sites. Utilising the designed primers gRNA sequences are confirmed by PCR and Sanger sequencing of the amplified region (Section 3. 2. 4. 4 & 3. 2. 4. 5.). A visual methodology for using ChopChop is seen in Appendix 1, as well as, all gRNA confirmation primers in Appendix 2.

3. 2. 2. CRISPR-Cas9 DNA constructs

3. 2. 2. 1. Endogenous U6 pDCC6 constructs

For the knockout of genes via CRISPR-Cas9 NHEJ, the plasmid backbone pDCC6 (addgene #59985) was used (Figure 17). pDCC6 is a bicistronic construct capable of expressing the entire CRISPR-Cas9 NHEJ system (330). The plasmid contains a *D. melanogaster U6-2* promoter for expression of gRNAs attached to a gRNA scaffold (for formation of the CC9-RNP), and hSpCas9 expressed by the *hsp70* promoter (245). This plasmid was chosen for its ability to elicit mutations via CRISPR-Cas9 NHEJ in *D. melanogaster* and *Ae. aegypti/albopictus* (232,330).

Target gene gRNAs are incorporated in this plasmid using the Golden Gate Assembly method. Briefly, the gRNAs are synthesised (Integrated DNA Technologies, USA) as single-stranded oligonucleotides

with an overhang matching the restriction site of the Type IIS restriction endonuclease *BpiI* (CTTCTGNNNNNN) on both the 5' and 3' end. The pDCC6 plasmid is digested twice via *BpiI* (ThermoFisher, USA) removing a section between the U6 promoter and gRNA scaffold. Following digestion, the linearised plasmid is de-phosphorylated using alkaline phosphatase (ThermoFisher, USA). Oligonucleotides are annealed and phosphorylated before being ligated into the linear pDCC6 and transformed into NEB® 5-alpha Competent *E. coli* (New England Biolabs, USA). Bacterial colonies formed are screened via PCR and Sanger sequencing (Section 3. 2. 4. 4 & 3. 2. 4. 5.) utilizing primers flanking the insertion region (Appendix 2). *E. coli* colonies confirmed to carry edited pDCC6 constructs are stored at -70°C in 10% glycerol LB media until required. When plasmids are required, colonies are amplified in liquid LB media and the plasmid is extracted by a Monarch® Plasmid Miniprep Kit (New England Biolabs, USA) following manufacturer's instructions.

Initial transfections in *L. longipalpis* cell lines showed no confirmation of gene mutations with the standard pDCC6 plasmid. One theorised reason for this was the *dU6-2* promoter, which has been shown to have limited function in insects other than *D. melanogaster* (331). The decision was made to remove the *dU6-2* promoter an incorporate endogenous *U6* promoters from both *L. Longipalpis* and *P. papatasi.* Orthologues of the *D. melanogaster U6* gene (FBgn0266758) were identified using VectorBase. The 400bp upstream of the *U6* start codon was noted and key promoter sequences such as the pol III proximal sequence element A (PSEA) and TATA box were identified within this region (Figure 17C). The *U6* promoter in pDCC6 was replaced via Gibson Assembly® following standard protocols (Gibson Assembly® Cloning Kit, New England Biolabs, USA). Pairs of primers were designed using the 5' and 3' promoter ends with 30bp overlaps of the genome/insert site (Appendix 2). Insertion of the *U6* promoters into the pDCC6 plasmid were confirmed via PCR and Sanger sequencing (Section 3. 2. 4. 4 & 3. 2. 4. 5., with primers shown in Appendix 2). The adapted plasmids were hereon referred to as *Llon1*-pDCC6 and *Ppap1*-pDCC6.

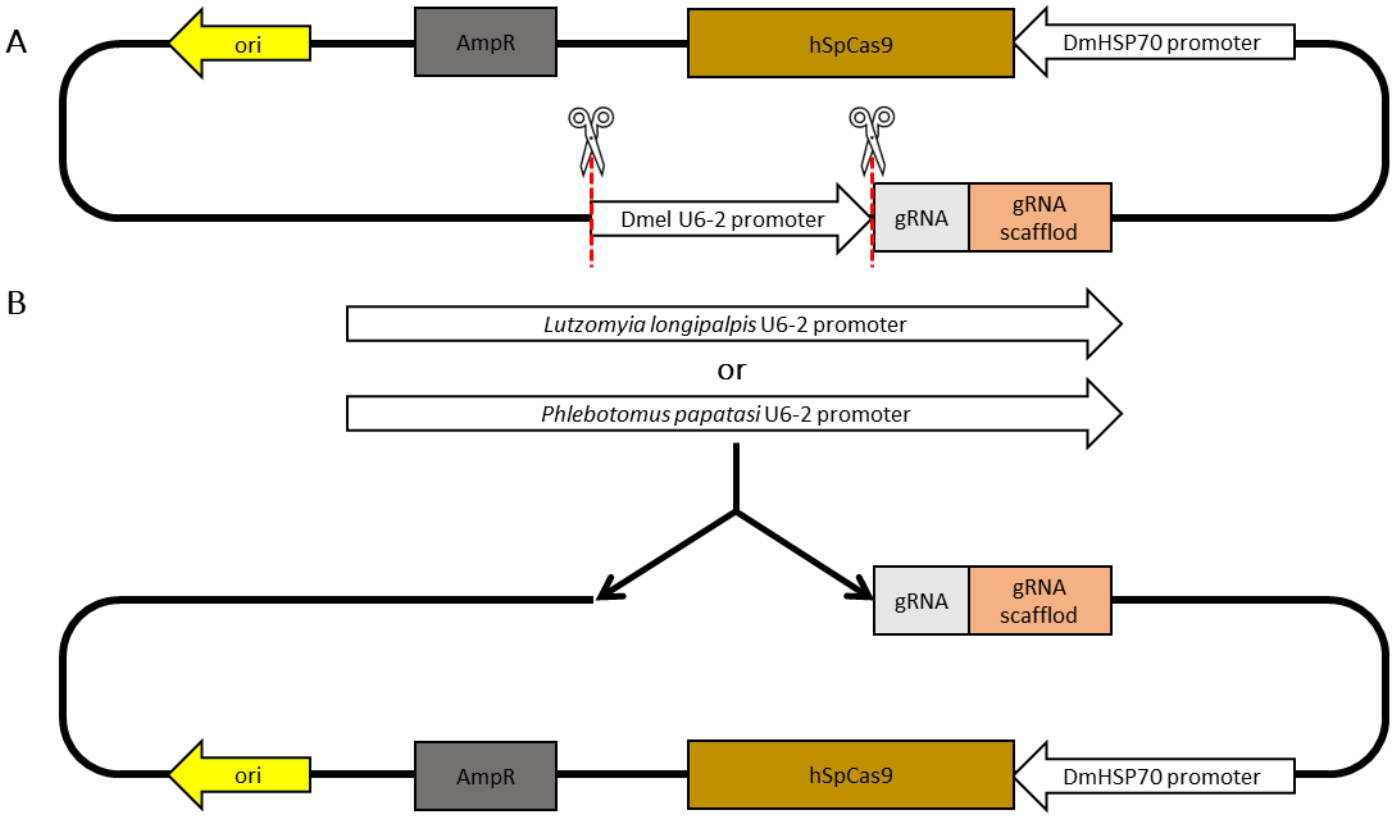

C

>Dmel-U6-2 (FBgn0266758)

GTTCGACTTGCAGCCTGAAATACGGCACGAGTAGGAAAAGCCGAGTCAAATGCCGAATGCAGAGTCTCATTACAGCACAAT
CAACTCAAGAAAAACTCGACACTTTTTTACCATTTGCACTTAAATCCTTTTTTTATTCGTTATGTATACTTTTTTTGGTCCC
TAACCAAAACAAAACCAAACTCTCTTAGTCGTGCCTCTATATTTAAAACTATCAATTTATTATAGTCAATAAATCGAACTG
TGTTTTCAACAAACGAACAATAGGACACTTTGATTCTAAAGGAAATTTTGAAAATCTTAAGCAGAGGGTTCTTAAGACCAT
TTGCCAATTCTTATAATTCTCAACTGCTCTTTCCTGATGTTGATCATTTATATAGGTATGTTTTCCTCAATACTTC

> Llon1 (LLOJ000483)

ATTGAAGTGACAATTGAATATCCAACGGTTACTTTTAGTTCAATTTTATTCCACTCACATACCAATGGCGCTAAATTCTCT
TTCCAGTCTTTCCAATGCTTTCCAAGGAAAAGGGAATTTATTTTTCCTCATTGATCTTGAGAAAAAAAGCTTTTCTTGTGC
TATATAGATTGTAATTTATTTATATCGAATAAAAAGAACAAAACACATCCGCCTACAATTTTCCATGCAATTTTCACATCA
CCTTTTTGAATTCCCCCTTGTTCCCCTTCAAACAACATTTGAAGTGTTTCCATTTGCAACATTTAAATGGAAGATTTTTTA
TCGTTAAATCATATACTTCGGGGGAACTATTTTTCACGCACAAAGTTTATAAGGAAAATAGATTTGCCATGGAATT

>Ppap1 (PPAI002629)

TGTGATATCCCGTGGGCCAAATTTGAAATGATGCAGAAGAACAGGTTCTGAGACGGCTTCTGCCATGATTTATATTTGTTT
TCACTGAGATTCTTCTGCACTATGAGGTTTTGGGAGTTTATTTATCAATTTCCGGGATTTCCTGGGAGTTCTTCCTGGCCA
ATTGCGAAATTCACAAAAAATTCACGACAAAAGAATAACAAATGACAAGCTGTTTGCAACGGATAAATTAATTTCAAGTTG
AGAACATAGAGGCGCAGCTGATGGTTTGAAAATTCAAACATTTAAAGGGTTTCACCTTAACATTTGATGGGTTTTTCTTTA
CAGTTACCGTGTATACTTCAGGGGAGATGGTTTCAGAGCCTCTGAGTTCATATATCAATTCGATTTCTATGCATTT

Figure 17. An illustration of the replacement of the *D. melanogaster U6* promoter in pDCC6 with endogenous sand fly promoters.

A) the structure of pDCC6 with the *D. melanogaster* based *U6-2* promoter being removed by Gibson Assembly®. B) the *D. melanogaster U6-2* promoter being replaced with endogenous *L. longipalpis* or *P. papatasi U6* promoters by Gibson Assembly®. C) sequences of the original *D. melanogaster* (Dmel) *U6-2* promoter with the replacement *L. longipalpis* (*Llon*) and *P. papatasi* (*Ppap*) promoters. Gene IDs for locating these promoters are in brackets. Green text highlights the pol III proximal sequence element A (PSEA) and the red text highlights the TATA box.

3. 2. 2. 2. pDsRed-attP

The pDsRed-attP (addgene #51019) plasmid is a double-stranded DNA (dsDNA) donor plasmid that facilitates the insertion of exogenous DNA into a target genome via CRISPR-Cas9 HDR. The pDsRed-attP plasmid was delivered in tandem with the endogenous pDCC6 plasmids which are required to cause a CRISPR-Cas9 double-stranded break. pDsRed-attP was designed to transcribe a dsDNA cassette containing a DsRed-Express fluorescent marker promoted by *3xP3* (297). Within the cassette loxP recombination sites flank the fluorescent marker and an attP ΦC31 docking site to facilitate subsequent modifications of transgenic insects by recombinase-mediated cassette exchange (332). The entire cassette is flanked by 800bp homology arms that complement the 800bp upstream and downstream of the target gene insertion site as required by HDR.

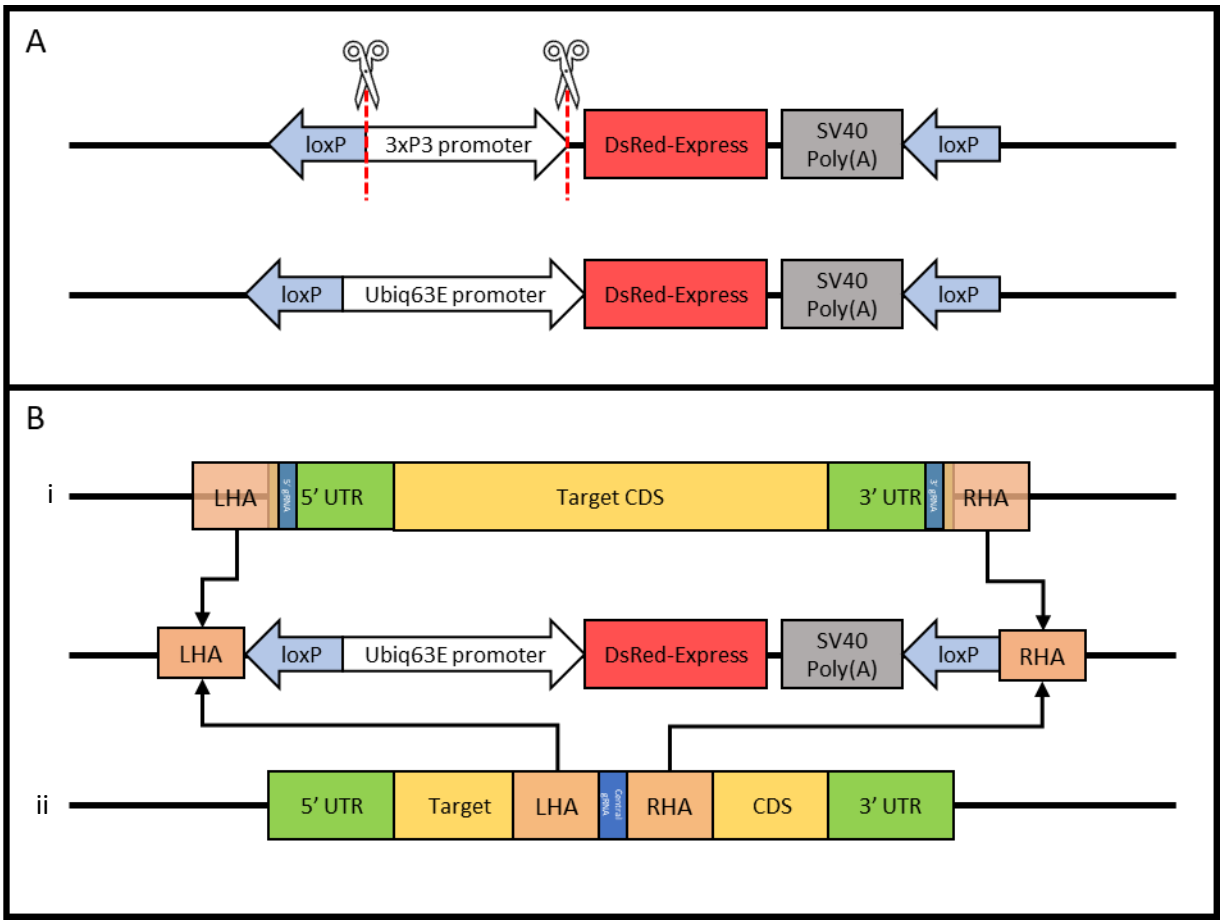

Figure 18. The design and methodologies utilized by the pDsRed-attP plasmid.
A) a diagram of the removal and replacement of the *3xP3* promoter via Gibson Assembly®. B) a diagram of the two strategies taken for exogenous DNA insertion via CRISPR-Cas9 HDR (Section 3. 2. 2. 2.). B, i) the HUTR gRNA approach. B, ii) the HSC gRNA approach.

As this chapter assessed this plasmid in both *in vitro* and *in vivo* methodologies, the eye specific *3xP3* promoter was replaced with the ubiquitous *Ubi-63e* promoter (Figure 18A). This was due to unknown expression activity for the eye-specific *3xP3* promoter in sand fly cell lines. The *Ubi-63e*

promoter was amplified from the Ubiq-Cas9.874W plasmid (Addgene #112686) with 30bp overhangs complimentary to the sequence flanking the *3xp3* promoter in pDsRed-attP. In tandem, the pDsRed-attP vector was amplified with primers complementary to those used for the *Ubi-63e* promoter. The insertion was then performed via Gibson Assembly® following standard protocols (Gibson Assembly® Cloning Kit, New England Biolabs, USA). Successful *Ubi-63e* promoter insertion was confirmed by PCR and Sanger sequencing (Section 3. 2. 4. 4 & 3. 2. 4. 5.). This resultant plasmid is referred to hereon as pDsRed-*Ubi63e*-attP.

Modifying the pDsRed-*Ubi63e*-attP plasmid to target specific genes, the homology arms must be replaced with those complimentary to the gRNA cleavage site (targeted by endogenous pDDC6 plasmids). For this chapter, two gRNA targeting approaches were assessed, a multiplexed gRNA approach which would replace the entire gene CDS with the dsDNA cassette (HUTR); and a single central gRNA approach (HSC) that would knockout gene function by placing the dsDNA cassette in the centre of the gene's CDS (Figure 18B). The HUTR approach uses two gRNAs identified from the 5' or 3' untranslated regions (UTRs) of the target gene. The homology arms are designed to be complimentary to upstream of the 5' UTR gRNA and downstream of the 3' UTR gRNA. Whereas the HSC gRNA approach has homology arms designed directly upstream and downstream of a single gRNA located within the gene's protein coding sequence. Homology arms are replaced within pDsRed-*Ubi63e*-attP via Gibson Assembly®, one at a time, using primers with 30bp overlaps matching the genome site and the pDsRed-*Ubi63e*-attP plasmid. For amplifying the vector two universal primers were designed for amplification of the pDsRed-*Ubi63e*-attP vector. Universal primer 1 (ataatgtatgctatacgaagttatcgtacgcgcgcagatcgccgatgggcgtggcgccgg) is located at the 5' end of the *Ubi-63e* promoter in the forward direction. Universal primer 2 (atagcatacattatacgaagttataccggttaagatacattgatgagtttggacaaacca) is located on the 3' end of the SV40 poly(A) signal in the reverse direction. All primers for homology arm amplification are found in Appendix 2.

3. 2. 3. Delivery of the CRISPR-Cas9 NHEJ constructs to sand flies *in vivo*

Sand fly microinjections were carried out with the assistance of Mrs Barbora Kykalová (Charles University, Prague, Czech Republic) and Dr Rhodri Edwards (LSHTM, London, UK). Rearing of the colonies and breeding of transgenic lines was primarily carried out by Mrs Kykalová. The majority of the microinjections were performed by Dr Edwards and Mrs Kykalová and the delivery of CRISPR-Cas9 HDR plasmids via microinjections was performed by me.

3. 2. 3. 1. Sand fly colony rearing

The *L. longipalpis* and *P. papatasi* sand fly colonies used in this research were reared and maintained in the laboratory of Professor Petr Volf (Charles University, Prague, Czech Republic), following his maintenance procedures (333,334). These species were used due to availability and ease of rearing over other sand fly species available to us within Professor Petr Volf's laboratory.

Sand fly adults were maintained in large (50 x 50 cm) cages, with cotton wool soaked with 30% sugar solution placed on top of the cage. Cages were maintained at 25-28°^{C}, 80% relative humidity, and a 14hr dark: 10hr light cycle. Female sand flies were offered blood 1-2 times a week. 5-6 days after feeding, gravid females were aspirated into 10cm diameter plastic containers with a plaster of paris base. The containers were sealed with a mesh cover to prevent escape of adult females and allow airflow. Females lay eggs 6-10 days post blood-feeding and were removed once oviposition has occurred. Larvae hatch from eggs 6-10 days later. Larvae feed on a mixture of rabbit faeces and rabbit pellets, air-dried and ground to a powder, which is applied to the larval pot surface. Larval pots were placed within plastic boxes containing a base of moist sand until they pupate (around 3 weeks). The pupal stage lasts for ~7-10 days. Emerging adults were then moved back to new colony cages and the cycle repeats.

3. 2. 3. 2. Sand fly embryo microinjection

3. 2. 3. 2. 1. Pulling of microinjection needles

Microinjection needles were pulled with a Narishige PC-10 needle puller (Narishige, Japan) using Narishige G-1 borosilicate glass capillaries (Narishige, Japan). A two-step pulling method was used with the following settings: heater #1= 65.1; heater #2= 75; upper shutter= 2.5; lower shutter= 5; Weight was set to the highest possible setting. Following pulling, the aperture at the tip of the needle is opened by using a micro-grinder beveller set at 20-30°. Prepared needles are stored horizontally in a petri dish attached in place by putty adhesive.

3. 2. 3. 2. 2. Microinjection methodology

The sand fly microinjection methodologies were adapted from Jefferies *et al.,*(152). 15- 20 female sand flies were collected 3 days post blood feeding and transferred to custom laying containers (Figure 19A). These containers were constructed from 50ml centrifuge tubes cut in half with mesh covering the open end, and 2% agar in the screw top to act as the oviposition surface (Figure 19A). The sand flies were incubated to oviposit in the dark for 1 hour. Following oviposition, the cap was removed and replaced with a fresh 2% agar lid to allow the sand flies to continue laying (Figure 19B).

Laid eggs in the screw top were gently removed with a damp paint brush and placed on a glass microscope slide aligned against a damp piece of Hybond™ hydrophilic membrane (Cytiva, USA) (Figure 19C). Aligned embryos were then microinjected with a steady flow of injection mixture by piercing the egg in the lower third of its length. The microinjections were carried out using a manual Narishige IM-9B microinjector and Narishige MMO-4 micromanipulator (Narishige, Japan) mounted on a Leica DMi8 inverted microscope (Leica, Germany). Following injection eggs remained on the slide and were moved to a petri dish lined with damp filter paper where they were incubated for 3 days at 25- 28°C and 80% relative humidity, absent of light. After incubation, the eggs were brushed into a traditional oviposition container and reared using the methods outlined in Section 3. 2. 3. 1.

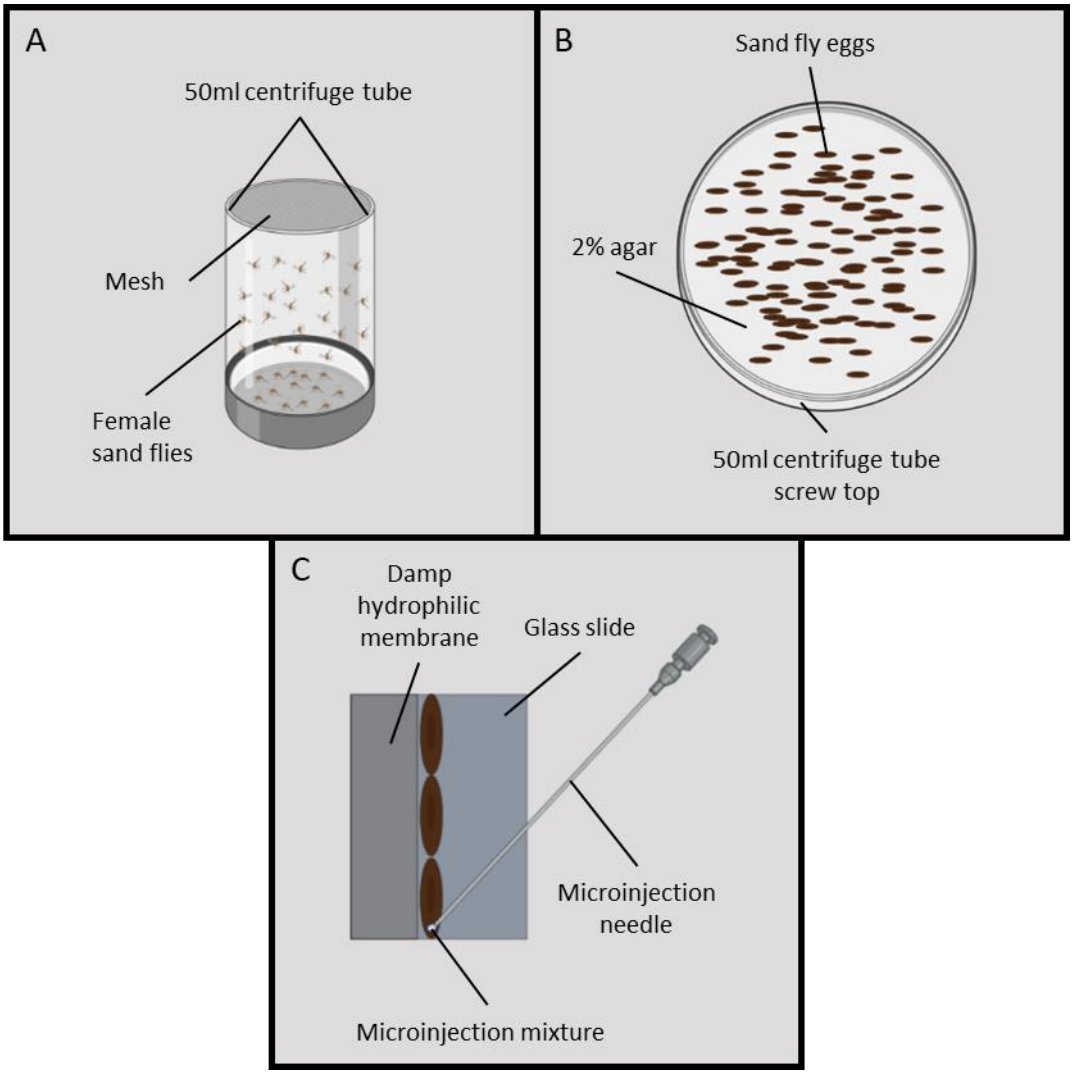

Figure 19. Methodology for the microinjection of sand flies.
A) graphic of the oviposition of eggs onto agar in a custom-made oviposition container. B) the removal of the screw top showing freshly laid eggs ready for microinjection. C) alignment and microinjection of sand fly embryos on a glass slide with a Narishige IM-9B microinjector. Further information on microinjection methodologies is found in section 3. 2. 3. 2. 2.

Microinjection mixtures were made up to 10µL, 20 minutes prior to injections commencing. They are incubated at 37°C prior to being loaded into the backend of a microinjection needle and fixed into

the Narishige IM-9B microinjector. This mixture contains plasmids extracted from *E. coli* colonies directly into DEPC water. The concentrations of these plasmid mixtures can be found in Table 5. When multiple plasmids were combined, they were mixed in equal measures by molecular weight to give a similar copy number.

3. 2. 4. Confirmation of CRISPR-Cas9 genome modification in sand flies

Imaging of putative transgenic sand flies was primarily performed by Mrs Kykalová, with a small proportion imaged by Dr Rhodri Edwards and me. Genomic DNA extraction of all adult sandflies was performed by Mrs Kykalová and Dr Edwards. The PCR, Sanger sequencing and T7EI digestion was ran primarily by Dr Rhodri Edwards, whilst I analysed CRISPR-Cas9 HDR transfected samples. Algorithmic deconvolution and densitometric analysis results presented in this chapter were produced by me.

3. 2. 4. 1. Imaging of transfected insects

To identify potential phenotypic mutations caused by transfection of CRISPR-Cas9 plasmids, sand flies were imaged on a Leica M205 FA microscope (Leica, Germany). Sand flies were imaged at multiple life stages; L1-4 larvae; pupal stage; and adults prior to mating. Sand flies are assessed for phenotypic mutations in both generations 0 and 1 (G0 and G1).

3. 2. 4. 2. Outcrossing and backcrossing of transfected sand flies

For outcrossing and backcrossing of potentially modified sand flies, multiple approaches were taken. For the pDCC6 (NHEJ) injections of *L. longipalpis* all G0 adults were mated with their siblings. For *P. papatasi* G0 adults were outcrossed with wild-type populations, and G1 showing phenotypic changes were sibling crossed. Females were separated before oviposition, so that offspring could be traced back to specific females. Further downstream analysis such as DNA extraction was carried out after males were separated from the females and after oviposition for females. Out crossing was carried out with *P. papatasi* as low numbers of adults emerged and wild-types were used in an effort to increase potential G1 offspring following low numbers from *L. longipalpis*.

For the pDsRed-*Ubi63e*-attP injected flies, female survivors were crossed with wild-type males in separate cages. Males were immediately processed by DNA extraction after fluorescence was imaged (Section 3. 2. 5. 2. 1.). Females were processed by DNA extraction after oviposition.

3. 2. 4. 3. Genomic DNA extraction

Genomic DNA was extracted using either the DNeasy® Blood and Tissue Kit (Qiagen, Germany) or the Monarch® Genomic DNA Purification Kit (New England biolabs, USA). For the DNeasy® kit, the

insect tissue protocol was followed, whilst the animal tissue protocol was followed for the Monarch® kit. Some alterations to the protocols were carried out. All samples were homogenised using a sterile microcentrifuge pestle. Following homogenisation, the lysis incubation was carried out in a shaking incubator at 1,400rpm for both kits. For the Dneasy® kit, elution was carried out in 50µL of preheated (56°C) elution buffer. Elution of the Monarch® kit was collected with 30µL of preheated (56°C) elution buffer. Extracted genomic DNA was quantified using a Ds-11 FX+ spectrophotometer (Denovix, USA).

3. 2. 4. 4. PCR amplification

PCR amplifications were carried out using a Phusion® High-Fidelity PCR Kit (New England Biolabs, USA) following the manufacturers' protocol. Reactions are made up to 20µL with DEPC water. The annealing temperatures for primers was estimated using the NEB® Tm Calculator (335) set to Phusion® High-Fidelity PCR Kit (HF Buffer) at a primer concentration of 200nM. The extension stage is set for 30 seconds per 1,000bp plus 15 seconds (e.g., a 2,000bp product would have a 1 minute 15 second extension). Primers for relevant PCR amplification can be found in Appendix 2. PCR products were purified by the Monarch® PCR & DNA Cleanup Kit (New England Biolabs, USA). If unexpected amplicons were amplified desired PCR products were purified by the Monarch® DNA Gel Extraction Kit (New England Biolabs, USA).

3. 2. 4. 5. Sanger sequencing of PCR products

Sanger sequencing of PCR products was conducted by GeneWiz® (Azenta Life Sciences, Germany). Purified PCR products (Section 3. 2. 4. 4.) are provided to GeneWiz® at a concentration of 50ng/µL of DNA with 5mM of primer mixed a 1:1 ratio. Sequencing results are returned in a .ab1 file format.

3. 2. 4. 6. Algorithmic deconvolution analysis of sequence data

Sanger sequencing often amplifies the most abundant allele within a pooled sample. When transfection efficiencies are low, mutated DNA will not be the most abundant alleles and may not be detected as high peaks on the ab1 file chromatogram. An algorithmic deconvolution analysis (ADA) searches sequencing metadata to find estimated trends in low level peaks for confirmation of indels caused by gene editing techniques. There are a number of webtools using ADA to validate sequencing for CRISPR-Cas9 NHEJ mutations. These tools use gRNA and a wild-type sequences to search for mismatches surrounding the predicted cut sight. Some examples of these tools include CRISP-ID, CRISPResso2, DECODR v3, Synthego ICE Analysis tool v3 (ICE), and TIDE (336–340).

The webtools above were all assessed for ease of use and result quality using a known positive file set. Following this assessment, the ICE tool was chosen as my personal preference due to its ease of use, bulk uploading, and appealing visual readout. Therefore, all further ADAs were carried out using ICE.

ICE outputs include a discordance graph; an indel size-frequency histogram and an aligned trace file (Section 3. 3. 1. 4. 2.). The discordance graph shows the difference between the control wild-type sample and putative edited DNA sample. The graph contains a black dotted line at the estimated cut site and an orange section highlighting the potential interference window where a mutation would cause discordance on the graph. The red highlighted area is the sequence used by ICE to align the control and edited samples.

The indel size histogram quantifies the various predicted frame shifts in the edited DNA. Whilst the trace file shows the sequence mismatches surrounding the cut site. Further statistical data output by the ICE analysis includes an indel percentage, knockout-score, and R^2 value. The indel percentage is an estimated sum of all of the indel alleles in the sample against the wild-type alleles. The knockout score is the percentage of the indels that would likely cause gene function loss due to frameshifts. The R^2 value is the Pearson correlation coefficient measuring how well the ICE algorithm and indels fit the edited DNA sequence data. An R^2 value of 1 infers that the edited DNA is consistent with the ICE algorithm's prediction perfectly. Values lower than 1 represent the percentage that match the prediction, e.g. 0.6 would be 60% matching the ICE algorithm whilst 40% are unexplained. An R^2 value of ≥0.8 would be seen as a good fit. Lower scores potentially indicate poor sequencing quality and may lead to false positive/negative results.

3. 2. 4. 7. Detection of mutagenesis via T7 Endonuclease I heteroduplex assay

The T7 Endonuclease I heteroduplex assay (T7EI assay) can detect mutations in amplified DNA caused by CRISPR-Cas9 NHEJ. For this research the EnGen® Mutation Detection Kit (NEB, USA) was used following the manufacturer's protocol.

Briefly, a target region is amplified via PCR (Section 3. 2. 4. 4.). If indels have occurred following transfection, the PCR product will be an amplicon pool of homoduplexes of unmodified DNA and homoduplexes of mutated DNA. The PCR product is subjected to denaturation and annealing, heteroduplexes can form between the amplicons with a modified locus and un-modified locus, in addition to re-formation of homoduplexes. The T7EI recognises indels in the heteroduplexes and cleaves both strands resulting in fragmentation. Gel electrophoresis is used to separate and visualise DNA products, and the size of the fragments generated can be used to determine if a mutation has

occurred at the expected site based on gRNA location (Section 3. 3. 1. 4. 3.). Efficiency of transfection can be inferred by the intensity of fluorescence from the DNA products on the gel, compared to an unmodified DNA PCR product. The fluorescence intensity is analysed by Image Lab Software (BioRad, USA) using their standard densitometric analysis method. Briefly, the uncut and cleaved DNA strands are highlighted with the lane profile tool, and background is removed by selecting high and low boundaries for each band. A percentage fluorescence for each band is given based on the entire fluorescence of the lane. By comparison of the lane fluorescence data, a percentage modification can be estimated based on this equation designed by New England Biolabs:

%modification= 100 x [1-√(1-M)]

M (modified DNA) = % fluorescence of digested products / (% fluorescence of digested products+ % fluorescence of undigested products)

A positive control comprised was used based on a pJet plasmid backbone with a single nucleotide polymorphism. The mutated pJet plasmid is mixed with DNA from an unmutated pJet backbone. These create heteroduplexes that are cleaved at a mutation percentage of ~20%.

3. 2. 5. Delivery of exogenous DNA to sand flies via CRISPR-Cas9 HDR

3. 2. 5. 1. Assessment of pDsRed-Ubi63e-attP in vitro

3. 2. 5. 1. 1. Transfection of LLE/LULS45 cells

Transfection of LLE/LULS45 cell lines with pDsRed-*Ubi63e*-attP and *Llon1*-pDCC6 were performed with FlyFectin™ following the methods outlined in section 2. 2. 3. 3. Cells were transfected with the plasmids designed in section 3. 2. 2., following either the HSC or HUTR gRNA approach. Transfection controls were: untreated wild-type; pAc5-STABLE-NEO-RFP as an RFP positive control; and the appropriate *Llon1*-pDCC6 to confirm CRISPR-Cas9 cleavage.

3. 2. 5. 1. 2. Confirmation of genomic integration

48-72 hours following transfection cells were imaged by the live cell imaging protocol described in section 2. 2. 4.

Following fluorescent imaging genomic DNA was extracted from transfected cells using the Monarch® genomic DNA purification kit (New England biolabs, USA) following the cultured cells protocol. 35µL of DNA was extracted per sample and then quantified using a Ds-11 FX+ spectrophotometer (Denovix, USA).

Confirmation of exogenous DNA insertion was confirmed by PCR amplification (Section 3. 2. 4. 4.) of the target region utilizing the primers found in Appendix 2. Primers confirm insertion from within the HDR DNA cassette to a primer 100-200bp downstream of the right homology arm. Confirmation is seen as the presence of a band following gel electrophoresis of around 1,300bp. The wild-type DNA will not amplify with these primers. Any bands present were excised and confirmed via Sanger sequencing (Section 3. 2. 4. 5.).

For the *Llon1*-pDCC6 control, sequences were amplified by PCR (Section 3. 2. 4. 4.) using the gRNA confirmation primers (Appendix 2). These were then analysed for mutations via the T7EI assay (Section 3. 2. 4. 7.) and Sanger sequenced for ADA (Section 3. 2. 4. 5. & 3. 2. 4. 6.).

3. 2. 5. 2. Assessment of pDsRed-Ubi63e-attP in vivo

Rearing, imaging, and genomic DNA extraction for this section was carried out by Barbora Kykalová. Confirmation of genomic insertion (Section 3. 2. 5. 1. 2.) was produced by me.

3. 2. 5. 2. 1. Fluorescent microscopy of emerged sand flies

To validate DsRed-Express expression, sand flies were imaged on a Leica M205 FA microscope (Leica, Germany). Sand flies were imaged at multiple life stages; L1-4 larvae; pupal stage; and adults prior to mating. Sand flies are assessed for mutations in both the generations 0 and 1 (G0 and G1). Fluorescence was excited at wavelengths of 485nm for green fluorescence, and 558nm for red fluorescence. Green fluorescence was used as an artifact control.

3. 2. 5. 2. 2. Confirmation of genomic integration

Genomic DNA extraction from sand flies was carried out following the methods outlined in section 3. 2. 4. 3. Confirmation of exogenous DNA insertion was carried out following the protocols outlined in section 3. 2. 5. 1. 2.

3. 3. Results

3. 3. 1. Transfection of sand flies via CRISPR-Cas9 NHEJ techniques

3. 3. 1. 1. Identification and incorporation of phenotypic markers into NHEJ constructs

Several hundred putative non-lethal phenotypic genes were identified using previously published literature in model insects. These were assessed for their potential in sand flies based on whether the phenotype would be clearly visible in either target sand fly species. Following this, orthologues within the target genomes were assessed for amino acid sequence alignment, conserved functions, and paralogues (Section 3. 2. 1. 2.). Those that were found to show minimal phenotypic changes in a target organism; vastly different amino acid sequences; or multiple paralogues without a conserved gRNA, were excluded from selection. Table 4 shows the candidate phenotypic genes chosen for CRISPR-Cas9 construct production against sand flies and lists the target gRNAs designed in ChopChop v3. Phenotypic genes were grouped under three main functions: cuticle tanning, eye phenotypes and wing phenotypes. These are visible in Figure 16 following function knockout in *D. melanogaster*.

Selected cuticle tanning genes include *ebony* and *yellow.* The *ebony* gene encodes N-β-alanyl dopamine (NBAD), a key protein needed in the melanin synthesis pathway (309). NBAD breaks down cuticular hydrocarbons (CH) forming shorter CHs that are visible as a paler colour in an insect's cuticle. Loss of function in this gene is exhibited as longer CHs forming leading to a dark pigmentation in the cuticle and has been shown to alter neurological functions due to the lack of dopamine metabolization (308). *L. longipalpis* produces a dark pigmented cuticle in wild-type insects, therefore, *ebony* phenotypes would likely be indistinguishable with wild type populations. As *P. papatasi* is pale coloured in wild-type populations, *ebony* mutations were selected as a phenotypic knockout for this species. The *yellow* gene is also involved in the melanin formation pathway, being directly involved in the synthesis of black dopamine melanin (308). Loss of this gene reduces the formation of long CHs, and due to this cuticle pigmentation in knockout insects is lighter in colour (309). *L. longipalpis* presents a dark cuticle in wild-type populations, a loss of function in the *yellow* gene would cause an obvious phenotype.

Multiple eye phenotype genes were selected, these include *cinnabar, eyeless, scarlet,* and *white.* The *cinnabar* gene encodes kynurenine 3-monooxygenase, which is involved in the tryptophan degradation pathway, metabolising kynurenine to 3-hydrokynurenine. This process is essential to the formation of ommochromes, the pigment visible to us as eye colour (341). In *Drosophila* loss of function leads to an increase kynurenic acid build up in the brain causing neurotoxicity similar to that found in Huntingdon's disease (341). The potential neurological effects are not ideal and therefore

cinnabar was ranked low against the other selected genes. The *eyeless* gene encodes a Pax6 homologue required for brain and eye development (315). Knockout of this gene will result in eyes not being formed and potentially lethal lack of brain development. An intact paralogue of the gene is required for viable insects to form, therefore, this target is ranked low compared to other target genes. The *white* gene encodes an ATP-binding cassette (ABC) guanine transporter, which is known for transporting molecules such as ommochromes throughout insects (342,343). Loss of function mutations of the *w* gene show a complete lack of pigmentation to the eye, and are commonly used as a phenotypic marker in insects (314,344). The *scarlet* gene encodes a transporter of the ABC family which is linked to the *white* gene. The function of *scarlet* is to transport brown pigment precursors in the eyes of insects in tandem with the *white* gene transporters, leading to a lightening of the eye pigmentation if function is lost (342,345). Loss of function of this gene has shown good viability in multiple insect species, it is a good candidate for CRISPR-Cas9 knockout in sand flies (299).

Two wing phenotype expressing genes were selected, these are *rudimentary* and *vestigial*. The *rudimentary* gene encodes a carbamoyl-phosphate synthase, required in pyrimidine biosynthesis (346). Loss of function to this pathway can cause lethal pyrimidine auxotrophy, however, it more commonly causes a non-lethal reduction in wing size (347). This stunted wing phenotype can be used in sand flies as a marker of CRISPR-Cas9 mutagenesis. The *vestigial* gene encodes a transcriptional activator linked to the wing/haltere identify selector gene, *scalloped* (348). Loss of function in *vestigial* causes a number of wing phenotypes including malformed shortened wings as well as a lack of wings forming. This is an obvious phenotypic marker for gene knockout and was selected for further investigation in sand flies.

The phenotypic genes above were selected for further investigation and gRNAs with high estimated knockout efficiencies were designed and placed into the pDCC6 plasmid backbone (Section 3. 2. 1. 3.). Initial transfections of LLE/LULS45 cells with pDCC6 targeting the *cinnabar, ebony, eyeless,* and *white* genes were performed using Lipofectamine™ 3000 as a chemotransfection reagent (Section 2. 2. 3. 4.). These transfections were assessed via PCR, Sanger sequencing, and ADA, showing no detectable indels at the target site. Following consultation with Dr Andrew Hammond (Imperial College London, UK), it was decided to replace the *D. melanogaster* U6-2 promoter driving gRNA transcription with an endogenous U6 promoter from the target insect. Orthologues of the *D. melanogaster U6* gene were located in *L. longipalpis* and *P. papatasi* and the 400bp promoter region was amplified and inserted into the pDCC6 plasmid via Gibson Assembly®. Another limitation of the early transfections was the low transfection efficiencies limiting the amplification of mutated alleles (Section 2. 3. 1.). It was decided that endogenous pDCC6 plasmids were assessed *in vivo* targeting

ebony, rudimentary, and *vestigial.* Once the gRNAs were designed, they were incorporated into the novel endogenous pDCC6 plasmids and readied for *in vivo* transfection.

Table 4. Sand fly genes selected for editing via CRISPR-Cas9 NHEJ.
The gRNA sequences used for knockout of function are present. Red gRNAs were used in NHEJ based CRISPR-Cas9 constructs. Green gRNAs were used in HDR based CRISPR-Cas9 constructs.

Gene name	Function	Reference gene	*L. longipalpis* orthologue	*L. longipalpis* gRNA sequence	*P. papatasi* orthologue	*P. papatasi* gRNA sequence	Relevant references
caspar (casp)	Implicated in the Imd immune pathway in Drosophila.	FBgn0034068	N/A	N/A	PPAI005190	GGATTCTGAGAGTTCCATGG TATCCTCAAGAATCTCAATG GATGAAGCAACGCTGTAGGG TGAGGCTATCTATTTGCTAG	(349)
cinnabar (cn)	Loss of function reduces the formation of ommochromes causing eyes to lose brown pigmentation.	FBgn0000337	LLOJ009814	GATTTGATCATCGGCTGCGA	N/A	N/A	(341)
ebony (e)	Supresses melanin formation in specific cuticle cells.	FBgn0000527	LLOJ008326	GCCTCAATTGTCGATTCTCA	PPAI005863	TCGCATTCAGCACATCCTTG AAAGTGCATGGTAATCAGGA CACATTTCCATATGGCCAGG GTGGCTATCAAGTTGTCCGA	(308,309)
eyeless (ey)	A Pax6 homolog, required in the development of insect eyes and brains.	FBgn0005558	LLOJ006069	GTTGCATTGATGTTGACACG	N/A	N/A	(315)
rudimentary (r)	Associated with the development of wing tip cells and fertility in females.	FBgn0003189	LLOJ009278	AGCATTGGAAGACACAGGGT TTGTAGCCCATCTTCACGA GGAACTATGGCATTCCGTG	N/A	N/A	(347)

scarlet (st)	Required for the transport of brown pigment precursors in the eye.	FBgn0003515	LLOJ001495	5'- GCGCATCATCAATAACGTGA 3'- GCAGGTACACACTACGAATG SC- CAAGACATGCCAGTGCAAGG	N/A	N/A	(342,345)
vestigial (vg)	Regulates cell proliferation in the wing/haltere identity selector gene.	FBgn0003975	LLOJ009695	TCATCATTACGGTTCCTACG GGAAAATTTCTCGCCGACAT TCGCGGACACGTATTGTGCT	PPAI008343	CGTGGAGTAACTTCCGTCTG ACCACAATATGGCCCAGTAT TGTGGTGATGATGGTAAGCG GTATGCTGCGGCACTCTCGA	(348)
white (w)	Required for the transport of brown pigment precursors in the eye.	FBgn0003996	LLOJ001311	GCCACCACAGTTCAGTCGTG	N/A	N/A	(342,343,345)
yellow (y)	Required for the formation of melanin in cuticle cells.	FBgn0004034	LLOJ007802	TCGATACACCCTCCACACTG AACTCACCGTCCTTCCATCG CCCGTGGGCATTGAGCATTG	PPAI006879	CGTCTCGGTCGACAACATCG AGTCGATCTTGACGTCAGCG GAGATCAATGTACGTCAGAG GAAGTGGAGCTTGGAAGATG	(309)

3. 3. 1. 2. Microinjection procedure and survivorship

Following gRNA design and pDCC6 production, the microinjection of sand fly embryos was performed following the methods outlined in section 3. 2. 3. 2. 2. Injections were carried out in batches based on embryo availability and processing speed each day. Plasmids injected, concentrations and survivorship data can be seen in Table 5. In total, 4,369 sand fly embryos were injected with CRISPR-Ca9 DNA constructs.

Table 5. *In vivo* transfection conditions and survivorship.
Text in red identifies the CRISPR-Cas9 NHEJ mutation approach. Text in green identifies the CRISPR-Cas9 HDR mutation approach. The * symbol refers to larvae being difficult to identify in oviposition containers and therefore some may not have been counted.

Species	Plasmid	Concentration of plasmids injected (ng/µl)	Eggs injected	Larvae hatched*	Adult male emerged	Adult female emerged	Adult survival from eggs injected (%)
L. longipalpis	*rudimentary* 1-3 & *vestigial* 1-3 *Llon1*-pDCC6	317.58	579	6 (1.04%)	3	3	1.04
L. Longipalpis	HUTR pDsRed-*Ub63e*-attP & 5/3' HUTR *Llon1*-pDCC6	300	701	3 (0.43%)	1	2	0.43
L. longipalpis	HUTR pDsRed-*Ubi63e*-attP	300	539	4 (0.74%)	2	2	0.74
P. papatasi	*Caspar 1-4 Ppap1*-pDCC6	214.48	1,516	12 (0.79%)	2	4	0.40
P. papatasi	*ebony* 1-4 *Ppap1*-pDCC6	278.48	1,034	8 (0.77%)	6	6	1.16

Constructs with gRNAs targeting wing phenotypes (*rudimentary* and *vestigial*) in *L. longipalpis* were pooled together to give the best chances at eliciting a phenotypic change by multiplexing. For *P. papatasi,* due to a lack of resources, *ebony* was targeted as the only phenotypic marker. Further constructs targeting an immune pathway gene (*caspar*) were also used to provide a platform for future *Leishmania* infection studies. Further plasmids for *yellow* in *L. longipalpis* and *vestigial* in *P. papatasi* were constructed but due to time constraints and rearing capacity were not injected into sand flies.

Adult survivorship data following the injection of pDCC6 plasmids (G0) shows an average of 1.04% for *L. longipalpis*. For *P. papatasi*, microinjection survivorship showed an average of 0.78%. This survivorship rate is similar to sand fly targeting publications, however, it is much lower than the 9.95% survivorship quoted in one study (152,222,319).

3. 3. 1. 3. Phenotypic and genotypic analysis of sand flies

Following emergence sand flies are screened for phenotypic changes (Section 3. 2. 4.). Following phenotypic screening, the sand flies are crossed following methods section 3. 2. 4. 2., their offspring (G1) are also screened for phenotypic changes as these are more likely to be present in the following generation (Figure 20 and Figure ***22***).

Following phenotypic analysis injected sand flies and their offspring were assessed for mutations via the molecular techniques found in section 3. 2. 4. Genotypic analysis comprised of PCR and sanger sequencing (Sections 3. 2. 4. 4. & 3. 2. 4. 5.); an ICE algorithmic deconvolution analysis (Section 3. 2. 4. 6.); and a T7 endonuclease I heteroduplex assay (Section 3. 2. 4. 7.). The initial PCR and Sanger sequencing of the target gRNA regions to observe SNPs compared to wild-type DNA. Genotypic analysis is particularly important to this research due to no previous studies having targeted these phenotypic genes in sand flies. Therefore, phenotypic changes are not known and may not occur following genomic mutations via CRISPR-Cas9 NHEJ.

The ICE algorithmic deconvolution analysis provides an estimated likelihood of mutations from the Sanger sequencing chromatograms of transfected insects against control wild-type populations. Briefly, the output from the ICE analysis provides an Indel %, Knockout-score, and R^2 fit value. The Indel % represents an estimated percentage of alleles in the transfected samples that have indels compared to a wild-type control sample. The Knockout-score shows the percentage of indels that could result in loss of gene function, providing and estimated gene knockout efficiency. The R^2 value is a measurement of good fit between the transfected sequence and the wild-type. A high R^2 means that the result is likely accurate and not down to bad quality sequencing. In tandem with the ADA, gRNA regions were assessed for mutations using a The T7EI assay. Briefly, T7EI heteroduplexes are able to confirm small indels created by CRISPR-Cas9 NHEJ mutations by cleavage of mismatched DNA using a T7 endonuclease I enzyme. This mismatched DNA occurs when an amplicon pools of homoduplexes of unmodified DNA and homoduplexes of mutated DNA are subjected to a series of denaturing and annealing, which re-forms them as heteroduplexes. Gel electrophoresis is used to separate and visualise the cleaved DNA products, and the size of the fragments generated can be used to determine if a mutation has occurred at the expected site based on gRNA location.

3. 3. 1. 3. 1. caspar targeted Phlebotomus papatasi

Loss of function in the *caspar* gene is not related to a visual phenotype and therefore phenotypic analysis was not carried out on *caspar* targeted insects. Six G0 *caspar* targeted sand flies developed to adulthood (two male, four female), after backcrossing, their genomic DNA was extracted and four produced an allele at the expected size via PCR. Those presenting alleles were F1, F2, F4 and M2. No indels or SNPs were observed at the target sites in the Sanger sequencing chromatogram. No indels were reported from the ICE analysis of sequences from *caspar* gene. T7EI heteroduplex assays were also performed for *caspar* gRNA regions showing no successful cleavage following T7EI treatment. Due to time constraints no analysis was performed on G1 *caspar* targeted sand flies.

3. 3. 1. 3. 2. ebony targeted Phlebotomus papatasi

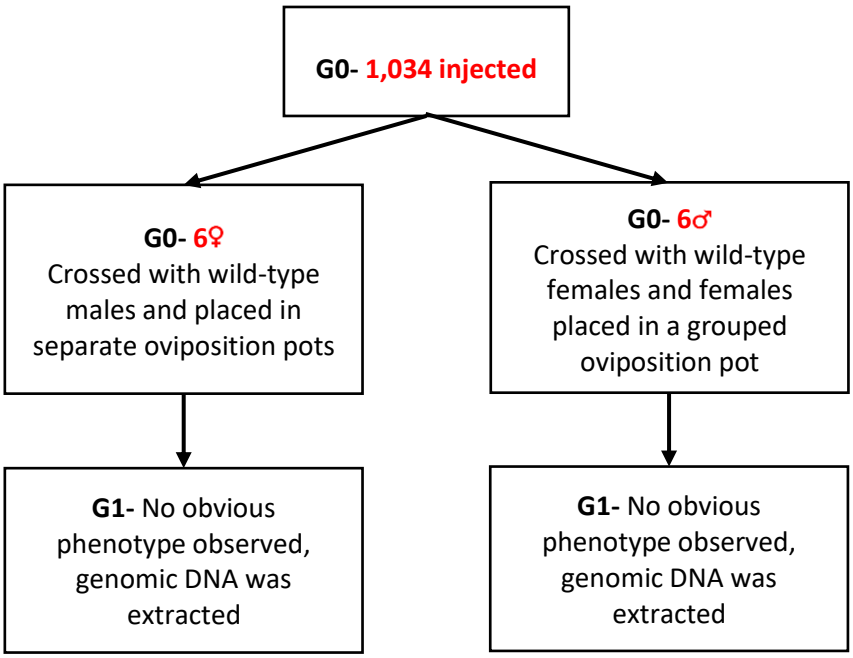

Figure 20. The processing pipeline for conformation of mutations in *P. papatasi* sand flies transfected with CRISPR-Cas9 plasmids targeting the *ebony* gene (PPAI005863).

For *ebony* targeting transfections in *P. papatasi*, two G0 sand flies showed a dark banding in the pupal stages (Figure 21). 50 wild-type pupae of a similar age were monitored whilst developing and none showed the dark banding phenotype. The *ebony* G0 adults were compared to these ~50 wild-type sand flies and showed a darkened cuticle in comparison (Figure 21).

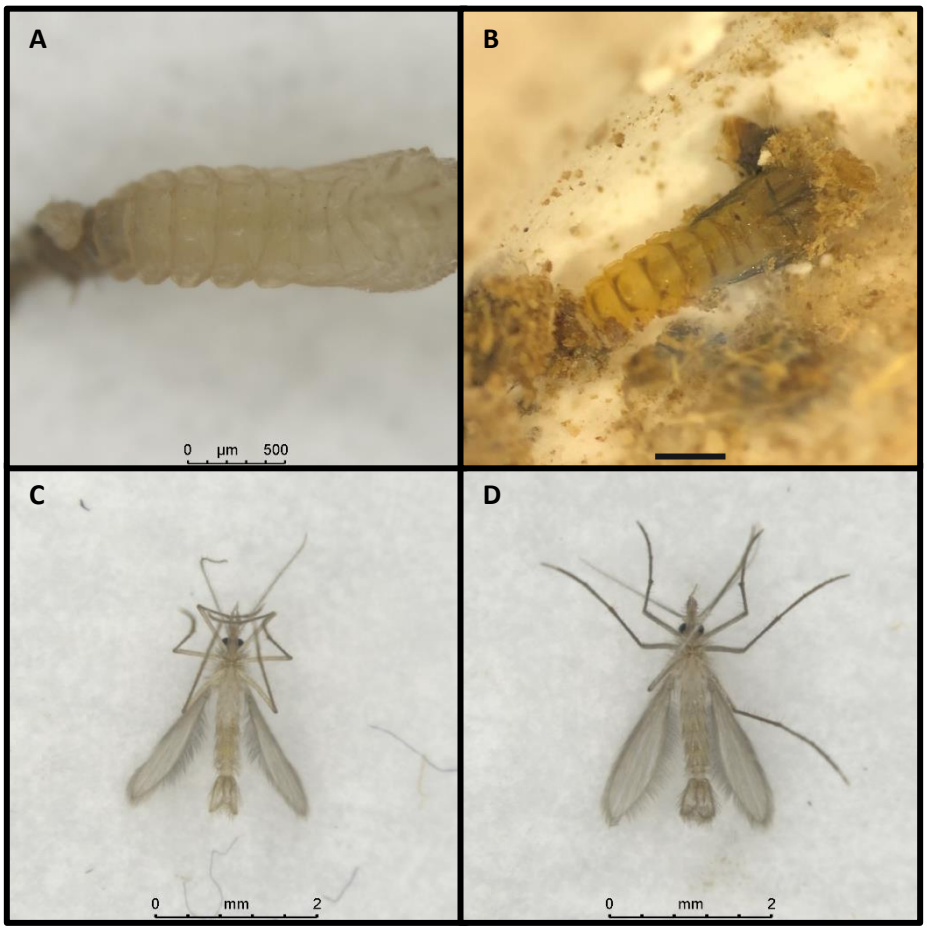

Figure 21. Phenotypic mutations observed in *P. papatasi* following transfection with a CRISPR-Cas9 plasmid targeting the *ebony* gene (PPAI005863).
A and B) *P. papatasi* pupae at 7 days post pupal case formation. C and D) adult sand flies 2 days post emergence. A and C) wild type sand flies. B and D) G0 sand flies following injection with a CRISPR-Cas9 plasmid targeting the *ebony* gene. All images were taken on a Leica M205 FA microscope (Leica, Germany). The scale bar in B represents 500µm.

The four gRNA regions (Table 4) of G0 adults injected with *ebony* 1-4 *Ppap1*-pDCC6 were amplified by PCR. Five male sand flies (out of six) and four female sand flies (out of six) demonstrated a amplicon of the expected size following PCR. Sequence analysis of the target regions showed no indels or SNPs present for any samples. The PCR fragments for G0 females 2 and 5 could not be assessed by Sanger sequencing due to bad read quality. ICE analysis of sequences from *ebony* gene targeted insects showed no indels in any sample. T7EI heteroduplex assays were also performed for *ebony* gRNA regions showing no successful cleavage following T7EI treatment. Due to time constraints no analysis was performed on G1 *ebony* targeted sand flies.

3. 3. 1. 3. 3. Wing phenotype targeted Lutzomyia longipalpis

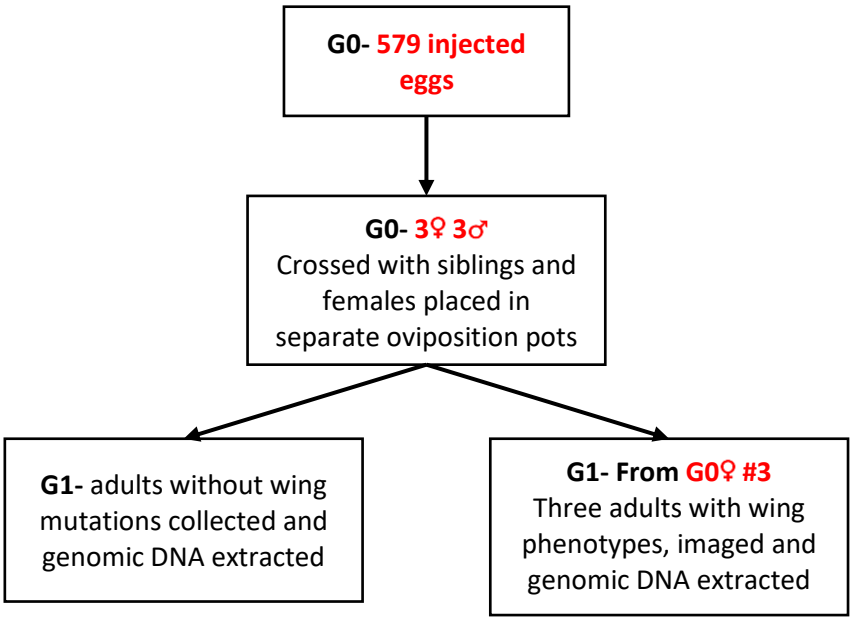

Figure 22. The processing pipeline for conformation of mutations in *L. longipalpis* sand flies transfected with CRISPR-Cas9 plasmids targeting the *rudimentary* and *vestigial* genes (LLOJ009278 and LLOJ009695).

Phenotypic analysis of the G0 wing phenotype targeting *L. longipalpis* survivors presented one female (G0-f1) with a putative "stunted" wing, related to a mutation in the *rudimentary* gene (Figure 23b).

Of the six G0 *L. longipalpis* targeted for mutations to the wing phenotype genes, *rudimentary* and *vestigial*, all showed alleles of the expected sizes following PCR of the six gRNA regions. Following manual screening of the Sanger sequencing chromatograms, two samples (G0-F1 and G0-M3) showed mismatches around the expected cut site for the *r* gRNA2, and two samples (G0- F1 and G0-M1) showed expected mismatches surrounding the *r* gRNA3 region. Unfortunately, the Sanger sequencing quality was low and multiple sequence alignment was not possible. The low Sanger sequencing quality for *r* gRNA1 and all three *vg* gRNAs meant that potential mismatches could not be validated.

Four of the six G0 wing phenotype targeting survivors were successfully ran through the ICE analysis for the r gRNA 2 and 3. As seen in Table 6, indels were found in sample G0-M3 for gRNA2 and indels surrounding gRNA3 were found in samples G0-F1 (Figure 25) and G0-F2.

T7EI heteroduplex assays were carried out on all *rudimentary* and *vestigial* gRNA regions for G0 sand flies. However, the poor-quality PCR products produced a range of off target cleavages in the controls making confirmation of mutations inconclusive.

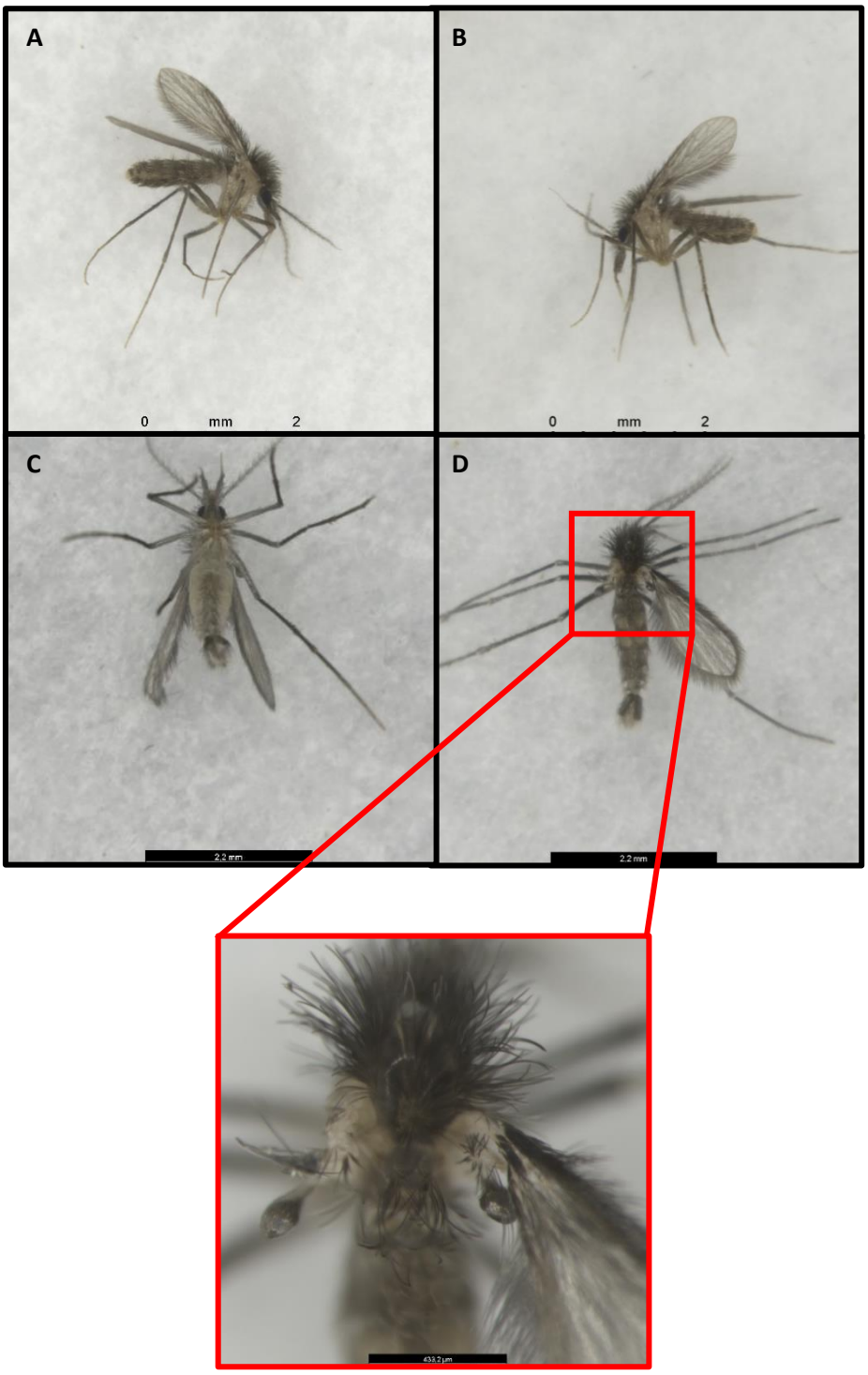

Figure 23. *L. longipalpis* adults exhibiting a phenotypic change following mutations to the *rudimentary* and *vestigial* genes *(*LLOJ009278 *and* LLOJ009695*)* via CRISPR-Cas9 transfection.
A) a wild-type *L. longipalpis* adult. B) a G0 adult showing stunted wing phenotypes. C) a G1 sand fly showing a crumpled wing phenotype. D) a G1 adult missing its left wing following transfection. All images were taken on a Leica M205 FA microscope (Leica, Germany).

Following sibling crossing, two G1 adults presented a phenotypic change in the wing structure (Figure 23C and D). One male (G1-D) presented with a "crumpled" wing characteristic of a *vestigial* mutation (Figure 23C). Another male (G1-Z) was missing a wing which infers a *vestigial* mutation (Figure 23D).

Following phenotypic analysis all G1 sand flies were screened to genotypic analysis. Twenty-six G1 *L. longipalpis* sand flies (labelled A-Z), targeted for wing phenotypes, amplified an allele of the expected size targeting the 6 gRNA regions. Of the twenty-six amplified *rudimentary* gene alleles, twelve sequences aligned with the gRNA1 (Figure 24Ai); sixteen with gRNA2 (Figure 24Aii); and seven with gRNA3. Due to conserved regions within the *rudimentary* gene the gRNA3 confirmation primers were split across the gene and were unable to confirm mutations. One sample (G1-B) for *r* gRNA1 showed a mutation around the expected cut site following alignment. All samples aligned with *vg* gRNA1 (Figure 24Bi) and twenty samples aligned with gRNA2 (Figure 24Bii). One sample (G1-F) potentially has multiple base pair substitutions surrounding the *vg* gRNA1 region (Figure 24Bi). One sample (G1-Y) presents multiple base pair substitutions surrounding the *vg* gRNA2 region (Figure 24Bii). Sequences for the *vg* gRNA3 region were too low in quality to be used in any analysis.

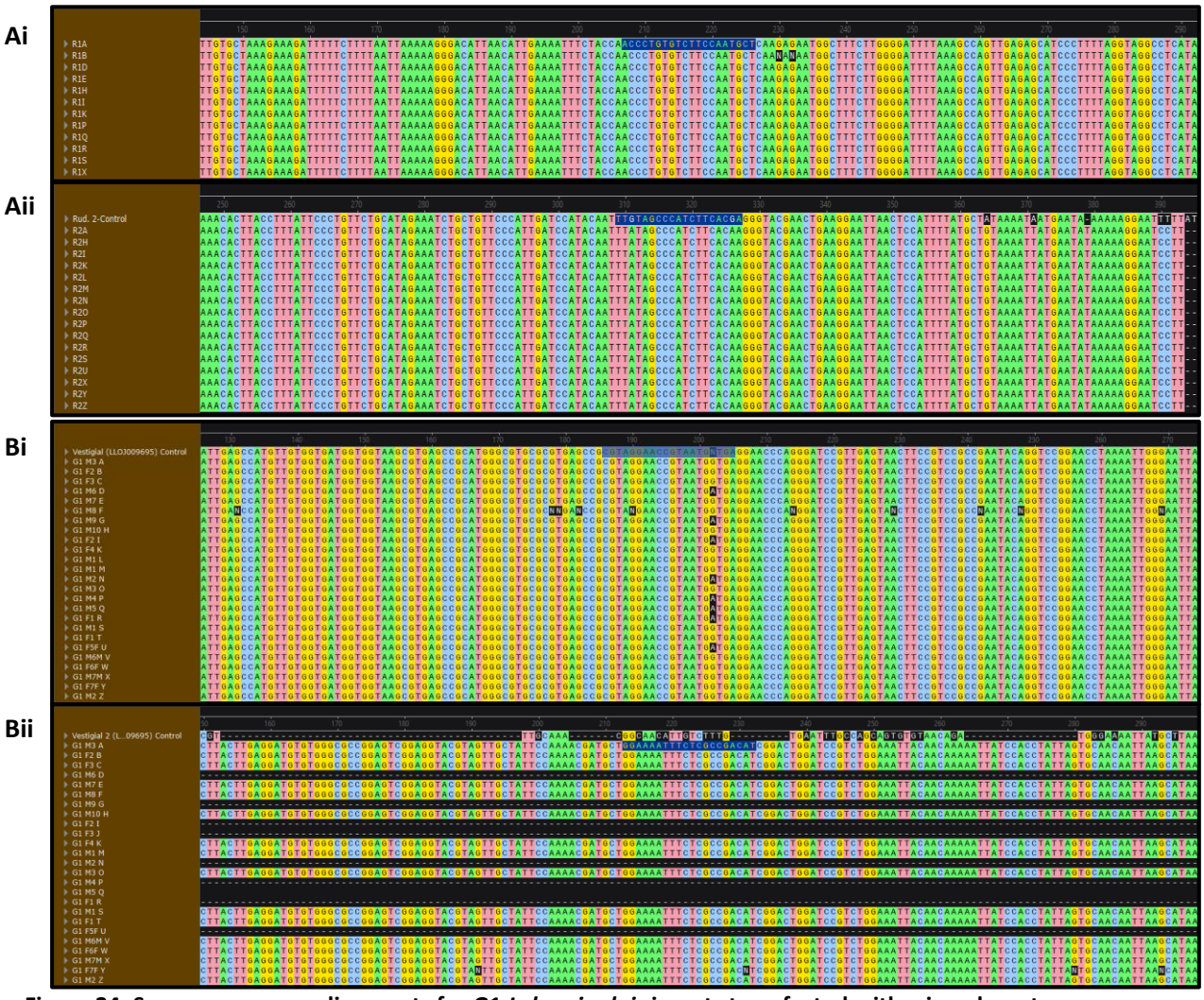

Figure 24. Sanger sequence alignments for G1 *L. longipalpis* insects transfected with wing phenotype inducing CRISPR-Cas9 plasmids.
A) alignments of the *rudimentary* gene (LLOJ009278) focusing on the regions surrounding target gRNAs (Ai for gRNA1 and Aii for gRNA2). B) alignments of the *vestigial* gene (LLOJ009695) focusing on the regions surrounding target gRNAs (Bi for gRNA1 and Bii for gRNA2). gRNA sequences are highlighted in blue.

Alignments were carried out using SnapGene software v6.2 (Dotmatics, USA) under the MUSCLE alignment tool.

Sequence data from the r gRNAs 2 and 3 were successfully analysed via ICE ADA. The other four gRNAs (r gRNA1, vg gRNA 1-3) failed to analyse due to poor sequence read quality. Sixteen G1 sand flies were positive for indels surrounding the *r* gRNA2 site (Table 6). Two sand flies were positive for indels in the *r* gRNA3 site (Table 6). All of the *r* gene ICE ADAs show low R^2 values of between 0.52-0.57, which infers possible errors in indel identification.

Table 6. ICE analysis summary of positive results for *L. longipalpis* transfected with CRISPR-Cas9 plasmids targeting the *rudimentary* gene (LLOJ009278).
gRNA regions can be found in Table 4. Indel % represents the percentage of alleles present in the sample with indels compared to a wild-type control sample. KO-score represents the percentage of indels found that would cause loss of function in the target gene. R^2 is a model fit estimation. Orange text is data from G0 sand flies and green text is from G1.

Transfected *L. longipalpis*	gRNA region analysed	Indel %	KO-score	R^2
G0-M3	2	23	19	0.54
G0-F1	3	54	54	0.54
G0-F3	3	57	0	0.57
G1-A	2	22	17	0.53
G1-H	2	22	18	0.53
G1-I	2	22	18	0.53
G1-K	2	22	18	0.53
G1-L	2	22	18	0.53
G1-M	2	22	18	0.53
G1-N	2	22	18	0.53
G1-O	2	22	18	0.53
G1-P	2	21	17	0.52
G1-Q	2	21	17	0.52
G1-R	2	22	18	0.53
G1-S	2	22	18	0.53
G1-U	2	22	18	0.53
G1-X	2	22	18	0.53
G1-Y	2	22	18	0.53
G1-Z	2	22	17	0.53
G1-F	3	54	54	0.54
G1-G	3	55	55	0.55

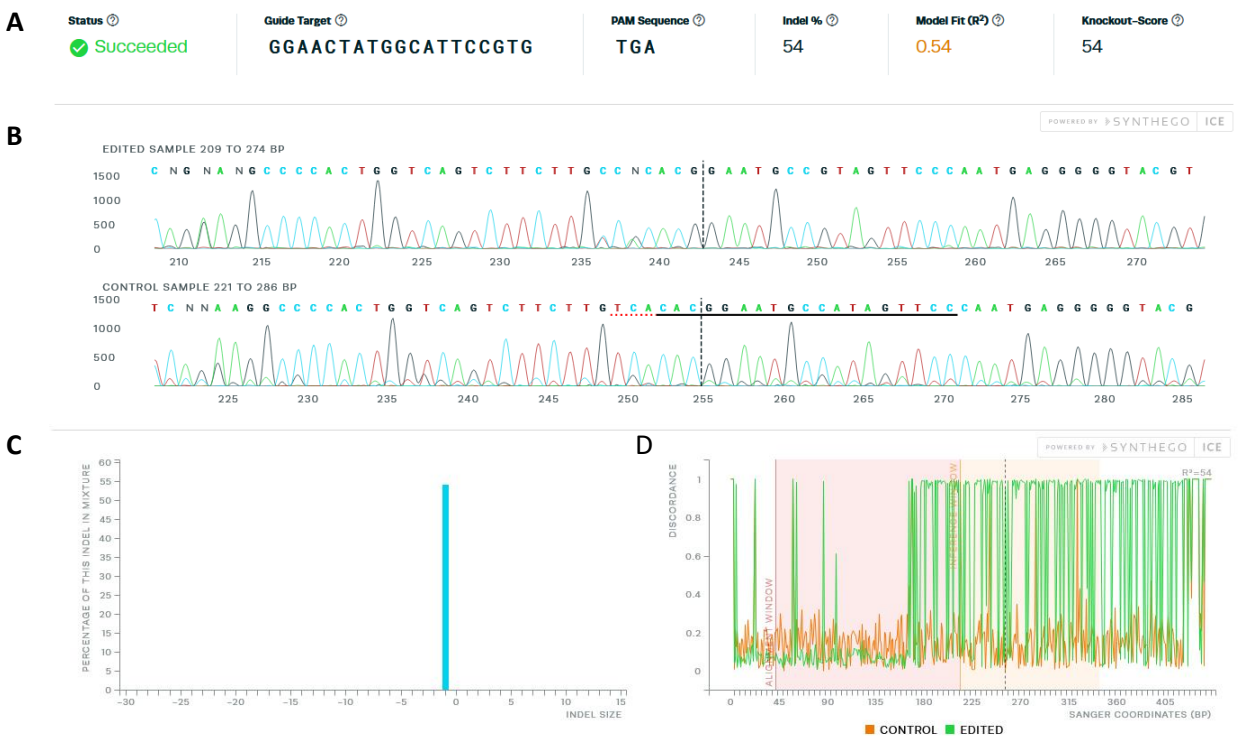

Figure 25. ICE analysis graphical output for a *L. longipalpis* sand fly (G0-F1) transfected with CRISPR-Cas9 plasmids targeting the *rudimentary* gene (LLOJ009278).
A) the text output for the ICE analysis, where; Indel % represents the percentage of alleles present in the sample with indels compared to a wild-type control sample; KO-score represents the percentage of indels found that would cause loss of function in the target gene; R^2 is a model fit estimation. B) the trace file output from the ICE analysis focusing on the predicted cut site from the target gRNA in both the mutated sample and wild-type control. C) an indel size-frequency histogram, showing the size of indels against their percentage frequency in the mutated sample. D) a discordance graph visualising the difference between the mutated trace file (green) and the control trace file (orange). The black dotted line on the graph shows the predicted cut site.

Assessing mutations within the *vestigial* gene was successful for G1 sand flies with amplicons of the expected size for gRNA1 (577bp) and gRNA2 (567bp) being produced for all samples except J (for gRNA1 and 2) and L (for gRNA2). T7EI cleavage of the gRNA1 region would have created bands of 222bp and 355bp. Ten samples showed successful cleavage producing bands of the expected size (Figure 27). Following densitometric analysis these ten samples showed mutation percentages ranging from 1.67-19.21% (Table 7). The expected T7EI cleavage of gRNA2 would have produced bands of 261bp and 306bp. For nine samples successful cleavage of this size was observed (Figure 27). Following densitometric analysis of these samples the estimated mutation percentage ranged from 6.43-18.77% (Table 7). Multiple unexpected bands were seen in the negative PCR controls for both gRNAs, but bands of the expected positive cleavage size were not seen. For *vg* gRNA3, no amplicons of the expected size could be amplified. Therefore, T7EI cleavage could not be assessed on *vg* gRNA3.

For the *rudimentary* gene gRNAs, no cleavage was obtained for gRNAs 1 and 2. Unfortunately, due to a lack of PCR amplification samples A, I, K, N, and T were not assessed for gRNA1 and B, C, D, E, F, G,

I, S, T, U, V, W, X, Y, and Z were not assessed for gRNA2. For gRNA 3 amplicons of the expected size (534bp) were seen in all samples A-Z. If heteroduplexes had formed T7E1 cleavage would result in bands of 244bp and 290bp. Following the T7EI assay, no expected cleavage occurred. A band around 400bp (Figure 26) was visible in six T7EI treated samples. However, this band was also present in thirteen untreated PCR controls.

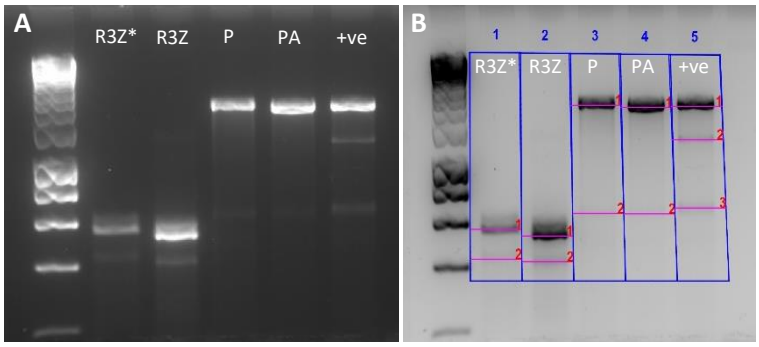

Figure 26. T7 endonuclease I heteroduplex assay of a G1 *L. longipalpis* fly targeting the *rudimentary* gene (LLOJ009278) by CRISPR-Cas9.
A) DNA products imaged following cleavage by T7EI. B) a densitometric image showing the lanes highlighted in blue and the bands selected for analysis highlighted by a purple line. In both A and B the sample highlighted with a * shows treatment with T7EI. The expected gRNA region length was 534bp which would have been cleaved into two 244bp and 290bp fragments following T7EI treatment. P and PA are positive plasmid samples ran independently from each other, with the +ve lane showing the formation of heteroduplexes which are cleaved with T7EI (Section 3. 2. 4. 7.). A Meridian bioscience HyperLadder™ 1kb is present in the far-left lane.

Table 7. Densitometric analysis results inferring mutations in the *vestigial* gene (LLOJ009695) of G1 *L. longipalpis* insects transfected with CRISPR-Cas9 plasmids.

gRNA targeted	Sample ID	Band No.	Band Volume	% of Lane	% Modification
***vg* gRNA 1**	H	1	37120086	48.69	5.72
		2	15853477	6.02	
		3	8723622	0.07	
	I	1	21126130	25.75	9.87
		2	10864555	5.39	
		3	5385579	0.56	
	P	1	12604560	45.56	19.21
		3	9449882	20.91	
		4	5986006	3.32	
	R	1	13916288	53.64	16.89
		4	11030382	21.96	
		5	5421318	2.06	
	T	1	13617298	58.88	4.12
		3	6670638	3.77	
		4	5302476	1.39	
	V	1	7863466	26.31	14.96
		3	5877952	7.48	
		4	5223538	2.59	
	W	1	15231032	65.23	1.67
		2	4013600	1.26	
		3	4563440	0.98	

	X	1	23972661	35.90	1.75
		3	7524171	1.21	
		4	4507503	0.08	
	Y	1	23961574	29.31	9.29
		3	12554566	5.82	
		4	5469950	0.49	
	Z	1	31433380	42.10	2.56
		3	7959746	1.01	
		4	8935564	1.22	
***vg* gRNA 2**	G	1	23000206	55.95	18.77
		2	16980790	24.72	
		3	7716669	4.13	
	H	1	14169853	44.86	17.71
		2	13569351	17.87	
		3	6242141	3.53	
	I	1	16881906	57.70	12.62
		2	10961964	11.23	
		3	9083935	6.64	
	K	1	16377043	55.37	11.27
		2	8569396	8.98	
		3	7818149	5.98	
	N	1	20982937	66.02	6.43
		2	5750612	4.23	
		3	6882527	4.26	
		4	3903322	0.89	
	O	1	12965368	46.74	17.30
		2	9565198	10.63	
		3	9713819	10.96	
	Q	1	12390472	52.27	15.15
		2	8287553	10.07	
		3	8706571	10.26	
	R	1	28939678	13.84	11.70
		2	17224530	2.08	
		3	14329750	1.83	
	U	1	45787124	24.83	15.24
		2	23882834	7.67	
		3	15698586	2.06	

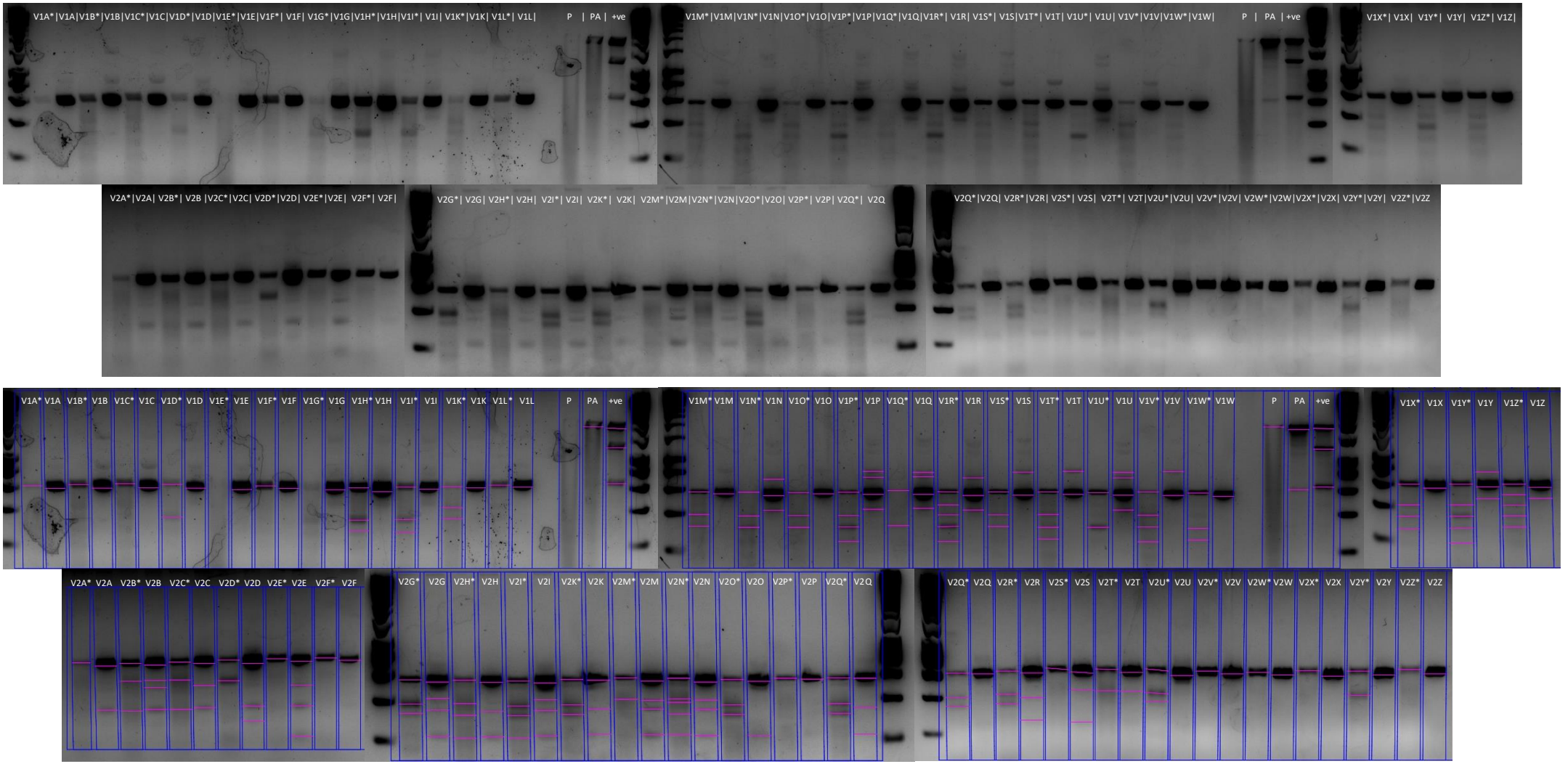

Figure 27. T7 endonuclease I heteroduplex assay of G1 *L. longipalpis* flies targeting the *vestigial* gene (LLOJ009695) by CRISPR-Cas9 gRNA1 and gRNA2.
A) DNA products imaged following cleavage by T7EI. B) A densitometric image showing the lanes highlighted in blue and the bands selected for analysis highlighted by a purple line. In both A and B, the samples highlighted with a * shows cleavage with T7EI. Expected fragment sizes are found in section 3. 3. 1. 4. 3. P and PA are positive samples ran independently from each other, with the +ve lane showing the formation of heteroduplexes, which are cleaved with T7EI (Section 3. 2. 4. 7.). A Meridian bioscience HyperLadder™ 1kb was used.

In summary, the genotypic analysis of transfected sand flies revealed 22 *L. longipalpis* sand flies mutated within the *rudimentary* gene (1 G0 via Sanger sequence alignment, 3 G0 via ADA 18 G1 via ADA) and 21 mutated within the *vestigial* gene (2 G1 via Sanger sequence alignment, 19 G1 via T7EI assay). This is important as no previous literature has achieved a CRISPR-Cas9 genomic mutation with *L. longipalpis* sand flies.

3. 3. 2. Integration of exogenous DNA into sand fly genomes via CRISPR-Cas9 HDR

The endogenous pDCC6 plasmids successfully forming mutations in the previous section, facilitated the ability to deliver exogenous DNA cassettes into sand flies via CRISPR-Cas9 HDR. This approach has been a major omission in previous literature on sand fly genome engineering as insertion of exogenous DNA is required for population control techniques such as gene-drives.

3. 3. 2. 1. Transfection of LLE/LULS45 cells

To assess the integration of exogenous DNA into the genome of sand flies via CRISPR-Cas9 HDR approaches, the LLE/LULS45 cell line (*L. longipalpis* Jacobina strain) was transfected with DNA constructs. The CRISPR-Cas9 elements (gRNA and Cas9) were delivered by a *Llon1*-pDCC6 and the exogenous DNA cassette was delivered by pDsRed-*Ubi63e*-attP. The *scarlet* gene was targeted with two NHEJ cleavage approaches, one targeting the gene centrally (HSC), and an approach utilizing two gRNA targeting either the 5' or 3' UTR to remove the gene's coding region (HUTR). Nine wells (3 replicates within 3 rounds of transfection) of ~2 million attached cells were transfected for each approach with control wells as mentioned in section 3. 2. 5. 1. 1. This approach demonstrated an important step for CRISPR-Cas9 HDR genome editing in *L. longipalpis* sand flies.

3. 3. 2. 1. 1. Fluorescent microscopy

The DNA cassette within pDsRed-*Ubi63e*-attP contains a DsRed-Express fluorescent tag, visible under red wavelengths of light during fluorescent microscopy (629nm). This was the initial screening method for HDR insertion into the genome of LLE/LULS45 cells (Section 3. 2. 5. 1. 2.). Figure 28 shows, expression of the DsRed-Express was achieved with both gRNA approaches. Expression was also observed in all wells containing pDsRed-*Ubi63e*-attP, including control cells without the *Llon1*-pDCC6 plasmids and without chemotransfection reagents.

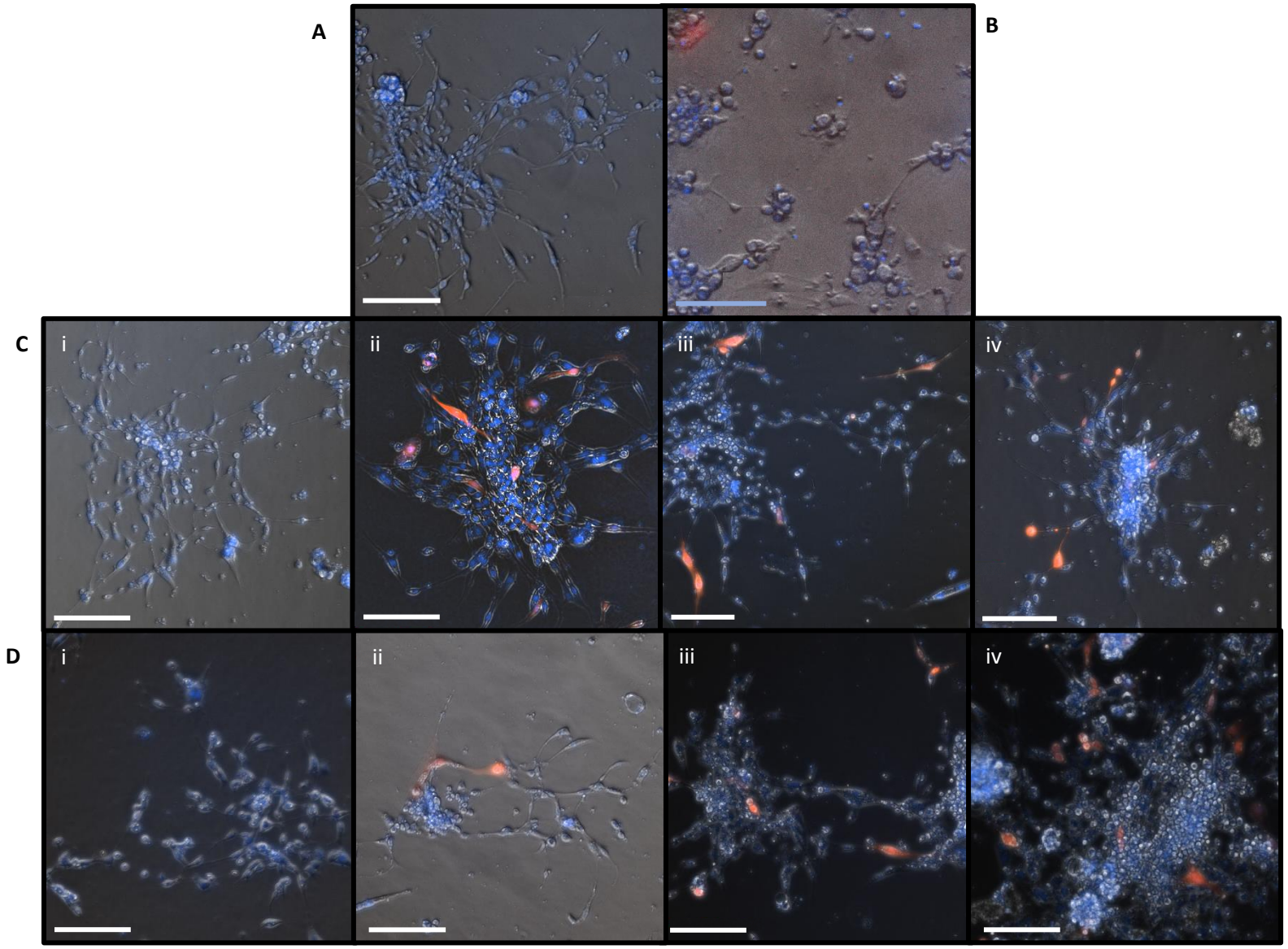

Figure 28. Fluorescent micrographs of LLE/LULS45 cells expressing DsRed-Express after integration into the *scarlet* gene (LLOJ001495) via CRISPR-Cas9 HDR.
A) wild-type control; B) RFP positive control; C) cells transfected with plasmid mixtures targeting the scarlet gene with the HSC approach. D) cells transfected with plasmid mixtures targeting the scarlet gene with the HUTR approach. i) cells transfected with only pDCC6 plasmids; ii) cells transfected with *Llon1*-pDCC6 and pDsRed-*Ubi63e*-attP plasmids without chemotransfection reagents; iii) Cells transfected with only pDsRed-Ubi63e-attP plasmids; and iv) Cells transfected with *Llon1*- pDCC6 and pDsRed-*Ubi63e*-attP plasmids with transfection reagents. All micrographs are composite images of fluorescence in blue, green, red and phase channels. Blue colour represents Hoescht 33342 DNA stain excited at a wavelength of 455nm. Red colour represents DsRed-Express fluorescence excited at a wavelength of 629nm. Green colour represents excitation of artifacts at a wavelength of 530nm. Images A; C. i-iv; and D. i-iv were imaged at a magnification of 200x. Image B was taken at a magnification of 400x. All micrographs were imaged on a Nikon Eclipse Ti2 inverted fluorescent microscope. Scale bars with a white colour represent 100µm and blue scale bars represent 50µm.

3. 3. 2. 1. 2. Genotypic analysis

In an attempt to confirm that DsRed-Express expression within LLE/LULS45 cells was due to integration in the genome, the 5' and 3' ends of the integration site were amplified and sequenced. Utilizing primers within the DNA cassette and downstream from either RHA (HSC/HUTR) we were able to confirm insertion into the genome (primers found in Appendix 2). These primers will not produce an amplicon in wild-type DNA. However, if intact pDsRed-*Ubi63e*-attP constructs are present in the PCR solution then an allele of the expected positive size may form. This infers that results by PCR and sanger sequencing cannot confirm integration with these primer sets. In Figure 29A and B, an amplicon of the expected size (1234bp) was produced for all pDsRed-*Ubi63e*-attP transfected cells. When sequenced by Sanger sequencing the amplicon confirmed genomic integration at the target site for both approaches (Figure 29C and D). An allele around 3kbp was also amplified and sequenced for the pDsRed-Ubi63e-attP treated cells (Figure 29A and B). This allele was confirmed to be the pDsRed-Ubi63e-attP plasmid remaining in cells/media following DNA extraction.

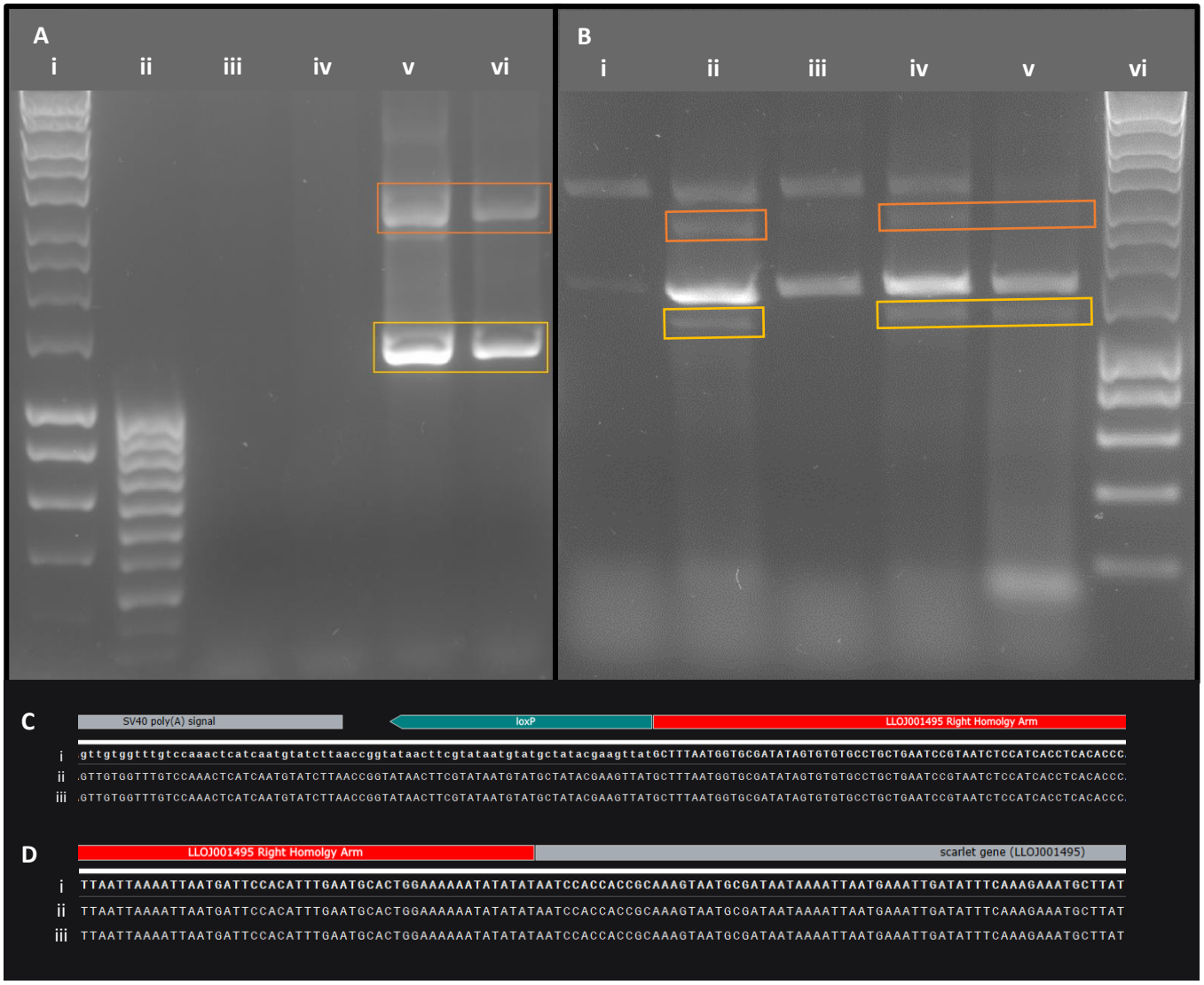

Figure 29. Confirmation of exogenous DNA integration into the *scarlet* gene (LLOJ001495) within LLE/LULS45 cells via CRISPR-Cas9 HDR.
A) PCR amplicons corelating to DNA insertion at the target site via the HUTR approach; B) PCR amplicons corelating to DNA insertion at the target site via the HSC gRNA approach; C) the sequence upstream of the right homology arm against the pDsRed-*Ubi63e*-attp construct confirming exogenous DNA insertion into the scarlet gene; D) the sequence downstream of the right homology arm against the *st* gene confirming exogenous DNA insertion into the *st* gene. The loading plan for the gels are as follows A. i) Meridian bioscience HyperLadder™ 1kb; ii) Meridian bioscience HyperLadder™ 100bp; iii) wild-type DNA; iv) transfection with Llon1-pDCC6 plasmids only; v) transfection with pDsRed-*Ubi63e*-attP only; vi) transfection with *Llon1*-pDCC6 and pDsRed-*Ubi63e*-attp. B. i) wild-type DNA; ii) transfection with *Llon1*-pDCC6 and pDsRed-*Ubi63e*-attP without chemotransfection reagents; iii) transfection with Llon1-pDCC6 plasmids only; iv) transfection with pDsRed-*Ubi63e*-attP only; v) transfection with *Llon1*-pDCC6 and pDsRed-*Ubi63e*-attp; vi) Meridian bioscience HyperLadder™ 1kb. Bands highlighted with an orange box show amplification of pDsRed-*Ubi63e*-attp plasmid. Bands highlighted with a yellow box show successful integration of endogenous DNA into the *st* gene. The aligned sequences are labelled as follows: C. i) template DNA focused on the endogenous DNA 3' end; D. i) template DNA focused on the downstream end of the right homology arm of the *st* gene; C & D. ii) amplified DNA from cells transfected with only pDsRed-*Ubi63e*-attP; C & D. iii) amplified DNA from cells transfected with *Llon1*-pDCC6 and pDsRed-*Ubi63e*-attP.

When processing these results, we were unaware of the formation of heteroduplexes between wild-type and DNA constructs in the PCR reaction above (Figure 29). We assumed that HDR integration was successful and attempted to confirm that the *Llon1*-pDCC6 plasmids were cleaving genomic DNA and forming indels via NHEJ. To do this amplification of the gRNA target regions by PCR was carried out, followed by analysis of CRISPR-Cas9 mutations via Sanger sequencing, algorithmic deconvolution analysis, and T7EI heteroduplex assays (Sections 3. 2. 4. 4., 3. 2. 4. 5., 3. 2. 4. 6., 3. 2. 4. 7.). The ICE algorithmic deconvolution assay did not detect indels around the target sites of the gRNAs in either approach (Figure 30 and Table 8). The T7EI heteroduplex assay demonstrated cleavage and amplicons around the expected sizes for the HSC gRNA (246 and 260bp) and 5' HUTR gRNA (267 and 326bp) (Figure 31). A densitometric analysis of the T7EI assay under multiple camera exposure times (0.4-4 seconds) inferred modification percentages of 2.2-3.49% for the HSC gRNA, and 1.85-5.75% for the 5' UTR gRNA (Table 8). The modification percentages are in line with those recorded following *in vivo* transfection (Section 3. 3. 1. 4. 3). The positive T7EI assay provides evidence that the *Llon1*-pDCC6 plasmids are capable of cleaving genomic DNA within the LLE/LULS45 cells.

Table 8. The analytical data for LLE/LULS45 cells treated with CRISPR-Cas9 Llon1-pDCC6 plasmids targeting the *scarlet* gene (LLOJ001495) utilizing three different gRNAs.
Outputs from an algorithmic deconvolution assay on Sanger sequencing and a T7 endonuclease I heteroduplex densitometric analysis.

gRNA analysed	Indel %	Knockout-score	R^2	Band No.	Volume	% of Lane	% modified
***st* central**	0	0	1	1	557961968	55.31	3.49
				2	212430760	2.20	
				3	264136968	1.87	
3' UTR	Failed	Failed	Failed	1	609784648	67.66	N/A
5' UTR	0	0	0.99	1	831706680	64.59	5.75
				2	366264328	7.11	
				3	239268080	1.01	

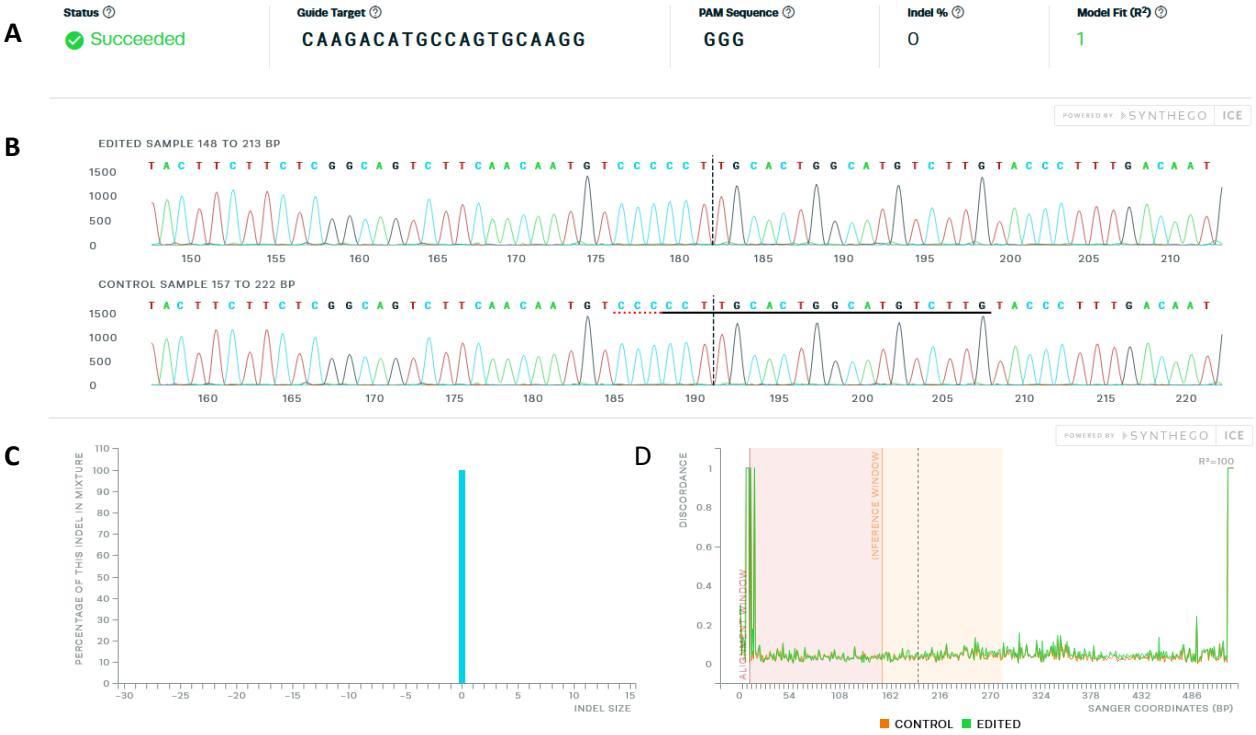

Figure 30. ICE algorithmic deconvolution analysis for LLE/LULS45 cells transfected with Llon1-pDCC6 plasmids targeting the *scarlet* gene (LLOJ001495).
A) the text output for the ICE analysis, where; Indel % represents the percentage of alleles present in the sample with indels compared to a wild-type control sample; KO-score represents the percentage of indels found that would cause loss of function in the target gene; R^2 is a model fit estimation. B) the trace file output from the ICE analysis focusing on the predicted cut site from the target gRNA in both the mutated sample and wild-type control. C) an indel size-frequency histogram, showing the size of indels against their percentage frequency in the mutated sample. D) a discordance graph visualising the difference between the mutated trace file (green) and the control trace file (orange). The black dotted line on the graph shows the predicted cut site.

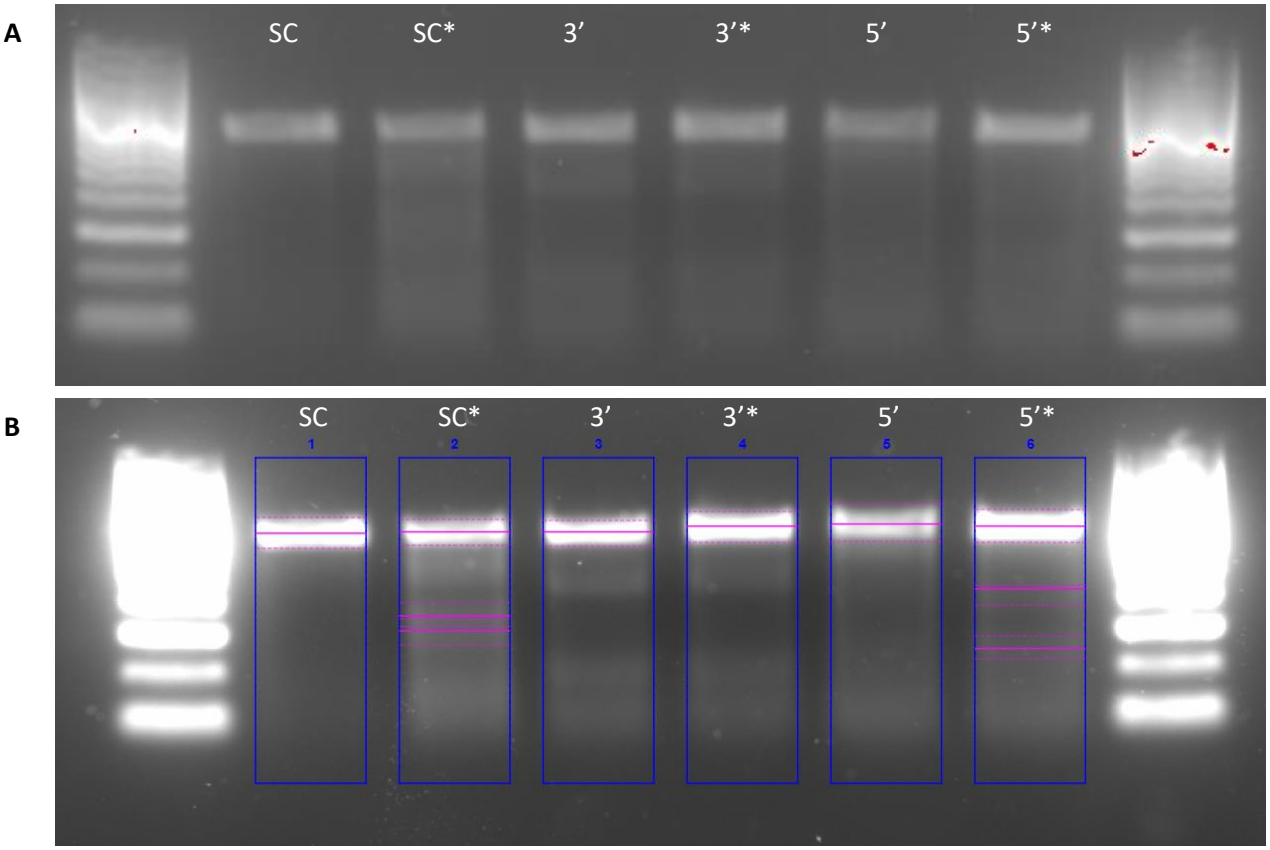

Figure 31. A T7 endonuclease I heteroduplex assay for LLE/LULS45 cells transfected with Llon1-pDCC6 plasmids targeting the *scarlet* gene (LLOJ001495).

A) DNA products following cleavage by T7EI. B) a densitometric analysis with lanes highlighted in blue and the bands selected for analysis highlighted by a purple line with high and low band boundaries in dotted purple lines. In both A and B, the samples are all treated with T7EI and those highlighted with a * show transfected cell DNA, those without a * are the gRNA region from wild-type cell DNA. A Meridian bioscience HyperLadder™ 100bp was used.

3. 3. 2. 2. Microinjection of L. longipalpis sand flies

Following our early interpretation of the CRISPR-Cas9 HDR results within LLE/LULS45 cells, *in vivo* approaches were attempted. Transfection of *L. longipalpis* embryos was carried out via microinjection of the HUTR approach CRISPR-Cas9 constructs at Charles University, Prague, Czech Republic. 701 *L. longipalpis* embryos were injected with the pDsRed-*Ubi63e*-attP plasmid and *Llon1*-pDCC6 plasmid, whilst 539 embryos were injected with only the pDsRed-*Ubi63e*-attP construct. Adult survivorship data is seen in Table 5 and breeding pathways of these lines are seen in Figure 32.

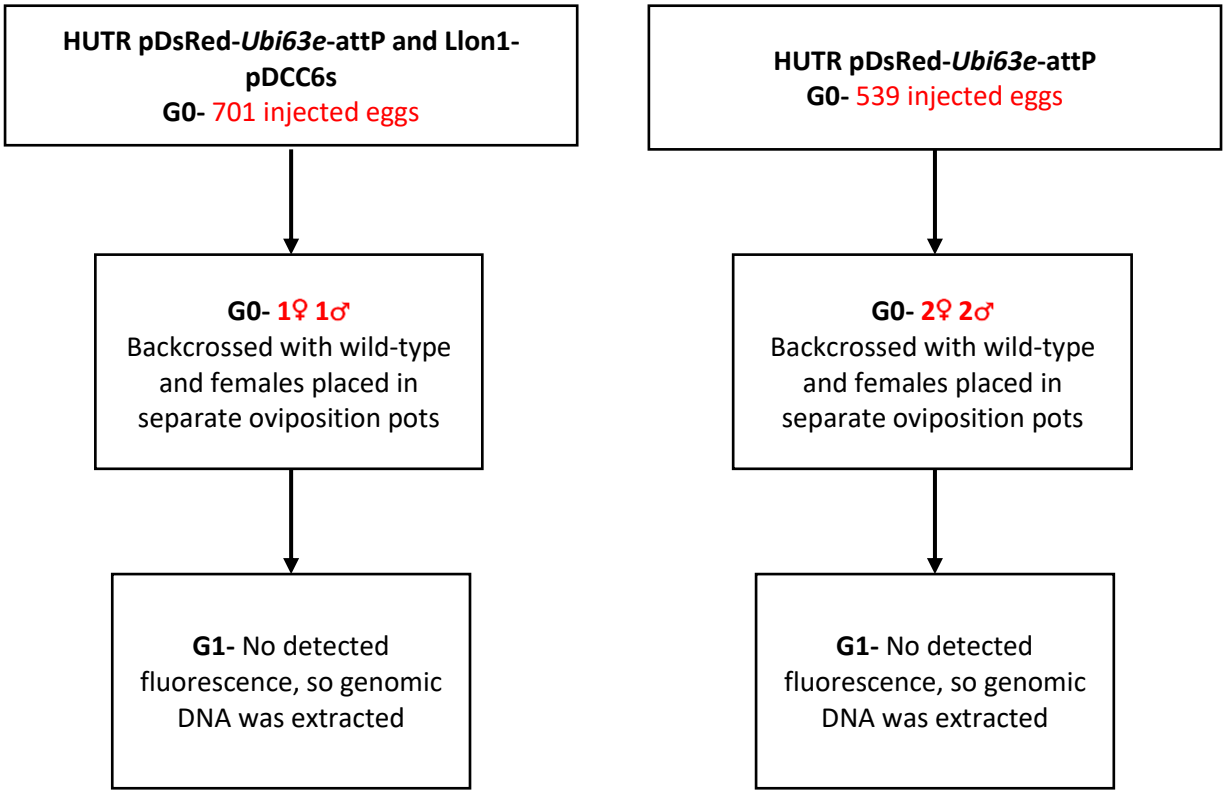

Figure 32. The processing pipeline for conformation of mutations in *L. longipalpis* sand flies transfected with CRISPR-Cas9 HDR plasmids for the insertion of an exogenous DNA cassette into the *scarlet* gene (LLOJ001495).

3. 3. 2. 2. 1. Fluorescent microscopy

To validate the expression of DsRed-Express from the integrated DNA cassette, larval and adult sand flies were imaged under a fluorescent stereomicroscope. No fluorescence was observed in either the G0 or G1 populations (Figure 33). As no fluorescence was observed genomic DNA was extracted from adults post death to confirm DNA cassette integration.

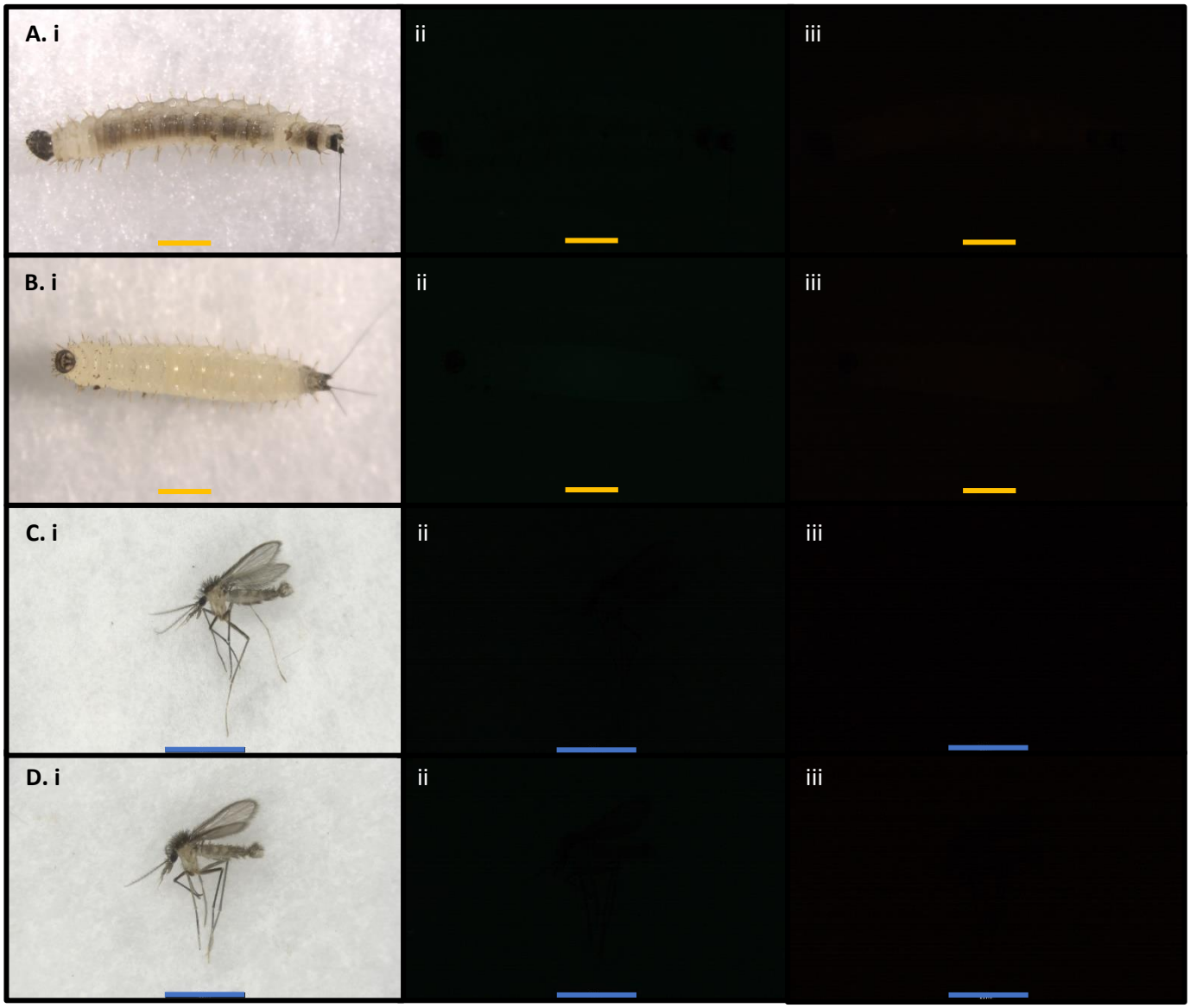

Figure 33. Fluorescent micrographs of G1 *L. longipalpis* sand flies following parental transfections with HUTR pDsRed-*Ubi63e*-attP and *Llon1*-pDCC6 plasmids.
A) a wild-type larvae. B) a G1 larvae C) a wild-type adult. D) a G1 adult. i) white light micrographs. ii) green light micrographs taken at a wavelength of 530nm to highlight artifacts. iii) red light micrographs taken at a wavelength of 629nm to highlight DsRed-Express expression. All images were taken on a Leica M205 FA microscope (Leica, Germany). The yellow scale bars represent 500µm, the blue scale bars represent 2.2mm.

3. 3. 2. 2. 2. Genotypic analysis

Following the absence of fluorescence, genomic DNA was extracted from the six G0 adults and the four G1 adults that developed. These were assessed via PCR amplification utilizing primers within the DNA cassette and downstream from the RHA. These primers should have only produced an amplicon if the DNA cassette was present as seen in Figure 29. No amplicon was amplified for the G0 or G1 adults (Figure 34).

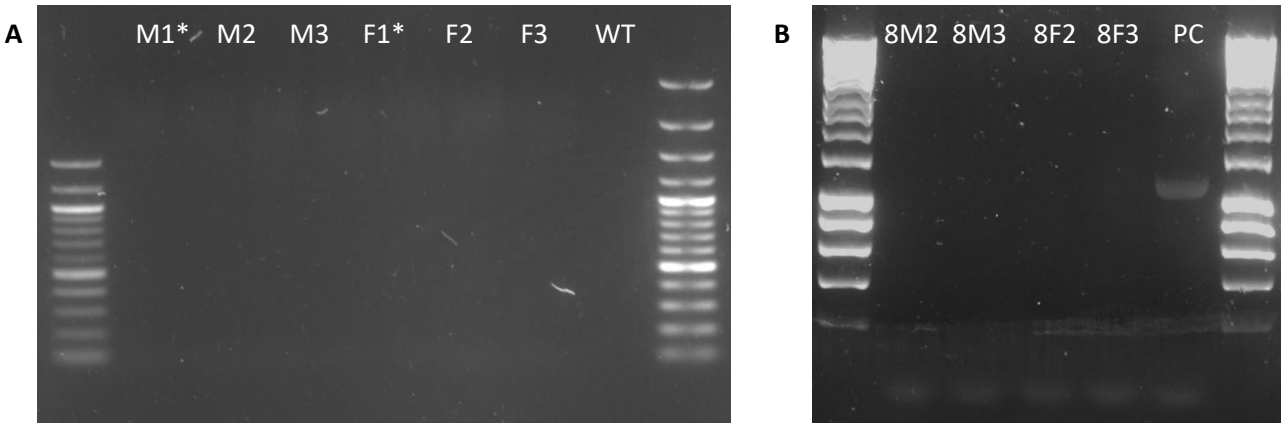

Figure 34. PCR confirmation of transfection in *L. longipalpis* adults with HUTR pDsRed-*Ubi63e*-attP.
A) G0 adults, those marked with a * were injected with both pDsRed-*Ubi63e*-attP and *Llon1*-pDCC6. B) G1 adults and a positive control from transfected LLE/LULS45 cells.

3. 4. Discussion

The results outlined above demonstrate evidence supporting the first successful mutation of genomic DNA via CRISPR-Cas9 NHEJ plasmids in *L. longipalpis*. These results are supported by phenotype expression, Sanger sequencing, algorithmic deconvolution assays, and T7EI heteroduplex assays. These results also provide the reported attempt to integrate exogenous DNA into the genome of *L. longipalpis* via *in vitro* transfection of CRISPR-Cas9 HDR plasmids. With further genotypic analysis needed to validate these results. We have achieved validation for the use of CRISPR-Cas9 NHEJ in phlebotomine sand flies, paving the way for future work into Leishmaniasis control.

3. 4. 1. CRISPR-Cas9 gene knockout via NHEJ

Initially the *in vitro* platform assessed in section 2, was to be used to assess the pDCC6 plasmids targeting phenotypic marker genes (*cinnabar, ebony, eyeless,* and *white* genes) which could be validated *in vivo* at a later stage. Initially no mutations were detected via PCR and Sanger sequencing. This was theorised to be due to the *D. melanogaster* U6-2 promoter transcribing the gRNAs. In previous research this promoter has shown low level expression in mosquitoes, whilst, high expression is seen from endogenous promoters amplified from upstream of *DU6-2* gene orthologues (136,331,350). Therefore, endogenous U6 promoters for *L. longipalpis* and *P. papatasi* were designed. It was decided that these would be assessed via *in vivo* approaches. This was due to a belief that the low transfection efficiencies in cells (Section 2. 3. 1.) led to unmutated DNA being amplified by PCR over the mutated alleles, reducing the sensitivity of Sanger sequencing and ADAs. At the time the T7EI heteroduplex assay had not been fully assessed which has been shown to show a much higher level of sensitivity over standard PCR and Sanger sequencing (351). If possible we would have preferred validation of mutations via amplicon sequencing which would have allowed us to sequence low copy mutated alleles (352). We were limited to *in vitro* methods due to a lack of viable sand fly colonies at the LSHTM and the COVID-19 pandemic restricting travel to collaborators abroad. The construction of *Llon1/Ppap1*-pDCC6 plasmids coincided with the lifting of multiple travel bans in Europe, allowing us to collaborate with Prof. Petr Volf's team at Charles University.

In vivo transfection approaches for sand flies continues to be logistically difficult due to the fragility of sand fly embryos. Currently, we rely on microinjection of recently laid embryos prior to melanisation providing only a short window (2-3 hours) to undertake transfection experiments. This is due to microinjection needles fracturing on the surface of the chorion before penetration. However, unmelanised embryos are prone to rupturing from the pressure of the injection mixture as

well as failing to heal the injection site. These disadvantages, partially explain the low survivorship rates observed in this research and others (152,222,319). The one study siting 9.95% survivorship was related to a single batch of embryos and further research from the same group showed a survivorship of 2.04% (222,319). The main difference between our approach and this study is the use of halocarbon oil to limit embryo desiccation, this could have increased survivorship. It is also important to ensure the integration of mutations in pre-blastoderm cell genomes to increase the likelihood of the entire developing embryo receiving the intended trait. This is done by injecting embryos at the posterior end where pole cells form. Whilst the timeline for this stage is well understood in mosquitoes, little has been done to identify this state in sand flies (353). One study, theorised this stage will occur in the first 36-60 hours of development for *P. papatasi* (354). Following this, we based our times off of the first 2-3 hours post oviposition to increase our chances. As the sandfly embryos are perfectly symmetrical (north to south), the location of the pole cells was unknown during injection. Embryos were instead injected ¾ of the way to the south hoping that this would place the mixture close to the pole cell end without damaging cells. This could have reduced contact of the plasmid mixture with early cells reducing transfection efficiencies. If the mixture is injected too close to the cells, the increase in pressure could cause damage, reducing viability. Manual handling of the embryos following injection would have also had an effect on survivorship (152). Currently, there is no replacement for microinjection in sand flies but potentially chemotransfection or electroporation could be explored as alternatives. These approaches could reduce the manual handling of embryos, increasing viability.

The survivors of pDCC6 plasmid microinjections produced multiple positive results. Putative phenotypes for loss of gene function in the *ebony*, *rudimentary* and *vestigial* genes were observed visually (Figures Figure 21 and Figure 23). Molecular validation inferred mutations in twenty-two *L. longipalpis* adults targeting wing phenotype genes (out of 32 adults analysed). One sample (G1-Z) was positive for a mutation by presentation of a mutant phenotype and by the genetic approaches ADA and T7EI. Due to time constraints, a large number of G1 offspring were not assessed for mutations by any molecular techniques. Repeats of those which failed to amplify by PCR were not possible due to having limited sample DNA. As mentioned above, PCR and Sanger sequencing will amplify the most dominant alleles in the DNA sample. This creates a problem *in vivo* as microinjection techniques are unlikely to result in all pole cells being transfected. This would lead to G0 adults presenting mosaic mutations, which if integrated into the germline could lead to heterozygous offspring with ubiquitous phenotypic mutations. This mosaic formation has been previously documented in insect CRISPR-Cas9 studies and they found amplicon sequencing of the G0 generation can detect the low level mutated amplicons (300). As seen in Table 6, ADA results for the

rudimentary gene have low R^2 values potentially showing bad DNA quality. This could have been due to the PCR amplification, or the DNA extraction being contaminated by bacteria or fungi in the decomposing sand fly. Spectrophotometer readings on the extracted genomic DNA often read a 260/280 ratio of around 1 (expected to be 1.8 for purified DNA). This would indicate contamination in the sample potentially by proteins or chemicals that absorb light at the 280nm wavelength. Ideally, with more resources and time, the DNA samples would be sequenced by amplicon sequencing. This approach would allow us to sequence individual alleles, identifying small populations of mutated cells and removing background sequences caused by contamination. This approach is seen as the gold standard for G0 insects and assessing mutation copy numbers within the genome for many other insect CRISPR-Cas9 studies (168,300,355). Molecular analysis of dead larvae and pupae would also be analysed as previous research has shown the knockout of the *vg* gene can lead to development failures in the pupal stage (311).

As amplicon sequencing was not available, the T7EI heteroduplex assay was used to identify low level mutations which would not be picked up via Sanger sequencing. This method was able to identify mutations at potential efficiencies ranging from 1.67-19.21%. T7EI assays are dependent on DNA quality and large indel sized mutations (356). The negative controls for *r* gRNA3 and both *vg* gRNA1/2 showed multiple background amplicons, which could have been cleaved causing fragments in the test sample. By only carrying out the densitometric analysis on bands of the expected size, we hopefully avoided anomalous DNA. However, without sequencing these bands further we cannot confirm they are related to the CRISPR-Cas9 mutations.

For *P. papatasi,* the phenotype exhibited in the *ebony* gene targeting transfections is promising (Figure 21). After consulting with Prof. Petr Volf and his team, we are confident that this is a mutant phenotype. This theory is supported by the lack of dark banding in the wild-type *P. papatasi* pupae screened. The phenotype was also not present in wild-type adult flies or in *caspar* targeted survivors. The lack of molecular evidence could be due to the problems with ADA and T7EI outlined above. Given more time and resources, DNA from these samples would be assessed by amplicon sequencing and further *P. papatasi* transfections would be carried out to at least G1 to demonstrate germline transformation.

3. 4. 2. Expression of exogenous DNA via CRISPR-Cas9 HDR

Genetic manipulation via CRISPR-Cas9 HDR has become a powerful tool for control of insects. No previous research has been published using this technique in phlebotomine sand flies. Here we provide reported attempt of insertion of a DNA cassette containing a fluorescent marker into *L.*

longipalpis cell lines via CRISPR-Cas9 HDR. With further genotypic evidence this *in vitro* approach could lay the groundwork for future vector control *in vivo*.

Expression of the DsRed-Express following integration into the *scarlet* gene was high, with fluorescence intensity during microscopy visually higher than that of other markers used in section 2. 3. and the Ac5-STABLE-neo-RFP plasmid control (Figure 28). Unfortunately, access to the flow cytometry equipment at LSHTM was limited, preventing quantitative measurements of these transfections. Transient expression of DsRed within the HDR donor plasmid is possible so confirmation via sequencing is required.

Confirmation of genomic integration was attempted by PCR and Sanger sequencing (Figure 29). Obtaining positive results via PCR and Sanger sequencing was should be more sensitive for HDR, due to the primer pair spanning the 3' end of the DNA cassette/integration site. In wild-type DNA these primer pairs do not amplify via PCR. This creates a relatively rapid and easy to use CRISPR-Cas9 validation method. However, if intact DNA constructs are present in the PCR solution amplification of a heteroduplexes formed from single primers amplifying genomic DNA and plasmid DNA would occur. This could create alleles of the expected positive size following repetitive PCR cycles. Confirmation of genome integration was not possible for our *in vitro* cultures at the time and would need to be further validated by utilizing techniques such as amplicon sequencing or inverse PCR (300,357,358). Due to the low levels of plasmid in adult tissues and G1 insects any positive results *in vivo* would provide robust evidence using the primer set found in Figure 29. If the research was to continue *in vivo*, future transfections would use the HDR approach with new targeted gRNAs and HAs designed for the successful phenotypic targets from section 3. 3. 1 (e.g. *ebony*, *rudimentary,* and *vestigial* genes). Alternatively, to further assess the HDR approach *in vitro*, drug selection markers such as zeocin™ could be integrated to select for stable transgenic lines (359). As the HDR plasmids are non-replicative within insect cells these lines would eventually degrade the plasmid DNA reducing the risk of false positives due to heteroduplexes forming.

Unexpectedly, the negative controls for the *in vitro* CRISPR-Cas9 HDR transfections presented positive alleles for integration. The cells treated without chemotransfection reagents showed transfection efficiencies at similar rates to those with reagents (estimated by counting cells during microscopy). This is most likely due to heteroduplexes forming in the PCR reaction between the HDR constructs and wild-type DNA as described above. However, to provide an alternative theory, transient transfection has been observed in mammalian cells following nutrient shock (360). In this context, the lack of serum and high plasmid concentrations could have damaged cell membranes, up taking plasmids and recovering once serum rich media was returned. Alternatively, the poly-D-lysine

or polyethyleneimine coating the culture flasks is known to induce transfections in mammalian and insect cells (361–363). The cell line is also heterogenous with the possibility of certain cell types showing higher transfection efficiencies (Section 2. 4.). It is possible that both the nutrient shock and adherence chemicals made certain cell types more susceptible to transfections.

A further unexpected result was positive alleles for the cell transfected without *Llon1*-pDCC6 plasmids. Once again, this is most likely due to the formation of heteroduplexes within the PCR reaction. However, HDR is a mechanism used to repair genomic DNA with complimentary DNA found in cells. Usually the break from CRISPR-Cas9 NHEJ causes an increase in HDR if a complimentary piece of DNA is present. It has been reported, that genetic modification can occur at low rates in the presence of DNA cassettes with HAs (364). Long length HAs (700-1000bp) can cause high efficiency insertions especially with older transgenic techniques such as TALEN/ZFNs (365). These long HAs could facilitate integration without CRISPR-Cas9 NHEJ elements, which should increase HDR greatly and reduce the need for long HAs (366). To overcome concerns that the pDCC6 plasmids were not functioning as intended, amplification of the gRNA regions and molecular mutation validation was assessed (Sections 3. 2. 4. 4., 3. 2. 4. 5., 3. 2. 4. 6., 3. 2. 4. 7.). Although Sanger sequencing and ADA showed no cleavage, they are prone to the errors mentioned in section 3. 4. 1. Outputs from the T7EI assay demonstrated cleavage for the HSC and 5' gRNA (Figure 31), providing evidence for the successful expression of pDCC6 elements at a low rate (1.85-5.75%). To increase HDR efficiencies, future work would focus on reducing the length of the HAs to increase the dependency on the CRISPR-Cas9 NHEJ cleavage.

Previous research into optimising HDR efficiencies suggested that a multiplexed gRNA approach would increase integration efficiencies (366,367). To maximise our chances with successful integration we utilised a two-gRNA approach targeting the *scarlet* gene's UTRs, alongside a single central gRNA approach. Following transfections, microscopy could not easily identify if one methodology led to a higher number of cells expressing DsRed-Express. We had intended to use flow cytometry data to infer which methodology produced increased transfection rates. Unfortunately, as mentioned above, this service was not available when transfections occurred. The similar levels of expression might be due to transient expression of the plasmid in both cases rather than genome integration which still needs to be confirmed by inverse PCR and sequencing. Due to this it was decided to assess the HDR approaches *in vivo* instead.

In vivo assessment of HDR transfections did not demonstrate DsRed-Express expression or genetic integration. It is likely that the limitations outlined in section 3. 4. 1. also applied to the HDR approaches. However, amplification via PCR should have yielded more obvious results due to its

increased sensitivity. Adult survivorship numbers were low, and this limited potential back crossing. We were also limited by time and resources at Charles Univeristy, which meant that only a few rounds of HDR plasmid injections could occur and only the HUTR approach was attempted. Previous research into insect transfections of CRISPR-Cas9 HDR have microinjected thousands of embryos and not seen expression till G1 to G3 (137,297). Further collaborations with Prof. Petr Volf's team would focus on repeating the HUTR microinjections as well as the HSC plasmids. A *P. papatasi* targeting HDR construct based on *ebony* gRNA 3 was also constructed but not microinjected due to logistical constraints. One further pathway that was considered was the integration of a gene-drive elements integrated into the genome via *piggyBac* constructs. This approach has been very successful in *Aedes* mosquitoes and removes the need for complex HDR approaches (168,291).

In summary, we provide evidence of genome modifications within phlebotomine sand flies via CRISPR-Cas9 NHEJ and HDR approaches. With further development this approach could form a platform for the future vector control of leishmaniasis. It also furthers the adaption of CRISPR-Cas9 approaches to non-model insects contributing practical knowledge to the whole molecular entomology field.

4. A novel chemotransfection methodology for the delivery of genome editing DNA constructs to *Rhodnius prolixus* embryos

4. 1. Introduction

An increase in insecticide resistance and limited resources for vector control of Chagas disease has resulted in the need for novel approaches to triatomine bug control (38,368,369). To my knowledge, no previous research has reported the genetic modification of triatomine bugs. This is potentially due to the lack of available methods for the delivery of genome engineering elements (302). This limits the capacity for research into vector-parasite interactions and novel vector control strategies. This chapter describes a novel methodology for delivering transfection macromolecules to *R. prolixus* bugs.

4. 1. 1. Delivery of transfection agents to Hemiptera via microinjection

The genetic modification of insects for population control could revolutionise the way we prevent crop destruction, habitat loss and disease transmission (355,370,371). Approaches such CRISPR-Cas9 or RNAi have become vital tools for targeting specific genes, allowing researchers to produce detailed gene function assessments. This can be applied to control efforts reducing populations by interfering with reproductive fitness (157,355). Alternatively, by understanding the functions of genes involved in disease pathways or sensory cues these can be interrupted on a population scale, reducing disease transmission (85,141,372–375). Whilst these approaches have been well studied in multiple insect orders, there is a lack of research into the genetic modification of Hemiptera. One theory for this is the difficulty in delivering genetic modification elements to preblastodermal embryos (302). Therefore, the identification and validation of transfection element delivery methods is vital to the control of insects.

Microinjection of recently laid embryos is the most widely used approach for delivering transfection elements in insect orders such as Diptera and Lepidoptera (298,300,310,311,318). These elements could include double-stranded RNA for RNAi or Cas9 endonucleases and transcribed gRNAs or DNA constructs for CRISPR-Cas9 (79,376). When adapting microinjection methodologies to Hemiptera, multiple alterations are needed to overcome the oviposition surface, egg size and chorion thickness (302). Alterations are required as hemipteran insects are often magnitudes larger in size than Diptera (such as mosquitos) and lay eggs attached to surfaces or with chorions that are more robust than those of most dipterans. In the glassy-winged sharpshooter (*Homalodisca vitripennis*), CRISPR-Cas9 macromolecules were microinjected through leaf epidermis as to not damage embryos by removing them from leaves (300). To remove leaves from the oviposition process, the Western tarnished plant bug (*Lygus Hesperus*) were induced to oviposit on parafilm which could be stretched to gently dislodge embryos post microinjection (377). Some hemipterans have large eggs which are

more easily microinjected, however, microinjection of small eggs (<0.3mm) can be damaged by the needle or injection mixture. To increase viability and transfection efficiencies in these smaller embryos, finer microinjection needles must be pulled and used in more controlled microinjectors such as those with robotic arms (378). Chorion thickness can be a major limitation to microinjection, with some insect embryos damaged by chorion shards or fracturing microinjection needles before the injection reaches the pole cells. To overcome this, European firebug (*Pyrrhocoris apterus)* embryos were soaked in water prior to microinjection (138). As outlined above with appropriate adaptations, microinjection into the embryos of insects can become a viable and highly efficient method of delivering genetic elements.

A less commonly used alternative to embryo microinjections is the direct injection of transfection components into the ovaries of adult insects. This reduces the trauma to the embryo caused by chorion fractures, injection solution pressure and secondary infections. Ovary injections of RNAi and CRISPR-Cas9 components have been validated in a number of insect species including the silverleaf whitefly (*Bemisia tabaci),* German cockroach *(Blattella germanica),* deer tick (*Ixodes scapularis),* kissing bug *(Rhodnius prolixus),* red spider mite *(Tetranychus urticae)* and red fluor beetle *(Tribolium castaneum)* (379–384). The advantage of this is especially important in *T. urticae* embryos, which have a diameter of ~100µm. To aid inclusion in developing embryos, transfection macromolecules can be packaged by Receptor-Mediated Ovary Transduction of Cargo (ReMOT) (385). ReMOT functions by attaching CRISPR-Cas9 ribonucleoproteins (RNPs) to peptides which are incorporated into insect oocytes, which facilitates migration of the RNPs from the insect haemolymph to the ovaries. This approach has since been successfully adapted to multiple insect orders including Hemiptera (380,385). The ReMOT system is limited to the delivery of CRISPR-Cas9 RNPs and therefore cannot deliver the DNA cassettes required for homology-directed repair (HDR) approaches (386). RNAi injections into *R. prolixus* nymphs and adults*,* have been applied to screen potential phenotypic genes, which could be used for CRISPR-Cas9 studies in both adults and emergent nymphs (383). Vieira *et al.,* was able to interrupt embryo development by injecting dsRNA targeting the RpATG6 gene (382). Both of these studies show that injections into *R. prolixus* bugs have the potential to deliver transfection agents to embryos.

Microinjection has been shown as a versatile methodology for the application of genetic modifications in insects (298,300,310,311,318,379–381). However, the adaptations create further complications such as processing speed and reduced viability. With further research, less traumatic approaches could be developed for insect transgenics.

4. 1. 2. Delivery of transfection agents to insects via non-microinjection methodologies

Whilst microinjection of embryos is the most common delivery method of transfection elements in insects, other methodologies have been assessed. These include biolistic delivery, chemotransfection, electroporation, and ingestion (304–306,387–389).

Biolistic delivery has been used for decades to deliver DNA constructs to *in vitro* cell lines and tissue sections such as plant leaves (390,391). The technique coats gold microparticles in packaged DNA/RNA, which is propelled at high speeds into cells/tissue using pressurised helium gas (390). Biolistic delivery has been adapted to embryo transfections of multiple insect species including the silk moth (*Bombyx mori)* and fruit fly (*Drosophila melanogaster)* (303,304,392). Typically, embryos were aligned vertically on agar and dsRNA was delivered into embryos at a fairly high throughput rate compared to microinjection (~200 embryos transfected with each bombardment). However, due to the random nature of particle dispersal and variance in quality of microparticle coating, discrepancies between samples were often recorded (305). This technique was initially assessed in insects before microinjection became widely available and standardised. More recent developments in plant biolistics, including more accurate ejection barrels, could standardise this technique making it a viable approach for large scale insect transfections (393).

Electroporation has been assessed as a possible delivery method of transfection elements in both embryos and developed larvae (Section 2. 1. 3.). This technique had limited results when applied to delivering DNA constructs from a solution, generally exhibiting low expression of transient plasmids (305). Further refinement of this technique has been applied to Asian blue tick (*Rhipicephalus microplus)* embryos to deliver RNAi macromolecules showing a ~50% efficiency with ~25% reduced embryonic viability (306). This is important as the small size of tick eggs (~500µm diameter) makes them difficult to microinject. Electroporation following microinjection of transfection agents has also been shown to dramatically increase the efficiency of DNA/RNA delivery to cells (387,394,395). This post injection technique has been applied to multiple insect species (Asian malaria mosquito *Anopheles sinensis, B. mori,* Asian swallowtail *Papilio xuthus* and *T. castaneum*) with expression levels up to ~76% higher than standard microinjection and ~5% viability reduction (387,394,395).

The ingestion of transgenic elements has resulted in the loss of gene function via RNAi in multiple insect species (396–399). There are two ingestion approaches currently utilised, the feeding of transcribed dsRNAs or the feeding of microorganisms that express dsRNA. Both approaches have been assessed as a possible pest control methodology. Although, one theory for its success as a pest control method is due to an increase in RNases and gut microbiota following dsRNA ingestion (397).

For direct dsRNA feeding, loss of function in essential genes (e.g. *Fak, Snf7, Mad1, Srp54k, Actin, Snap,* and *Shihas*) been recorded in the sweet potato weevil (*Cylas puncticollis)* and willow leaf beetle *(Plagiodera versicolora)* (396,397). Expression of dsRNA within microorganisms such as *E. coli* and *Saccharomyces cerevisiae*, can increase efficiency of RNAi due to protection from RNAases and continued expression within insect organs (398,399). The microorganism delivery method has been validated as a pest control method in multiple insects such as emerald ash borer (*Agrilus planipennis)* and spotted wing Drosophila *(Drosophila suzukii),* as well as being adapted for high-throughput gene screening in *R. prolixus* (388,398,399). In *R. prolixus*, the expression of egg development genes was successfully limited, resulting in a reduction to oviposition rates by 84% (388). Whilst these examples show future promise for RNAi, there is a need to establish ingestion as an approach as a means to deliver DNA constructs for use in genome engineering methodologies such as CRISPR-Cas9.

Whilst chemotransfection is the most common delivery method for *in vitro* gene modifications (Section 2. 1. 3.), it is under-researched for delivery to *in vivo* embryos, with very limited current applications. Injecting EGFP expressing plasmids packaged by FlyFectIN™ into squinting bush brown butterfly (*Bicyclus anynana)* pupae increases transfection efficiencies by up to 30% over electroporation alone (400). To my knowledge no studies have attempted to transfect embryos by immersion in chemotransfection reagents, similar to *in vitro* protocols. This is potentially due to egg chorions preventing liquid from reaching the embryo. Most insect embryos require respiratory diffusion to ambient air from aeropiles (pores in the chorion for air intake) protected by hairs, ridges or wax to inhibit external liquid contact with the embryo surface (389,401). A study by Bomfim *et al.,* focuses on exploiting these aeropiles on *R. prolixus* eggs (Figure 35B) to deliver potential insecticides (389). Ethanol was applied to strip the wax surrounding the aeropiles which enabled liquid insecticides to reach the embryonic membranes. There is an air cavity between the chorion and vitelline membrane (Figure 35C), which could be exploited to deliver chemotransfection reagents to the embryos. This was theorised by Bomfim *et al*., although to date no further research has attempted this approach. By adapting the delivery method discovered by Bomfim *et al.,* we could create a rapid easy-to-use chemotransfection methodology to genetically modify triatomine bugs.

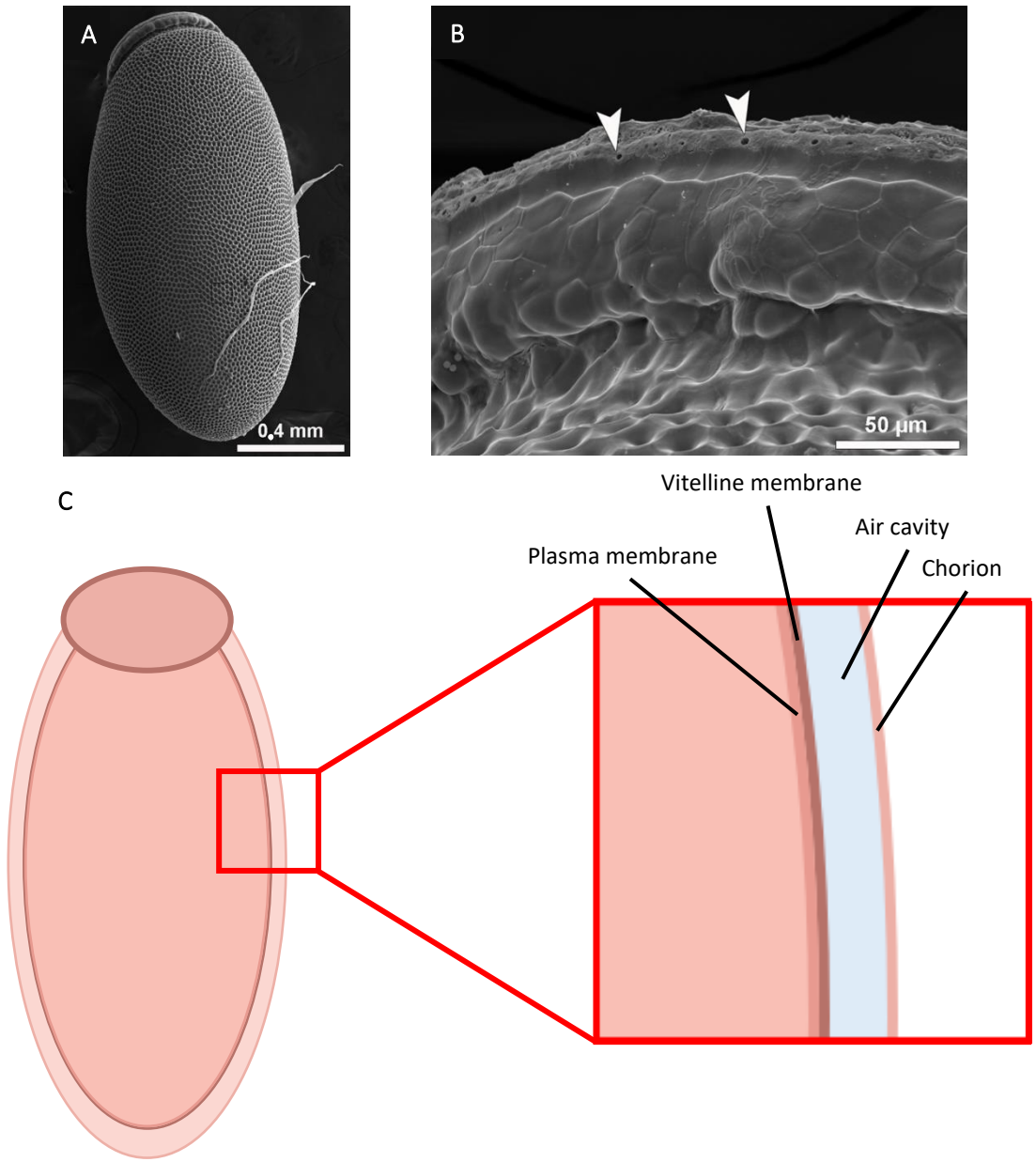

Figure 35. The egg structure of *Rhodnius prolixus* demonstrating a possible delivery route of transfection reagents to the embryo.
Images A and B are field emission scanning electron micrographs of a *Rhodnius prolixus* egg (389). A) the whole egg structure. B) the aeropiles on the rim of the operculum. C) the egg structure focusing on the air cavity and embryonic membranes that delivery of macromolecules must pass for successful transfection.

4. 1. 3. Aims

To date, the genetic modification of triatomine bugs has not been achieved in published literature. A major barrier is the lack of delivery methods for transfection reagents. Here we aim to develop a delivery methodology capable of successfully transfecting *Rhodnius prolixus* embryos. To validate this methodology multiple objectives must be achieved; the delivery of transfection macromolecules to a developing embryo; assessment of viability following treatment; and the demonstration of successful delivery of DNA constructs capable of integrating exogenous DNA into the genome.

4. 2. Methods

4. 2. 1. *Rhodnius prolixus* colony rearing

The *R. prolixus* colony used in this study was maintained by me at the London School of Hygiene and Tropical Medicine (LSHTM, UK) with the assistance of Shahida Begum. This colony was derived from insects originating from Venezuela and maintained at the LSHTM since the late 1920s (402).

The *R. prolixus* bugs were maintained in glass jars (H9.5 cm × D14 cm) with qualitative Whatman™ filter paper QL100 (Cytiva, USA) lining the base, and with folded filter paper running the vertical length of the jar to allow resting surfaces for the bugs. The colony is incubated at 26 °C ± 2 °C, at 70% relative humidity with a 12h light: 12h dark cycle. Bugs are fed every 4–6 weeks on defibrinated horse blood (TCS Microbiology, Buckingham, UK) using a Hemotek® membrane feeding system with 5ml reservoirs (Hemotek Ltd., Blackburn, UK).

4. 2. 2. Ethanol-chemotransfection methodology validation via Hoechst 33342

To assess the ethanol wax stripping methodology, embryos were stained with Hoechst 33342 DNA stain following the stripping of hydrophobic wax by ethanol. Embryos were collected ~96 hours post oviposition from the *R. prolixus* colony and placed in a 1.5ml microcentrifuge tube (max 40 per reaction). To remove the wax, 200µl of 95% ethanol was added to the tube and embryos are incubated at room temperature for 5 minutes. The ethanol was removed, and embryos were air dried on sterile filter paper for 1 minute. The embryos were placed in a new tube and coated with 200µl of Hoechst 33342 diluted in *phosphate-buffered saline* (PBS) at a final concentration of 20µg/ml. These were incubated at room temperature for 5 minutes then the solution was removed. The embryos were washed with PBS three times before being air dried on filter paper. The embryos were incubated at room temperature in a 9cm petri dish containing a sterile saline wipe for 1 hour. Following incubation, the embryos were then prepared for imaging following the methods described in Section 4. 2. 5. excluding the Hoechst 33342 staining step.

As a control, embryos were treated in the Hoechst solution for 5 minutes without wax stripping via ethanol then washed 3 times in PBS and prepared following the methods in Section 4. 2. 5.

4. 2. 3. Click-iT™ Plus EdU Kit for plasmid DNA

The Click-iT™ Plus EdU Imaging Kit (ThermoFisher, USA) is a commercial product for evaluating the replication of DNA in cell samples. It does this by incorporating EdU into replicating DNA, replacing the thymine bases. EdU contains an alkyne that can bind covalently to a picolyl azide attached to a fluorescent tag. This allows for DNA to be tagged after fixation and imaged using fluorescent microscopy. By incorporating EdU into a DNA plasmid replicating within *E. coli*, we can later tag this plasmid (with fluorescent probes) within a fixed embryo to confirm delivery to cells.

The Click-iT™ Plus EdU Alexa Fluor™ 594 Imaging kit (ThermoFisher, USA) was used to incorporate EdU into plasmid DNA. The EdU solution was added to *E. coli* replicating the ^{i}hyPBase plasmid (277), following the manufacturers protocol for cells. After EdU incorporation and replication, ^{i}hyPBase plasmids were purified using a Monarch® Plasmid Miniprep Kit (New England Biolabs, USA). Purified plasmids were then transfected into *R. prolixus* embryos 24 hours post oviposition using the Nucleic Acid Squaramide Carriers (NASC) based ethanol-chemotransfection (EC) methodology (Section 4. 2. 4. 1.). After 72 hours of incubation, transfected embryos were dissected and fixed in paraformaldehyde (PFA) as described in Section 4. 2. 5. Fixed embryos were tagged with Alexa Fluor™ 594 (red) following the Click-iT Plus EdU Imaging Kit protocol, excluding any steps that required pelleting cells. The embryos were then imaged following standard protocols (Section 4. 2. 6.).

4. 2. 4. Chemotransfection methodologies for *Rhodnius prolixus* embryos

An adapted protocol based on the Bomfim *et al.* method was assessed to deliver DNA constructs *to R. prolixus* embryos (389). Briefly, this protocol hereon referred to as ethanol-chemotransfection (EC), uses ethanol to wash away the hydrophobic wax surrounding aeropiles on the operculum rim. Once the wax was cleared, liquid was able to enter the cavity between the chorion and vitelline membrane (Figure 35C). Using chemotransfection reagents packaged DNA constructs can pass through the vitelline and plasma membranes to reach embryonic cells. Multiple approaches were taken to validate this transfection approach.

4. 2. 4. 1. Ethanol-chemotransfection via Nucleic Acid Squaramide Carriers

Nucleic acid squaramide carriers (NASC) are a novel chemotransfection reagent designed and assessed by Asst. Prof. Francisco Olmo (LSHTM, UK). NASC use polarity to deliver packaged DNA or proteins into cells. Transfection efficiencies in mammalian cells have been shown to be up to 10-fold

higher than electroporation with reduced toxicity (unpublished data, Olmo *et al*.,). This method was used for the Click-iT™ Plus EdU method as well as viability assays post EC (Section 4. 3. 2. & 4. 3. 3.).

The protocol is as follows, embryos 1-4 hours post oviposition were collected from the *R. prolixus* colony and placed in a 1.5ml microcentrifuge tube (max of 40 per reaction). To remove the wax, 200µl of 95% ethanol was added to the tube and embryos were incubated at room temperature for 5 minutes. The ethanol was removed, and embryos were air dried on sterile filter paper for 1 minute (NASC can be damaged by ethanol). The embryos were placed in a new tube and immersed in 200µl of a solution containing 1µg of plasmid DNA packaged by NASC in serum free RPMI media at a concentration of 160 µM. The embryos were incubated at room temperature for 5 minutes then the solution was removed. Embryos were then gently pressed into the surface of putty adhesive in a 9cm petri dish containing a sterile saline wipe for humidity. The dish was incubated under normal colony conditions (Section 4. 2. 1.) for 72 hours before being prepared for embryo imaging (Section 4. 2. 5.) or until nymphs emerge (9-14 days).

4. 2. 4. 2. Ethanol-chemotransfection via Cellfectin® II

For the transfection of embryos with DNA constructs, Cellfectin® II (Invitrogen, USA) was used as a chemotransfection reagent in the EC methodology. Cellfectin® II is a cationic lipid based chemotransfection reagent which has been commercially optimised for insect cell lines such as Sf9 and High Five™ cells.

Cellfectin® II transfection mixtures were produced as follows: 3µl of Cellfectin® II reagent was diluted in 100µl of RPMI media and incubated at room temperature for 15-30 minutes. Whilst in tandem, a solution of 1µg of plasmid DNA and 2µl of PLUS™ reagent in 100µl of RPMI medium was incubated at room temperature for 5 minutes. The two solutions were combined and incubated at room temperature for 5-15 minutes. Whilst the packaging reaction was occurring, embryos 1-4 hours post oviposition were collected from the *R. prolixus* colony and placed in a 1.5ml microcentrifuge tube (max of 40 per reaction). To remove the wax, 200µl of 95% ethanol was added to the tube and embryos were incubated at room temperature for 5 minutes. The ethanol was removed, and embryos were air dried on sterile filter paper for 1 minute. The embryos were placed in a new tube and coated with 200µl of plasmids packaged by Cellfectin® II. These were incubated at room temperature for 5 minutes then the solution was removed. Embryos were then gently pressed into the surface of putty adhesive in a 9cm petri dish containing a sterile saline wipe for humidity. The dish was incubated under normal colony conditions (Section 4. 2. 1.) for 72 hours before being prepared for embryo imaging (Section 4. 2. 5.) or until nymphs emerged (9-14 days).

4. 2. 4. 3. Ethanol-chemotransfection via FlyFectIN™

For the transfection of embryos with DNA constructs, FlyFectIN™ (OZ Biosciences, France) was used as a chemotransfection reagent in the EC methodology. FlyFectIN™ is a catatonic lipid and polymer based chemotransfection reagent which acts by exploiting endosomal escape methodologies. It has been commercially optimised within multiple insect cell lines such as Bm5, High Five™, S2 and Sf9.

FlyFectIN™ transfection mixtures were produced as follows; 2µl of FlyFectIN™ reagent was diluted in 100µl of RPMI medium and incubated at room temperature for 5 minutes. Whilst in tandem, a solution of 1µg of plasmid DNA in 100µl of RPMI medium was incubated at room temperature for 5 minutes. The two solutions were combined and incubated at room temperature for a further 15-30 minutes. Whilst the packaging reaction was occurring, embryos 1-4 hours post oviposition were collected from the *R. prolixus* colony and placed in a 1.5ml microcentrifuge tube (max of 40 per reaction). To remove the wax, 200µl of 95% ethanol was added to the tube and embryos were incubated at room temperature for 5 minutes. The ethanol was removed, and embryos were air dried on sterile filter paper for 1 minute. The embryos were placed in a new tube and coated with 200µl of plasmids packaged by FlyFectIN™. These were incubated at room temperature for 5 minutes then the solution was removed. Embryos were then gently pressed into the surface of putty adhesive in a 9cm petri dish containing a sterile saline wipe for humidity. The dish was incubated under normal colony conditions (Section 4. 2. 1.) for 72 hours before being prepared for embryo imaging (Section 4. 2. 5.) or until nymphs emerged (9-14 days).

4. 2. 5. Preparation of *Rhodnius prolixus* embryos for imaging

Following treatment, embryos were prepared for imaging by fluorescence microscopy. As the chorion is highly auto-fluorescent in multiple wavelengths of light, chorions were removed from the embryo via dissection.

The dissection methodology for a *R. prolixus* embryos was performed as follows (Figure 36). Using a cyanoacrylate adhesive, the embryos were attached to a glass microscope slide. Once the adhesive had dried the embryos were covered with a few drops of sterile PBS (Figure 36A). Using a 10A Surgical scalpel blade (Swann-Morton, UK) the operculum of the embryo was removed and discarded (Figure 36B). Both vertical sides of the chorion were then cut making sure to avoid cutting the vitelline membrane and leaving a small section of chorion attached at the posterior pole (Figure 36C). The upper half of the chorion was then gently lifted back using the scalpel blade and severed at the posterior pole (Figure 36D). The embryo was removed using a pipette fitted with a wide-bore 1mL pipette tip and placed into a 1.5mL microcentrifuge tube (Figure 36E). For fixation, the PBS

surrounding the embryo was replaced with a 4% PFA solution and incubated at room temperature for 30 minutes. For transfection experiments, the PFA was then removed and replaced with a solution of Hoechst 33342 diluted in PBS at a final concentration of 20µg/mL and incubated for 1 hour at room temperature. The Hoechst solution was then removed and replaced with PBS. The embryos were then stored in complete darkness at 4°C until microscopy was performed.

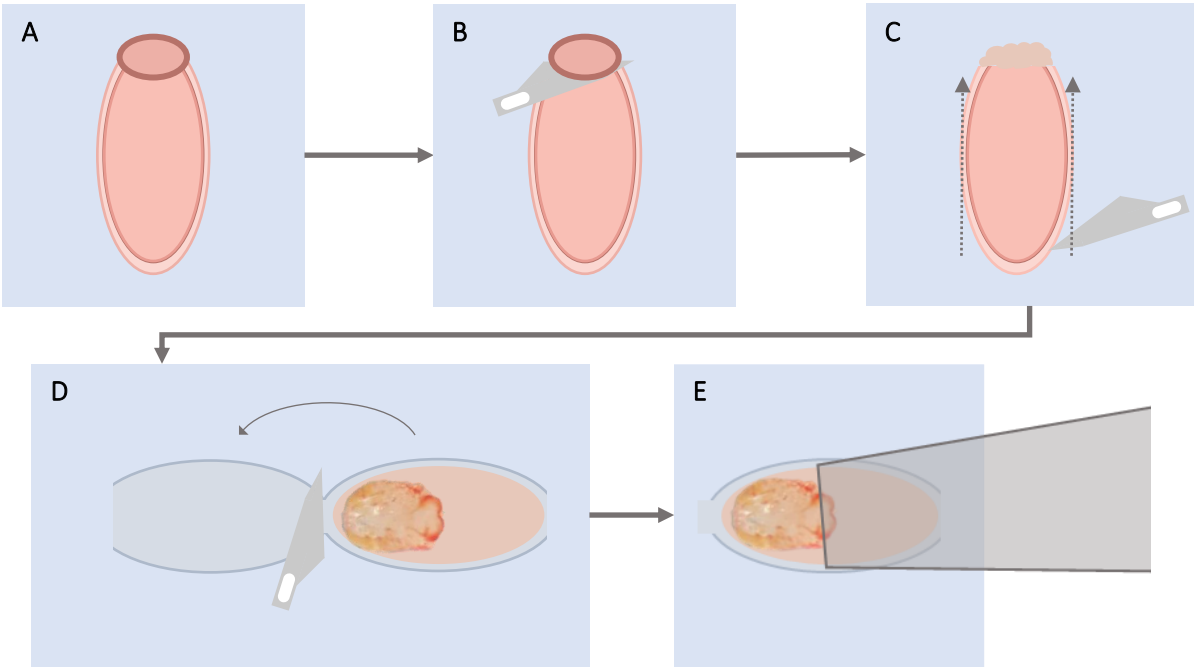

Figure 36. Methodology for dissection of a *Rhodnius prolixus* embryo.
A) an embryo is glued to a glass microscope slide and covered in a drop of PBS. B) the operculum is removed by scalpel blade. C) both sides of the chorion are cut making sure not to cut the vitelline membrane and leaving a small section at the posterior pole uncut. D) the upper half of the chorion is folded back to reveal the embryo. E) the embryo is gently removed by a wide-bore 1ml pipette tip and placed into 4% PFA for further processing.

4. 2. 6. Fluorescent imaging of *Rhodnius prolixus* embryos

Following fixation and staining, embryos were placed into an uncoated µ-Dish glass coverslip imaging dish (Ibidi, Germany), and 2mL of PBS applied. The embryos were imaged on either a Nikon Eclipse Ti2 inverted fluorescent microscope (Nikon, Japan) or a Zeiss LSM880 with Airyscan (Zeiss, Germany). Images were captured and processed using the NIS-Elements software (Nikon, Japan) or Zen microscopy software (Zeiss, Germany). Emission wavelengths for fluorescent molecules were 460nm for blue, 530nm for green and 600nm for red.

4. 3. Results

4. 3. 1. Assessment of wax stripping methodology

To assess the potential of the ethanol-chemotransfection method, we first attempted to demonstrate that the stripping of wax with ethanol facilitates the absorption of chemicals into the embryo. An experiment performed by Bomfim *et al.,* was adapted to treat embryos with Hoechst 33342 diluted in PBS (389). This was to mimic the solutions used for chemotransfection reagents in future experiments and infer our ability to deliver DNA constructs to embryonic cells.

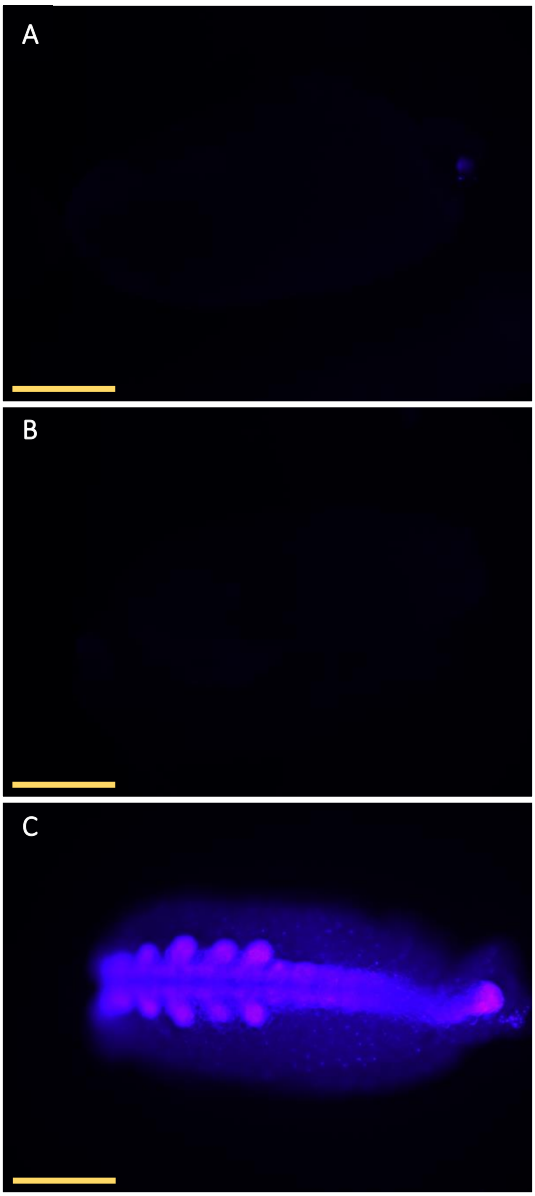

Figure 37. Validation of the wax stripping ethanol methodology in *R. prolixus* embryos.
A) a wild-type embryo; B) an embryo immersed in Hoechst 33342 stain in PBS without wax stripping; C) an embryo treated with ethanol for 5 minutes then immersed in Hoechst diluted in PBS. The embryos were imaged on a Nikon Eclipse Ti2 inverted fluorescent microscope at a magnification of 40x. The micrographs only show blue light exciting the Hoechst 33342 stain at 455nm. The scale bars represent 500µm.

As seen in Figure 37, dewaxing with ethanol facilitates the delivery of Hoechst stain to the entire embryo (45 embryos treated with EC-Hoechst). The control embryos did not exhibit nuclear staining (25 embryos for each control). The artifact present in the wild-type embryo image (Figure 37A) is autofluorescence from a chorion piece remaining from the dissection. The experiment demonstrated that the removal of wax surrounding aeropiles is crucial for successful chemical solution delivery. This experiment was carried out on a single occasion to validate molecule delivery, which once achieved we progressed to validate chemotransfection of DNA constructs.

4. 3. 2. Delivery of a Click-iT™ EdU tagged DNA construct

As wax stripping facilitates the delivery of molecules to *R. prolixus* embryos, validation of DNA construct delivery was needed. We used the Click-iT™ Plus EdU Imaging Kit to tag transfected plasmid DNA following fixation of embryos allowing us to visualise successful delivery to embryonic cells.

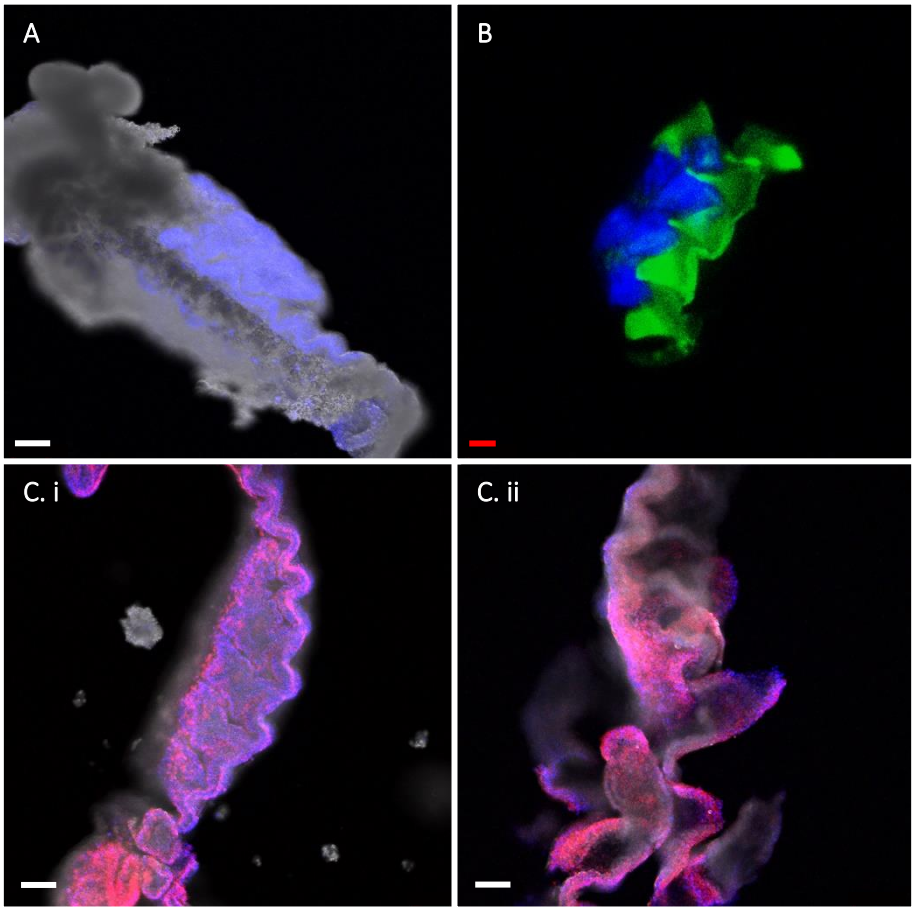

Figure 38. *Rhodnius prolixus* embryos transfected with a DNA construct via an ethanol-chemotransfection methodology.
A) an embryo which was treated with ethanol and stained with Hoechst 33342 after fixation; B) a cluster of cells from an embryo treated with a GFP tagged NASC transfection reagent; C) two embryos transfected with a ^{i}hyPBase plasmid which was tagged and stained using a Click-iT™ Plus EdU Alexa Fluor™ 594 (red) kit (ThermoFisher, UK). All images were taken on a Zeiss LSM880 with Airyscan. Multiple light emission wavelengths were used, for blue light at 405nm, green light at 488nm, red light at 543nm. White scale bars

represent 100µm and the red scale bar represents 10µm. A) and C) were imaged at a magnification of 100x. B) was imaged at a magnification of 630x.

Following transfection and embryo fixation (Sections 4. 2. 4. 1. And 4. 2. 5.) plasmid DNA was tagged with Alexa Fluor™ 594 which is visible as red light excitation during fluorescent microscopy. DNA constructs were successfully delivered to developed *R. prolixus* embryos (20 embryos per treatment). Fluorescent microscopy confirmed ubiquitous uptake of DNA constructs to the developed embryos (Figure 38C). GFP tagged NASC were also delivered without a packaged plasmid and demonstrated high binding efficiencies with cell membranes providing evidence of their ability to deliver packaged DNA (Figure 38B).

We delivered the ^{i}hyPBase plasmid to cells using a novel chemotransfection reagent known as NASC (Figure 38C). This chemotransfection reagent is currently being assessed by Asst. Prof. Francisco Olmo (LSHTM, UK) in several organisms (unpublished data from Asst. Prof. Francisco Olmo). We delivered the ^{i}hyPBase plasmid as it was known to not reduce viability in other insect species (Section 2. 3. 2.) and expressed no fluorescent markers (Section 2. 2. 2.).

The successful delivery of DNA demonstrated here formed the basis of the EC methodology that we would carry forward for further optimisation with alternative chemotransfection reagents (Section 4. 3. 4.) following a viability assay (Section 4. 3. 3.). Therefore this experiment was carried out on a single occasion to validate DNA construct delivery, which once achieved we progressed to survivability experiments

4. 3. 3. Viability assays of ethanol-chemotransfection methodology

Following successful delivery of plasmid DNA, potential toxicity was assessed by a viability assay under multiple treatment conditions recording emergence from embryos. The conditions used were untreated embryos, wax stripping with ethanol immersion for 5 minutes (Ethanol), the NASC-based EC methodology without a plasmid (NASC), and NASC-EC transfecting embryos with the piggyBac based pHome-T and ^{i}hyPBase plasmids in combination (pHome-T). pHome-T transfections were carried out over fifteen rounds due to availability of eggs. At least one untreated control embryo was present for each of these experimental rounds.

Ethanol treatment does not significantly reduce viability of embryos (Table 9). treatment with the NASC reagent appeared to increase viability in embryo by 30%. EC with the pHome-T plasmid appeared to reduce the viability of embryos by 40-70%. A low embryo numbers were used in this experiment, however, further transfection experiments showed similar results (Section 5. 3. 3.).

Emerged pHome-T transfected nymphs were screened for the presence of fluorescence, none was observed.

Table 9. Survivorship following the ethanol-chemotransfection methodology in *R. prolixus* embryos.

Treatment	No. of embryos treated	No. of hatched nymphs	Survivorship rate
Untreated	28	17	60.7%
Ethanol	30	18	60.0%
NASC	43	39	90.7%
pHome-T	246	51	20.7%

4. 3. 4. Chemotransfection of GFP expressing DNA constructs

To further confirm the EC methodology, transfection of plasmids containing fluorescent expression markers (GFP) was performed. Ac5-STABLE1-neo (addgene #32425) is a transient expressing plasmid using the *Actin5c* promoter for eGFP expression (278). Ubiq-Cas9.874W (addgene #112686) is a piggyBac based plasmid for genomic integration of a cassette at semi-random location which expresses GFP under the ubiquitous *Ubi-63E* promoter (183). The ^{i}hyPBase plasmid which expresses a hyperactive helper transposase, was transfected with the Ubiq-Cas9.874W to facilitate integration of the expression cassette into the genome. Due to the potential toxicity of plasmid DNA seen in the survivorship assessment (Table 9), we decided to dissect and image embryos 72 hours post transfection.

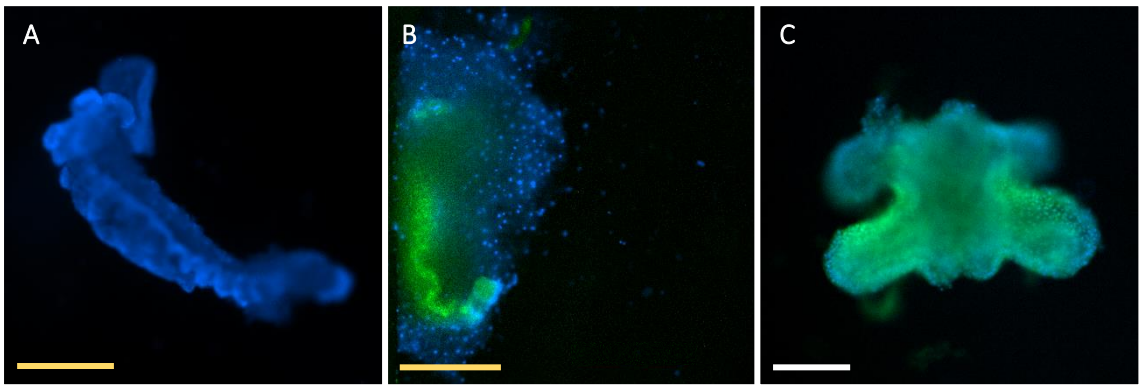

Figure 39. *Rhodnius prolixus* embryos transfected with transient and integrative plasmids.
A) an untreated embryo. B) an embryo transfected with Ac5-STABLE1-neo (addgene #32425) expressing GFP. C) an embryo transfected with Ubiq-Cas9.874W (addgene #112686) and an ^{i}hyPBase helper plasmid expressing GFP. A) and B) were imaged at 40x magnification. C) was imaged at 200x. Emission wavelengths of 460nm (blue) and 530nm (green) were used to capture these images. All micrographs were taken on a Nikon Eclipse Ti2 inverted fluorescent microscope. Scale bars with a white colour represent 100µm and yellow scale bars represent 500µm.

Expression of GFP was observed for both the transient Ac5-STABLE1-neo plasmid (Figure 39B) and the integrative Ubiq-Cas9.874W (Figure 39C). For this experiment two further chemotransfection

reagents were also validated. For the Ac5-STABLE1-neo, Cellfectin® II was used (Section 4. 2. 4. 2.), and FlyFectIN™ was used for the Ubiq-Cas9.874W transfections (Section 4. 2. 4. 3.). These results, validate the EC methodology for transfection of plasmid DNA to *R. prolixus* embryos. To my knowledge this is the first recorded evidence of a transfection within triatomine bugs with plasmid DNA. The expression of GFP in the Ubiq-Cas9.874W transfected embryos does not confirm genome integration as transient expression could be occurring. To validate integration into the genome sequencing confirmation via inverse PCR could be attempted (355,357,358). The EC technique overcomes an important barrier for the delivery of gene editing constructs to triatomine bugs.

4. 4. Discussion

In this chapter we demonstrate a novel transfection methodology for *R. prolixus* embryos with successful delivery and expression of DNA constructs. In comparison with microinjection approaches this methodology is easy-to-use, rapid, and has comparable survivorship rates. The results here provide the basis for future genetic modification research in triatomine bugs.

Initial validations with Hoechst 33342, provided evidence of chemical delivery to embryos past the vitelline and plasma membranes. We showed uniform ubiquitous fluorescence following delivery, however, Bomfim *et al.,* showed an increase in delivery when Hoechst was diluted in ethanol (389). We diluted Hoechst in PBS to mimic the delivery methods required for NASC chemotransfection reagent which is degraded in ethanol. Other chemotransfection reagents such as Lipofectamine™ are not damaged in the presence of ethanol (403). Delivery of packaged plasmids in ethanol would reduce the time taken to transfect embryos and reduce damage done by manual handling during washing stages. The toxicity of ethanol appears to be minimal as the viability of ethanol control embryos was not significantly reduced from the non-treated controls (Table 9). Given more time and resources, we would conduct assessments on multiple chemotransfection reagents (such as Cellfectin® II, FlyFectIN™, Lipofectamine™ 3000) in the absence and presence of ethanol to compare both transfection efficiencies and viability.

We achieved successful transfection with multiple chemotransfection reagents. This validates the EC approach is an effective alternative to microinjection. The use of multiple chemotransfection reagents was due to the varied structure of NASC. As NASC are currently in development, their structure changed multiple times throughout the course of this research. With each structural change the NASC became more efficient and less toxic in standardised cell lines (BSR T7/5 cells, HEK293 cells, and *T. cruzi* CL-Luc:Neon parasites). However, older structures were discontinued and unavailable for us to use for repeating experiments. We had concerns that early experiments may

not be comparable to later NASC transfections. Therefore, for the purpose of this chapter the only NASC results presented were those performed with a single compound structure early on in its development. We subsequently utilised commercial compounds (Cellfectin® II and FlyFectIN™) with stable structures for plasmid transfections. These reagents previously demonstrated reduced transfection efficiencies compared to NASC *in vitro* with mammalian and parasite lines (unpublished data, Olmo *et al*.,). Once NASC are commercially released, they could be assessed for transfection efficiencies with the EC methodology.

EC with all transfection reagents was shown to deliver DNA constructs to whole embryos at both preblastodermal and developed stages. This is key to successful integration of mutations in early cells as partial delivery can cause mosaic mutations to form in G0 progeny (136). Research using microinjection (primarily in mosquitos) shows the expression of inherited traits often occurs in G1 and onwards (201,291). This is due to the successful delivery of traits to germ cells in G0, which will integrate the mutation into at least one chromosome of every G1 cell. If the inherited trait is dominant or homozygous then presentation of the phenotype will occur in all cells. *R. prolixus* are slow to develop, taking 5-6 months to reach adulthood. Backcrossing to achieve ubiquitous expression in G1, would be a lengthy and resource consuming process. Reducing mosaics would therefore reduce the time and resources needed to induce desired traits. In other insects, CRISPR-Cas9 components are typically delivered by microinjection of solutions containing unpackaged DNA/RNA, this potentially reduces transfection efficiencies, increasing the chances of mosaic expression. The ubiquitous transfection seen across all chemotransfection reagents (Figures Figure 38 and Figure 39) using EC, shows the potential of this method to reach early embryonic cells. This would hopefully increase the likelihood of integration into the germline and inherited mutations in G1. A time-course experiment could assess the chances of mosaics forming by dissecting and imaging embryos across multiple time points post transfection with an integrative fluorescent protein plasmid. High resolution imaging of single cells could allow us to estimate the percentage of cells expressing the integrated cassette and link this to the potential for mosaics in the G0 populations. Quantitative PCR of the integrated DNA cassette would also provide a measurement of uptake within the embryos for comparison of transfection reagents but would not allow us to identify if the entire embryo was transfected.

Viability of embryos was comparable or lower to that of microinjection in other insects. With 20.7% of nymphs hatching post plasmid transfection compared to <10% in some insects and 50-90% seen in model insects such as mosquitoes (136,223,300,318). The benefit of this method is its ease to use, low skill barrier and throughput speed. The EC method can transfect ~40 embryos in less than 30

minutes. This is in contrast to microinjection which requires the time consuming lining up of delicate unmelanised embryos on a slide and the level of skill needed to microinject embryos without causing significant mortality (152,319). Tradition microinjection is also not available to insect embryos such as triatomine bugs due to chorion thickness. The loss in viability when pHome-T was transfected could have multiple explanations. Firstly, endotoxins can be found in plasmid solutions following extraction from bacteria. These endotoxins are known to cause loss of viability during transfections of cell lines (404). No previous published research has assessed *R. prolixus'* susceptibility to endotoxins. Secondly, the pHome-T plasmid is a piggyBac based construct which semi-randomly integrates into the genome of transfected cells. This integration could occur within essential genes causing developmental issues. Multiple transfected embryos were observed with delayed or altered development (Appendix 5), which could have reduced their viability. Finally, the insectaries used to rear triatomine bugs at the LSHTM do not have controlled humidity and have fluctuating temperature. Whilst efforts were made to keep a consistent temperature and humidity for all samples, spikes in temperature and dips in humidity often caused contamination or desiccation of embryos. This occurred more frequently in transfected embryos potentially due to the open aeropiles allowing contaminated water droplets or dry air to enter the embryo reducing their viability.

In summary, this novel transfection methodology facilitates the genetic modification of triatomine bugs with a low resource intensive approach. The results in this chapter provide robust evidence of DNA construct delivery and transient expression *in vivo*. With further confirmation (inverse PCR or amplicon sequencing) piggyBac cassette integration could be validated. The EC methodology could easily be adapted to other genome engineering approaches such as CRISPR-Cas9, which is being utilised in other insect orders. This technique could become a vital tool in the understanding of vector-parasite interactions and the development and implementation of GM vector control strategies.

5. Application of a CRISPR-Cas9 system to triatomine bugs (*Rhodnius prolixus*)

5. 1. Introduction

Genome editing in insects has revolutionised the study of functional genomics, especially in understanding the role of genes implicated in the transmission of human disease. For triatomine bugs, the insect vectors of Chagas disease, several studies have focused on reducing expression of genes via RNAi (405–407,388,408,382,409–412). However, to my knowledge, no published literature has provided evidence of genome editing in triatomine bugs. The lack of tools for genetically modifying triatomine bugs limits potential research into their vector-parasite interactions as well as vector control methodologies. In this chapter we aim to address this gap in knowledge and apply our ethanol-chemotransfection methodology (Section 4. 2. 4.) to assess a CRISPR-Cas9 system in the triatomine bug, *Rhodnius prolixus*.

5. 1. 1. CRISPR-Cas9 in Hemiptera insects

Whilst multiple genetic modification (GM) techniques have been applied to insects, CRISPR-Cas9 remains one of the most important, enabling targeted mutations and the insertion of exogenous DNA providing a desired inheritable trait (Section 1. 5.) CRISPR-Cas9 has been widely applied to Diptera, proving its utility in *Drosophila* and mosquitoes (genera including *Anopheles*, *Aedes* and *Culex*) particularly the development of novel insect control strategies for disease vectors (137,158,292,311,330,413). Briefly these strategies have been split into either population replacement or suppression. With replacement strategies focused on the integration of exogenous DNA and/or targeted loss of genes, which reduces their transmission capacity following population uptake (85,201). Population suppression techniques target genes relating to fecundity or mating behaviour (157,291,355). These strategies, whilst highly developed in dipteran model insects are far less common in hemipteran insects.

As the morphology of hemipteran insects differs greatly from Diptera, the development of hemipteran CRISPR-Cas9 methodologies must undergo novel adaptations. Currently, multiple pilot studies have been carried out for the validation of the CRISPR-Cas9 system in hemipteran insects (302). Many hemipteran insects are agricultural pests, this has driven research towards the adoption of CRISPR-Cas9 systems for pest control. To my knowledge, CRISPR-Cas9 gene modifications have been achieved for nine hemipteran insects. These insects are the pea aphid (*Acyrthosiphon pisum),* silverleaf whitefly *(Bemisia tabaci),* brown stink bug *(Euschistus heros),* glassy-winged sharpshooter *(Homalodisca vitripennis),* western tarnished plant bug *(Lygus Hesperus),* brown planthopper *(Nilaparvata lugens),* large milkweed bug *(Oncopeltus fasciatus),* corn planthopper *(Peregrinus maidis),* and European firebug *(Pyrrhocoris apterus)* (138,300,318,377,380,414–417). These were

novel approaches in these insects, focusing on the validation of the CRISPR-Cas9 system by targeting phenotypic genes including *cardinal, cinnabar, stylin-01, white,* and *yellow.* Further studies have investigated biological pathways or potential pest control targets using CRISPR-Cas9 NHEJ. These include the loss of circadian rhythm genes such as *pigment dispersing factor*, which when lost caused *P. apterus* to display nocturnal behaviours due to alterations in photoperiod-dependent diapause induction (138,418). Xue *et al*., targeted the second paralogue of the *insulin receptor* gene in *N. lugens,* inducing reduced wing structures that would limit the insect's ability to search for mates (419). Chen *et al.,* observed the loss of a *cysteine sulfinic acid decarboxylase* gene in *N. lugens* caused reduced fecundity and a loss in viability of embryos (420). These *N. lugens* gene targets could be used for pest control if integrated into a population suppression system such as gene drives (Section 1. 5. 2.). With the development of precise gene editing techniques and further understanding of potential gene targets CRISPR-Cas9 can be utilised for the control of Hemipteran insects.

5. 1. 2. Gene silencing in triatomine bugs

Whilst the genetic modification of triatomine bugs has yet to be achieved in published literature, the silencing of genes to further understand their function has been used across multiple *Reduviidae* species. RNAi knockdown of genes has been the primary tool for the understanding of gene functions in *Reduviidae.* There are two main approaches; for the study of essential biological processes and for identifying potential phenotypic markers for gene editing studies. Genes previously silenced in *R. prolixus* could be targeted for the assessment of CRISPR-Cas9 methodologies or towards the implementation of GM vector control strategies.

Phenotypic genes are often targeted first for proof of principle methodology studies. Initially studies interested in embryo development of *R. prolixus* produced phenotypic mutations via RNAi silencing to gap genes. These include the *giant* gene, which resulted in a lack of gnathal segments and the shortening/fusing of the clypeus and labrum (406). Bugs showing strong *giant* phenotypes had their abdominal segments reduced (11 to 4) with the loss of limbs due to a lack of thoracic segments. The *krüppel* gene was also investigated, with silenced insects exhibiting a loss of thoracic segments, limbs and the fusing of abdominal segments 1-4 (421). As both of these genes are linked to embryonic development, mutations often produce non-viable nymphs due to difficulties emerging from their operculum. When attempting to assess the viability of GM techniques, it is important to create phenotypically distinct viable insects capable of producing offspring. This allows researchers the tracking of mutations across multiple generations. Pigmentation altering phenotypes were often favoured for their increased viability. When inhibited, the *tyrosine hydrolase* gene in the two-

spotted assassin bug (*Platymeris biguttatus)* was able to induce a complete loss of melanisation in 5th instar nymphs (422). Similar approaches have been assessed to target pigmentation in *R. prolixus,* Berni *et al.,* targeted the *aaNAT, cinnabar, ebony, scarlet, tan, white,* and *yellow* genes (410). The *cinnabar, scarlet* and *white* genes produced eye phenotypes (Figure 40A) with *scarlet* being their marker of choice due to a single *scarlet* targeted insect exhibiting no pigment in the ommochromes. This study was able to induce cuticle tanning phenotypes (Figure 40B) with the *aaNAT* and *yellow* genes being chosen as their preferred targets. None of their preferred genes caused reduced fitness or fecundity making them ideal candidates for validation of genetic modifications.

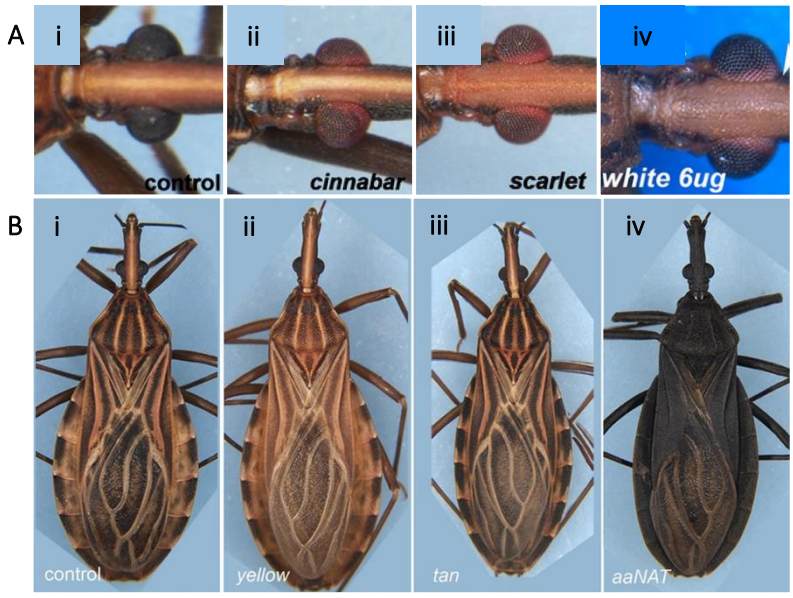

Figure 40. *R. prolixus* adults exhibiting loss of function in phenotypic genes following RNAi injections into 5th instar nymphs.
A) loss of function in eye phenotypic genes. Ai) a wild-type adult. Aii) *cinnabar*. Aiii) *scarlet*. Aiv) *white*. B) loss of function in cuticle tanning genes. Bi) wild-type control. Bii) *yellow*. Biii) *tan*. Biv) *aaNAT*. Figure adapted from (410).

Several genes with potential utility for GM vector control strategies have been identified in *R. prolixus* via RNAi. One of these is the *nitrophorin 2* gene, which when lost, leads to a reduction in anticoagulant in the saliva, limiting their ability to feed, leading to malnutrition (405). A key olfactory *odorant receptor co-receptor* gene (*RproOrco*) was identified and silenced in *R. prolixus*, resulting in a significant reduction in host seeking behaviour (408). In targeting this gene for vector control, we could limit transmission by reducing contact with humans and with further investigation into olfactory genes we could potentially produce populations of insects favouring sylvatic hosts. Several studies have investigated the genes responsible for oogenesis and embryogenesis. Using RNAi approaches and previous research in Diptera, the genetic pathway of oogenesis and embryonic patterning in *R. prolixus* was investigated (411). A novel *Bicaudal-D* gene was discovered to be responsible for the development of the blastoderm post-oviposition. The ovary *ecdysone response* genes were found to decrease the expression of vitellogenin when lost (412). This is an important

protein in the production of embryo chorions, leading to non-viable eggs. Both of these targets are candidates for population suppression systems as they do not reduce adult viability but reduce viable embryo production.

These previously characterised genes give valuable targets for both the validation of a CRISPR-Cas9 system and the potential of vector control strategies. In this chapter, we aim to use the prior hemipteran research as a basis to demonstrate phenotypes following CRISPR-Cas9 modifications within *Rhodnius prolixus*.

5. 1. 3. Aims

The genetic modification of triatomine bugs has not previously been achieved, limiting research into Chagas disease control. We aim to provide evidence of genetically modified *Rhodnius prolixus* insects via CRISPR-Cas9 methodologies to provide a platform for future research. To achieve this, genes would be successfully targeted by the CRISPR-Cas9 NHEJ approach and exogenous DNA will be inserted into their genomes via CRISPR-Cas9 HDR. Achieving this would provide a significant step for the developing of gene editing tools in triatomines for functional studies, such as investigating host vector interactions and Chagas disease transmission blocking targets.

5. 2. Methods

5. 2. 1. *Rhodnius prolixus* genome assembly

The *R. prolixus* genome assembly used to identify gene of interest in this chapter was hosted on VectorBase (320). The genome assembly versions used for this chapter were RproC3.3-5 (423). This assembly was sequenced by the Washington University School of Medicine Genome Sequencing Center (WUGSC, USA) using DNA isolated from the *R. prolixus* colony at the CDC (Atlanta, USA). Utilizing a whole-genome shotgun approach 454 reads were assembled using the CABOG assembler. The assembly is a total of 706.8Mb, with 47,726 contigs, 16,537 scaffolds, and 15,068 protein coding genes. ~20% (144Mb) of the assembly is known to be padding characters.

5. 2. 2. Design and production of CRISPR-Cas9 DNA constructs

5. 2. 2. 1. Rationalisation of gene targets

Genes were screened for their ability to induce a phenotypic change. The rationalisation of which was based on previously published literature following loss of function in dipteran or hemipteran insects. The literature search methodology and orthologue identification followed a similar search pattern to section 3. 2. 1. 2. Target genes previously assessed in hemipteran insects were favoured over dipteran. Due to the slow development of *R. prolixus* (5-6 months) to adulthood, genes expressing wing phenotypes were not selected. Instead, genes likely to elicit a change in 1st instar nymphs were ranked highly.

5. 2. 2. 2. Identification of gRNAs

The identification of gRNAs follows the same methodology as section 3. 2. 1. 3. Initially the ChopChop webtool did not have an *R. prolixus* genome in their system. Therefore, we submitted the RproC3.3 genome assembly to the ChopChop team via their submission method. For the design of HDR constructs only the single central gRNA approach was used (Section 3. 2. 2. 2.). This meant that no gRNAs were designed using the UTR region setting on ChopChop. All other setting selected followed the same methods as outlined in section 3. 2. 1. 3. or Appendix 1

5. 2. 2. 3. pDCC6

Initial transfections of *R. prolixus* embryos were carried out with the bicistronic CRISPR-Cas9 plasmid pDCC6 (addgene #59985). These transfections targeted the *white* gene by incorporation of identified gRNAs (Section 5. 3. 1.) using the Golden Gate Assembly method (Section 3. 2. 2. 1.). Following transfection, a phenotypic change was visible, but genetic confirmation provided no evidence of mutations. Genetic confirmation was carried out on pooled populations, which could have diluted

positive results to non-traceable levels (Section 3. 4. 1.). Due to this and lack of mutations in sand fly cell lines (Section 3. 3. 1. 1.), it was theorised the *D. melanogaster U6-2* promoter may be causing reduced expression of CRISPR RNPs. The U6 promoter was replaced with an endogenous *R. prolixus* promoter following methods found in section 3. 2. 2. 1. The sequence of the endogenous promoter can be seen in Figure 41. The primers used for the Gibson Assembly® kit can be found in Appendix 6. This new DNA construct was named *Rpro*-pDCC6. All further gRNAs used in HDR insertion were incorporated into the *Rpro*-pDCC6 construct using the Golden Gate Assembly method described in Section 3. 2. 2. 1.

```
>Dmel-U6-2 (FBgn0266758)
GTTCGACTTGCAGCCTGAAATACGGCACGAGTAGGAAAAGCCGAGTCAAATGCCGAATGCAGAGTCTCATTACA
GCACAATCAACTCAAGAAAAACTCGACACTTTTTTACCATTTGCACTTAAATCCTTTTTTATTCGTTATGTATA
CTTTTTTTGGTCCCTAACCAAAACAAAACCAAACTCTCTTAGTCGTGCCTCTATATTTAAAACTATCAATTTAT
TATAGTCAATAAATCGAACTGTGTTTTCAACAAACGAACAATAGGACACTTTGATTCTAAAGGAAATTTTGAAA
ATCTTAAGCAGAGGGTTCTTAAGACCATTTGCCAATTCTTATAATTCTCAACTGCTCTTTCCTGATGTTGATCA
TTTATATAGGTATGTTTTCCTCAATACTTCGTTCTTGCTTCGGCAGAACATATACTAAAATTGGAACGATACAG
AGAAGATTAGCATGGC

>Rpro1 (RPRC017522)
GTTGTTCTTACTGTGGGAAAATCCATTGTGAAGTAAAAAGAAATCACTAACACTAGAACAGACGAGTGGAAAAG
TAGAAATGGCTGTTTCTGGGTAAACTCATTATCGTAACAAATGTGTTCTCCTTGAGAATTGGTTATTTTTTTTC
ATGGTCAAAACTAATGCAATGTTAGCTTAGTTTGAGATAACAACTTGAGAATCTGTAAGAATCAAATTTATTCA
TTTTGATACAGCAAGCTCTATAATTTAAATTTAATATTAGAATCTCTCACAAGTTTAGATTATTTATTTTTTTT
AATTATAATATCCCTAAATTTGCCAAAAAAAACAATAAAAAATATTATTTTACATTTTTGTGCCTAAAGATAAC
TATATAAGCCAGAAAAAATCTCTTCTAGCTGTACTCGCTTCGGCGGTACATATACTAAAATTGGAACGATACAG
AGAAGATTAGCATGGC
```

Figure 41. Sequences for the replacement of the *D. melanogaster U6* promoter in pDCC6 with the endogenous promoter from *R. prolixus*.
Gene IDs for locating the U6 gene are in brackets above the sequences. Green text highlights the pol III proximal sequence element A (PSEA), and the red text highlights the TATA box.

5. 2. 2. 4. pDsRed-Ubi63e-attP

The pDsRed-*Ubi63e*-attP construct was used for the expression of a donor DNA cassette required for CRISPR-Cas9 HDR editing of the *R. prolixus* genome. This construct was adapted from pDsRed-attP (addgene #51019) to incorporate a ubiquitin promoter for DsRed expression following the Gibson Assembly® methods outlined in section 3. 2. 2. 2. If successfully incorporated into the genome the DNA cassette will express DsRed-Express, a fluorescent marker visualised in red wavelengths of light.

The HDR approach taken in this chapter utilised a single central gRNA from the target phenotypic gene. This approach utilizes the genomic sequence 800bp upstream and downstream of the gRNA sequence to design homology arms (HA). These were incorporated into pDsRed-Ubi63e-attP following the Gibson Assembly® protocols found in section 3. 2. 2. 2. (Figure 422A). When successfully transfected into *R. prolixus* embryos, the HAs will guide the cells to repair broken genomic DNA with the DNA cassette at the gRNA site (Figure 42B).

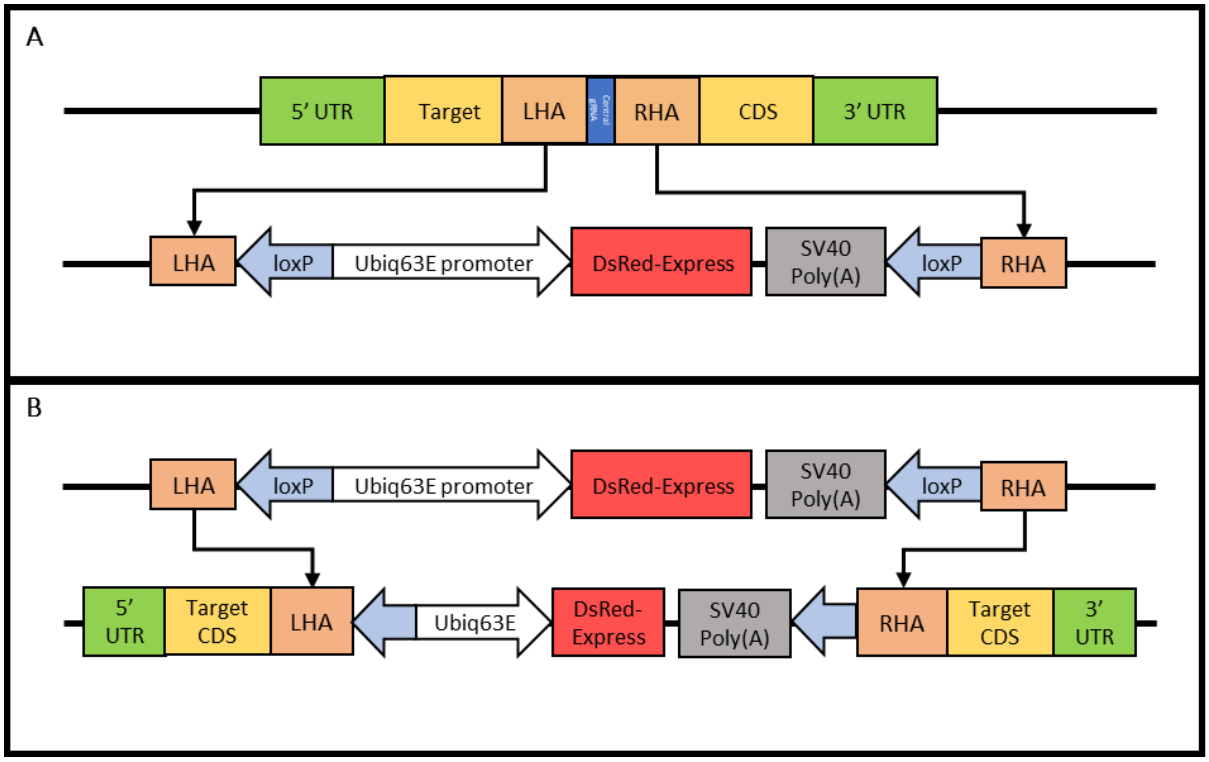

Figure 42. The design and methodologies utilized by the pDsRed-*Ubi63E*-attP plasmid for *R. prolixus* CRISPR-Cas9 HDR transfections.
A) homology arms are amplified from the target gene's coding sequence, surrounding a central gRNA. These homology arms are incorporated into the pDsRed-*Ubi63E*-attP plasmid forming the 5'/3' ends of the HDR DNA cassette. B) the DNA cassette in pDsRed-*Ubi63E*-attP is integrated into the genome using the homology arms as a guide following a double strand break at the gRNA site. This divides the gene's coding sequence, causing loss of function to the desired gene.

5. 2. 3. Delivery of DNA constructs to *R. prolixus* embryos

Delivery of DNA constructs to *R. prolixus* embryos was performed following the methods outlined in section 4. 2. 4. All embryos were treated between 1-4 hours post oviposition. The chemotransfection reagents used were CellFectin® II, FlyFectIN™, and NASC. Our sand fly *in vitro* transfections indicated that there was no significant difference in chemotransfection reagent efficiencies (Section 2. 3. 1.). The transfection reagent used was based on availability at the time. Details of which reagent and constructs were used for each experimental run can be found in the results tables Table ***11*** and Table ***12***.

Following transfection, eggs were initially mounted in putty adhesive in a 9cm petri dish containing a sterile saline wipe to maintain humidity. However, following multiple batches of treated embryos desiccating or becoming contaminated during incubation, the adhesive putty was replaced with a 5cm petri dish within the 9cm petri dish for HDR based transfections (Section 5. 3. 3.).

5. 2. 4. Confirmation of CRISPR-Cas9 genome modification

5. 2. 4. 1. Imaging of 1st instar nymphs

Following transfection, emergent 1st instar nymphs were screened for loss of phenotypic genes under an Olympus SZ51 stereo microscope (Olympus, Japan). Images were captured for all transfected nymphs potentially expressing a pigment phenotype (*aaNAT, white* and *yellow*) and were only taken when a phenotype was visually observed for those targeting *eyeless* and *krüppel*. Images were taken using an iPhone 12 Pro camera (Apple, USA) mounted to the microscope with a Celestron NexYZ™ smartphone adapter (Celestron, USA) at 40x magnification. Nymphs were imaged in a glass petri dish under a 22mm diameter #1.5 thick glass cover slip to restrict movement.

For screening of DsRed-Express expression following transfection of HDR constructs, nymphs were placed into an uncoated µ-Dish glass coverslip imaging dish (Ibidi, Germany) and were covered with a 22 mm diameter #1.5 thick glass cover slip. The nymphs were screened for red fluorescence (Ex λ 554nm) on a Nikon Eclipse Ti2 inverted fluorescent microscope (Nikon, Japan).

All imaging occurred 48-96h post emergence and was compared to wild-type (WT) nymphs which were oviposited in the same batch as the treated embryos.

5. 2. 4. 2. Mean grey scale analysis

Following image capture, a mean grey scale analysis (MGA) was performed for the nymphs which would demonstrate a pigment change following mutation (*aaNAT* and *yellow* targeted) in terms of light intensity. For each MGA, wild-type nymphs from the same oviposition collection were also analysed. The analysis was carried out using the Fiji package for the ImageJ software (424). Regions of interest (ROI) were initially identified on a wild-type insect then placed in the corresponding location on all analysed nymphs. The ROIs were then measured for mean grey scale value (MGV, measured in arbitrary units, a.u.), as well as minimum and maximum grey scale values (a.u.). Scatter plots for the MGVs were produced using GraphPad Prism software (version 9.5.1; GraphPad, USA). The data was analysed for significance using GraphPad Prism by an unpaired t-test reporting two-tailed P values. A P-value of 0.05 was used as the threshold for statistical significance throughout the analyses.

ROI identification was carried out in two different ways (Figure 43). For the MGA of all imaged *aaNAT* and *yellow* targeted nymphs ROI's were placed on different dorsal areas including the head, thorax, tergite 3, and tergite 7 (Figure 43A). For the MGA of the *yellow 1* nymph, four ROIs covering

the majority of the surface area of the turga were selected (Figure 43B). Images of all ROIs analysed can be found in Appendix 6.

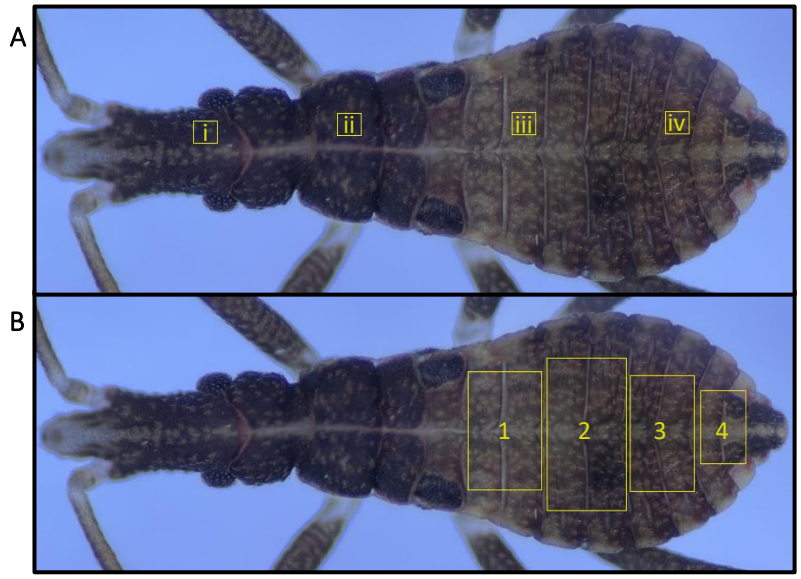

Figure 43. Regions of interest (ROI) selected for mean grey scale analysis (MGA).
A) the ROIs analysed for the *aaNAT* and *yellow* MGA. i) head. ii) thorax. iii) tergite 3. iv) tergite 7. B) the ROIs analysed for the MGA of the *yellow 1* nymph.

5. 2. 4. 3. Molecular confirmation of CRISPR-Cas9 mutations via NHEJ

Following phenotypic screening the genomic DNA of nymphs was collected using the Monarch® Genomic DNA Purification Kit (New England biolabs, USA) as per the manufacturers protocol. Nymphs exhibiting a suspected phenotype were isolated and genomic DNA was extracted individually. Remaining nymphs not visually demonstrating a phenotypic change were pooled in batches up to 10 for genomic DNA extraction.

To confirm mutations in the target gene the gRNA region was amplified via PCR using the Phusion® High-Fidelity PCR Kit (New England Biolabs, USA) with the confirmation primers found in Appendix 6 (Section 3. 2. 4. 4.). Amplified alleles of the expected size were sequenced via Sanger sequencing conducted by GeneWiz® (Azenta Life Sciences, Germany). Sequences were screen for mutations at the predicted gRNA cut site by the algorithmic deconvolution analysis tool Synthego ICE Analysis tool v3 (Synthego, USA). The detailed methodologies of ICE analysis are found in section 3. 2. 4. 6.

5. 2. 4. 4. Molecular confirmation of CRISPR-Cas9 mutations via HDR

Following phenotypic screening of emerged nymphs, genomic DNA was extracted with the Monarch® Genomic DNA Purification Kit (New England biolabs, USA) using the manufacturers protocol. Nymphs with a visible phenotype due to loss of gene function or expression of DsRed-

Express were isolated and genomic DNA was extracted individually. Nymphs with no obvious phenotypic change were pooled in groups of up to 20 for genomic DNA extraction.

To confirm integration of exogenous DNA into the target site two PCR approaches were taken. Amplification of the gRNA site with primers 100-200bp upstream/downstream of the HAs were used. If successful integration occurred, this would result in amplified alleles of ~5,000bp, compared to wild-type alleles of around ~2,000bp. The alternate amplification method used a primer within the DNA cassette just upstream of the 3' end, with the second primer placed 100-200bp downstream of the right HA. This amplification method was predicted to amplify an allele of ~1300bp in genomic DNA with integration of exogenous DNA at the correct site. PCR amplification was carried out using the Phusion® High-Fidelity PCR Kit (Section 3. 2. 4. 4.), using primers for both approaches found in Appendix 6. Amplified alleles of the expected size were sequenced via Sanger sequencing conducted by GeneWiz® (Azenta Life Sciences, Germany). Sequences were screened for the correct genomic location and DNA cassette sequence at both the 5' and 3' ends.

5. 3. Results

5. 3. 1. Identification and rationalisation of target genes

Using previously published literature phenotypic genes were identified and assessed for mutations in *R. prolixus* based on a morphological change to the nymphal stages of triatomine bugs. Phenotypic changes affecting body development, cuticle tanning, and eye pigmentation were favoured over wing or sexual organ phenotypes due to nymphs lacking wings or developed genitalia. Once phenotypes were selected, putative genes were identified in the *R. prolixus* genome via orthologue searches assessing their amino acid sequence alignment, conserved functions, and paralogues to estimate loss of function causing a phenotypic change. Target genes were taken forward to gRNA assessment if amino acid sequences were conserved with the model organism's orthologue, and they had no known functional paralogues. Target genes selected for CRISPR-Cas9 transfections and the gRNA sequences used can be found in Table 10.

The gene (*kr*) encodes a zinc finger transcription factor that in *D. melanogaster* is responsible for the formation of the thoracic and anterior embryonic segments and Malpighian tubules (425). Loss of function for *krüppel* has been researched in a number of insect species (*Gryllus bimaculatus, O. fasciatus, R. prolixus* and *Tribolium castaneum*) with similar results (421,426–428). These studies showed variation in phenotypic effect, with one *G. bimaculatus* orthologue of *Drosophila krüppel* gene forming only a single thoracic segment and a significantly reduced abdomen following loss of function (426). In *T. castaneum*, an orthologue altered eve stripe formation past the 5th stripe

causing a reduction and loss of jaw segments (428). Most importantly in the context of this chapter, loss of the *krüppel* gene in *R. prolixus* following RNAi injections, caused reduced formation of the thoracic and abdominal segments resulting in lost limbs and Malpighian tubule formation (421). We rationalise that *krüppel* is viable candidate for CRISPR-Cas9 mutations for this chapter.

The yellow gene was selected as a viable target due to its involvement in the formation of black melanin (309). As previously mentioned (Section 3. 3. 1. 1.), *yellow* is involved in the formation of long cuticular hydrocarbon molecules which form the dark pigmentation of melanin (308). The yellow gene has previously been validated as a phenotypic marker in many insect species including the hemipteran insects *E. heros, Pl. biguttatus, O. fasciatus and R. prolixus* (318,422,429,410). Another gene known to be involved in the cuticle tanning pathway is *aaNAT* (430). This gene codes arylalkylamine-N-acetyltransferase (aaNAT), which catalyses the conversion of dopamine to N-acetyl dopamine (NADA), the precursor to colourless sclerotin. If the *aaNAT* is lost sclerotin hardens with a dark, almost black colour, as reported in multiple insects such as *Bombyx mori, Periplaneta americana, Pl. biguttatus,* and *R. prolixus* (383,422,429,431). Both of the *yellow* and *aaNAT* genes have been assessed in *R. prolixus* via RNAi knockdowns (383). When gene function was lost, both these genes induce an obvious phenotypic change, as such they were selected as candidates for assessment of our CRISPR-Cas9 methodologies.

Finally, two eye-specific phenotypic genes were selected for assessment of the CRISPR-Cas9 approach, these were the *eyeless* and *white* genes. As previously described (Section 3. 3. 1. 1.), the *eyeless* gene encodes a Pax6 homologue required for protocerebrum and eye development (315). The *white* gene, encodes an ATP-binding cassette guanine transporter, which is vital in the transport of ommochromes to the eyes of insects (342,343). The phenotypic nature of these genes has been investigated in *Drosophila spp*. as well as being functionally conserved in hemipteran insects such as *N. lugens* and *T. castaneum* (415,432).

Following selection of candidate genes, gRNAs were designed favouring high predicted 'knockout' efficiencies (Table 10). These were then incorporated into the pDCC6 plasmid for CRISPR-Cas9 transfections. Multiple targets selected for CRISPR-Cas9 HDR assessment, had homology arms designed and incorporated into pDsRed-*Ubi63e*-attP plasmids for HDR genome integration of exogenous DNA (Table 10).

Table 10. *R. prolixus* genes selected for editing via CRISPR-Cas9.
Red gRNA sequences were used in NHEJ based CRISPR-Cas9 constructs. Green gRNA sequences were used in HDR based CRISPR-Cas9 approaches.

Common name	Function	Reference gene	*R. prolixus* orthologue	*R. prolixus* gRNA sequence	Relevant references
eyeless (ey)	A Pax6 homolog, required in the development of insect eyes and the protocerebrum.	FBgn0005558	RPRC003362	AGTGGTGTGAACCAACTGGG	(315)
krüppel (kr)	Involved in the segmentations of embryos and the formation of Malpighian tubules.	FBgn0001325	RPRC000102	AGACACCTAAGGGTACACAC	(421,425)
aaNAT (aN)	Important in the production of arylalkylamine-N-acetyltransferase which leads to colourless sclerotin.	FBgn0287831	RPRC015310	ATATATTTAGAGGCTCATCG	(383)
white (w)	Required for the transport of brown pigment precursors in the eye.	FBgn0003996	RPRC012709	GCCAGCGTTTTAGCATTCAC	(342,343)
yellow (y)	Required for the formation of melanin in cuticle cells.	FBgn0004034	RPRC005424	ATTAAAAGGTGATTTCAACG	(309,383)

5. 3. 2. Assessment of the CRISPR-Cas9 NHEJ approach in *R. prolixus*

Initially to validate CRISPR-Cas9 modifications in *R. prolixus*, the NHEJ based pDCC6 plasmid was used to target the *white* gene (RPRC012709). The pDCC6 plasmid used in the NHEJ-based transfections contained the *Dmel*-U6-2 promoter for gRNA expression. Transfection with the *w*-pDCC6 was performed by the ethanol-chemotransfection (EC) methodology using NASC as the chemotransfection reagent (Section 4. 2. 4. 1.). Phenotypes were screened 48 hours post emergence.

Table 11. *In vivo* CRISPR-Cas9 NHEJ transfection conditions and survivorship in *R. prolixus*.

Gene targeted	Plasmid for transfection	Chemotransfection reagent	# of embryos treated	# of nymph emerged	Survival rate (%)
Negative control	N/A	N/A	22	19	86.36
white	DmelU6-pDCC6	NASC	838	84	10.02

As seen in Table 11, 10.02% of transfected embryos emerged. Nymphs were screened by stereomicroscopy for phenotypic changes to eye pigmentation. One nymph (*w6*) presented a light pigment around the edge of the eyes (Figure 44). At the time of assessment, we were unsure this was a sign of a *white* mutation, so, *w6* was pooled with other insects for molecular analysis.

Figure 44. *R. prolixus* 1st instar nymph (*w6*) exhibiting a putative phenotypic change following mutations to the *white* gene (RPRC012709) via CRISPR-Cas9 transfection.
A) a wild-type *R. prolixus* nymph. B) a nymph presenting a putative eye phenotype. Both nymphs were imaged 48 hours post emergence. Images were taken using an Olympus SZ51 microscope at 40x magnification. The scale bars represent 500µm.

For molecular analysis, genomic DNA was extracted in pools of up to 10 insects (8 extractions of n=10 insects, one extraction of n=4 insects). The gRNA region was amplified by PCR and sequenced via Sanger sequencing to screen for mutations (Sections 3. 2. 4. 4 & 3. 2. 4. 5.). Sequencing chromatograms showed no evidence of mutations around the CRISPR-Cas9 cleavage site in any pooled sample. To further assess this the sequences were analysed with the ICE webtool. This analysis also showed no evidence of indels in the pooled samples (Figure 45).

Figure 45. ICE analysis graphical output for a pool sample of *R. prolixus* nymphs (including *w6*) transfected with CRISPR-Cas9 plasmids targeting the *white* gene (RPRC012709).

A) the text output for the ICE analysis, where; Indel % represents the percentage of alleles present in the sample with indels compared to a wild-type control sample; KO-score represents the percentage of indels found that would cause loss of function in the target gene; R2 is a model fit estimation. B) the trace file output from the ICE analysis focusing on the predicted cut site from the target gRNA in both the mutated sample and wild-type control.

5. 3. 3. CRISPR-Cas9 mutations in *R. prolixus* via the HDR approach

Following positive results with sand fly transfections (Section 3. 3. 2.), further transfections with *R. prolixus* embryos were performed utilising a novel endogenous *U6* promoter within the pDCC6 plasmid. The novel *Rpro*-pDCC6 plasmid was transfected in tandem with the HDR based pDsRed-*Ubi63E*-attP plasmid. The HDR approach was assessed for 4 target genes *eyeless*, *krüppel*, *aaNAT*, and *yellow*. As *white* gene mutations were theorised to be a minimal change, we decided not to target the gene for HDR.

Table 12. *In vivo* CRISPR-Cas9 HDR transfection conditions and survivorship in *R. prolixus*.

Gene targeted	Plasmid for transfection	Chemotransfection reagent	# of embryos treated	# of nymph emerged	Survival rate (%)
Negative control	N/A	N/A	131	100	76.34
eyeless	*ey-Rpro*-pDCC6 + *ey*-pDsRed-*Ubi63E*-attP	Cellfectin® II	198	69	34.85
krüppel	*kr-Rpro*-pDCC6 + *kr*-pDsRed-*Ubi63E*-attP	Cellfectin® II	119	40	33.61
aaNAT	*aN-Rpro*-pDCC6 + *pro*-pDsRed-*Ubi63E*-attP	FlyFectIN™	278	12	4.32
yellow	*y-Rpro*-pDCC6 + *y*-pDsRed-*Ubi63E*-attP	Cellfectin® II	121	20	16.53

For the transfections of HDR based transfections, NASC availability and consistency was uncertain, therefore, chemotransfection reagents Cellfectin® II and FlyFectIN™ were used for transfections (Table 12). Survivorship rates increased Cellfectin® II where 29.45% of the transfect nymphs emerged. Whilst only 4.32% of FlyFectIN™ transfected embryos emerged.

Emerged nymphs were screened by microscopy for phenotypic changes relating to the target gene and also presence of the DsRed-Express fluorescent marker. Phenotypic mutations were not

observed for nymphs targeted for *eyeless* or *krüppel* mutations. As pigment changes can be subtle images of *aaNAT* and *yellow* targeted nymphs were analysed via MGA to infer a pigmentation change over wild-type standards. Due to alterations in microscopy conditions and image quality, the data was split into screening sessions as well as combined for each targeted gene.

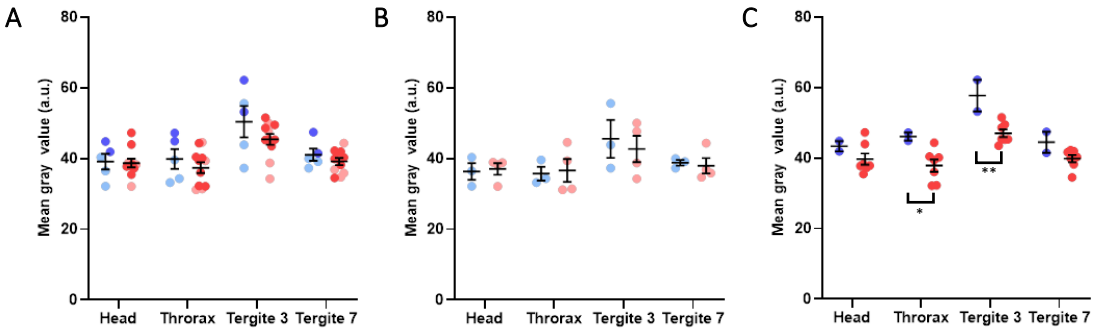

		Wildtype			aaNAT			
		Mean	SEM	N	Mean	SEM	N	P value
Combined data	Head	39.15	2.21	5	38.73	1.20	11	0.8587
	Thorax	39.86	2.78		37.40	1.52		0.4141
	Tergite 3	50.43	4.41		45.45	1.55		0.1976
	Tergite 7	41.08	1.73		39.16	1.00		0.3254
Session 1	Head	36.33	2.37	3	37.05	1.66	4	0.8068
	Thorax	35.72	1.97		36.64	3.26		0.8356
	Tergite 3	45.59	5.36		42.69	3.71		0.6643
	Tergite 7	38.81	0.79		37.96	2.17		0.7625
Session 2	Head	43.37	1.46	2	39.69	1.61	7	0.2905
	Thorax	46.07	1.16		37.84	1.72		0.0463*
	Tergite 3	57.71	4.50		47.03	1.10		0.0077**
	Tergite 7	44.48	2.98		39.84	1.03		0.0941

Figure 46. Confirmation of a phenotypic change in *R. prolixus* nymphs via a grey scale analysis following mutations in the *aaNAT* gene.
The graphs show the mean grey value of four ROIs on the dorsal side of nymphs. A) combined data from screening sessions 1 (pale blue and red) and 2 (dark blue and red). B) screening session 1. C) screening session 2. Data points corresponding to wild-type nymphs are in blue. Potentially transfected nymphs are in pink/red. Error bars provide standard error of the mean (SEM). The table shows the mean values, SEM, N value and P values when compared to wild-type controls. Results are expressed as mean (black line). P-values (two-tailed t-test) are expressed as *P < 0.05, **P < 0.01, ***P < 0.001, ****P < 0.0001.

The MGA for aaNAT target nymphs presented a significant difference in light intensities for insects imaged in session two on the thorax (P= 0.0463) and tergite 3 (P= 0.0077) (Figure 46C). In session 2, the average MGV of treated nymphs trended towards a darker light intensity over wild-types. Showing decreases of mean light intensity of 3.68% for the head ROI, 8.23% for the thorax ROI, 10.68% for the tergite3 ROI, and 4.64% for the tergite 7 ROI. This trend is supportive of mutations in

multiple insects following CRISPR-Cas9 transfections targeting the *aaNAT* gene. No significant difference in light intensity was observed in insects imaged in session 1.

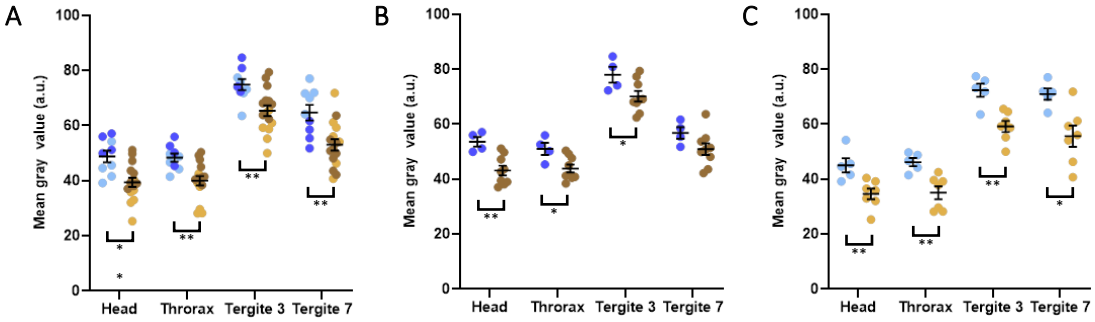

		Wildtype			Yellow			
		Mean	SEM	N	Mean	SEM	N	P value
Combined data	Head	48.85	2.14	9	39.43	1.66	16	0.0022**
	Thorax	48.36	1.48		40.02	1.68		0.003**
	Tergite 3	74.90	2.00		65.37	1.95		0.0043**
	Tergite 7	64.71	2.85		53.01	2.07		0.0028**
Session 1	Head	53.59	1.77	4	43.15	1.74	9	0.0041**
	Thorax	51.05	2.23		43.87	1.44		0.0193*
	Tergite 3	78.01	2.89		70.17	1.93		0.0454*
	Tergite 7	56.87	2.12		50.95	2.13		0.1214
Session 2	Head	45.05	2.55	5	34.65	1.92	7	0.0077**
	Thorax	46.21	1.50		35.06	2.31		0.0043**
	Tergite 3	72.40	2.41		59.20	2.02		0.0018**
	Tergite 7	70.99	2.07		55.66	3.84		0.0109*

Figure 47. Confirmation of a phenotypic change in *R. prolixus* nymphs via a grey scale analysis following mutations in the *yellow* gene.
The graphs show the mean grey value of four ROIs on the dorsal side of nymphs. A) combined data from screening sessions 1 (dark blue and brown) and 2 (pale blue and yellow). B) screening session 1. C) screening session 2. Data points corresponding to wild-type nymphs are in blue. Potentially transfected nymphs are in brown/yellow. Error bars provide standard error of the mean (SEM). The table shows the mean values, SEM, N value and P values when compared to wild-type controls. A * symbol refers to the level of significance. Results are expressed as mean (black line). P-values (two-tailed t-test) are expressed as *P < 0.05, **P < 0.01, ***P < 0.001, ****P < 0.0001.

The MGA on *yellow* targeted nymphs presents highly significant changes in light intensity across almost all ROI (session 1, tergite 7 showed no significance) (Figure 47A). Unfortunately, the trend of this data presents MGVs showing lower light intensities inferring the transfected nymphs are darker than the wild-types. This is evident from mean light intensities decreasing at a range of 10.41-15.32% for session 1, and 5.92-10.45% for session 2.

Due to this unexpected trend we decided to select images with nymphs that were visually lighter in colour and run separate MGAs on the selected nymphs. A single *yellow* targeted nymph (*y1*) presented reduced pigment in its abdomen visually (Figure 48A). This nymph was reanalysed via MGA to focus on the surface are of the terga. The results of this compared to the four wild-type

nymphs imaged in the same session resulted in a 6.69% increase in light intensity over the four ROI (Figure 48D). However, the *y1* nymph did not show fluorescence when imaged under fluorescent microscopy. None of the treated nymphs for any of the gene targets showed evidence of DsRed-Express expression under fluorescent microscopy.

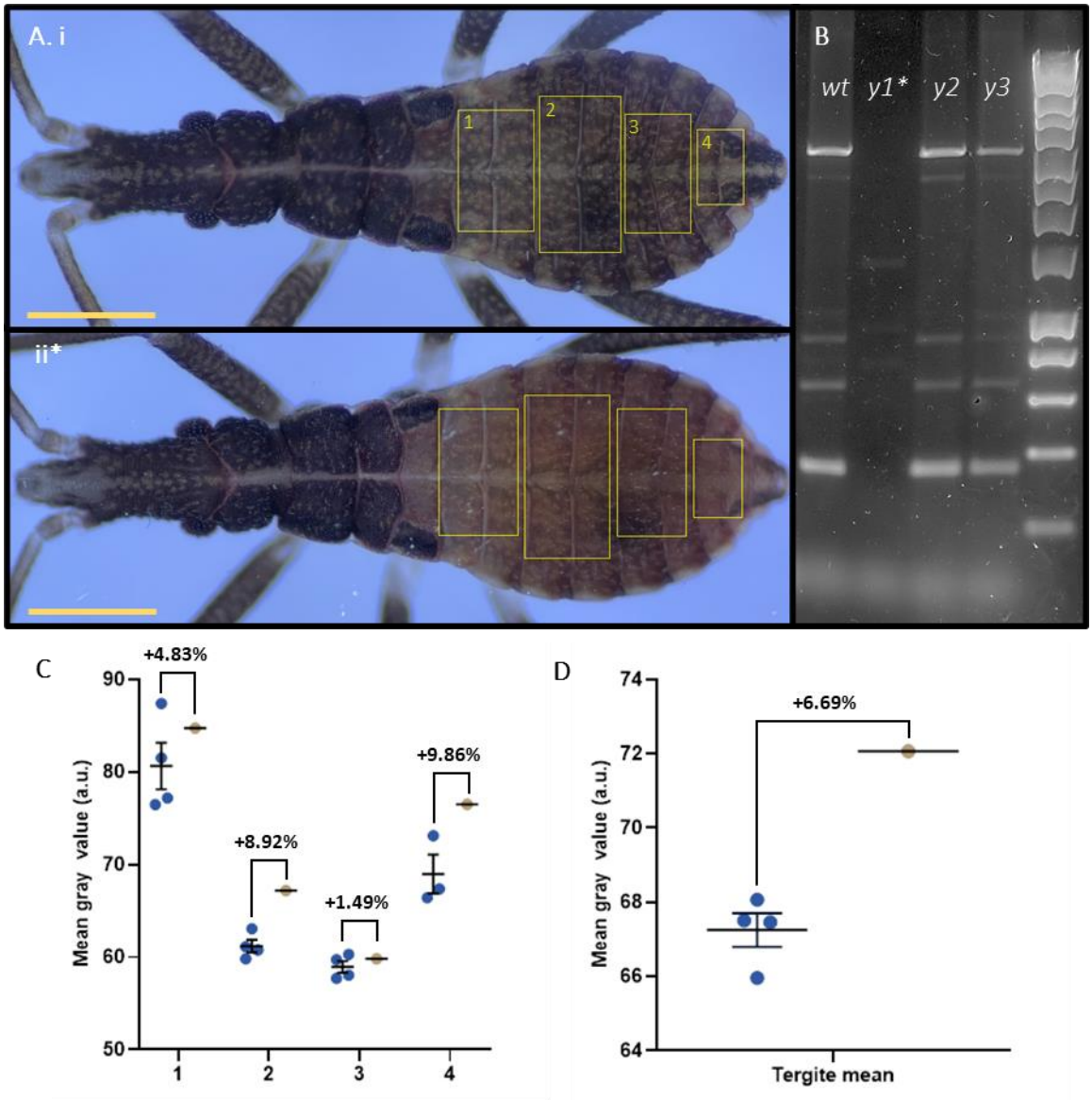

Figure 48. Confirmation of a mutation to the *yellow* gene (RPRC005424) via CRISPR-Cas9 HDR transfection in a *R. prolixus* 1st instar nymph.
Ai) a wild-type *R. prolixus* nymph. Aii) a transfected nymph presenting a cuticle tanning phenotype. Both nymphs were imaged 96 hours post emergence. Images were taken using an Olympus SZ51 microscope at 40x magnification. The scale bars represent 500µm. The yellow boxes show the ROIs selected for mean grey scale analysis. B) PCR amplification of the right homology arm region following HDR insertion. If HDR insertion has occurred a band of 1,285bp would be seen. The 1,285bp allele will not amplify in wild-type DNA. A Meridian bioscience HyperLadder™ 1kb was used in the gel. The * symbol signifies the PCR sample matches the nymph in the microscopy image. C) mean grey scale analysis for y1 (yellow) against four wild-type nymphs (blue) using the four ROIs seen in A. D) the average grey value for the four ROIs. Percentages on graphs show the average increase in grey value compared to the wild-type. Error bars provide standard error of the mean (SEM).

Nymphs without obvious phenotypic mutations were pooled for molecular confirmation of insertion of the DNA cassette. Initial confirmation was performed by PCR amplification of the right homology

arm (RHA) using a primer within the DNA cassette and a primer downstream from the RHA in the genome (Appendix 6). If integration of the DNA cassette has occurred then amplification of a ~1,300bp allele would occur, whilst no band should occur for the wild-type DNA. Sample *y1* showed a band of ~1,300bp across all genomic DNA assessed (Figure 48B). The allele amplified in nymph *y1* was extracted and sent for Sanger sequencing, however, the sequence was of too poor quality to confirm insertion. Multiple PCR repeats were attempted to increase DNA quality, but none were successful in creating a clean sequencing read of the potentially successful allele.

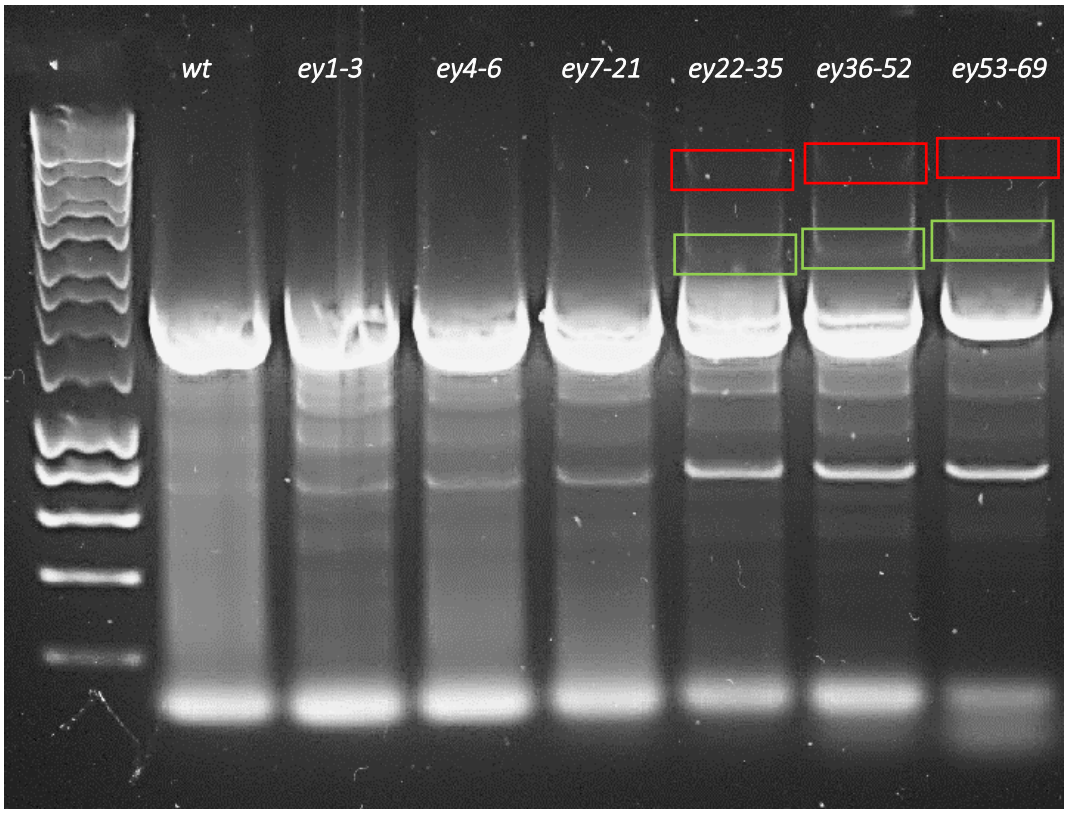

Figure 49. PCR confirmation of mutations to the *eyeless* gene (RPRC003362) via CRISPR-Cas9 HDR transfections in pooled *R. prolixus* nymph samples.
HDR insertion results in an amplicon of 4,984bp. An amplicon of 2,097bp would indicate wild-type DNA. A Meridian bioscience HyperLadder™ 1kb was used in the gel. Green boxes highlight alleles of the expected size following HDR insertion. Red boxes highlight an unexpected band which could be related to HDR insertion. Both green and red alleles were sequenced and confirmed to be genomic DNA at the HDR insertion site.

Further analysis of genomic DNA was taken to amplify the gRNA/HA region. Primers were designed 100-200bp upstream/downstream of the left and right HAs (Appendix 6). Wild-type DNA would produce an amplicon of ~2,000-2,100bp, whilst a DNA cassette integrated into the target region would produce an amplicon of ~4,800bp. Three pooled eyeless targeting samples produced alleles of the expected size for DNA integration (Figure 49). These samples (*ey22-69*) were genomic DNA extracted from 14-17 nymphs for each sample. Sanger sequencing of the ~5kb alleles showed the expected genomic site with the 5' and 3' ends matching both the ends of the HAs as expected in the genome (Figure 50). Unfortunately, the sequencing read was not able to confirm the DNA cassette sequence. However, on the basis of the allele size and genomic sequence confirmation can infer integration of the DNA cassette. No integration alleles were observed when amplifying this region for treated nymphs targeted in the *krüppel*, *aaNAT*, and *yellow* genes.

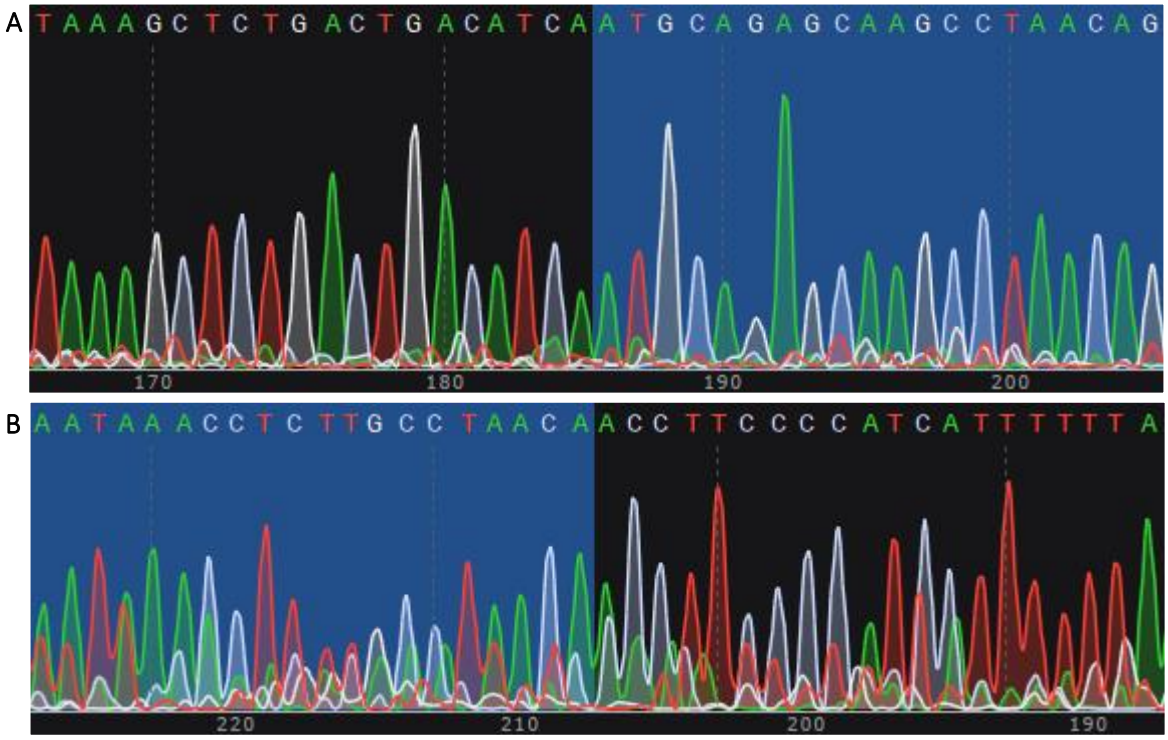

Figure 50. Sequence confirmation of the ~5kb amplicon spanning the HDR insertion region of the *eyeless* gene (RPRC003362) in transfected *R. prolixus* insects.
A) the 5' end of the left homology arm and upstream genomic DNA. B) the 3' of the right homology arm and downstream genomic DNA. A blue highlight represents DNA within the HAs found in the *ey*-pDsRed-*Ubi63e*-attP construct.

The results outlined above provide evidence of CRISPR-Cas9 mutations within *Rhodnius prolixus* via homology directed repair techniques incorporating exogenous DNA within the *yellow* and *eyeless* genes. This result demonstrates GM techniques within triatomine bugs with the potential for research to target genes involved in disease transmission, reducing a huge burden of human suffering.

5. 4. Discussion

The results presented in this chapter provide, to my knowledge, the first evidence of genetic modifications in triatomine bugs. This was achieved using CRISPR-Cas9 based DNA constructs providing supportive evidence for both the NHEJ and HDR methodologies. These methods were validated for genome engineering by phenotype expression (*aaNAT, white* and *yellow*), PCR amplification (*eyeless* and *yellow*), and sequencing (*eyeless*). We demonstrated targeted insertion of exogenous DNA into the genome of *R. prolixus* insects at the *eyeless* and *yellow* gRNA sites. These results contribute important proof of principle research validating the CRISPR-Cas9 system within triatomine bugs, which with further development could limit transmission of Chagas disease.

5. 4. 1. Survivorship following the ethanol-chemotransfection methodology

The EC methodology showed high survivorship following transfection of CRISPR-Cas9 constructs. This level of survivorship (29.45% for Cellfectin® II) is similar to that of microinjection in model insects such as *An. gambiae* and *D. melanogaster,* which routinely see survivorship levels of ~18-24% (186,330). As previously mentioned (Section 3. 4.), a potential reason for the reduction in viability could be due to endotoxins extracted from bacteria when purifying plasmids (404). The quality of incubation following treatment likely also reduced viability in all transfections, especially for the *white* and *aaNAT* targeted embryos.

During the transfection of *white* targeted embryos, the triatomine colonies were relocated to a new insectary which was not well suited to the rearing of insects. The new insectary circulates dry air leading to desiccation of embryos and developed insects. Measures were taken to increase humidity in the colony, but this was unstable and often led to high humidities which increasing contamination from bacteria and fungi. These fluctuating conditions increased the risk of contamination from putty adhesive which led to its removal. *w*-pDCC6 transfections had concluded before incubation conditions had been stabilised to standard conditions (26 °C ± 2 °C, at 70%) (433).

Transfections targeting the *aaNAT* gene were performed when we no longer had access to the CellFectin® II reagent. Therefore, *aaNAT* targeting transfections were carried out with the remaining stock of FlyFectIN™ from the sand fly cell line transfections. Multiple embryo batches were contaminated, with no embryos surviving. No CRISPR-Cas9 transfections were carried out in a microbiological safety cabinet and therefore contamination from the open air is likely. We also had major fluctuations in humidity and temperature during incubation, which desiccated whole batches of embryos. Future transfections would be carried out within a microbiological safety cabinet and incubated within a sealed climate-controlled incubator.

5. 4. 2. Genetic modification of *R. prolixus* embryos via CRISPR-Cas9 NHEJ constructs

Successful delivery of *w*-pDCC6 constructs resulted in a single *R. prolixus* nymph exhibiting a mutated phenotype. The reduction in pigment around the outer edge of the eye is consistent with *R. prolixus* adults showing loss of function in the *cinnabar* and *scarlet* genes (410). Initially, we expected the phenotypic mutation to be observable as a pale or white coloured eye as seen in other insect species such as the silk moth (*Bombyx mori),* southern house mosquito *(Culex quinquefasciatus), H. vitripennis,* and Indianmeal moth (*Plodia interpunctella)* (300,314,413,434). However, many insects (including the southern green stink bug *Nezara viridula* and *N. lugens*) have shown the loss of the *white* orthologues results in a reduction in pigmentation of the pigment cells, whilst the rhabdom and other compound eye components are still pigmented, similar to the phenotype seen in our research (415,435). Access to a higher magnification stereomicroscope would allow for more detailed viewing of the eye, potentially identifying the type of pigment loss exhibited.

The ambiguous result from the *white* phenotypic nymph, led to us pooling the DNA of the phenotype expressing *w6* nymph with other potentially unmutated nymphs for molecular analysis. This likely resulted in the mutation brought on by CRISPR-Cas9 being diluted by wild-type DNA when amplified by PCR. This preferential amplification of wild-type DNA could have been below the detection levels of the ICE analysis resulting in a lack of indels at the target site. As previously mentioned (Section 3. 4. 1.), other molecular techniques such as amplicon sequencing or the T7EI heteroduplex assay would be able to identify potential mutated alleles at a greater efficacy (351,352). When the *w*-pDCC6 transfections had been performed the T7EI assay had not been assessed by our group and future NHEJ based transfections would be assessed using this assay. Assessing the G1 offspring of potentially transgenic insects would also increase the likelihood of confirming mutations via sanger sequencing.

Ultimately, the HDR approach was favoured over NHEJ for future transfections. The rationale was that we had seen favourable results for HDR in *L. longipalpis* cell lines (Section 3. 3. 2.), and the PCR-based screening method would increase specificity when screening CRISPR-Cas9 mutations in *R. prolixus*.

5. 4. 3. Integration of exogenous DNA into the *R. prolixus* genome via CRISPR-Cas9 HDR constructs

5. 4. 3. 1. Phenotypic screening of putative HDR transfected nymphs

Phenotypic screening of the transfected embryos resulted in the expression of a *yellow* phenotype in two nymphs (*y1* and *y9*). Nymphs were imaged 96 hours post emergence, as full melanisation occurs during this period of time. As expected with loss of the *yellow* gene, putatively transgenic nymphs exhibited pale abdomen and they did not develop to a darkened cuticle following 20 days. This phenotype was not seen in any observed wild-type nymphs found in the colony. The phenotype resembles that of a *yellow* gene loss via RNAi seen in Berni *et al.,* (410). Unfortunately, the pigmentation was not greatly reduced on the head, thorax, or legs. However, there was a significant pigment colour change to the melanised sections of tergites 9-11 in *y1* and *y9* over the wild-type nymphs. The phenotype was only noticed in *y1* during initial observations. Therefore, the genomic DNA of *y1* was extracted individually, whilst *y9* was pooled with other nymphs (Section 5. 4. 3. 2.).

Utilizing the mean grey scale analysis previously applied in other insect studies, we were able to create quantifiable data for pigment change (410,420). This data demonstrates a positive trend (darkening of ROIs) for the *aaNAT* targeted nymphs potentially indicating mutations via CRISPR-Cas9 (Figure 466). The data for the *yellow* targeted insect also provided a decrease in light intensity (darkening), despite at least one insect being visibly paler. This led to the *y1* insect being individually compared to wild-type insects focusing only on the terga. Following this MGA, results followed the expected trend of a paler insect (Figure 48). The *y1* analysis was limited by the lack of data corresponding to the head, thorax, or limbs.

The imaging for the MGA was hindered by the equipment available to us. Limitations include screening under a simple stereomicroscope with a maximum magnification of 40x and using a phone camera to capture images. The magnification was not able to provide full detail and the lighting was inconsistent due to a ring light without a fixed position. The phone camera utilises computational image processing post capture. This post-capture processing can alter the image's brightness, contrast, and introduce digital artefacts without the ability to access the original image. The phone also produced images of varied pixel density, which altered the area measured for the MGA. A further limitation was the live imaging of nymphs. This meant they were often moving, which made the reflection of light different for each insect. Data from the MGA was split into sessions for statistical analysis to avoid variances in imaging conditions. Each session had the phone and ring light fixed in the same position providing a similar environmental conditions for each image, but the

insect's position or the post-capture processing could be slightly altered leading to photons scattering in different patterns. If further transfections were to be performed, we would use a complete insect imaging system like that of the Leica M205FA used in section 3. 3. 1. 3. We would also euthanise the insects prior to imaging, this would allow us to manipulate them more easily and create standard positions for imaging. To assist calibration, we would take background images without insects to remove the background and compare to matched wildtype insects in ImageJ for normalising the data. This would allow us to use the whole dorsal surface of the nymph for MGA, increasing the sensitivity for pigmentation mutations in both cuticle and eye phenotypes.

Transfection targeting *aaNAT, eyeless* and *krüppel* did not result in obvious phenotypic mutations. The *eyeless* gene should have produced insects lacking eyes or sections of the head (315). As *eyeless* is a *Pax6* gene it is responsible for early neurological development (436). The different alleles produced from *eyeless* mutations can form various phenotypes including lethal developmental changes (315,432). It is possible that non-viable phenotypes formed within our transfected populations. To assess non-viable phenotypes, further embryos would be dissected and observed for head formation mutations. A known paralogue of the *eyeless* gene, *twin of eyeless* (*toy*), leads to similar phenotypes when mutated in other insects (437). The *toy* gene has been discovered to function as a regulator of eyeless and therefore it's loss results in the eyeless phenotype (438). The *toy* gene's protein sequence is highly conserved with *eyeless* across multiple insect genomes, with the *toy* orthologue within *R. prolixus* (RPRC001429) presenting 84% shared identity with the *eyeless* gene (RPRC003362). This high amino acid sequence conservation infers eye formation could have remained following the loss of eyeless if replaced by the *toy* gene. No known paralogues of these genes exist within the *R. prolixus* genome, therefore, a dual CRISPR-Cas9 construct approach targeting both *eyeless* and *toy* could lead to an eyeless phenotype expressing.

The lack of obvious *aaNAT* phenotypes is likely due to the reduced viability discussed in Section 5. 4. 1. Improving incubation techniques and repeating these transfections in higher numbers may have led to a dark pigmentation phenotype as seen in Figure 40 (410).

Screening of putative *krüppel* gene mutations were not fully optimised prior to assessment. The *krüppel* gene is known to cause large developmental changes to the thoracic segments and anterior abdomen (428). These mutations can result in lost limbs and reduced body mass, which would hinder a nymphs ability to emerge through the operculum (421). Alternative methodologies for the screening of *krüppel* targeted nymphs should have been put in place, to observe mutations in embryos development without the need for insects to emerge. These include the dissection of embryos 9 days post transfection. This technique would be supplemented with *in situ* hybridization

targeting germband related genes to be able to visualise mutations in formation or loss of segments. These two techniques have been used to assess *krüppel* loss of function in multiple insects such as *G. bimaculatus, O. fasciatus, R. prolixus* and *T. castaneum* (421,426–428).

Ultimately, the lack of a phenotype in G0 is common within CRISPR-Cas9 insect studies (136,415,416,434). Within multiple hemipteran insects such as *T. castelium* and *N. lugens,* mosaic mutation phenotypes occurred within G0 populations, phenotypes became uniform when backcrossing the insects led to inherited mutations being found in the G1 (136,415). This provided evidence that the mutations were integrated into germline cells. The developmental time of *R. prolixus* (5 months to adult) meant that the backcrossing of transfected nymphs was not within the remit of this research. With more time phenotypic mutations would be assessed through to at least G1.

The DNA cassette for insertion into *R. prolixus* contained an integrative DsRed-Express fluorescent marker. Expression of this marker was not seen in any emergent nymphs. This is likely due to the ubiquitous nature of the expression and the melanised cuticle blocking fluorescent signal. Melanised cuticles have previously been shown to limit fluorescent microscopy within *D. melanogaster* and *R. prolixus* (410,439). Phenotypes that over expressed black melanin led to a reduction in fluorescent light being visible under fluorescent microscopy. In this chapter, the cuticle of the *R. prolixus* nymphs was melanised when they were imaged on the 4th day. Another limitation was our access to a fluorescent stereomicroscope. We were limited to using inverted fluorescent microscopes which are not suited to whole insect microscopy, due to light having to pass through the object to be captured in the lenses below. To overcome this, future work would use a fluorescent stereomicroscope, imaging embryos as close to emergence as possible to avoid melanisation of the cuticle. We would also design new plasmids with DNA cassettes expressing under the 3xP3 promoter for eye specific expression. Eyes have regions between the ommatidium that can allow the passage of fluorescent light (440). Further experiments could also image developing embryos which will not form melanised cuticles and could be homogenised to visualise DsRed expression in single cells. By adapting our methodologies in this way, we would be able to validate these CRISPR-Cas9 HDR constructs for a range of gene function studies.

5. 4. 3. 2. Molecular confirmation of HDR transfections in R. prolixus nymphs

Molecular confirmation of inserted DNA cassettes was primarily assessed via PCR amplification of the insertion region. Initial amplification with primers based within the DNA cassette and downstream of the right HA, validated insertion of the DNA cassette into a single *yellow* targeted

nymph (*y1*) (Figure 48B). Sanger sequencing of this allele did not successfully confirm genomic DNA due to poor quality.

To increase the PCRs sensitivity, we designed primers spanning insertion region from outside the HAs. These primers would create a band in wild-type DNA of ~2,000-2,100bp, and an allele of ~4,800bp for integrated DNA. These primer sets created multiple offsites in wild-type DNA (Figure 49), which would be excluded from confirmation results. Three pooled samples for the *eyeless* targeted nymphs (*ey22-69*) showed positive amplicons indicating genomic integration (Figure 49). Sequencing was able to confirm the ~4,800bp amplicon was located within the target regions by identification of the outer borders of the HAs (Figure 50). This provides evidence for genomic integration of the DNA cassette in at minimum, one nymph from each pooled sample. If possible, these amplicons could be sequenced long read nanopore sequencing to obtain full coverage of the ~4,800bp. The low UV intensity of positive amplicons in the electrophoresis gel, infers a low level of mutated DNA in the sample. A quantitative result for these amplicons could have been provided using techniques such as qPCR and amplicon sequencing. These approaches have been used in other CRISPR-Cas9 studies to estimate transfection efficiencies with high success rates (300,352,355,441). This is particularly important in pooled samples where wild-type alleles will be more prevalent than transfected alleles. qPCR would be the preferred choice for further HDR integration studies due to its ability to assess primers via melt curves, ease of use and reduced cost compared to amplicon sequencing. Further experiments could include the further rearing of insects and screening of G1 offspring. This would produce genotypic heterozygous mutations, which would limit the wild-type bias to 50% of gene copies found in G1 by PCR and sequencing.

We attempted the T7EI heteroduplex analysis on a small number (*ey1-3* and *aN1*) of ~2,000bp alleles from the pooled samples. However, the high level of off target amplicons produced by the primer set, resulted in a large number of fragments which could not be distinguished from potential positive results following T7EI cleavage. Therefore, the T7EI analysis was not used on the remaining samples and was not recorded in the results section.

In summary, we provided evidence of the successful integration of exogenous DNA into the genome of *R. prolixus* at two specific target sites (*eyeless* and *yellow*). The integrated DNA caused a phenotypic change following loss of the *yellow* gene as confirmed by MGA and PCR. This research provides the first known evidence of genetic modification in triatomine bugs. In validating the CRISPR-Cas9 system in triatomine bugs we have provided a novel methodology for the molecular research of Chagas disease.

6. Discussion and Future Research

6. 1. Discussion

Chagas disease and leishmaniasis are currently prevalent in an estimated 11 million people leading to ~1 million disability-adjusted life years lost and mortality in the thousands annually (1,2). Chemotherapies for these diseases exist but resistance to antileishmanial drugs is on the rise and treatments for the chronic phase of Chagas disease offer marginal benefit over non-treatment (25,28). Human vaccines are currently not available. Therefore, prevention is key to reducing burden of disease, and vector control has been the most effective approach for limiting transmission (33,43). However, factors such as resistance to insecticides, funding and geopolitical conflicts have affected vector control efforts in endemic areas (368,369,442–445). Due to this, novel self-sustaining vector control approaches are needed to overcome these limitations. Recent developments in the genetic modification of insects such as mosquitos have created vector control strategies that last generations with the use of gene drives (168,201,355). The approaches are yet to be adapted to sand flies or triatomine bugs with research into gene editing techniques for these insects still in its infancy (222).

This thesis describes the development and application of genome editing tools for both sand flies and triatomine bugs. We provide robust evidence of targeted mutations using both *in vitro* and *in vivo* CRISPR-Cas9 NHEJ methodologies (Sections 3. 4. 1. & 5. 4. 2) for sand flies (*L. longipalpis* and *Phlebotomus papatasi*) and triatomine bugs (*Rhodnius prolixus*). Furthering this we were able to integrate an exogenous DNA cassette into the genomes of sand flies (*in vitro*) and triatomine bugs (*in vivo*) via CRISPR-Cas9 HDR, which is a novel result for both insect subfamilies. These targeted mutations occurred in genes eliciting non-lethal phenotypes, which were initially identified using bioinformatic webtools. We also showed expression of fluorescent markers following transfection of piggyBac transposons (sand flies *in vitro,* triatomine bugs *in vivo*), with integration into the genome of these organisms to be confirmed by sequencing and inverse PCR in future experiments. We developed a novel transfection methodology for the embryos of triatomine bugs overcoming the barrier of DNA construct delivery due to microinjection limitations.

This research made use of two novel *L. longipalpis* cell lines LLE/LULS40 and LLE/LULS45 which we developed as an *in vitro* platform for transfection and gene editing methodologies. The chemotransfection of different plasmid constructs, enabled us to evaluate expression promoters for use in gene editing systems driving crucial elements such as Cas9 and helper transposases. An increased interest for *in vivo* experiments in sand flies is occurring despite the labour-intensive rearing techniques required (334). The establishment of a stable insect cell line is not easily achieved, we attempted to produce a *Rhodnius prolixus* cell line within our laboratory over several

months but could not obtain attached replicating cells in a stable culture. Following this we formed a collaboration with Bell-Sakyi *et al.,* and her group was able to establish a *R. prolixus* cell line (433). However, this line took 6-8 weeks to become 50% confluent within a flask and therefore was not preferable for *in vitro* transfection experiments as *in vivo* methods would provide results in a shorter time span. This further shows the importance of these two sand fly cell lines as they were stable and provided more ease of use than *in vivo* approaches with sand flies. We consider our development of an *in vitro* platform an important one, as *in vitro* systems allow molecular techniques to be optimised for sand fly species before being attempted *in vivo*, providing an efficient screening technique for future molecular research.

The transfection of plasmids Ac5-STABLE1-Neo, ^{i}hyPBase, pmaxGFP™, and Ubiq-Cas9.874W confirm the promoters *Ac5, CMV, hsp70, OpIE2,* and *Ubi-63E* for expression of proteins within sand flies. The *Ac5, OpIE2 and Ubi-63E* promoters had not previously been assessed in sand flies, in validating them here we have provided ubiquitous expression systems which are key for heterogenous cell lines and ubiquitous expression *in vivo*. These promoters were later incorporated into a CRISPR-Cas9 system for targeted mutagenesis in sand flies. eGFP expression was visible following the transfection of Ubiq-Cas9.874W constructs, however, this is not a sign of genome integration via piggyBac transposons without being confirmed by further molecular techniques such as inverse PCR and sequencing. With further development the piggyBac system would be of great benefit to sand fly research as multiple piggyBac based vector control systems are currently being developed for dipteran insects (110,184).

Transfection efficiencies within both LLE/LULS cell lines were low when assessed by flow cytometry previously within our lab (Section 2. 3. 1.). When comparing the expression of eGFP following Ac5-STABLE1-Neo transfections, S2 cells showed ~90 fold more fluorescent events over LLE/LULS cells (max odds ratios of 3.86 for LLE/LULS and 348.91 for S2). This difference in efficiencies could be due to the heterogeneous nature of the LLE/LULS cell lines, with certain differentiated cells being more susceptible to transfection (446,447). Flow cytometry also found no significant difference between the chemotransfection reagents tested (Cellfectin® II , FlyFectin™ reagent, and Lipofectamine™ 3000 reagent). These chemotransfection reagents use lipid-mitigated transfection, certain cell types possess higher numbers of membrane surface glycoproteins, increasing their capacity to intake lipid-packaged DNA by endocytosis (448). Despite the relatively low transfection numbers, the cell lines provided positive results for the validation of molecular methods for assessment of subsequent *in vivo* tools.

The research presented here shows the first reported *in vivo* genome mutations to *L. longipalpis* sand flies via CRISPR-Cas9 NHEJ DNA constructs. We were successful in eliciting mutations to produce a *vestigial* phenotype confirmed visually, by an algorithmic deconvolution assay (ADA) and by a T7 Endonuclease I heteroduplex assay (T7EI) (Section 3. 3. 1.). We were also able to induce indels in the *rudimentary* gene (*L. longipalpis*) and the *ebony* gene (*P. papatasi)*. Previously, CRISPR-Cas9 mutations within *P. papatasi* have only been achieved in a single published study, with our research furthering the CRISPR-Cas9 NHEJ approach within sand flies by the use of DNA constructs over a sgRNA/Cas9 injection mixture (222). Whilst we were able to achieve mutations within our genes of interest, confirmation could have been improved by the use of high depth sequencing such as amplicon sequencing or with the use of high quality tissue PCR kits such as the Phire Tissue Direct PCR kit (ThermoFisher, USA), which would provide clean, quantified results (168,222,355). The success of these mutations lays a foundation for further genome engineering techniques to be used in sand flies and potentially the development of population control techniques (Section 1. 5.) (110,157,159,161).

Following the successful demonstration of CRISPR-Cas9 NHEJ mutations formed in sand flies, we subsequently produced a CRISPR-Cas9 HDR system targeting the *L. longipalpis scarlet* gene as an integration site. We utilized two approaches for homology arm design, one directly surrounding the gRNA region (HSC) and another using homology arms within the 5'/3' untranslated regions (HUTR). Both of these approaches produced the expected amplicons of integrated DNA cassettes as confirmed by Sanger sequencing. However, due to the presence of DNA constructs within the extracted DNA solution, heteroduplexes could form during PCR amplification causing false positive results with wild-type DNA. To validate integration, genomic DNA from these cells must be assessed via inverse PCR and sequencing. The HUTR approach has the potential to remove entire genes from the genome and use their promoters to drive expression of potential anti-parasite effector molecules. We also noted the insertion of DNA cassettes without the CRISPR-Cas9 constructs to form a double-stranded break. These false positives are likely due to the heteroduplexes formed from the PCR. An alternative less likely theory for these positive results is that the long homology arms (800bp) lead to homologous insertion during cell replication, the use of CRISPR-Cas9 cleavage *in vivo* should increase the HDR integration efficiencies in non-replicating cells (364–366).

When considering gene modifications in triatomine bugs, the delivery of transfection agents was previously the biggest limitation (302). In this thesis we were able to develop a novel ethanol-chemotransfection methodology (EC) in *R. prolixus*. EC was able to effectively strip the wax surrounding aeropiles on triatomine egg chorions without excessive mortality (Section 4. 3. 3.). This

allowed packaged DNA to cross embryonic membranes via chemotransfection reagents (Figure 38). After validation with Hoechst 33342, we were able to deliver plasmid constructs including the transiently expressing Ac5-STABLE1-Neo and piggyBac-based Ubiq-Cas9.874W. To my knowledge, there is no published literature demonstrating the genome engineering of triatomine embryos, with previous functional genomics research focusing on RNAi (405,408,410,412). We are the first to present evidence of integrated exogenous DNA transfected into *R. prolixus* genomes via CRISPR-Cas9 HDR approaches. This novel methodology has the potential to revolutionise molecular research in triatomine bugs due to its ease of use and high viability compared to microinjection (20.7% viability) (136,222,300,318).

Utilizing our novel EC methodology, we have provided putative evidence of integrated exogenous DNA cassettes in the *eyeless* and *yellow* genes of *R. prolixus* via CRISPR-Cas9 HDR DNA constructs. We also achieved putative mutations within the *white* gene following CRISPR-Cas9 NHEJ transfections with one nymph (out of 838 transfected) showing a putative eye phenotype. Confirmation of NHEJ mutations were limited by poor DNA extraction and Sanger sequencing. Potential HDR integrated DNA was amplified by PCR within pooled populations of *eyeless* targeted nymphs (Section 5. 3. 3.). The amplicons produced by PCR were of the expected size following HDR insertion but only the genomic DNA upstream/downstream of the homology arms could be confirmed by Sanger sequencing. The use of long read sequencing such as Oxford nanopore could confirm the integrated cassette. A single yellow targeted nymph (*y1*) was shown to have a 6.69% increase in light intensity indicating a lightening of pigment following transfection, which was confirmed by PCR of the target area (Figure 48). This phenotype aligns with similar experiments carried out by Berni *et al.,* using RNAi, inferring that this is the first confirmed phenotypic mutation in triatomine bugs using gene editing methodologies (410). Confirmation of integrated DNA cassettes is more reliable *in vivo* as the transient HDR donor plasmids will likely have degraded during development of the embryo and genome DNA will be at a higher concentration than any remaining DNA constructs. Backcrossing of the putative transgenic insects to G1 would further remove the DNA constructs and mutated DNA would be higher in concentration due to germline cell integration. These results demonstrate the utility of the CRISPR-Cas9 system we have developed within triatomine bugs, which could be utilised by other researchers for the understanding and prevention of Chagas disease.

6. 1. 1. Impact of COVID-19

The COVID-19 global pandemic had a significant impact on this research, resulting in a number of modifications to the aims. Sand fly based *in vivo* experiments were delayed by two years due to the

inability to travel to Charles University in Prague, Czech Republic, where the colonies used in this research were based. The process of microinjection and backcrossing of insects is labour intensive and time consuming and due to our limited time within the Czech Republic we had to scale back the number of targets assessed. We had initially aimed to assess piggyBac constructs within the sand fly colonies and to target gut attachment genes to be assessed by challenging parasites to transgenic colonies. We also produced several CRISPR-Cas9 HDR constructs targeting both *L. longipalpis* and *P. papatasi,* which due to time constraints we were unable to microinject. Due to the three national lockdowns within the UK, we had multiple delays to the *in vitro* work as cells had to be resuscitated from cryostorage. Unfortunately, the LLE/LULS cell lines took 3-6 months to recover steady growth rates (1-week doubling rate) following cryopreservation. This severely delayed the assessment of plasmid constructs due to the optimization of chemotransfection methodologies being performed, and an inability to share lab spaces with other researchers, limiting the number of experiments which could be carried out weekly. Despite this the results we achieved are novel and lay the foundations for future vector control research.

6. 2. Future research

This research presents evidence for the implementation of CRISPR-Cas9 vector control systems within phlebotomine sand flies and triatomine bugs. There is scope for creating a genome engineering platform for vector-parasite research. A key future objective would be the optimisation of the LLE/LULS cell lines to create an *in vitro* platform for modelling gene editing targets. Additionally, the successful results for CRISPR-Cas9 HDR transfections could be further developed for an *in vivo* gene drive system within sand flies and triatomine bugs. The detailed aspects of these potential approaches are outlined here.

The LLE/LULS cell lines are uncharacterised heterogenous cultures (240,241). The heterogenous nature of these cells creates biases which can affect transfection efficiencies and result in differential expression (283). For research aims such as sex determination or the localised expression of anti-parasitic molecules it is imperative that the cell type is characterised. For example, a characterised clonal line of gut epithelial cells could be used for modelling the expression of antimicrobial peptides (Section 1. 5. 3., Table 1) in a midgut targeting gene drive system (201,278). To achieve this multiple clonal lines could be created from the LLE/LULS cells using approaches such as semisolid agar or fluorescence-activated cell sorting (FACS)(284,449). Clonal lines would be characterized using morphological approaches as well as western blotting with RT-PCR for gene expression assays (450,451). Once characterised optimisation of transfection methodologies could be performed and localised gene targets for vector control can be assessed.

The creation of a clonal cell line expressing Cas9 was of particular interest to our group. ACas9 expressing cell line would increase productivity ofCRISPR-Cas9 mutations by allowing the delivery of purified gRNAs, facilitating the rapid screening of gene targets via transfection systems such as Lipofectamine™ CRISPRMAX™ (Invitrogen, USA). Briefly this line could be derived by FACS following transfections of the Ubiq-Cas9.874W plasmid (183). The DNA cassette within the Ubiq-Cas9.874W plasmid could also be integrated *in vivo* to derive a colony of sand flies or triatomines, such as cas9 expressing lines used in dipteran studies (280,291). This would significantly increase the capacity of gene target screening as gRNA delivery is often regarded as simpler than large DNA constructs or proteins.

Furthering the successful CRISPR-Cas9 HDR transfections, the natural progression would be the development and assessment of a gene drive system within sand flies and triatomine bugs. Multiple approaches to gene drive development have been assessed within insects such as daisy-drives and reverse drives (Section 1. 5. 1.) (157,160,161). Gene drives are reliant on a germline specific

promoter driving Cas9 endonucleases for the inheritance of desired traits within offspring. Two promising promoters currently used for gene drive constructs are from the *nanos* and *zero population growth* (*zpg*) genes (158,355). The *nanos* gene is involved in embryogenesis forming an mRNA repressor complex with *pumilio* proteins (452). When integrated into gene drive systems *nanos* reduced somatic expression over previously used germline promoters (*vasa*) limiting the formation of mutations which have a fitness cost (158). The *zpg* germline specific gene is involved in the formation of insect gonad development, therefore, mutations within the gene cause a reduction in female fecundity which can be used for population control (453,454). The *zpg* gene is conserved across multiple Diptera, when incorporated into gene drives the *zpg* promoter elicits fewer resistance alleles than *nanos* based drives (355,455). Constructs incorporating gene drive elements for sand flies and triatomine bugs could be transfected using our CRISRP-Cas9 platform or piggyBac plasmids (109).

Gene drives within sand flies and triatomines have the potential to limit parasite transmission via population control. Multiple gene targets for population suppression have previously been assessed in other insects, including *β2-tubulin, doublesex*, *filial 1, fruitless* and *nix* (157,167,172,179,164,293). Genes linked to parasite attachment and vector competency include *caspar*, galectins, and glycoproteins, which have the potential to be used in population replacement drives (189–192,456). The expression of anti-microbial peptides (AMPs) within mosquitos has been shown to reduce malaria transmission in caged experiments (201). In previous literature, a number of AMPs have been identified to be active against *Leishmania spp.* and *T. cruzi.* The most promising of which include cathelicidins, immunity-related proteins, and insect venoms (Section 1. 5. 3., Table Table ***1*** Table 2)(204,207,209,211–214,219). The peptides were assessed against parasites via different methodologies. Therefore, we would aim to reassess their active concentrations against parasites using a standardised approach and carry out toxicity assays for the insect vectors via the feeding of tainted blood. Once assessed the peptides could be introduced into a population via a gene-drive which is localised to gut expression via promoters such as *carboxypeptidase A1*, *gambicin1*, or G12 (86,201,247). Furthering this, once successful candidates have been integrated into populations via gene drives, we would need to assess multigenerational inheritance and efficacy of transmission interruption within large cage experiments, mimicking field conditions before release (355)

However, when applying gene-drives to sand flies and triatomine bugs, a number of considerations must be applied. Triatomine bugs are considerably longer lived than that of mosquitos or other Diptera, with *R. prolixus* taking 5-6 months from egg emergence to oviposition (402). This means that populations studies for control would take several years and in wild populations edited insects

have a higher risk of mortality before they are able to pass on traits. Another factor in the spread of gene-drives, is the evidence that triatomine populations do not migrate between households in large numbers, with most novel domestic infestations coming from sylvatic populations (457). This could be overcome by releasing gene-drive insects within sylvatic environments or by mass roll out within domestic environments, however, there are ethical complications when considering releasing blood-feeding disease vectors within households. Phlebotomine sand flies are also known to show low dispersal of populations (≤500m), which could be useful to limit the spread of gene-drives outside of disease endemic areas, whilst allowing traits to be driven through populations within a targeted area (458–460). For both Chagas disease and leishmaniasis multiple species of vectors can be present in the same geographical area (Section 1. 3.). Whilst there is evidence of cross species hybridization potentially spreading gene-drives this is limited and theorised to mostly occur between those within the same genus (461–463). To overcome this all-potential vectors within the target area would need to be characterised, transfected, and reared on mass to produce a stable transgenic line for release. This is a costly and labour intensive endeavour for a single species, which may not be feasible for the estimated 120 triatomine species and 988 phlebotomine sand fly species which transmit their respective parasites (54,55,66,464).

The implementation of CRISPR-Cas9 systems to sand flies and triatomine bugs is not limited to vector control strategies and is of great benefit to functional genomics studies, in particular vector-parasite interactions. In sand flies, there are a number of unknown interactions which could be vital to leishmania control. Multiple potential vaccine targets are being produced from sand fly saliva antigens (465). With gene editing potential antigens could be removed to assess which are vital for successful transmission of *Leishmania* by assessing immune responses in mice. Immune responses to *Leishmania* infection in the sand flies are also not fully understood with many citing these as an important area for transmission control (67). This was the focus of the first CRISPR-Cas9 gene editing in sand flies, which targeted the *relish* gene showing a reduction in gut bacteria when functionally removed (222). Other immune pathways are also theorised to be involved in *Leishmania* control and could be studied using gene editing techniques, our research targeted the *caspar* gene with the intention of challenging parasites to transgenic insects if a line had been achieved (192). In triatomines, the attachment molecule for epimastigotes in the hind gut is still not known. Previous research theorises a hydrophobic molecule which attaches to a hemidesmosome-like material under parasite plasma membranes is responsible (466). By identifying potential attachment proteins using the *R. prolixus* genome, we could screen genes via CRISPR-Cas9 mutations potentially creating insects which pass parasites before they develop to trypomastigotes. A number of antimicrobial molecules have been identified in the immune pathways of triatomine bugs, such as cathepsin D,

defensins, and nitric oxides (467–469). These have the potential to block parasite infection and may be responsible for the genotype specific nature of insects like *R. prolixus* (467). If investigated further or integrated into other insects via HDR these peptides could block transmission of multiple genotypes. These examples among others show the potential of gene editing in these vectors for furthering our understanding of parasite interactions and potentially discovering novel pathways which can be developed into control programs.

In summary, genome engineering in sand flies and triatomines is limited and the research outlined here addresses this omission. We have demonstrated sand fly and triatomine specific gene editing platforms, through both *in vitro* and *in vivo* assessment, to detect mutagenesis and integrate exogenous DNA cassettes. These results are novel, with CRISPR-Cas9 based mutations being achieved for the first time in *Lutzomyia longipalpis* (HDR) and *Rhodnius prolixus* (NHEJ & HDR). Our findings may be of interest to the wider vector control research community, reducing an enormous burden of human suffering.

7. References

1. Wang H, Abbas KM, Abbasifard M, Abbasi-Kangevari M, Abbastabar H, Abd-Allah F, et al. Global age-sex-specific fertility, mortality, healthy life expectancy (HALE), and population estimates in 204 countries and territories, 1950–2019: a comprehensive demographic analysis for the Global Burden of Disease Study 2019. The Lancet. 2020 Oct 17;396(10258):1160–203.

2. Vos T, Lim SS, Abbafati C, Abbas KM, Abbasi M, Abbasifard M, et al. Global burden of 369 diseases and injuries in 204 countries and territories, 1990–2019: a systematic analysis for the Global Burden of Disease Study 2019. The Lancet. 2020 Oct 17;396(10258):1204–22.

3. Ready PD. Epidemiology of visceral leishmaniasis. Clin Epidemiol. 2014 May 3;6:147–54.

4. Auwera GV der, Dujardin JC. Species Typing in Dermal Leishmaniasis. Clin Microbiol Rev. 2015 Apr 1;28(2):265–94.

5. Alvar J, Yactayo S, Bern C. Leishmaniasis and poverty. Trends Parasitol. 2006 Dec 1;22(12):552–7.

6. Schmunis GA. Epidemiology of Chagas disease in non endemic countries: the role of international migration. Mem Inst Oswaldo Cruz. 2007 Aug 31;102(suppl 1):75–86.

7. Castillo-Riquelme M. Chagas disease in non-endemic countries. Lancet Glob Health. 2017 Apr 1;5(4):e379–80.

8. Rassi A, Rassi A, Marin-Neto JA. Chagas disease. The Lancet. 2010 Apr 17;375(9723):1388–402.

9. Moretti E, Basso B, Castro I, Carrizo Paez M, Chaul M, Barbieri G, et al. Doença de Chagas: estudo da transmissão congênita nos casos da infecção materna aguda. Rev Soc Bras Med Trop. 2005 Feb;38(1):53–5.

10. Silva-dos-Santos D, Barreto-de-Albuquerque J, Guerra B, Moreira OC, Berbert LR, Ramos MT, et al. Unraveling Chagas disease transmission through the oral route: Gateways to Trypanosoma cruzi infection and target tissues. PLoS Negl Trop Dis [Internet]. 2017 Apr 5 [cited 2019 Jun 10];11(4). Available from: https://www.ncbi.nlm.nih.gov/pmc/articles/PMC5397068/

11. Gómez-P CF, Mantilla-H JC, Rodriguez-Morales AJ. Fatal Chagas Disease Among Solid-Organ Transplant Recipients in Colombia. Open Forum Infect Dis [Internet]. 2014 Jun 7 [cited 2019 Jun 10];1(1). Available from: https://www.ncbi.nlm.nih.gov/pmc/articles/PMC4324190/

12. Rassi A, Rassi A, Marcondes de Rezende J. American Trypanosomiasis (Chagas Disease). Infect Dis Clin North Am. 2012 Jun;26(2):275–91.

13. Villarreal MR. *Leishmania donovani*. In: Wikipedia [Internet]. 2019 [cited 2019 Jun 10]. Available from: https://en.wikipedia.org/w/index.php?title=Leishmania_donovani&oldid=889450308

14. Zhang JR, Guo XG, Chen H, Liu JL, Gong X, Chen DL, et al. Pathogenic Leishmania spp. detected in lizards from Northwest China using molecular methods. BMC Vet Res. 2019 Dec 9;15:446.

15. Kamhawi S. Phlebotomine sand flies and Leishmania parasites: friends or foes? Trends Parasitol. 2006 Sep;22(9):439–45.

16. Rogers ME, Chance ML, Bates PA. The role of promastigote secretory gel in the origin and transmission of the infective stage of *Leishmania mexicana* by the sandfly *Lutzomyia longipalpis*. Parasitology. 2002 May;124(5):495–507.

17. Kaye P, Scott P. Leishmaniasis: complexity at the host–pathogen interface. Nat Rev Microbiol. 2011 Jul 11;9(8):604–15.

18. Laskay T, van Zandbergen G, Solbach W. Neutrophil granulocytes--Trojan horses for Leishmania major and other intracellular microbes? Trends Microbiol. 2003 May;11(5):210–4.

19. Ndjamen B, Kang BH, Hatsuzawa K, Kima PE. Leishmania parasitophorous vacuoles interact continuously with the host cell's endoplasmic reticulum; Parasitophorous vacuoles are hybrid compartments. Cell Microbiol. 2010 Oct;12(10):1480–94.

20. De Trez C, Magez S, Akira S, Ryffel B, Carlier Y, Muraille E. iNOS-Producing Inflammatory Dendritic Cells Constitute the Major Infected Cell Type during the Chronic Leishmania major Infection Phase of C57BL/6 Resistant Mice. Mansfield JM, editor. PLoS Pathog. 2009 Jun 26;5(6):e1000494.

21. Peters NC, Egen JG, Secundino N, Debrabant A, Kimblin N, Kamhawi S, et al. In vivo imaging reveals an essential role for neutrophils in leishmaniasis transmitted by sand flies. Science. 2008 Aug 15;321(5891):970–4.

22. Pérez-Molina JA, Molina I. Chagas disease. The Lancet. 2018 Jan 6;391(10115):82–94.

23. Weltgesundheitsorganisation, editor. Control of chagas disease: second report of the WHO Expert Committee. Geneva: WHO; 2002. 109 p. (Control of Chagas disease).

24. Murphy N, Macchiaverna NP, Victoria Cardinal M, Bhattacharyya T, Mertens P, Zeippen N, et al. Lineage-specific rapid diagnostic tests can resolve Trypanosoma cruzi TcII/V/VI ecological and epidemiological associations in the Argentine Chaco. Parasit Vectors. 2019 Sep 16;12(1):424.

25. Pérez-Molina JA, Pérez-Ayala A, Moreno S, Fernández-González MC, Zamora J, López-Velez R. Use of benznidazole to treat chronic Chagas' disease: a systematic review with a meta-analysis. J Antimicrob Chemother. 2009 Dec 1;64(6):1139–47.

26. Torres-Guerrero E, Quintanilla-Cedillo MR, Ruiz-Esmenjaud J, Arenas R. Leishmaniasis: a review. F1000Research [Internet]. 2017 [cited 2019 Sep 6];6. Available from: https://www.ncbi.nlm.nih.gov/pmc/articles/PMC5464238/

27. Bocxlaer KV, Gaukel E, Hauser D, Park SH, Schock S, Yardley V, et al. Topical Treatment for Cutaneous Leishmaniasis: Dermato-Pharmacokinetic Lead Optimization of Benzoxaboroles. Antimicrob Agents Chemother [Internet]. 2018 May [cited 2019 Sep 6];62(5). Available from: https://www.ncbi.nlm.nih.gov/pmc/articles/PMC5923108/

28. Rajasekaran R, Chen YPP. Potential therapeutic targets and the role of technology in developing novel antileishmanial drugs. Drug Discov Today. 2015 Aug 1;20(8):958–68.

29. Dinc R. Leishmania Vaccines: the Current Situation with Its Promising Aspect for the Future. Korean J Parasitol. 2022 Dec;60(6):379–91.

30. Santos CV dos, Bedin C, Wilhelms TS, Villela MM, Santos CV dos, Bedin C, et al. Assessment of the Housing Improvement Program for Chagas Disease Control in the Northwestern municipalities of Rio Grande do Sul, Brazil. Rev Soc Bras Med Trop. 2016 Oct;49(5):572–8.

31. Sanofi Espoir Foundation - CEDIC - Fighting Chagas disease in indigenous communities of the Paraguayan Chaco [Internet]. [cited 2019 Jun 14]. Available from: http://fondation-sanofi-espoir.com/en/ngo_cedic.php

32. WHO EMRO | Leishmaniasis: Iraq improves field vector control | Iraq-news | Iraq [Internet]. [cited 2019 Jun 14]. Available from: http://www.emro.who.int/irq/iraq-news/leishmaniasis-field-vector-control.html

33. Dias JCP. Southern Cone Initiative for the elimination of domestic populations of Triatoma infestans and the interruption of transfusion Chagas disease: historical aspects, present situation, and perspectives. Mem Inst Oswaldo Cruz. 2007 Oct;102:11–8.

34. Schofield CJ, Dias JCP. The Southern Cone Initiative against Chagas Disease. In: Advances in Parasitology [Internet]. Elsevier; 1999 [cited 2019 Sep 5]. p. 1–27. Available from: https://linkinghub.elsevier.com/retrieve/pii/S0065308X08601475

35. Schmunis GA, Zicker F, Moncayo A. Interruption of Chagas' disease transmission through vector elimination. The Lancet. 1996 Oct 26;348(9035):1171.

36. Picollo MIS, Vassena C, Orihuela PS, Barrios S, Zaidemberg M, Zerba E. High Resistance to Pyrethroid Insecticides Associated with Ineffective Field Treatments in Triatoma infestans (Hemiptera: Reduviidae) from Northern Argentina. J Med Entomol. 2005;42(4):6.

37. Coura JR, Coura JR. Chagas disease: control, elimination and eradication. Is it possible? Mem Inst Oswaldo Cruz. 2013 Dec;108(8):962–7.

38. Gurevitz JM, Sol Gaspe M, Enríquez GF, Vassena CV, Alvarado-Otegui JA, Provecho YM, et al. Unexpected Failures to Control Chagas Disease Vectors With Pyrethroid Spraying in Northern Argentina. J Med Entomol. 2012 Dec 1;49(6):1379–86.

39. Waleckx E, Gourbière S, Dumonteil E. Intrusive versus domiciliated triatomines and the challenge of adapting vector control practices against Chagas disease. Mem Inst Oswaldo Cruz. 2015 Mar 14;110(3):324–38.

40. Fronza G, Roca-Acevedo G, Mougabure-Cueto GA, Sierra I, Capriotti N, Toloza AC. Insecticide Resistance Mechanisms in Triatoma infestans (Reduviidae: Triatominae): The Putative Role of Enhanced Detoxification and Knockdown Resistance (kdr) Allele in a Resistant Hotspot From the Argentine Chaco. J Med Entomol. 2020 May 4;57(3):837–44.

41. Lima MM, Carvalho-Costa FA, Toma HK, Borges-Pereira J, de Oliveira TG, Sarquis O. Chagas disease and housing improvement in northeastern Brazil: a cross-sectional survey. Parasitol Res. 2015 May 1;114(5):1687–92.

42. Rojas-de-Arias A. Chagas disease prevention through improved housing using an ecosystem approach to health. Cad Saúde Pública. 2001;17(suppl):S89–97.

43. González U, Pinart M, Sinclair D, Firooz A, Enk C, Vélez ID, et al. Vector and reservoir control for preventing leishmaniasis. Cochrane Infectious Diseases Group, editor. Cochrane Database Syst

Rev [Internet]. 2015 Aug 6 [cited 2019 Jun 17]; Available from: http://doi.wiley.com/10.1002/14651858.CD008736.pub2

44. Picado A, Singh SP, Rijal S, Sundar S, Ostyn B, Chappuis F, et al. Longlasting insecticidal nets for prevention of Leishmania donovani infection in India and Nepal: paired cluster randomised trial. BMJ. 2010 Dec 29;341:c6760.

45. Dhiman RC, Yadav RS. Insecticide resistance in phlebotomine sandflies in Southeast Asia with emphasis on the Indian subcontinent. Infect Dis Poverty [Internet]. 2016 Nov 7 [cited 2019 Jun 17];5. Available from: https://www.ncbi.nlm.nih.gov/pmc/articles/PMC5098277/

46. Gomes B, Purkait B, Deb RM, Rama A, Singh RP, Foster GM, et al. Knockdown resistance mutations predict DDT resistance and pyrethroid tolerance in the visceral leishmaniasis vector Phlebotomus argentipes. PLoS Negl Trop Dis. 2017 Apr 17;11(4):e0005504.

47. Balaska S, Fotakis EA, Chaskopoulou A, Vontas J. Chemical control and insecticide resistance status of sand fly vectors worldwide. PLoS Negl Trop Dis. 2021 Aug 12;15(8):e0009586.

48. Ratcliffe NA, Furtado Pacheco JP, Dyson P, Castro HC, Gonzalez MS, Azambuja P, et al. Overview of paratransgenesis as a strategy to control pathogen transmission by insect vectors. Parasit Vectors. 2022 Mar 31;15:112.

49. Beard CB, Mason PW, Aksoy S, Tesh RB, Richards FF. Transformation of an insect symbiont and expression of a foreign gene in the Chagas' disease vector Rhodnius prolixus. Am J Trop Med Hyg. 1992 Feb;46(2):195–200.

50. Hurwitz I, Fieck A, Klein N, Jose C, Kang A, Durvasula R. A Paratransgenic Strategy for the Control of Chagas Disease. Psyche J Entomol. 2012 Mar 12;2012:e178930.

51. Durvasula RV, Kroger A, Goodwin M, Panackal A, Kruglov O, Taneja J, et al. Strategy for Introduction of Foreign Genes into Field Populations of Chagas Disease Vectors. Ann Entomol Soc Am. 1999 Nov 1;92(6):937–43.

52. Hurwitz I, Hillesland H, Fieck A, Das P, Durvasula R. The paratransgenic sand fly: A platform for control of Leishmania transmission. Parasit Vectors. 2011 May 19;4(1):82.

53. Ghassemi M, Akhavan AA, Zahraei-Ramazani A, Yakhchali B, Arandian MH, Jafari R, et al. Rodents as vehicle for delivery of transgenic bacteria to make paratransgenic sand fly vectors of cutaneous leishmaniasis in field condition. Sci Rep. 2023 Sep 9;13(1):14912.

54. Sandoval CM, Duarte R, Gutíerrez R, Rocha D da S, Angulo VM, Esteban L, et al. Feeding sources and natural infection of Belminus herreri (Hemiptera, Reduviidae, Triatominae) from dwellings in Cesar, Colombia. Mem Inst Oswaldo Cruz. 2004 Mar;99(2):137–40.

55. Panzera F, Hornos S, Pereira J, Cestau R, Canale D, Diotaiuti L, et al. Genetic Variability and Geographic Differentiation among Three Species of Triatomine Bugs (Hemiptera-Reduviidae). Am J Trop Med Hyg. 1997 Dec 1;57(6):732–9.

56. Schofield CJ, Dujardin JP. Chagas disease vector control in Central America. Parasitol Today. 1997 Apr 1;13(4):141–4.

57. Khatchikian CE, Foley EA, Barbu CM, Hwang J, Ancca-Juárez J, Borrini-Mayori K, et al. Population Structure of the Chagas Disease Vector Triatoma infestans in an Urban Environment. PLoS Negl Trop Dis. 2015 Feb 3;9(2):e0003425.

58. Chuit R, Cohen JE, Cecere MC, Segura EL, Lauricella MA, Gurtler RE. Influence of humans and domestic animals on the household prevalence of Trypanosoma cruzi in Triatoma infestans populations in northwest Argentina. Am J Trop Med Hyg. 1998 Jun 1;58(6):748–58.

59. Gourbière S, Dorn P, Tripet F, Dumonteil E. Genetics and evolution of triatomines: from phylogeny to vector control. Heredity. 2012 Mar;108(3):190–202.

60. Gaunt M, Miles M. The ecotopes and evolution of triatomine bugs (triatominae) and their associated trypanosomes. Mem Inst Oswaldo Cruz. 2000 Aug;95(4):557–65.

61. Zingales B, Andrade SG, Briones MRS, Campbell DA, Chiari E, Fernandes O, et al. A new consensus for Trypanosoma cruzi intraspecific nomenclature: second revision meeting recommends TcI to TcVI. Mem Inst Oswaldo Cruz. 2009 Nov;104:1051–4.

62. Messenger LA, Miles MA, Bern C. Between a bug and a hard place: Trypanosoma cruzi genetic diversity and the clinical outcomes of Chagas disease. Expert Rev Anti Infect Ther. 2015 Aug 3;13(8):995–1029.

63. Lewis MD, Francisco AF, Taylor MC, Jayawardhana S, Kelly JM. Host and parasite genetics shape a link between Trypanosoma cruzi infection dynamics and chronic cardiomyopathy. Cell Microbiol. 2016;18(10):1429–43.

64. de Abreu AP, Lucas da Silva HF, Sarto MPM, Iunklaus GF, Trovo JV, de Souza Fernandes N, et al. Infection susceptibility and vector competence of Rhodnius robustus Larrousse, 1927 and R. pictipes Stal, 1872 (Hemiptera, Reduviidae, Triatominae) for strains of Trypanosoma cruzi (Chagas, 1909) (Kinetoplastida, Trypanosomatidae) I, II and IV. Parasit Vectors. 2022 Jun 30;15(1):239.

65. Izeta-Alberdi A, Ibarra-Cerdeña CN, Moo-Llanes DA, Ramsey JM. Geographical, landscape and host associations of Trypanosoma cruzi DTUs and lineages. Parasit Vectors. 2016 Dec;9(1):1–20.

66. Bates PA, Depaquit J, Galati EA, Kamhawi S, Maroli M, McDowell MA, et al. Recent advances in phlebotomine sand fly research related to leishmaniasis control. Parasit Vectors. 2015 Feb 27;8(1):131.

67. Cecílio P, Cordeiro-da-Silva A, Oliveira F. Sand flies: Basic information on the vectors of leishmaniasis and their interactions with Leishmania parasites. Commun Biol. 2022 Apr 4;5(1):1–12.

68. Salomón OD, Feliciangeli MD, Quintana MG, Afonso MM dos S, Rangel EF. Lutzomyia longipalpis urbanisation and control. Mem Inst Oswaldo Cruz. 2015 Oct 23;110(7):831–46.

69. Schwabl P, Boité MC, Bussotti G, Jacobs A, Andersson B, Moreira O, et al. Colonization and genetic diversification processes of Leishmania infantum in the Americas. Commun Biol. 2021 Jan 29;4(1):1–13.

70. Chowdhury R, Kumar V, Mondal D, Das ML, Das P, Dash AP, et al. Implication of vector characteristics of Phlebotomus argentipes in the kala-azar elimination programme in the Indian sub-continent. Pathog Glob Health. 2016 May;110(3):87–96.

71. Flanley CM, Ramalho-Ortigao M, Coutinho-Abreu IV, Mukbel R, Hanafi HA, El-Hossary SS, et al. Population genetics analysis of Phlebotomus papatasi sand flies from Egypt and Jordan based on mitochondrial cytochrome b haplotypes. Parasit Vectors. 2018 Mar 27;11(1):214.

72. Trájer AJ, Grmasha RA. The potential effects of climate change on the climatic suitability patterns of the Western Asian vectors and parasites of cutaneous leishmaniasis in the mid- and late twenty-first century. Theor Appl Climatol [Internet]. 2023 Nov 15 [cited 2023 Dec 20]; Available from: https://doi.org/10.1007/s00704-023-04726-4

73. Morrison AC, Ferro C, Tesh RB. Host Preferences of the Sand Fly Lutzomyia longipalpis at an Endemic Focus of American Visceral Leishmaniasis in Colombia. Am J Trop Med Hyg. 1993 Jul 1;49(1):68–75.

74. Afonso MM dos S, Duarte R, Miranda JC, Caranha L, Rangel EF. Journal of Tropical Medicine. 2012 [cited 2019 Jun 13]. Studies on the Feeding Habits of Lutzomyia (Lutzomyia) longipalpis (Lutz & Neiva, 1912) (Diptera: Psychodidae: Phlebotominae) Populations from Endemic Areas of American Visceral Leishmaniasis in Northeastern Brazil. Available from: https://www.hindawi.com/journals/jtm/2012/858657/abs/

75. Noireau F, Diosque P, Jansen AM. Trypanosoma cruzi: adaptation to its vectors and its hosts. Vet Res [Internet]. 2009 [cited 2019 Jun 5];40(2). Available from: https://www.ncbi.nlm.nih.gov/pmc/articles/PMC2695024/

76. Jansen AM, Xavier SC das C, Roque ALR. Trypanosoma cruzi transmission in the wild and its most important reservoir hosts in Brazil. Parasit Vectors. 2018 Sep 6;11(1):502.

77. Roque ALR, Jansen AM. Wild and synanthropic reservoirs of Leishmania species in the Americas. Int J Parasitol Parasites Wildl. 2014 Aug 29;3(3):251–62.

78. Singh N, Mishra J, Singh R, Singh S. Animal Reservoirs of Visceral Leishmaniasis in India. J Parasitol. 2013 Feb;99(1):64–7.

79. Ran FA, Hsu PD, Wright J, Agarwala V, Scott DA, Zhang F. Genome engineering using the CRISPR-Cas9 system. Nat Protoc. 2013 Nov;8(11):2281–308.

80. Würtele H, Little KCE, Chartrand P. Illegitimate DNA integration in mammalian cells. Gene Ther. 2003 Oct;10(21):1791–9.

81. Kirchhoff J, Schiermeyer A, Schneider K, Fischer R, Ainley WM, Webb SR, et al. Gene expression variability between randomly and targeted transgene integration events in tobacco suspension cell lines. Plant Biotechnol Rep. 2020 Aug 1;14(4):451–8.

82. Nakatake Y, Fujii S, Masui S, Sugimoto T, Torikai-Nishikawa S, Adachi K, et al. Kinetics of drug selection systems in mouse embryonic stem cells. BMC Biotechnol. 2013 Aug 7;13:64.

83. Tomomura M, Rice DS, Morgan JI, Yuzaki M. Purification of Purkinje cells by fluorescence-activated cell sorting from transgenic mice that express green fluorescent protein. Eur J Neurosci. 2001;14(1):57–63.

84. Yamamoto DS, Sumitani M, Hatakeyama M, Matsuoka H. Malaria infectivity of xanthurenic acid-deficient anopheline mosquitoes produced by TALEN-mediated targeted mutagenesis. Transgenic Res. 2018 Feb 1;27(1):51–60.

85. Dong Y, Simões ML, Marois E, Dimopoulos G. CRISPR/Cas9 -mediated gene knockout of Anopheles gambiae FREP1 suppresses malaria parasite infection. PLOS Pathog. 2018 Mar 8;14(3):e1006898.

86. Nolan T, Petris E, Müller HM, Cronin A, Catteruccia F, Crisanti A. Analysis of Two Novel Midgut-Specific Promoters Driving Transgene Expression in Anopheles stephensi Mosquitoes. PLOS ONE. 2011 Feb 4;6(2):e16471.

87. Volohonsky G, Hopp AK, Saenger M, Soichot J, Scholze H, Boch J, et al. Transgenic Expression of the Anti-parasitic Factor TEP1 in the Malaria Mosquito Anopheles gambiae. PLOS Pathog. 2017 Jan 17;13(1):e1006113.

88. Fraser MJ, Smith GE, Summers MD. Acquisition of Host Cell DNA Sequences by Baculoviruses: Relationship Between Host DNA Insertions and FP Mutants of Autographa californica and Galleria mellonella Nuclear Polyhedrosis Viruses. J Virol. 1983 Aug;47(2):287–300.

89. Cary LC, Goebel M, Corsaro BG, Wang HG, Rosen E, Fraser MJ. Transposon mutagenesis of baculoviruses: analysis of Trichoplusia ni transposon IFP2 insertions within the FP-locus of nuclear polyhedrosis viruses. Virology. 1989 Sep;172(1):156–69.

90. Fraser MJ, Clszczon T, Elick T, Bauser C. Precise excision of TTAA-specific lepidopteran transposons piggyBac (IFP2) and tagalong (TFP3) from the baculovirus genome in cell lines from two species of Lepidoptera. Insect Mol Biol. 1996;5(2):141–51.

91. Sarkar A, Sim C, Hong YS, Hogan JR, Fraser MJ, Robertson HM, et al. Molecular evolutionary analysis of the widespread piggyBac transposon family and related 'domesticated' sequences. Mol Genet Genomics. 2003 Oct 1;270(2):173–80.

92. Chen Q, Luo W, Veach RA, Hickman AB, Wilson MH, Dyda F. Structural basis of seamless excision and specific targeting by piggyBac transposase. Nat Commun. 2020 Jul 10;11(1):3446.

93. Ding S, Wu X, Li G, Han M, Zhuang Y, Xu T. Efficient Transposition of the piggyBac (PB) Transposon in Mammalian Cells and Mice. Cell. 2005 Aug 12;122(3):473–83.

94. Wu SCY, Meir YJJ, Coates CJ, Handler AM, Pelczar P, Moisyadi S, et al. piggyBac is a flexible and highly active transposon as compared to Sleeping Beauty, Tol2, and Mos1 in mammalian cells. Proc Natl Acad Sci. 2006 Oct 10;103(41):15008–13.

95. Wilson MH, Coates CJ, George AL. PiggyBac transposon-mediated gene transfer in human cells. Mol Ther J Am Soc Gene Ther. 2007 Jan;15(1):139–45.

96. Cadiñanos J, Bradley A. Generation of an inducible and optimized piggyBac transposon system†. Nucleic Acids Res. 2007 Jun 15;35(12):e87.

97. Yusa K, Zhou L, Li MA, Bradley A, Craig NL. A hyperactive piggyBac transposase for mammalian applications. Proc Natl Acad Sci. 2011 Jan 25;108(4):1531–6.

98. Wright JA, Smith RC, Li X, Craig NL, Atkinson PW. IPB7 transposase behavior in Drosophila melanogaster and Aedes aegypti. Insect Biochem Mol Biol. 2013 Oct 1;43(10):899–906.

99. Labbé GMC, Nimmo DD, Alphey L. piggybac- and PhiC31-Mediated Genetic Transformation of the Asian Tiger Mosquito, Aedes albopictus (Skuse). PLoS Negl Trop Dis. 2010 Aug 17;4(8):e788.

100. Grossman GL, Rafferty CS, Clayton JR, Stevens TK, Mukabayire O, Benedict MQ. Germline transformation of the malaria vector, Anopheles gambiae, with the piggyBac transposable element. Insect Mol Biol. 2001;10(6):597–604.

101. Sumitani M, Yamamoto DS, Oishi K, Lee JM, Hatakeyama M. Germline transformation of the sawfly, Athalia rosae (Hymenoptera: Symphyta), mediated by a piggyBac-derived vector. Insect Biochem Mol Biol. 2003 Apr 1;33(4):449–58.

102. Raphael KA, Shearman DCA, Streamer K, Morrow JL, Handler AM, Frommer M. Germ-line transformation of the Queensland fruit fly, Bactrocera tryoni, using a piggyBac vector in the presence of endogenous piggyBac elements. Genetica. 2011 Jan;139(1):91–7.

103. Li X, Guan Z, Wang F, Wang Y, Asare E, Shi S, et al. Evolution of piggyBac Transposons in Apoidea. Insects. 2023 Apr;14(4):402.

104. Tamura T, Thibert C, Royer C, Kanda T, Eappen A, Kamba M, et al. Germline transformation of the silkworm Bombyx mori L. using a piggyBac transposon-derived vector. Nat Biotechnol. 2000 Jan;18(1):81–4.

105. Allen ML, Handler AM, Berkebile DR, Skoda SR. piggyBac transformation of the New World screwworm, Cochliomyia hominivorax, produces multiple distinct mutant strains. Med Vet Entomol. 2004 Mar;18(1):1–9.

106. Kuwayama H, Yaginuma T, Yamashita O, Niimi T. Germ-line transformation and RNAi of the ladybird beetle, Harmonia axyridis. Insect Mol Biol. 2006;15(4):507–12.

107. Lorenzen MD, Berghammer AJ, Brown SJ, Denell RE, Klingler M, Beeman RW. piggyBac-mediated germline transformation in the beetle Tribolium castaneum. Insect Mol Biol. 2003 Oct;12(5):433–40.

108. Schertzer MD, Thulson E, Braceros KCA, Lee DM, Hinkle ER, Murphy RM, et al. A piggyBac-based toolkit for inducible genome editing in mammalian cells. RNA. 2019 Aug;25(8):1047–58.

109. Verkuijl SAN, Gonzalez E, Li M, Ang JXD, Kandul NP, Anderson MAE, et al. A CRISPR endonuclease gene drive reveals distinct mechanisms of inheritance bias. Nat Commun. 2022 Nov 21;13:7145.

110. Li M, Kandul NP, Sun R, Yang T, Benetta ED, Brogan DJ, et al. Targeting Sex Determination to Suppress Mosquito Populations. bioRxiv. 2023 Apr 20;2023.04.18.537404.

111. Smith HO, Wilcox KW. A restriction enzyme from Hemophilus influenzae. I. Purification and general properties. J Mol Biol. 1970 Jul 28;51(2):379–91.

112. Li L, Wu LP, Chandrasegaran S. Functional domains in Fok I restriction endonuclease. Proc Natl Acad Sci U S A. 1992 May 15;89(10):4275–9.

113. Boch J, Scholze H, Schornack S, Landgraf A, Hahn S, Kay S, et al. Breaking the Code of DNA Binding Specificity of TAL-Type III Effectors. Science. 2009 Dec 11;326(5959):1509–12.

114. Kim YG, Cha J, Chandrasegaran S. Hybrid restriction enzymes: zinc finger fusions to Fok I cleavage domain. Proc Natl Acad Sci. 1996 Feb 6;93(3):1156–60.

115. Urnov FD, Rebar EJ, Holmes MC, Zhang HS, Gregory PD. Genome editing with engineered zinc finger nucleases. Nat Rev Genet. 2010 Sep;11(9):636–46.

116. Miller J, McLachlan AD, Klug A. Repetitive zinc-binding domains in the protein transcription factor IIIA from Xenopus oocytes. EMBO J. 1985 Jun 1;4(6):1609–14.

117. Bibikova M, Carroll D, Segal DJ, Trautman JK, Smith J, Kim YG, et al. Stimulation of Homologous Recombination through Targeted Cleavage by Chimeric Nucleases. Mol Cell Biol. 2001 Jan;21(1):289–97.

118. Segal DJ, Crotty JW, Bhakta MS, Barbas CF, Horton NC. Structure of Aart, a Designed Six-finger Zinc Finger Peptide, Bound to DNA. J Mol Biol. 2006 Oct 20;363(2):405–21.

119. Paschon DE, Lussier S, Wangzor T, Xia DF, Li PW, Hinkley SJ, et al. Diversifying the structure of zinc finger nucleases for high-precision genome editing. Nat Commun. 2019 Mar 8;10(1):1133.

120. Nakajima K, Nakajima T, Takase M, Yaoita Y. Generation of albino Xenopus tropicalis using zinc-finger nucleases. Dev Growth Differ. 2012;54(9):777–84.

121. Beumer KJ, Trautman JK, Bozas A, Liu JL, Rutter J, Gall JG, et al. Efficient gene targeting in Drosophila by direct embryo injection with zinc-finger nucleases. Proc Natl Acad Sci. 2008 Dec 16;105(50):19821–6.

122. Geurts AM, Cost GJ, Freyvert Y, Zeitler B, Miller JC, Choi VM, et al. Knockout Rats via Embryo Microinjection of Zinc-Finger Nucleases. Science. 2009 Jul 24;325(5939):433–433.

123. Doyon Y, McCammon JM, Miller JC, Faraji F, Ngo C, Katibah GE, et al. Heritable targeted gene disruption in zebrafish using designed zinc-finger nucleases. Nat Biotechnol. 2008 Jun;26(6):702–8.

124. Takasu Y, Kobayashi I, Beumer K, Uchino K, Sezutsu H, Sajwan S, et al. Targeted mutagenesis in the silkworm Bombyx mori using zinc finger nuclease mRNA injection. Insect Biochem Mol Biol. 2010 Oct;40(10):759–65.

125. Watanabe T, Ochiai H, Sakuma T, Horch HW, Hamaguchi N, Nakamura T, et al. Non-transgenic genome modifications in a hemimetabolous insect using zinc-finger and TAL effector nucleases. Nat Commun. 2012 Aug 21;3(1):1017.

126. Choudhury TP, Roy A. A review on principles, applications and the current challenges to genome editing in insects.

127. Joung JK, Sander JD. TALENs: a widely applicable technology for targeted genome editing. Nat Rev Mol Cell Biol. 2013 Jan;14(1):49–55.

128. Bhardwaj A, Nain V. TALENs—an indispensable tool in the era of CRISPR: a mini review. J Genet Eng Biotechnol. 2021 Aug 21;19(1):125.

129. Liu J, Li C, Yu Z, Huang P, Wu H, Wei C, et al. Efficient and Specific Modifications of the Drosophila Genome by Means of an Easy TALEN Strategy. J Genet Genomics. 2012 May 20;39(5):209–15.

130. Xu J, Dong Q, Yu Y, Niu B, Ji D, Li M, et al. Mass spider silk production through targeted gene replacement in Bombyx mori. Proc Natl Acad Sci U S A. 2018 Aug 28;115(35):8757–62.

131. Yang B, Fujii T, Ishikawa Y, Matsuo T. Targeted mutagenesis of an odorant receptor co-receptor using TALEN in Ostrinia furnacalis. Insect Biochem Mol Biol. 2016 Mar 1;70:53–9.

132. Ishino Y, Shinagawa H, Makino K, Amemura M, Nakata A. Nucleotide sequence of the iap gene, responsible for alkaline phosphatase isozyme conversion in Escherichia coli, and identification of the gene product. J Bacteriol. 1987 Dec;169(12):5429–33.

133. Garneau JE, Dupuis MÈ, Villion M, Romero DA, Barrangou R, Boyaval P, et al. The CRISPR/Cas bacterial immune system cleaves bacteriophage and plasmid DNA. Nature. 2010 Nov;468(7320):67–71.

134. Gasiunas G, Barrangou R, Horvath P, Siksnys V. Cas9–crRNA ribonucleoprotein complex mediates specific DNA cleavage for adaptive immunity in bacteria. Proc Natl Acad Sci. 2012 Sep 25;109(39):E2579–86.

135. Bassett AR, Tibbit C, Ponting CP, Liu JL. Highly Efficient Targeted Mutagenesis of Drosophila with the CRISPR/Cas9 System. Cell Rep. 2013 Jul 11;4(1):220–8.

136. Gilles AF, Schinko JB, Averof M. Efficient CRISPR-mediated gene targeting and transgene replacement in the beetle Tribolium castaneum. Development. 2015 Aug 15;142(16):2832–9.

137. Gantz VM, Jasinskiene N, Tatarenkova O, Fazekas A, Macias VM, Bier E, et al. Highly efficient Cas9-mediated gene drive for population modification of the malaria vector mosquito Anopheles stephensi. Proc Natl Acad Sci. 2015 Dec 8;112(49):E6736–43.

138. Kotwica-Rolinska J, Chodakova L, Chvalova D, Kristofova L, Fenclova I, Provaznik J, et al. CRISPR/Cas9 Genome Editing Introduction and Optimization in the Non-model Insect Pyrrhocoris apterus. Front Physiol [Internet]. 2019 [cited 2023 Apr 23];10. Available from: https://www.frontiersin.org/articles/10.3389/fphys.2019.00891

139. Hu XF, Zhang B, Liao CH, Zeng ZJ. High-Efficiency CRISPR/Cas9-Mediated Gene Editing in Honeybee (*Apis mellifera*) Embryos. G3amp58 GenesGenomesGenetics. 2019 May;9(5):1759–66.

140. Zhang Z, Aslam AFM, Liu X, Li M, Huang Y, Tan A. Functional analysis of Bombyx Wnt1 during embryogenesis using the CRISPR/Cas9 system. J Insect Physiol. 2015 Aug 1;79:73–9.

141. Li Y, Zhang J, Chen D, Yang P, Jiang F, Wang X, et al. CRISPR/Cas9 in locusts: Successful establishment of an olfactory deficiency line by targeting the mutagenesis of an odorant receptor co-receptor (Orco). Insect Biochem Mol Biol. 2016 Dec 1;79:27–35.

142. Ohde T, Takehana Y, Shiotsuki T, Niimi T. CRISPR/Cas9-based heritable targeted mutagenesis in Thermobia domestica: A genetic tool in an apterygote development model of wing evolution. Arthropod Struct Dev. 2018 Jul 1;47(4):362–9.

143. Awata H, Watanabe T, Hamanaka Y, Mito T, Noji S, Mizunami M. Knockout crickets for the study of learning and memory: Dopamine receptor Dop1 mediates aversive but not appetitive reinforcement in crickets. Sci Rep. 2015 Nov 2;5(1):15885.

144. Hu W, Wang X, Ma S, Peng Z, Cao Y, Xia Q. CRISPR-Mediated Endogenous Activation of Fibroin Heavy Chain Gene Triggers Cellular Stress Responses in Bombyx mori Embryonic Cells. Insects. 2021 Jun;12(6):552.

145. Huynh N, Zeng J, Liu W, King-Jones K. A Drosophila CRISPR/Cas9 Toolkit for Conditionally Manipulating Gene Expression in the Prothoracic Gland as a Test Case for Polytene Tissues. G3 GenesGenomesGenetics. 2018 Nov 1;8(11):3593–605.

146. Wilson AL, Courtenay O, Kelly-Hope LA, Scott TW, Takken W, Torr SJ, et al. The importance of vector control for the control and elimination of vector-borne diseases. PLoS Negl Trop Dis. 2020 Jan 16;14(1):e0007831.

147. Wang GH, Gamez S, Raban RR, Marshall JM, Alphey L, Li M, et al. Combating mosquito-borne diseases using genetic control technologies. Nat Commun. 2021 Jul 19;12(1):4388.

148. Otwell E, Telfer M. Gene drives spread their wings [Internet]. 2015 [cited 2023 May 26]. Available from: https://www.sciencenews.org/article/gene-drives-spread-their-wings

149. Dyby SD. Embryogenesis. In: Capinera JL, editor. Encyclopedia of Entomology [Internet]. Dordrecht: Springer Netherlands; 2008 [cited 2023 Dec 22]. p. 1301–6. Available from: https://doi.org/10.1007/978-1-4020-6359-6_3541

150. Abbassy MM, Helmy N, Osman M, Cope SE, Presley SM. Embryogenesis of the Sand Fly Phlebotomus papatasi (Diptera: Psychodidae): Cell Cleavage, Blastoderm Formation, and Gastrulation. Ann Entomol Soc Am. 1995 Nov 1;88(6):809–14.

151. Nunes-da-Fonseca R, Berni M, Tobias-Santos V, Pane A, Araujo HM. Rhodnius prolixus: From classical physiology to modern developmental biology. genesis. 2017;55(5):e22995.

152. Jeffries CL, Rogers ME, Walker T. Establishment of a method for Lutzomyia longipalpis sand fly egg microinjection: The first step towards potential novel control strategies for leishmaniasis. Wellcome Open Res [Internet]. 2018 Aug 15 [cited 2019 Jul 3];3. Available from: https://www.ncbi.nlm.nih.gov/pmc/articles/PMC6107984/

153. Alphey LS, Crisanti A, Randazzo F (Fil), Akbari OS. Opinion: Standardizing the definition of gene drive. Proc Natl Acad Sci U S A. 2020 Dec 8;117(49):30864–7.

154. Sinkins SP, Gould F. Gene drive systems for insect disease vectors. Nat Rev Genet. 2006 Jun;7(6):427.

155. Hammond A, Galizi R, Kyrou K, Simoni A, Siniscalchi C, Katsanos D, et al. A CRISPR-Cas9 gene drive system targeting female reproduction in the malaria mosquito vector *Anopheles gambiae*. Nat Biotechnol. 2016 Jan;34(1):78–83.

156. Gantz VM, Bier E. Genome editing. The mutagenic chain reaction: a method for converting heterozygous to homozygous mutations. Science. 2015 Apr 24;348(6233):442–4.

157. Kyrou K, Hammond AM, Galizi R, Kranjc N, Burt A, Beaghton AK, et al. A CRISPR–Cas9 gene drive targeting *doublesex* causes complete population suppression in caged *Anopheles gambiae* mosquitoes. Nat Biotechnol. 2018 Nov;36(11):1062–6.

158. Champer J, Liu J, Oh SY, Reeves R, Luthra A, Oakes N, et al. Reducing resistance allele formation in CRISPR gene drive. Proc Natl Acad Sci. 2018 May 22;115(21):5522–7.

159. Marshall JM, Buchman A, Sánchez C. HM, Akbari OS. Overcoming evolved resistance to population-suppressing homing-based gene drives. Sci Rep. 2017 Jun 19;7(1):3776.

160. Vella MR, Gunning CE, Lloyd AL, Gould F. Evaluating strategies for reversing CRISPR-Cas9 gene drives. Sci Rep. 2017 Sep 8;7(1):11038.

161. Noble C, Min J, Olejarz J, Buchthal J, Chavez A, Smidler AL, et al. Daisy-chain gene drives for the alteration of local populations. Proc Natl Acad Sci U S A. 2019 Apr 23;116(17):8275–82.

162. Girardin L, Calvez V, Débarre F. Catch Me If You Can: A Spatial Model for a Brake-Driven Gene Drive Reversal. Bull Math Biol. 2019 Dec 1;81(12):5054–88.

163. Edgington MP, Alphey LS. Modeling the mutation and reversal of engineered underdominance gene drives. J Theor Biol. 2019 Oct 21;479:14–21.

164. Hall AB, Basu S, Jiang X, Qi Y, Timoshevskiy VA, Biedler JK, et al. A male-determining factor in the mosquito Aedes aegypti. Science. 2015 Jun 12;348(6240):1268–70.

165. Galizi R, Hammond A, Kyrou K, Taxiarchi C, Bernardini F, O'Loughlin SM, et al. A CRISPR-Cas9 sex-ratio distortion system for genetic control. Sci Rep. 2016 Aug 3;6(1):31139.

166. Simoni A, Hammond AM, Beaghton AK, Galizi R, Taxiarchi C, Kyrou K, et al. A male-biased sex-distorter gene drive for the human malaria vector Anopheles gambiae. Nat Biotechnol. 2020 Sep;38(9):1054–60.

167. Chen J, Luo J, Wang Y, Gurav AS, Li M, Akbari OS, et al. Suppression of female fertility in Aedes aegypti with a CRISPR-targeted male-sterile mutation. Proc Natl Acad Sci. 2021 Jun;118(22):e2105075118.

168. Li M, Yang T, Bui M, Gamez S, Wise T, Kandul NP, et al. Suppressing mosquito populations with precision guided sterile males. Nat Commun. 2021 Sep 10;12(1):5374.

169. Navarro-Payá D, Flis I, Anderson MAE, Hawes P, Li M, Akbari OS, et al. Targeting female flight for genetic control of mosquitoes. PLoS Negl Trop Dis. 2020 Dec 3;14(12):e0008876.

170. O'Leary S, Adelman ZN. CRISPR/Cas9 knockout of female-biased genes AeAct-4 or myo-fem in Ae. aegypti results in a flightless phenotype in female, but not male mosquitoes. PLoS Negl Trop Dis. 2020 Dec;14(12):e0008971.

171. Tree of Sex Consortium. Tree of Sex: a database of sexual systems. Sci Data. 2014;1:140015.

172. Zhang Z, Niu B, Ji D, Li M, Li K, James AA, et al. Silkworm genetic sexing through W chromosome-linked, targeted gene integration. Proc Natl Acad Sci U S A. 2018 Aug 28;115(35):8752–6.

173. Gilbert LA, Horlbeck MA, Adamson B, Villalta JE, Chen Y, Whitehead EH, et al. Genome-Scale CRISPR-Mediated Control of Gene Repression and Activation. Cell. 2014 Oct 23;159(3):647–61.

174. Chase BA, Baker BS. A Genetic Analysis of Intersex, a Gene Regulating Sexual Differentiation in Drosophila Melanogaster Females. Genetics. 1995 Apr;139(4):1649–61.

175. Smith RC, Walter MF, Hice RH, O'Brochta DA, Atkinson PW. Testis-specific expression of the β2 tubulin promoter of Aedes aegypti and its application as a genetic sex-separation marker. Insect Mol Biol. 2007;16(1):61–71.

176. Burtis KC, Baker BS. Drosophila doublesex gene controls somatic sexual differentiation by producing alternatively spliced mRNAs encoding related sex-specific polypeptides. Cell. 1989 Mar 24;56(6):997–1010.

177. Basrur NS, De Obaldia ME, Morita T, Herre M, von Heynitz RK, Tsitohay YN, et al. Fruitless mutant male mosquitoes gain attraction to human odor. eLife. 9:e63982.

178. Clowney EJ, Iguchi S, Bussell JJ, Scheer E, Ruta V. Multimodal Chemosensory Circuits Controlling Male Courtship in Drosophila. Neuron. 2015 Sep 2;87(5):1036–49.

179. Tanaka R, Higuchi T, Kohatsu S, Sato K, Yamamoto D. Optogenetic Activation of the fruitless-Labeled Circuitry in Drosophila subobscura Males Induces Mating Motor Acts. J Neurosci. 2017 Nov 29;37(48):11662–74.

180. Vosshall LB, Amrein H, Morozov PS, Rzhetsky A, Axel R. A Spatial Map of Olfactory Receptor Expression in the Drosophila Antenna. Cell. 1999 Mar 5;96(5):725–36.

181. Xia Y, Zwiebel LJ. Identification and characterization of an odorant receptor from the West Nile Virus mosquito, Culex quinquefasciatus. Insect Biochem Mol Biol. 2006 Mar 1;36(3):169–76.

182. Dame DA, Curtis CF, Benedict MQ, Robinson AS, Knols BG. Historical applications of induced sterilisation in field populations of mosquitoes. Malar J. 2009 Nov 16;8(2):S2.

183. Kandul NP, Liu J, Sanchez C HM, Wu SL, Marshall JM, Akbari OS. Transforming insect population control with precision guided sterile males with demonstration in flies. Nat Commun. 2019 Jan 8;10(1):84.

184. Kandul NP, Liu J, Buchman A, Shriner IC, Corder RM, Warsinger-Pepe N, et al. Precision Guided Sterile Males Suppress Populations of an Invasive Crop Pest. GEN Biotechnol. 2022 Aug;1(4):372–85.

185. RESNIK DB. ETHICAL ISSUES IN FIELD TRIALS OF GENETICALLY MODIFIED DISEASE-RESISTANT MOSQUITOES. Dev World Bioeth. 2014 Apr;14(1):37–46.

186. Carballar-Lejarazú R, Tushar T, Pham TB, James AA. Microinjection Method for Anopheles gambiae Embryos. J Vis Exp. 2021 Jul 7;(173):62591.

187. Billker O, Lindo V, Panico M, Etienne AE, Paxton T, Dell A, et al. Identification of xanthurenic acid as the putative inducer of malaria development in the mosquito. Nature. 1998 Mar;392(6673):289–92.

188. Kamhawi S, Ramalho-Ortigao M, Van M. Pham, Kumar S, Lawyer PG, Turco SJ, et al. A Role for Insect Galectins in Parasite Survival. Cell. 2004 Oct;119(3):329–41.

189. R. Hall A, T. Blakeman J, M. Eissa A, Chapman P, L. Morales-García A, Stennett L, et al. Glycan–glycan interactions determine Leishmania attachment to the midgut of permissive sand fly vectors. Chem Sci. 2020;11(40):10973–83.

190. Alves CR, Albuquerque-Cunha JM, Mello CB, Garcia ES, Nogueira NF, Bourguingnon SC, et al. Trypanosoma cruzi: Attachment to perimicrovillar membrane glycoproteins of Rhodnius prolixus. Exp Parasitol. 2007 May 1;116(1):44–52.

191. de Fuentes-Vicente JA, Gutiérrez-Cabrera AE, Flores-Villegas AL, Lowenberger C, Benelli G, Salazar-Schettino PM, et al. What makes an effective Chagas disease vector? Factors underlying Trypanosoma cruzi-triatomine interactions. Acta Trop. 2018 Jul 1;183:23–31.

192. Telleria EL, Sant'Anna MRV, Ortigão-Farias JR, Pitaluga AN, Dillon VM, Bates PA, et al. Caspar-like Gene Depletion Reduces Leishmania Infection in Sand Fly Host Lutzomyia longipalpis. J Biol Chem. 2012 Apr 13;287(16):12985–93.

193. Yamamoto DS, Nagumo H, Yoshida S. Flying vaccinator; a transgenic mosquito delivers a Leishmania vaccine via blood feeding: Flying vaccinator mosquito. Insect Mol Biol. 2010 Mar 19;19(3):391–8.

194. Mishra P, Furey C, Balaraman V, Fraser MJ. Antiviral Hammerhead Ribozymes Are Effective for Developing Transgenic Suppression of Chikungunya Virus in Aedes aegypti Mosquitoes. Viruses. 2016 Jun;8(6):163.

195. Williams AE, Sanchez-Vargas I, Reid WR, Lin J, Franz AWE, Olson KE. The Antiviral Small-Interfering RNA Pathway Induces Zika Virus Resistance in Transgenic Aedes aegypti. Viruses. 2020 Nov;12(11):1231.

196. Yen PS, James A, Li JC, Chen CH, Failloux AB. Synthetic miRNAs induce dual arboviral-resistance phenotypes in the vector mosquito Aedes aegypti. Commun Biol. 2018 Feb 8;1(1):1–9.

197. Isaacs AT, Jasinskiene N, Tretiakov M, Thiery I, Zettor A, Bourgouin C, et al. Transgenic Anopheles stephensi coexpressing single-chain antibodies resist Plasmodium falciparum development. Proc Natl Acad Sci U S A. 2012 Jul 10;109(28):E1922–30.

198. Pham TB, Phong CH, Bennett JB, Hwang K, Jasinskiene N, Parker K, et al. Experimental population modification of the malaria vector mosquito, Anopheles stephensi. PLOS Genet. 2019 Dec 19;15(12):e1008440.

199. Adolfi A, Gantz VM, Jasinskiene N, Lee HF, Hwang K, Terradas G, et al. Efficient population modification gene-drive rescue system in the malaria mosquito Anopheles stephensi. Nat Commun. 2020 Nov 3;11(1):5553.

200. Nogueira NFS, Gonzales M, Garcia EM, de Souza W. Effect of Azadirachtin A on the Fine Structure of the Midgut ofRhodnius prolixus. J Invertebr Pathol. 1997 Jan 1;69(1):58–63.

201. Hoermann A, Habtewold T, Selvaraj P, Del Corsano G, Capriotti P, Inghilterra MG, et al. Gene drive mosquitoes can aid malaria elimination by retarding *Plasmodium* sporogonic development. Sci Adv. 2022 Sep 23;8(38):eabo1733.

202. Kückelhaus SAS, Leite JRSA, Muniz-Junqueira MI, Sampaio RN, Bloch C, Tosta CE. Antiplasmodial and antileishmanial activities of phylloseptin-1, an antimicrobial peptide from the skin secretion of Phyllomedusa azurea (Amphibia). Exp Parasitol. 2009 Sep 1;123(1):11–6.

203. Zhang R, Zhou M, Wang L, McGrath S, Chen T, Chen X, et al. Phylloseptin-1 (PSN-1) from Phyllomedusa sauvagei skin secretion: A novel broad-spectrum antimicrobial peptide with antibiofilm activity. Mol Immunol. 2010 Jul 1;47(11):2030–7.

204. Miranda A, Jouvensal L, Vovelle F, Bulet P, Daffre S. Gomesin: a powerful antimicrobial peptide isolated from the Brazilian tarantula spider Acanthoscurria gomesiana. 2009 [cited 2019 Jul 6]; Available from: https://hal.archives-ouvertes.fr/hal-00283559

205. Shigenaga T, Muta T, Toh Y, Tokunaga F, Iwanaga S. Antimicrobial tachyplesin peptide precursor. cDNA cloning and cellular localization in the horseshoe crab (Tachypleus tridentatus). J Biol Chem. 1990 Dec 5;265(34):21350–4.

206. Brand GD, Leite JRSA, Silva LP, Albuquerque S, Prates MV, Azevedo RB, et al. Dermaseptins from Phyllomedusa oreades and Phyllomedusa distincta. Anti-Trypanosoma cruzi activity without cytotoxicity to mammalian cells. J Biol Chem. 2002 Dec 20;277(51):49332–40.

207. Bera A, Singh S, Nagaraj R, Vaidya T. Induction of autophagic cell death in Leishmania donovani by antimicrobial peptides. Mol Biochem Parasitol. 2003 Mar;127(1):23–35.

208. Berrocal-Lobo M, Molina A, Rodríguez-Palenzuela P, García-Olmedo F, Rivas L. Leishmania donovani: Thionins, plant antimicrobial peptides with leishmanicidal activity. Exp Parasitol. 2009 Jul 1;122(3):247–9.

209. Borges A, Silva S, Op den Camp HJM, Velasco E, Alvarez M, Alfonzo MJM, et al. In vitro leishmanicidal activity of Tityus discrepans scorpion venom. Parasitol Res. 2006 Jul 1;99(2):167–73.

210. Yu Y, Zhao P, Cao L, Gong P, Yuan S, Yao X, et al. A Novel Anti-Microbial Peptide from Pseudomonas, REDLK Induced Growth Inhibition of Leishmania tarentolae Promastigote In Vitro. Korean J Parasitol. 2020 Apr;58(2):173–9.

211. Pitale DM, Kaur G, Baghel M, Kaur KJ, Shaha C. Halictine-2 antimicrobial peptide shows promising anti-parasitic activity against Leishmania spp. Exp Parasitol. 2020 Nov 1;218:107987.

212. Haines LR, Thomas JM, Jackson AM, Eyford BA, Razavi M, Watson CN, et al. Killing of Trypanosomatid Parasites by a Modified Bovine Host Defense Peptide, BMAP-18. PLoS Negl Trop Dis [Internet]. 2009 Feb 3 [cited 2018 Dec 18];3(2). Available from: https://www.ncbi.nlm.nih.gov/pmc/articles/PMC2628741/

213. Parente AMS, Daniele-Silva A, Furtado AA, Melo MA, Lacerda AF, Queiroz M, et al. Analogs of the Scorpion Venom Peptide Stigmurin: Structural Assessment, Toxicity, and Increased Antimicrobial Activity. Toxins [Internet]. 2018 Apr 18 [cited 2018 Dec 17];10(4). Available from: https://www.ncbi.nlm.nih.gov/pmc/articles/PMC5923327/

214. Jacobs T, Bruhn H, Gaworski I, Fleischer B, Leippe M. NK-Lysin and Its Shortened Analog NK-2 Exhibit Potent Activities against Trypanosoma cruzi. Antimicrob Agents Chemother. 2003 Feb;47(2):607–13.

215. Lima DB, Mello CP, Bandeira ICJ, Menezes RRPPB de, Sampaio TL, Falcão CB, et al. The dinoponeratoxin peptides from the giant ant Dinoponera quadriceps display in vitro antitrypanosomal activity. Biol Chem. 2018 Jan 26;399(2):187–96.

216. Monteiro ML, Lima DB, Menezes RRPPB de, Sampaio TL, Silva BP, Serra Nunes JV, et al. Antichagasic effect of hemocyanin derived from antimicrobial peptides of penaeus monodon shrimp. Exp Parasitol. 2020 Aug 1;215:107930.

217. Ramírez-Carreto S, Quintero-Hernández V, Jiménez-Vargas JM, Corzo G, Possani LD, Becerril B, et al. Gene cloning and functional characterization of four novel antimicrobial-like peptides from scorpions of the family Vaejovidae. Peptides. 2012 Apr 1;34(2):290–5.

218. Pedron CN, Freire KA, Torres MDT, Lima DB, Monteiro ML, Menezes RRPPB de, et al. Arg-substituted VmCT1 analogs reveals promising candidate for the development of new antichagasic agent. Parasitology. 2020 Dec;147(14):1810–8.

219. Hu C, Aksoy S. Innate immune responses regulate trypanosome parasite infection of the tsetse fly Glossina morsitans morsitans. Mol Microbiol. 2006 Jun 1;60(5):1194–204.

220. Santana CJC, Magalhães ACM, dos Santos Júnior ACM, Ricart CAO, Lima BD, Álvares A da CM, et al. Figainin 1, a Novel Amphibian Skin Peptide with Antimicrobial and Antiproliferative Properties. Antibiotics. 2020 Sep;9(9):625.

221. Larabi M, Yardley V, Loiseau PM, Appel M, Legrand P, Gulik A, et al. Toxicity and Antileishmanial Activity of a New Stable Lipid Suspension of Amphotericin B. Antimicrob Agents Chemother. 2003 Dec;47(12):3774–9.

222. Louradour I, Ghosh K, Inbar E, Sacks DL. CRISPR/Cas9 Mutagenesis in Phlebotomus papatasi: the Immune Deficiency Pathway Impacts Vector Competence for Leishmania major. mBio. 2019 Aug 27;10(4):e01941-19.

223. Louradour I, Monteiro C, Inbar E, Ghosh K, Merkhofer R, Lawyer P, et al. The midgut microbiota plays an essential role in sand fly vector competence for Leishmania major. Cell Microbiol. 2017 Jun 5;19.

224. Xu Y, Viswanatha R, Sitsel O, Roderer D, Zhao H, Ashwood C, et al. CRISPR screens in Drosophila cells identify Vsg as a Tc toxin receptor. Nature. 2022;610(7931):349–55.

225. Varjak M, Maringer K, Watson M, Sreenu VB, Fredericks AC, Pondeville E, et al. Aedes aegypti Piwi4 Is a Noncanonical PIWI Protein Involved in Antiviral Responses. mSphere. 2017 May 3;2(3):e00144-17.

226. Yee CM, Zak AJ, Hill BD, Wen F. The Coming Age of Insect Cells for Manufacturing and Development of Protein Therapeutics. Ind Eng Chem Res. 2018 Aug 8;57(31):10061–70.

227. Aulicino F, Pelosse M, Toelzer C, Capin J, Ilegems E, Meysami P, et al. Highly efficient CRISPR-mediated large DNA docking and multiplexed prime editing using a single baculovirus. Nucleic Acids Res. 2022 Jul 22;50(13):7783–99.

228. Nweke EE, Thimiri Govinda Raj DB. Development of insect cell line using CRISPR technology. Prog Mol Biol Transl Sci. 2021;180:1–20.

229. Fredericks AC, Russell TA, Wallace LE, Davidson AD, Fernandez-Sesma A, Maringer K. Aedes aegypti (Aag2)-derived clonal mosquito cell lines reveal the effects of pre-existing persistent infection with the insect-specific bunyavirus Phasi Charoen-like virus on arbovirus replication. PLoS Negl Trop Dis. 2019 Nov 6;13(11):e0007346.

230. Müller HM, Dimopoulos G, Blass C, Kafatos FC. A hemocyte-like cell line established from the malaria vector Anopheles gambiae expresses six prophenoloxidase genes. J Biol Chem. 1999 Apr 23;274(17):11727–35.

231. Hsu SH, Mao WH, Cross JH. Establishment of a Line of Cells Derived from Ovarian Tissue of Culex Quinquefasciatus Say1. J Med Entomol. 1970 Dec 1;7(6):703–7.

232. Rozen-Gagnon K, Yi S, Jacobson E, Novack S, Rice CM. A selectable, plasmid-based system to generate CRISPR/Cas9 gene edited and knock-in mosquito cell lines. Sci Rep. 2021 Jan 12;11(1):736.

233. Viswanatha R, Mameli E, Rodiger J, Merckaert P, Feitosa-Suntheimer F, Colpitts TM, et al. Bioinformatic and cell-based tools for pooled CRISPR knockout screening in mosquitos. Nat Commun. 2021 Nov 24;12(1):6825.

234. Saraiva E, Fampa P, Cedeno V, Bergoin M, Mialhe E, Miller LH. Expression of heterologous promoters in Lutzomyia longipalpis and Phlebotomus papatasi (Diptera: Psychodidae) cell lines. J Med Entomol. 2000 Nov;37(6):802–6.

235. Tesh RB, Modi GB. Development of a Continuous Cell Line from the Sand Fly Lutzomyia Longipalpis (Diptera: Psychodidae), and its Susceptibility to Infection with Arboviruses1. J Med Entomol. 1983 Mar 30;20(2):199–202.

236. Rey GJ, Ferro C, Bello FJ. Establishment and characterization of a new continuous cell line from Lutzomyia longipalpis (Diptera: Psychodidae) and its susceptibility to infections with arboviruses and Leishmania chagasi. Mem Inst Oswaldo Cruz. 2000 Jan;95(1):103–10.

237. Côrtes LM, Silva RM, Pereira BA, Guerra C, Zapata AC, Bello FJ, et al. Lulo cell line derived from Lutzomyia longipalpis (Diptera: Psychodidae): a novel model to assay Leishmania spp. and vector interaction. Parasit Vectors. 2011 Nov 14;4(1):216.

238. de Castro Côrtes LM, de Souza Pereira MC, da Silva FS, Pereira BAS, de Oliveira Junior FO, de Araújo Soares RO, et al. Participation of heparin binding proteins from the surface of Leishmania (Viannia) braziliensis promastigotes in the adhesion of parasites to Lutzomyia longipalpis cells (Lulo) in vitro. Parasit Vectors. 2012 Jul 17;5(1):142.

239. da Silva Gonçalves D, Iturbe-Ormaetxe I, Martins-da-Silva A, Telleria EL, Rocha MN, Traub-Csekö YM, et al. Wolbachia introduction into Lutzomyia longipalpis (Diptera: Psychodidae) cell lines and its effects on immune-related gene expression and interaction with Leishmania infantum. Parasit Vectors. 2019 Jan 15;12(1):33.

240. Bell-Sakyi L, Darby A, Baylis M, Makepeace BL. The Tick Cell Biobank: A global resource for in vitro research on ticks, other arthropods and the pathogens they transmit. Ticks Tick-Borne Dis. 2018 Jul;9(5):1364–71.

241. Bell-Sakyi L, Beliavskaia A, Hartley CS, Jones L, Luu L, Haines LR, et al. Isolation in Natural Host Cell Lines of Wolbachia Strains wPip from the Mosquito Culex pipiens and wPap from the Sand Fly Phlebotomus papatasi. Insects. 2021 Sep 26;12(10):871.

242. Lu C, Bentley WE, Rao G. A high-throughput approach to promoter study using green fluorescent protein. Biotechnol Prog. 2004;20(6):1634–40.

243. Yang-Tsung C, Keller EB. The TATA-dependent and TATA-independent promoters of the Drosophila melanogaster actin 5C-encoding gene. Gene. 1991 Oct 15;106(2):237–41.

244. Amin J, Mestril R, Schiller P, Dreano M, Voellmy R. Organization of the Drosophila melanogaster hsp70 heat shock regulation unit. Mol Cell Biol. 1987 Mar;7(3):1055.

245. Wakiyama M, Matsumoto T, Yokoyama S. Drosophila U6 promoter-driven short hairpin RNAs effectively induce RNA interference in Schneider 2 cells. Biochem Biophys Res Commun. 2005 Jun 17;331(4):1163–70.

246. Tsubota T, Uchino K, Suzuki TK, Tanaka H, Kayukawa T, Shinoda T, et al. Identification of a Novel Strong and Ubiquitous Promoter/Enhancer in the Silkworm Bombyx mori. G3 GenesGenomesGenetics. 2014 May 23;4(7):1347–57.

247. Moreira LA, Edwards MJ, Adhami F, Jasinskiene N, James AA, Jacobs-Lorena M. Robust gut-specific gene expression in transgenic Aedes aegypti mosquitoes. Proc Natl Acad Sci U S A. 2000 Sep 26;97(20):10895–8.

248. Pondeville E, Puchot N, Parvy JP, Carissimo G, Poidevin M, Waterhouse RM, et al. Hemocyte-targeted gene expression in the female malaria mosquito using the hemolectin promoter from Drosophila. Insect Biochem Mol Biol. 2020 May 1;120:103339.

249. Hammond A, Karlsson X, Morianou I, Kyrou K, Beaghton A, Gribble M, et al. Regulating the expression of gene drives is key to increasing their invasive potential and the mitigation of resistance. PLOS Genet. 2021 Jan 29;17(1):e1009321.

250. Port F, Chen HM, Lee T, Bullock SL. Optimized CRISPR/Cas tools for efficient germline and somatic genome engineering in Drosophila. Proc Natl Acad Sci. 2014 Jul 22;111(29):E2967–76.

251. Berghammer AJ, Klingler M, A. Wimmer E. A universal marker for transgenic insects. Nature. 1999 Nov;402(6760):370–1.

252. Schetelig MF, Handler AM. A Functional Comparison of the 3xP3 Promoter by Recombinase-Mediated Cassette Exchange in Drosophila and a Tephritid Fly, Anastrepha suspensa. G3 GenesGenomesGenetics. 2013 Apr 1;3(4):687–93.

253. Osanai-Futahashi M, Ohde T, Hirata J, Uchino K, Futahashi R, Tamura T, et al. A visible dominant marker for insect transgenesis. Nat Commun. 2012 Dec 18;3(1):1295.

254. Fyrberg EA, Kindle KL, Davidson N, Sodja A. The actin genes of drosophila: a dispersed multigene family. Cell. 1980 Feb 1;19(2):365–78.

255. Hudson AM, Cooley L. Understanding the Function of Actin-Binding Proteins Through Genetic Analysis of *Drosophila* Oogenesis. Annu Rev Genet. 2002 Dec;36(1):455–88.

256. Chung YT, Keller EB. Regulatory elements mediating transcription from the Drosophila melanogaster actin 5C proximal promoter. Mol Cell Biol. 1990 Jan;10(1):206–16.

257. Pinkerton AC, Michel K, O'Brochta DA, Atkinson PW. Green fluorescent protein as a genetic marker in transgenic Aedes aegypti. Insect Mol Biol. 2000 Feb;9(1):1–10.

258. Hochstrasser M. Origin and function of ubiquitin-like proteins. Nature. 2009 Mar;458(7237):422–9.

259. Anderson MAE, Gross TL, Myles KM, Adelman ZN. Validation of novel promoter sequences derived from two endogenous ubiquitin genes in transgenic Aedes aegypti. Insect Mol Biol. 2010 Aug;19(4):441–9.

260. Lu C, Kim J, Fuller MT. The polyubiquitin gene Ubi-p63E is essential for male meiotic cell cycle progression and germ cell differentiation in Drosophila. Dev Camb Engl. 2013 Sep 1;140(17):3522–31.

261. Chen X, Chereddy SCRR, Gurusamy D, Palli SR. Identification and characterization of highly active promoters from the fall armyworm, Spodoptera frugiperda. Insect Biochem Mol Biol. 2020 Nov 1;126:103455.

262. Kim TK, Eberwine JH. Mammalian cell transfection: the present and the future. Anal Bioanal Chem. 2010;397(8):3173–8.

263. Lee JM, Takahashi M, Mon H, Koga K, Kawaguchi Y, Kusakabe T. Efficient gene transfer into silkworm larval tissues by a combination of sonoporation and lipofection. Cell Biol Int. 2005 Nov;29(11):976–9.

264. Mann SG, King LA. Efficient transfection of insect cells with baculovirus DNA using electroporation. J Gen Virol. 1989 Dec;70 (Pt 12):3501–5.

265. Gong D, Zhang TH, Zhao D, Du Y, Chapa TJ, Shi Y, et al. High-Throughput Fitness Profiling of Zika Virus E Protein Reveals Different Roles for Glycosylation during Infection of Mammalian and Mosquito Cells. iScience. 2018 Mar 23;1:97–111.

266. Du X, Wang J, Zhou Q, Zhang L, Wang S, Zhang Z, et al. Advanced physical techniques for gene delivery based on membrane perforation. Drug Deliv. 2018 Nov;25(1):1516–25.

267. Jordan ET, Collins M, Terefe J, Ugozzoli L, Rubio T. Optimizing Electroporation Conditions in Primary and Other Difficult-to-Transfect Cells. J Biomol Tech JBT. 2008 Dec;19(5):328–34.

268. Batista Napotnik T, Polajžer T, Miklavčič D. Cell death due to electroporation – A review. Bioelectrochemistry. 2021 Oct 1;141:107871.

269. Dalby B, Cates S, Harris A, Ohki EC, Tilkins ML, Price PJ, et al. Advanced transfection with Lipofectamine 2000 reagent: primary neurons, siRNA, and high-throughput applications. Methods. 2004 Jun 1;33(2):95–103.

270. Atieh T, Nougairède A, Klitting R, Aubry F, Failloux AB, Lamballerie X de, et al. New reverse genetics and transfection methods to rescue arboviruses in mosquito cells. Sci Rep. 2017 Oct 25;7(1):1–7.

271. Cherbas L, Hackney J, Gong L, Salzer C, Mauser E, Zhang D, et al. Targeted insertion in well-characterized Drosophila cell lines using ϕC31 integrase. bioRxiv. 2015 Aug 8;024216.

272. Zhu X, Liu J, Bai J, Liu P, Zhang T, Jiang P, et al. Baculovirus expression of the N-terminus of porcine heat shock protein Gp96 improves the immunogenicity of recombinant PCV2 capsid protein. J Virol Methods. 2016 Apr 1;230:36–44.

273. Gurusamy D, Mogilicherla K, Shukla JN, Palli SR. Lipids help double-stranded RNA in endosomal escape and improve RNA interference in the fall armyworm, Spodoptera frugiperda. Arch Insect Biochem Physiol. 2020;104(4):e21678.

274. Claret S, Sanial M, Plessis A. Evidence for a Novel Feedback Loop in the Hedgehog Pathway Involving Smoothened and Fused. Curr Biol. 2007 Aug 7;17(15):1326–33.

275. Schneider I. Cell lines derived from late embryonic stages of Drosophila melanogaster. J Embryol Exp Morphol. 1972 Apr;27(2):353–65.

276. Vaughn JL, Goodwin RH, Tompkins GJ, McCawley P. The establishment of two cell lines from the insectspodoptera frugiperda (lepidoptera; noctuidae). In Vitro. 1977 Apr 1;13(4):213–7.

277. Eckermann KN, Ahmed HMM, KaramiNejadRanjbar M, Dippel S, Ogaugwu CE, Kitzmann P, et al. Hyperactive piggyBac transposase improves transformation efficiency in diverse insect species. Insect Biochem Mol Biol. 2018 Jul;98:16–24.

278. González M, Martín-Ruíz I, Jiménez S, Pirone L, Barrio R, Sutherland JD. Generation of stable Drosophila cell lines using multicistronic vectors. Sci Rep. 2011 Aug 31;1(1):75.

279. Huynh N, Depner N, Larson R, King-Jones K. A versatile toolkit for CRISPR-Cas13-based RNA manipulation in Drosophila. Genome Biol. 2020 Nov 17;21(1):279.

280. Kandul NP, Belikoff EJ, Liu J, Buchman A, Li F, Yamamoto A, et al. Genetically Encoded CRISPR Components Yield Efficient Gene Editing in the Invasive Pest Drosophila suzukii. CRISPR J. 2021 Oct;4(5):739–51.

281. Bleckmann M, Fritz MHY, Bhuju S, Jarek M, Schürig M, Geffers R, et al. Genomic Analysis and Isolation of RNA Polymerase II Dependent Promoters from Spodoptera frugiperda. PLOS ONE. 2015 Aug 11;10(8):e0132898.

282. Theilmann DA, Stewart S. Molecular analysis of the trans-activating IE-2 gene of Orgyia pseudotsugata multicapsid nuclear polyhedrosis virus. Virology. 1992 Mar;187(1):84–96.

283. Altschuler SJ, Wu LF. Cellular heterogeneity: when do differences make a difference? Cell. 2010 May 14;141(4):559–63.

284. Ryan JA, Park N. Clonal Growth of Cells in Semisolid Media. :4.

285. Rashid M, Coombs KM. Serum-reduced media impacts on cell viability and protein expression in human lung epithelial cells. J Cell Physiol. 2019 Jun;234(6):7718–24.

286. Fernandes F, Vidigal J, Dias MM, Prather KLJ, Coroadinha AS, Teixeira AP, et al. Flipase-mediated cassette exchange in *Sf9* insect cells for stable gene expression. Biotechnol Bioeng. 2012 Nov;109(11):2836–44.

287. Liu Z, Chen O, Wall JBJ, Zheng M, Zhou Y, Wang L, et al. Systematic comparison of 2A peptides for cloning multi-genes in a polycistronic vector. Sci Rep. 2017 May 19;7(1):2193.

288. Adolfi A, Pondeville E, Lynd A, Bourgouin C, Lycett GJ. Multi-tissue GAL4-mediated gene expression in all Anopheles gambiae life stages using an endogenous polyubiquitin promoter. Insect Biochem Mol Biol. 2018 May 1;96:1–9.

289. Grigoraki L, Grau-Bové X, Carrington Yates H, Lycett GJ, Ranson H. Isolation and transcriptomic analysis of Anopheles gambiae oenocytes enables the delineation of hydrocarbon biosynthesis. McConville MJ, Marletta MA, McConville MJ, Besansky N, editors. eLife. 2020 Jun 15;9:e58019.

290. Schulte C, Theilenberg E, Müller-Borg M, Gempe T, Beye M. Highly efficient integration and expression of piggyBac-derived cassettes in the honeybee (Apis mellifera). Proc Natl Acad Sci. 2014 Jun 17;111(24):9003–8.

291. Li M, Yang T, Kandul NP, Bui M, Gamez S, Raban R, et al. Development of a confinable gene drive system in the human disease vector Aedes aegypti. Walczak AM, Bellen HJ, editors. eLife. 2020 Jan 21;9:e51701.

292. Feng X, López Del Amo V, Mameli E, Lee M, Bishop AL, Perrimon N, et al. Optimized CRISPR tools and site-directed transgenesis towards gene drive development in Culex quinquefasciatus mosquitoes. Nat Commun. 2021 May 20;12(1):2960.

293. Liu P, Jin B, Li X, Zhao Y, Gu J, Biedler JK, et al. Nix is a male-determining factor in the Asian tiger mosquito Aedes albopictus. Insect Biochem Mol Biol. 2020 Mar 1;118:103311.

294. Markert MJ, Zhang Y, Enuameh MS, Reppert SM, Wolfe SA, Merlin C. Genomic Access to Monarch Migration Using TALEN and CRISPR/Cas9-Mediated Targeted Mutagenesis. G3 GenesGenomesGenetics. 2016 Apr 1;6(4):905–15.

295. Xu J, Xu X, Zhan S, Huang Y. Genome editing in insects: current status and challenges. Natl Sci Rev. 2019 May 1;6(3):399–401.

296. Sander JD, Joung JK. CRISPR-Cas systems for editing, regulating and targeting genomes. Nat Biotechnol. 2014 Apr;32(4):347–55.

297. Gratz SJ, Ukken FP, Rubinstein CD, Thiede G, Donohue LK, Cummings AM, et al. Highly Specific and Efficient CRISPR/Cas9-Catalyzed Homology-Directed Repair in Drosophila. Genetics. 2014 Apr;196(4):961–71.

298. Mazo-Vargas A, Concha C, Livraghi L, Massardo D, Wallbank RWR, Zhang L, et al. Macroevolutionary shifts of WntA function potentiate butterfly wing-pattern diversity. Proc Natl Acad Sci. 2017 Oct 3;114(40):10701–6.

299. Liu G, Liu W, Zhao R, He J, Dong Z, Chen L, et al. Genome-wide identification and gene-editing of pigment transporter genes in the swallowtail butterfly Papilio xuthus. BMC Genomics. 2021 Feb 17;22.

300. de Souza Pacheco I, Doss ALA, Vindiola BG, Brown DJ, Ettinger CL, Stajich JE, et al. Efficient CRISPR/Cas9-mediated genome modification of the glassy-winged sharpshooter Homalodisca vitripennis (Germar). Sci Rep. 2022 Apr 19;12(1):6428.

301. Chen X, Palli SR. Development of multiple transgenic CRISPR/Cas9 methods for genome editing in the fall armyworm, Spodoptera frugiperda. J Pest Sci [Internet]. 2022 Jul 30 [cited 2023 Mar 28]; Available from: https://doi.org/10.1007/s10340-022-01546-9

302. Pacheco ID, Walling LL, Atkinson PW. Gene Editing and Genetic Control of Hemipteran Pests: Progress, Challenges and Perspectives. Front Bioeng Biotechnol [Internet]. 2022 [cited 2023 Apr 20];10. Available from: https://www.frontiersin.org/articles/10.3389/fbioe.2022.900785

303. Yuen JL, Read SA, Brubacher JL, Singh AD, Whyard S. Biolistics for high-throughput transformation and RNA interference in *Drosophila melanogaster*. Fly (Austin). 2008 Sep 30;2(5):247–54.

304. Carthew RW. Delivery of dsRNA into Drosophila Embryos by Gene Gun. CSH Protoc. 2006 Aug 1;2006(3).

305. Thomas J luc. Electroporation, an alternative to biolistics for transfection of Bombyx mori embryos and larval tissues. J Insect Sci. 2003 Jun;3(17):1–12.

306. Ruiz N, Abreu LA de, Parizi LF, Kim TK, Mulenga A, Braz GRC, et al. Non-Invasive Delivery of dsRNA into De-Waxed Tick Eggs by Electroporation. PLOS ONE. 2015 Jun 19;10(6):e0130008.

307. Xu Q, Guerrero FD, Palavesam A, Pérez de León AA. Use of electroporation as an option to transform the horn fly, *Haematobia irritans* : a species recalcitrant to microinjection: Electroporation of horn fly Haematobia irritans. Insect Sci. 2016 Aug;23(4):621–9.

308. Massey JH, Akiyama N, Bien T, Dreisewerd K, Wittkopp PJ, Yew JY, et al. Pleiotropic Effects of ebony and tan on Pigmentation and Cuticular Hydrocarbon Composition in Drosophila melanogaster. Front Physiol [Internet]. 2019 [cited 2023 Jan 26];10. Available from: https://www.frontiersin.org/articles/10.3389/fphys.2019.00518

309. Wittkopp PJ, True JR, Carroll SB. Reciprocal functions of the Drosophila Yellow and Ebony proteins in the development and evolution of pigment patterns. Development. 2002 Apr 15;129(8):1849–58.

310. Bi HL, Xu J, He L, Zhang Y, Li K, Huang YP. CRISPR/Cas9-mediated ebony knockout results in puparium melanism in Spodoptera litura. Insect Sci. 2019;26(6):1011–9.

311. Li M, Bui M, Yang T, Bowman CS, White BJ, Akbari OS. Germline Cas9 expression yields highly efficient genome engineering in a major worldwide disease vector, *Aedes aegypti*. Proc Natl Acad Sci. 2017 Dec 5;114(49):E10540–9.

312. Perry M, Kinoshita M, Saldi G, Huo L, Arikawa K, Desplan C. Molecular logic behind the three-way stochastic choices that expand butterfly colour vision. Nature. 2016 Jul;535(7611):280–4.

313. Khan SA, Reichelt M, Heckel DG. Functional analysis of the ABCs of eye color in *Helicoverpa armigera* with CRISPR/Cas9-induced mutations. Sci Rep. 2017 Jan 5;7:40025.

314. Osanai-Futahashi M, Tatematsu K i, Futahashi R, Narukawa J, Takasu Y, Kayukawa T, et al. Positional cloning of a Bombyx pink-eyed white egg locus reveals the major role of cardinal in ommochrome synthesis. Heredity. 2016 Feb;116(2):135–45.

315. Clements J, Hens K, Merugu S, Dichtl B, de Couet HG, Callaerts P. Mutational analysis of the eyeless gene and phenotypic rescue reveal that an intact Eyeless protein is necessary for normal eye and brain development in Drosophila. Dev Biol. 2009 Oct 15;334(2):503–12.

316. Otto PA. Drosophila viewer: a program on the formal genetics, anatomy and developmental biology of Drosophila melanogaster for students and specialists. Genet Mol Biol. 2000 Dec;23:835–9.

317. Fujii T, Abe H, Shimada T. Molecular analysis of sex chromosome-linked mutants in the silkworm Bombyx mori. J Genet. 2010 Sep;89(3):365–74.

318. Cagliari D, Smagghe G, Zotti M, Taning CNT. RNAi and CRISPR/Cas9 as Functional Genomics Tools in the Neotropical Stink Bug, Euschistus heros. Insects. 2020 Dec;11(12):838.

319. Martin-Martin I, Aryan A, Meneses C, Adelman ZN, Calvo E. Optimization of sand fly embryo microinjection for gene editing by CRISPR/Cas9. PLoS Negl Trop Dis. 2018 Sep 4;12(9):e0006769.

320. Amos B, Aurrecoechea C, Barba M, Barreto A, Basenko EY, Bażant W, et al. VEuPathDB: the eukaryotic pathogen, vector and host bioinformatics resource center. Nucleic Acids Res. 2022 Jan 7;50(D1):D898–911.

321. Lutzomyia longipalpis, whole genome shotgun sequencing project [Internet]. 2013 [cited 2023 Feb 20]. Available from: http://www.ncbi.nlm.nih.gov/nuccore/AJWK00000000.1

322. Phlebotomus papatasi, whole genome shotgun sequencing project [Internet]. 2014 [cited 2023 Feb 20]. Available from: http://www.ncbi.nlm.nih.gov/nuccore/AJVK00000000.1

323. Gramates LS, Agapite J, Attrill H, Calvi BR, Crosby MA, dos Santos G, et al. FlyBase: a guided tour of highlighted features. Genetics. 2022 Apr 1;220(4):iyac035.

324. Madeira F, Pearce M, Tivey ARN, Basutkar P, Lee J, Edbali O, et al. Search and sequence analysis tools services from EMBL-EBI in 2022. Nucleic Acids Res. 2022 Apr 1;gkac240.

325. Carbon S, Ireland A, Mungall CJ, Shu S, Marshall B, Lewis S, et al. AmiGO: online access to ontology and annotation data. Bioinformatics. 2009 Jan 15;25(2):288–9.

326. Labun K, Montague TG, Krause M, Torres Cleuren YN, Tjeldnes H, Valen E. CHOPCHOP v3: expanding the CRISPR web toolbox beyond genome editing. Nucleic Acids Res. 2019 Jul 2;47(W1):W171–4.

327. Shen MW, Arbab M, Hsu JY, Worstell D, Culbertson SJ, Krabbe O, et al. Predictable and precise template-free CRISPR editing of pathogenic variants. Nature. 2018 Nov;563(7733):646–51.

328. Tsai SQ, Zheng Z, Nguyen NT, Liebers M, Topkar VV, Thapar V, et al. GUIDE-seq enables genome-wide profiling of off-target cleavage by CRISPR-Cas nucleases. Nat Biotechnol. 2015 Feb;33(2):187–97.

329. Thyme SB, Akhmetova L, Montague TG, Valen E, Schier AF. Internal guide RNA interactions interfere with Cas9-mediated cleavage. Nat Commun. 2016 Jun 10;7(1):11750.

330. Gokcezade J, Sienski G, Duchek P. Efficient CRISPR/Cas9 Plasmids for Rapid and Versatile Genome Editing in Drosophila. G3 GenesGenomesGenetics. 2014 Sep 17;4(11):2279–82.

331. Anderson MAE, Purcell J, Verkuijl SAN, Norman VC, Leftwich PT, Harvey-Samuel T, et al. Expanding the CRISPR Toolbox in Culicine Mosquitoes: In Vitro Validation of Pol III Promoters. ACS Synth Biol. 2020 Mar 20;9(3):678–81.

332. Bateman JR, Lee AM, Wu C ting. Site-Specific Transformation of Drosophila via ϕC31 Integrase-Mediated Cassette Exchange. Genetics. 2006 Jun;173(2):769.

333. Volf P, Volfova V. Establishment and maintenance of sand fly colonies. J Vector Ecol J Soc Vector Ecol. 2011 Mar;36 Suppl 1:S1-9.

334. Lawyer P, Killick-Kendrick M, Rowland T, Rowton E, Volf P. Laboratory colonization and mass rearing of phlebotomine sand flies (Diptera, Psychodidae). Parasite [Internet]. [cited 2019 Jul 12];24. Available from: https://www.ncbi.nlm.nih.gov/pmc/articles/PMC5687099/

335. NEB Tm Calculator [Internet]. [cited 2023 Feb 24]. Available from: https://tmcalculator.neb.com/#!/main

336. Dehairs J, Talebi A, Cherifi Y, Swinnen JV. CRISP-ID: decoding CRISPR mediated indels by Sanger sequencing. Sci Rep. 2016 Jul 1;6(1):28973.

337. Clement K, Rees H, Canver MC, Gehrke JM, Farouni R, Hsu JY, et al. CRISPResso2 provides accurate and rapid genome editing sequence analysis. Nat Biotechnol. 2019 Mar;37(3):224–6.

338. Bloh K, Kanchana R, Bialk P, Banas K, Zhang Z, Yoo BC, et al. Deconvolution of Complex DNA Repair (DECODR): Establishing a Novel Deconvolution Algorithm for Comprehensive Analysis of CRISPR-Edited Sanger Sequencing Data. CRISPR J. 2021 Feb;4(1):120–31.

339. Conant D, Hsiau T, Rossi N, Oki J, Maures T, Waite K, et al. Inference of CRISPR Edits from Sanger Trace Data. CRISPR J. 2022 Feb;5(1):123–30.

340. Brinkman EK, Chen T, Amendola M, van Steensel B. Easy quantitative assessment of genome editing by sequence trace decomposition. Nucleic Acids Res. 2014 Dec 16;42(22):e168–e168.

341. Campesan S, Green EW, Breda C, Sathyasaikumar KV, Muchowski PJ, Schwarcz R, et al. The Kynurenine Pathway Modulates Neurodegeneration in a Drosophila Model of Huntington's Disease. Curr Biol. 2011 Jun 7;21(11):961–6.

342. Sullivan DT, Sullivan MC. Transport defects as the physiological basis for eye color mutants of Drosophila melanogaster. Biochem Genet. 1975 Oct;13(9–10):603–13.

343. Mackenzie SM, Brooker MR, Gill TR, Cox GB, Howells AJ, Ewart GD. Mutations in the white gene of Drosophila melanogaster affecting ABC transporters that determine eye colouration. Biochim Biophys Acta BBA - Biomembr. 1999 Jul 15;1419(2):173–85.

344. Tejeda-Guzmán C, Rosas-Arellano A, Kroll T, Webb SM, Barajas-Aceves M, Osorio B, et al. Biogenesis of zinc storage granules in Drosophila melanogaster. J Exp Biol. 2018 Mar 15;221(6):jeb168419.

345. Mackenzie SM, Howells AJ, Cox GB, Ewart GD. Sub-cellular Localisation of the White/Scarlet ABC Transporter to Pigment Granule Membranes Within the Compound Eye of Drosophila Melanogaster. Genetica. 2000 May 1;108(3):239–52.

346. Zerges W, Udvardy A, Schedl P. Molecular characterization of the 5' end of the rudimentary gene in Drosophila and analysis of three P element insertions. Nucleic Acids Res. 1992 Sep 11;20(17):4639–47.

347. Roykhman M, Ibach SM, Harding D, Wolff B, Vowels M, Gelsthorpe ME, et al. The Generation and Analysis of Deficiencies Within a Small Genomic rRegion on the X Chromosome of Drosophila melanogaster Containing Two Genes, enhancer of rudimentary and CG15352. Fly (Austin). 2007 Jul 15;1(4):245–50.

348. Deng H, Bell JB, Simmonds AJ. Vestigial Is Required during Late-Stage Muscle Differentiation in Drosophila melanogaster Embryos. Mol Biol Cell. 2010 Oct;21(19):3304–16.

349. Kim M, Lee JH, Lee SY, Kim E, Chung J. Caspar, a suppressor of antibacterial immunity in Drosophila. Proc Natl Acad Sci. 2006 Oct 31;103(44):16358–63.

350. Matsuda T, Togami S, Masumi-Koizumi K, Kahar P, Katsuda T, Yamaji H. Applying the CRISPR-Cas9 system to targeted transgene integration in the development of recombinant lepidopteran insect cells [Internet]. In Review; 2022 Jun [cited 2023 Mar 30]. Available from: https://www.researchsquare.com/article/rs-1736661/v1

351. Vouillot L, Thélie A, Pollet N. Comparison of T7E1 and Surveyor Mismatch Cleavage Assays to Detect Mutations Triggered by Engineered Nucleases. G3 GenesGenomesGenetics. 2015 Mar;5(3):407.

352. Iida M, Suzuki M, Sakane Y, Nishide H, Uchiyama I, Yamamoto T, et al. A simple and practical workflow for genotyping of CRISPR–Cas9-based knockout phenotypes using multiplexed amplicon sequencing. Genes Cells. 2020;25(7):498–509.

353. Biedler JK, Hu W, Tae H, Tu Z. Identification of Early Zygotic Genes in the Yellow Fever Mosquito Aedes aegypti and Discovery of a Motif Involved in Early Zygotic Genome Activation. Aerts S, editor. PLoS ONE. 2012 Mar 23;7(3):e33933.

354. Abbassy MM, Helmy N, Osman M, Cope SE, Presley SM. Embryogenesis of the Sand Fly Phlebotomus papatasi (Diptera: Psychodidae): Organogenesis including Segmentation, Blastokinesis, Mouthparts, and Alimentary Canal. Ann Entomol Soc Am. 1995 Nov 1;88(6):815–20.

355. Hammond A, Pollegioni P, Persampieri T, North A, Minuz R, Trusso A, et al. Gene-drive suppression of mosquito populations in large cages as a bridge between lab and field. Nat Commun. 2021 Jul 28;12(1):4589.

356. Sentmanat MF, Peters ST, Florian CP, Connelly JP, Pruett-Miller SM. A Survey of Validation Strategies for CRISPR-Cas9 Editing. Sci Rep. 2018 Jan 17;8(1):1–8.

357. Atsumi S, Miyamoto K, Yamamoto K, Narukawa J, Kawai S, Sezutsu H, et al. Single amino acid mutation in an ATP-binding cassette transporter gene causes resistance to Bt toxin Cry1Ab in the silkworm, Bombyx mori. Proc Natl Acad Sci. 2012 Jun 19;109(25):E1591–8.

358. Nimmo DD, Alphey L, Meredith JM, Eggleston P. High efficiency site-specific genetic engineering of the mosquito genome. Insect Mol Biol. 2006 Apr;15(2):129–36.

359. Pfeifer TA, Hegedus DD, Grigliatti TA, Theilmann DA. Baculovirus immediate-early promoter-mediated expression of the Zeocin resistance gene for use as a dominant selectable marker in dipteran and lepidopteran insect cell lines. Gene. 1997 Apr 1;188(2):183–90.

360. Swiech K, Kamen A, Ansorge S, Durocher Y, Picanço-Castro V, Russo-Carbolante EM, et al. Transient transfection of serum-free suspension HEK 293 cell culture for efficient production of human rFVIII. BMC Biotechnol. 2011 Nov 24;11:114.

361. Puente-Massaguer E, Gòdia F, Lecina M. Development of a non-viral platform for rapid virus-like particle production in Sf9 cells. J Biotechnol. 2020 Oct 10;322:43–53.

362. Vancha AR, Govindaraju S, Parsa KV, Jasti M, González-García M, Ballestero RP. Use of polyethyleneimine polymer in cell culture as attachment factor and lipofection enhancer. BMC Biotechnol. 2004 Oct 15;4:23.

363. Sanchez-Martos M, Martinez-Navarrete G, Bernabeu-Zornoza A, Humphreys L, Fernandez E. Evaluation and Optimization of Poly-d-Lysine as a Non-Natural Cationic Polypeptide for Gene Transfer in Neuroblastoma Cells. Nanomaterials. 2021 Jul 5;11(7):1756.

364. Bozas A, Beumer KJ, Trautman JK, Carroll D. Genetic Analysis of Zinc-Finger Nuclease-Induced Gene Targeting in Drosophila. Genetics. 2009 Jul 1;182(3):641–51.

365. Paquet D, Kwart D, Chen A, Sproul A, Jacob S, Teo S, et al. Efficient introduction of specific homozygous and heterozygous mutations using CRISPR/Cas9. Nature. 2016 May;533(7601):125–9.

366. Di Stazio M, Foschi N, Athanasakis E, Gasparini P, d'Adamo AP. Systematic analysis of factors that improve homologous direct repair (HDR) efficiency in CRISPR/Cas9 technique. PLoS ONE. 2021 Mar 5;16(3):e0247603.

367. Acosta S, Fiore L, Carota IA, Oliver G. Use of two gRNAs for CRISPR/Cas9 improves bi-allelic homologous recombination efficiency in mouse embryonic stem cells. genesis. 2018;56(5):e23212.

368. Calderón JM, Fuya P, Santacoloma L, González C. Deltamethrin resistance in Chagas disease vectors colonizing oil palm plantations: implications for vector control strategies in a public health-agriculture interface. Parasit Vectors. 2020 Apr 3;13(1):163.

369. Mougabure-Cueto G, Picollo MI. Insecticide Resistance in Triatomines. In: Guarneri A, Lorenzo M, editors. Triatominae - The Biology of Chagas Disease Vectors [Internet]. Cham: Springer International Publishing; 2021 [cited 2023 Jul 4]. p. 537–55. (Entomology in Focus). Available from: https://doi.org/10.1007/978-3-030-64548-9_19

370. Kandul NP, Belikoff EJ, Liu J, Buchman A, Li F, Yamamoto A, et al. Genetically Encoded CRISPR components Yield Efficient Gene Editing in the Invasive Pest, Drosophila suzukii.

371. Lester PJ, Bulgarella M, Baty JW, Dearden PK, Guhlin J, Kean JM. The potential for a CRISPR gene drive to eradicate or suppress globally invasive social wasps. Sci Rep. 2020 Jul 24;10(1):12398.

372. Fandino RA, Haverkamp A, Bisch-Knaden S, Zhang J, Bucks S, Nguyen TAT, et al. Mutagenesis of odorant coreceptor Orco fully disrupts foraging but not oviposition behaviors in the hawkmoth Manduca sexta. Proc Natl Acad Sci. 2019 Jul 30;116(31):15677–85.

373. Myskova J, Svobodova M, Beverley SM, Volf P. A lipophosphoglycan-independent development of Leishmania in permissive sand flies. Microbes Infect. 2007 Mar 1;9(3):317–24.

374. Corfas RA, Vosshall LB. The cation channel TRPA1 tunes mosquito thermotaxis to host temperatures. Scott K, editor. eLife. 2015 Dec 15;4:e11750.

375. Fresquet N, Lazzari CR. Response to heat in Rhodnius prolixus: The role of the thermal background. J Insect Physiol. 2011 Oct 1;57(10):1446–9.

376. Fire A, Xu S, Montgomery MK, Kostas SA, Driver SE, Mello CC. Potent and specific genetic interference by double-stranded RNA in Caenorhabditis elegans. Nature. 1998 Feb 19;391(6669):806–11.

377. Heu CC, Gross RJ, Le KP, LeRoy DM, Fan B, Hull JJ, et al. CRISPR-mediated knockout of cardinal and cinnabar eye pigmentation genes in the western tarnished plant bug. Sci Rep. 2022 Mar 22;12(1):4917.

378. Joshi AS, Alegria AD, Auch B, Khosla K, Mendana JB, Liu K, et al. Multiscale, multi-perspective imaging assisted robotic microinjection of 3D biological structures. Annu Int Conf IEEE Eng Med Biol Soc IEEE Eng Med Biol Soc Annu Int Conf. 2021 Nov;2021:4844–50.

379. Shirai Y, Piulachs MD, Belles X, Daimon T. DIPA-CRISPR is a simple and accessible method for insect gene editing. Cell Rep Methods. 2022 May 23;2(5):100215.

380. Heu CC, McCullough FM, Luan J, Rasgon JL. CRISPR-Cas9-Based Genome Editing in the Silverleaf Whitefly (Bemisia tabaci). CRISPR J. 2020 Apr 1;3(2):89–96.

381. Sharma A, Pham MN, Reyes JB, Chana R, Yim WC, Heu CC, et al. Cas9-mediated gene editing in the black-legged tick, Ixodes scapularis, by embryo injection and ReMOT Control. iScience. 2022 Mar 18;25(3):103781.

382. Vieira PH, Bomfim L, Atella GC, Masuda H, Ramos I. Silencing of RpATG6 impaired the yolk accumulation and the biogenesis of the yolk organelles in the insect vector R. prolixus. PLoS Negl Trop Dis. 2018 May 16;12(5):e0006507.

383. Berni M, Bressan D, Simão Y, Julio A, Oliveira PL, Pane A, et al. Pigmentation loci as markers for genome editing in the Chagas disease vector Rhodnius prolixus. bioRxiv. 2020 Apr 29;2020.04.29.067934.

384. Dermauw W, Jonckheere W, Riga M, Livadaras I, Vontas J, Van Leeuwen T. Targeted mutagenesis using CRISPR-Cas9 in the chelicerate herbivore Tetranychus urticae. Insect Biochem Mol Biol. 2020 May 1;120:103347.

385. Chaverra-Rodriguez D, Macias VM, Hughes GL, Pujhari S, Suzuki Y, Peterson DR, et al. Targeted delivery of CRISPR-Cas9 ribonucleoprotein into arthropod ovaries for heritable germline gene editing. Nat Commun. 2018 Aug 1;9(1):3008.

386. Nuss A, Sharma A, Gulia-Nuss M. Genetic Manipulation of Ticks: A Paradigm Shift in Tick and Tick-Borne Diseases Research. Front Cell Infect Microbiol [Internet]. 2021 [cited 2023 Apr 23];11. Available from: https://www.frontiersin.org/articles/10.3389/fcimb.2021.678037

387. Xu Q, Guerrero FD, Palavesam A, Pérez de León AA. Use of electroporation as an option to transform the horn fly, *Haematobia irritans* : a species recalcitrant to microinjection: Electroporation of horn fly Haematobia irritans. Insect Sci. 2016 Aug;23(4):621–9.

388. Taracena ML, Oliveira PL, Almendares O, Umaña C, Lowenberger C, Dotson EM, et al. Genetically Modifying the Insect Gut Microbiota to Control Chagas Disease Vectors through Systemic RNAi. PLoS Negl Trop Dis. 2015 Feb 12;9(2):e0003358.

389. Bomfim L, Vieira P, Fonseca A, Ramos I. Eggshell ultrastructure and delivery of pharmacological inhibitors to the early embryo of R. prolixus by ethanol permeabilization of the extraembryonic layers. Lorenzo MG, editor. PLOS ONE. 2017 Sep 29;12(9):e0185770.

390. O'Brien JA, Lummis SCR. Biolistic transfection of neuronal cultures using a hand-held gene gun. Nat Protoc. 2006;1(2):977–81.

391. Sanford JC. Biolistic plant transformation. Physiol Plant. 1990;79(1):206–9.

392. Thomas JL, Bardou J, L'hoste S, Mauchamp B, Chavancy G. A helium burst biolistic device adapted to penetrate fragile insect tissues. J Insect Sci. 2001 Oct 4;1:9.

393. Miller K, Eggenberger AL, Lee K, Liu F, Kang M, Drent M, et al. An improved biolistic delivery and analysis method for evaluation of DNA and CRISPR-Cas delivery efficacy in plant tissue. Sci Rep. 2021 Apr 8;11(1):7695.

394. Ando T, Fujiwara H. Electroporation-mediated somatic transgenesis for rapid functional analysis in insects. Development. 2013 Jan 15;140(2):454–8.

395. Che LR, He ZB, Liu Y, Yan ZT, Han BZ, Chen XJ, et al. Electroporation-mediated nucleic acid delivery during non-embryonic stages for gene-function analysis in Anopheles sinensis. Insect Biochem Mol Biol. 2021 Jan 1;128:103500.

396. Prentice K, Christiaens O, Pertry I, Bailey A, Niblett C, Ghislain M, et al. RNAi-based gene silencing through dsRNA injection or ingestion against the African sweet potato weevil Cylas puncticollis (Coleoptera: Brentidae). Pest Manag Sci. 2017;73(1):44–52.

397. Xu L, Xu S, Sun L, Zhang Y, Luo J, Bock R, et al. Synergistic action of the gut microbiota in environmental RNA interference in a leaf beetle. Microbiome. 2021 May 4;9(1):98.

398. Leelesh RS, Rieske LK. Oral Ingestion of Bacterially Expressed dsRNA Can Silence Genes and Cause Mortality in a Highly Invasive, Tree-Killing Pest, the Emerald Ash Borer. Insects. 2020 Jul 14;11(7):440.

399. Murphy KA, Tabuloc CA, Cervantes KR, Chiu JC. Ingestion of genetically modified yeast symbiont reduces fitness of an insect pest via RNA interference. Sci Rep. 2016 Mar 2;6(1):22587.

400. Golden K, Sagi V, Markwarth N, Chen B, Monteiro A. In Vivo Electroporation of DNA into the Wing Epidermis of the Butterfly, Bicyclus anynana. J Insect Sci. 2007 Oct 25;7:53.

401. Costa WA, Costa SM da, Rangel EF, Santos-Mallet JR dos, Serrão JE. Eggshell as a characteristic to identify Lutzomyia (Nyssomyia) intermedia (Lutz & Neiva, 1912) and Lutzomyia (Nyssomyia) neivai (Pinto, 1926) (Diptera: Psychodidae: Phlebotominae), vectors of cutaneous leishmaniasis. Rev Pan-Amaz Saúde. 2012 Mar;3(1):19–24.

402. Buxton PA. The Biology of a Blood-Sucking Bug, Rhodnius prolixus. Trans Entomol Soc Lond [Internet]. 1930 [cited 2023 Apr 18];78. Available from: https://www.cabdirect.org/cabdirect/abstract/19312901218

403. Anji A, Shaik KA, Kumari M. Effect of ethanol on lipid-mediated transfection of primary cortical neurons. Ann N Y Acad Sci. 2003 May;993:95–102; discussion 123-124.

404. Butash KA, Natarajan P, Young A, Fox DK. Reexamination of the effect of endotoxin on cell proliferation and transfection efficiency. BioTechniques. 2000 Sep;29(3):610–4, 616, 618–9.

405. Araujo RN, Santos A, Pinto FS, Gontijo NF, Lehane MJ, Pereira MH. RNA interference of the salivary gland nitrophorin 2 in the triatomine bug Rhodnius prolixus (Hemiptera: Reduviidae) by dsRNA ingestion or injection. Insect Biochem Mol Biol. 2006 Sep 1;36(9):683–93.

406. Lavore A, Pagola L, Esponda-Behrens N, Rivera-Pomar R. The gap gene giant of Rhodnius prolixus is maternally expressed and required for proper head and abdomen formation. Dev Biol. 2012 Jan;361(1):147–55.

407. Paim RMM, Araujo RN, Lehane MJ, Gontijo NF, Pereira MH. Long-term effects and parental RNAi in the blood feeder Rhodnius prolixus (Hemiptera; Reduviidae). Insect Biochem Mol Biol. 2013 Nov 1;43(11):1015–20.

408. Franco TA, Oliveira DS, Moreira MF, Leal WS, Melo ACA. Silencing the odorant receptor co-receptor RproOrco affects the physiology and behavior of the Chagas disease vector Rhodnius prolixus. Insect Biochem Mol Biol. 2016 Feb 1;69:82–90.

409. Brito T, Julio A, Berni M, Poncio L de C, Bernardes ES, Araujo H, et al. Transcriptomic and functional analyses of the piRNA pathway in the Chagas disease vector Rhodnius prolixus. PLoS Negl Trop Dis. 2018 Oct 10;12(10):e0006760.

410. Berni M, Lima L, Bressan D, Julio A, Bonfim L, Simão Y, et al. Atypical strategies for cuticle pigmentation in the blood-feeding hemipteran Rhodnius prolixus. Genetics. 2022 Jun 1;221(2):iyac064.

411. Pascual A, Rivera-Pomar R. Dynamics of maternal gene expression in Rhodnius prolixus. Sci Rep. 2022 Apr 20;12(1):6538.

412. Benrabaa S, Orchard I, Lange AB. A critical role for ecdysone response genes in regulating egg production in adult female Rhodnius prolixus. PLOS ONE. 2023 Mar 20;18(3):e0283286.

413. Li M, Li T, Liu N, Raban R, Wang X, Akbari OS. Methods for the generation of heritable germline mutations in the disease vector *Culex quinquefasciatus* using CRISPR/Cas9 [Internet]. Bioengineering; 2019 Apr [cited 2019 May 23]. Available from: http://biorxiv.org/lookup/doi/10.1101/609206

414. Le Trionnaire G, Tanguy S, Hudaverdian S, Gleonnec F, Richard G, Cayrol B, et al. An integrated protocol for targeted mutagenesis with CRISPR-Cas9 system in the pea aphid. Insect Biochem Mol Biol. 2019 Jul;110:34–44.

415. Xue WH, Xu N, Yuan XB, Chen HH, Zhang JL, Fu SJ, et al. CRISPR/Cas9-mediated knockout of two eye pigmentation genes in the brown planthopper, Nilaparvata lugens (Hemiptera: Delphacidae). Insect Biochem Mol Biol. 2018 Feb 1;93:19–26.

416. Reding K, Pick L. High-Efficiency CRISPR/Cas9 Mutagenesis of the white Gene in the Milkweed Bug Oncopeltus fasciatus. Genetics. 2020 Aug;215(4):1027–37.

417. Klobasa W, Chu FC, Huot O, Grubbs N, Rotenberg D, Whitfield AE, et al. Microinjection of Corn Planthopper, Peregrinus maidis, Embryos for CRISPR/Cas9 Genome Editing. J Vis Exp JoVE. 2021 Mar 26;(169).

418. Kotwica-Rolinska J, Damulewicz M, Chodakova L, Kristofova L, Dolezel D. Pigment Dispersing Factor Is a Circadian Clock Output and Regulates Photoperiodic Response in the Linden Bug, Pyrrhocoris apterus. Front Physiol [Internet]. 2022 [cited 2023 May 15];13. Available from: https://www.frontiersin.org/articles/10.3389/fphys.2022.884909

419. Xue WH, Xu N, Chen SJ, Liu XY, Zhang JL, Xu HJ. Neofunctionalization of a second insulin receptor gene in the wing-dimorphic planthopper, Nilaparvata lugens. PLOS Genet. 2021 Jun 28;17(6):e1009653.

420. Chen JX, Li WX, Lyu J, Hu YT, Huang G, Zhang WQ. CRISPR/Cas9-mediated knockout of the NlCSAD gene results in darker cuticle pigmentation and a reduction in female fecundity in Nilaparvata lugens (Hemiptera: Delphacidae). Comp Biochem Physiol A Mol Integr Physiol. 2021 Jun;256:110921.

421. Lavore A, Esponda-Behrens N, Pagola L, Rivera-Pomar R. The gap gene Krüppel of Rhodnius prolixus is required for segmentation and for repression of the homeotic gene sex comb-reduced. Dev Biol. 2014 Mar;387(1):121–9.

422. Zhang Y, Li H, Du J, Zhang J, Shen J, Cai W. Three Melanin Pathway Genes, TH, yellow, and aaNAT, Regulate Pigmentation in the Twin-Spotted Assassin Bug, Platymeris biguttatus (Linnaeus). Int J Mol Sci. 2019 Jan;20(11):2728.

423. Mesquita RD, Vionette-Amaral RJ, Lowenberger C, Rivera-Pomar R, Monteiro FA, Minx P, et al. Genome of *Rhodnius prolixus* , an insect vector of Chagas disease, reveals unique adaptations to hematophagy and parasite infection. Proc Natl Acad Sci. 2015 Dec 1;112(48):14936–41.

424. Schindelin J, Arganda-Carreras I, Frise E, Kaynig V, Longair M, Pietzsch T, et al. Fiji: an open-source platform for biological-image analysis. Nat Methods. 2012 Jul;9(7):676–82.

425. Romani S, Jimenez F, Hoch M, Patel NH, Taubert H, Jäckle H. Krüppel, a Drosophila segmentation gene, participates in the specification of neurons and glial cells. Mech Dev. 1996 Nov 1;60(1):95–107.

426. Mito T, Okamoto H, Shinahara W, Shinmyo Y, Miyawaki K, Ohuchi H, et al. Krüppel acts as a gap gene regulating expression of hunchback and even-skipped in the intermediate germ cricket Gryllus bimaculatus. Dev Biol. 2006 Jun 15;294(2):471–81.

427. Liu PZ, Kaufman TC. Kruppel is a gap gene in the intermediate germband insect Oncopeltus fasciatus and is required for development of both blastoderm and germband-derived segments. Dev Camb Engl. 2004 Sep;131(18):4567–79.

428. Cerny AC, Bucher G, Schröder R, Klingler M. Breakdown of abdominal patterning in the Tribolium Krüppel mutant jaws. Development. 2005 Dec 15;132(24):5353–63.

429. Liu J, Lemonds TR, Marden JH, Popadić A. A Pathway Analysis of Melanin Patterning in a Hemimetabolous Insect. Genetics. 2016 May 1;203(1):403–13.

430. Hiragaki S, Suzuki T, Mohamed AAM, Takeda M. Structures and functions of insect arylalkylamine N-acetyltransferase (iaaNAT); a key enzyme for physiological and behavioral switch in arthropods. Front Physiol. 2015 Apr 13;6:113.

431. Dai F yin, Qiao L, Tong X ling, Cao C, Chen P, Chen J, et al. Mutations of an Arylalkylamine-N-acetyltransferase, Bm-iAANAT, Are Responsible for Silkworm Melanism Mutant *. J Biol Chem. 2010 Jun 18;285(25):19553–60.

432. Posnien N, Koniszewski NDB, Hein HJ, Bucher G. Candidate Gene Screen in the Red Flour Beetle Tribolium Reveals Six3 as Ancient Regulator of Anterior Median Head and Central Complex Development. PLOS Genet. 2011 Dec 22;7(12):e1002416.

433. Penrice-Randal R, Hartley C, Beliavskaia A, Dong X, Brandner-Garrod L, Whitten M, et al. New Cell Lines Derived from Laboratory Colony Triatoma infestans and Rhodnius prolixus, Vectors of Trypanosoma cruzi, Do Not Harbour Triatoma Virus. Insects. 2022 Oct 5;13(10):906.

434. Heryanto C, Hanly JJ, Mazo-Vargas A, Tendolkar A, Martin A. Mapping and CRISPR homology-directed repair of a recessive white eye mutation in Plodia moths. iScience. 2022 Mar 18;25(3):103885.

435. Souza D, Christensen SA, Wu K, Buss L, Kleckner K, Darrisaw C, et al. RNAi-induced knockdown of white gene in the southern green stink bug (Nezara viridula L.). Sci Rep. 2022 Jun 21;12(1):10396.

436. Zhu J, Palliyil S, Ran C, Kumar JP. Drosophila Pax6 promotes development of the entire eye-antennal disc, thereby ensuring proper adult head formation. Proc Natl Acad Sci U S A. 2017 Jun 6;114(23):5846–53.

437. Czerny T, Halder G, Kloter U, Souabni A, Gehring WJ, Busslinger M. twin of eyeless, a second Pax-6 gene of Drosophila, acts upstream of eyeless in the control of eye development. Mol Cell. 1999 Mar;3(3):297–307.

438. Punzo C, Plaza S, Seimiya M, Schnupf P, Kurata S, Jaeger J, et al. Functional divergence between eyeless and twin of eyeless in Drosophila melanogaster. Development. 2004 Aug 15;131(16):3943–53.

439. Flaven-Pouchon J, Moussian B. Fluorescent Microscopy-Based Detection of Chitin in Intact Drosophila melanogaster. Front Physiol. 2022 Apr 26;13:856369.

440. Rylee JC, Siniard DJ, Doucette K, Zentner GE, Zelhof AC. Expanding the genetic toolkit of Tribolium castaneum. PLOS ONE. 2018 Apr 12;13(4):e0195977.

441. Shy BR, MacDougall MS, Clarke R, Merrill BJ. Co-incident insertion enables high efficiency genome engineering in mouse embryonic stem cells. Nucleic Acids Res. 2016 Sep 19;44(16):7997–8010.

442. Rocha D de A, Costa LM da, Pessoa GDC, Obara MT. Methods for detecting insecticide resistance in sand flies: A systematic review. Acta Trop. 2021 Jan 1;213:105747.

443. Roy L, Uranw S, Cloots K, Smekens T, Kiran U, Pyakurel UR, et al. Susceptibility status of the wild-caught Phlebotomus argentipes (Diptera: Psychodidae: Phlebotominae), the sand fly vector of visceral leishmaniasis, to different insecticides in Nepal. PLoS Negl Trop Dis. 2022 Jul 14;16(7):e0010304.

444. Fonseca B de P, Albuquerque PC, Zicker F. Neglected tropical diseases in Brazil: lack of correlation between disease burden, research funding and output. Trop Med Int Health. 2020;25(11):1373–84.

445. Berry I, Berrang-Ford L. Leishmaniasis, conflict, and political terror: A spatio-temporal analysis. Soc Sci Med 1982. 2016 Oct;167:140–9.

446. Alabdullah AA, Al-Abdulaziz B, Alsalem H, Magrashi A, Pulicat SM, Almzroua AA, et al. Estimating transfection efficiency in differentiated and undifferentiated neural cells. BMC Res Notes. 2019 Apr 15;12(1):225.

447. Chong ZX, Yeap SK, Ho WY. Transfection types, methods and strategies: a technical review. PeerJ. 2021 Apr 21;9:e11165.

448. Chesnoy S, Huang L. Structure and Function of Lipid-DNA Complexes for Gene Delivery. Annu Rev Biophys Biomol Struct. 2000 Jun;29(1):27–47.

449. Kato T, Yoshizuka K, Park EY. New strategy for rapid isolation of stable cell lines from DNA-transformed insect cells using fluorescence activated cell-sorting. J Biotechnol. 2010 May 17;147(2):102–7.

450. Goodman CL, Wang AA, Nabli H, Mcintosh AH, Wittmeyer JL, Grasela JJ. Development and partial characterization of heliothine cell lines from embryonic and differentiated tissues. Vitro Cell Dev Biol - Anim. 2004 Mar 1;40(3):89–94.

451. He X, Lu L, Huang P, Yu B, Peng L, Zou L, et al. Insect Cell-Based Models: Cell Line Establishment and Application in Insecticide Screening and Toxicology Research. Insects. 2023 Feb;14(2):104.

452. De Keuckelaere E, Hulpiau P, Saeys Y, Berx G, van Roy F. Nanos genes and their role in development and beyond. Cell Mol Life Sci CMLS. 2018 Jun;75(11):1929–46.

453. Tazuke SI, Schulz C, Gilboa L, Fogarty M, Mahowald AP, Guichet A, et al. A germline-specific gap junction protein required for survival of differentiating early germ cells. Dev Camb Engl. 2002 May;129(10):2529–39.

454. Magnusson K, Mendes AM, Windbichler N, Papathanos PA, Nolan T, Dottorini T, et al. Transcription Regulation of Sex-Biased Genes during Ontogeny in the Malaria Vector Anopheles gambiae. PLOS ONE. 2011 Jun 30;6(6):e21572.

455. Bier E. Gene drives gaining speed. Nat Rev Genet. 2022 Jan;23(1):5–22.

456. Kamhawi S, Ramalho-Ortigao M, Van M. Pham, Kumar S, Lawyer PG, Turco SJ, et al. A Role for Insect Galectins in Parasite Survival. Cell. 2004 Oct 29;119(3):329–41.

457. Arias AR de, Messenger LA, Rolon M, Vega MC, Acosta N, Villalba C, et al. Dynamics of Triatoma infestans populations in the Paraguayan Chaco: Population genetic analysis of household reinfestation following vector control. PLoS ONE [Internet]. 2022 [cited 2023 Dec 23];17(2). Available from: https://www.ncbi.nlm.nih.gov/pmc/articles/PMC8830694/

458. Morrison AC, Ferro C, Morales A, Tesh RB, Wilson ML. Dispersal of the sand fly Lutzomyia longipalpis (Diptera: Psychodidae) at an endemic focus of visceral leishmaniasis in Colombia. J Med Entomol. 1993 Mar;30(2):427–35.

459. Casanova C, Costa AI, Natal D. Dispersal pattern of the sand fly Lutzomyia neivai (Diptera: Psychodidae) in a cutaneous leishmaniasis endemic rural area in Southeastern Brazil. Mem Inst Oswaldo Cruz. 2005 Nov;100:719–24.

460. Orshan L, Elbaz S, Ben-Ari Y, Akad F, Afik O, Ben-Avi I, et al. Distribution and Dispersal of Phlebotomus papatasi (Diptera: Psychodidae) in a Zoonotic Cutaneous Leishmaniasis Focus, the Northern Negev, Israel. PLoS Negl Trop Dis. 2016 Jul 18;10(7):e0004819.

461. Courtier-Orgogozo V, Danchin A, Gouyon P, Boëte C. Evaluating the probability of CRISPR-based gene drive contaminating another species. Evol Appl. 2020 Apr 17;13(8):1888–905.

462. Ghosh KN, Mukhopadhyay JM, Guzman H, Tesh RB, Munstermann LE. Interspecific hybridization and genetic variability of Phlebotomus sandflies. Med Vet Entomol. 1999;13(1):78–88.

463. Azevedo LMS, Cesaretto NR, de Oliveira J, Ravazi A, dos Reis YV, Tadini SCAF, et al. First evidence of gonadal hybrid dysgenesis in Chagas disease vectors (Hemiptera, Triatominae): gonad atrophy prevents events of interspecific gene flow and introgression. Parasit Vectors. 2023 Oct 27;16(1):390.

464. Metchanun N, Borgemeister C, Amzati G, von Braun J, Nikolov M, Selvaraj P, et al. Modeling impact and cost-effectiveness of driving-Y gene drives for malaria elimination in the Democratic Republic of the Congo. Evol Appl. 2022 Jan 7;15(1):132–48.

465. Cecílio P, Oristian J, Meneses C, Serafim TD, Valenzuela JG, Cordeiro da Silva A, et al. Engineering a vector-based pan-Leishmania vaccine for humans: proof of principle. Sci Rep. 2020 Oct 29;10(1):18653.

466. Zimmermann D, Peters W, Schaub GA. Differences in binding of lectin-gold conjugates by Trypanosoma cruzi and Blastocrithidia triatomae (Trypanosomatidae) in the intestine of Triatoma infestans (Reduviidae). Parasitol Res. 1987;74(1):5–10.

467. Borges EC, Machado EMM, Garcia ES, Azambuja P. Trypanosoma cruzi: Effects of infection on cathepsin D activity in the midgut of Rhodnius prolixus. Exp Parasitol. 2006 Feb 1;112(2):130–3.

468. Waniek PJ, Jansen AM, Araújo CAC. Trypanosoma cruzi infection modulates the expression of Triatoma brasiliensis def1 in the midgut. Vector Borne Zoonotic Dis Larchmt N. 2011 Jul;11(7):845–7.

469. Whitten M, Sun F, Tew I, Schaub G, Soukou C, Nappi A, et al. Differential modulation of Rhodnius prolixus nitric oxide activities following challenge with Trypanosoma rangeli, T. cruzi and bacterial cell wall components. Insect Biochem Mol Biol. 2007 May;37(5):440–52.

8. Appendix

Appendix 1. A visual methodology of gRNA design using ChopChop v3.
A) the search page for ChopChop. gRNAs are located within genes by searching with gene IDs from the selected genome. Ai) the general settings tab. Aii) the Cas9 settings tab. Aiii) the primer settings tab. B) the gRNA ranking readout. C) the primer design readout. All settings altered from default are highlighted with a red box. The gRNA region placed into a DNA construct is highlighted in blue.

Ai

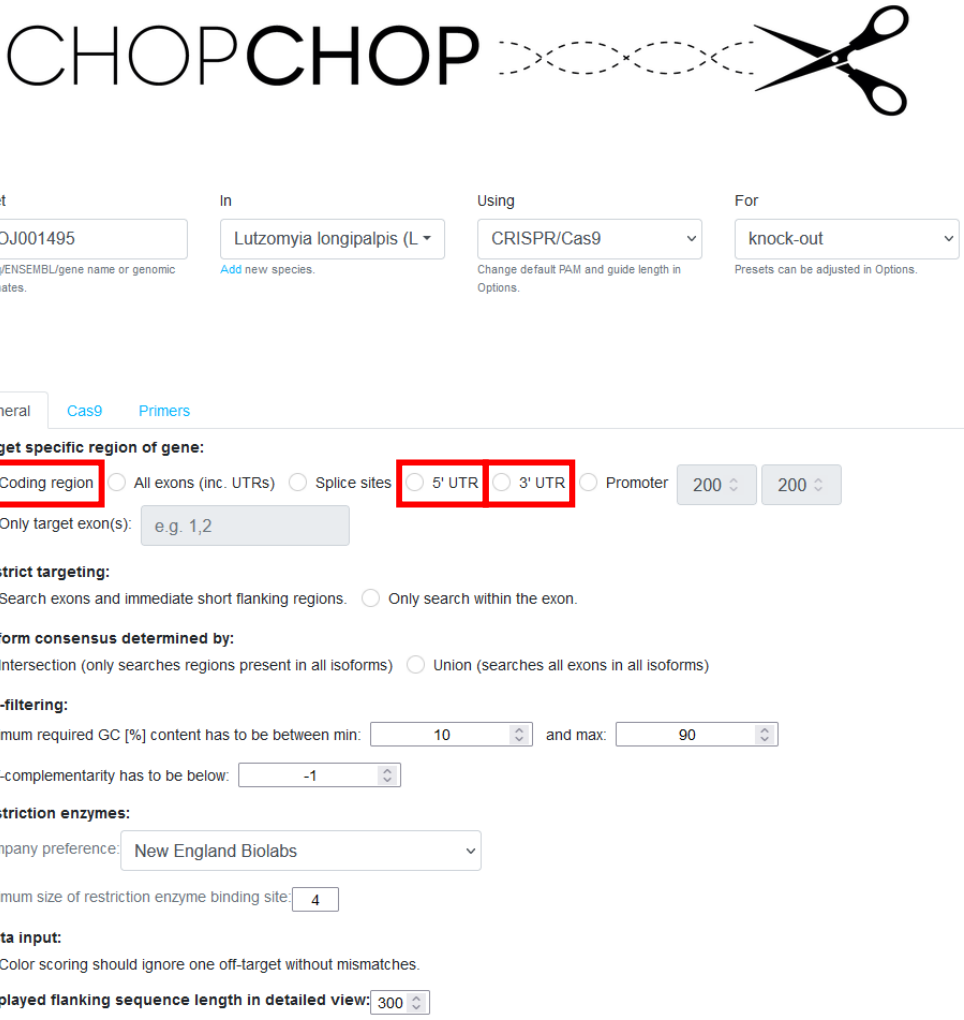

Aii

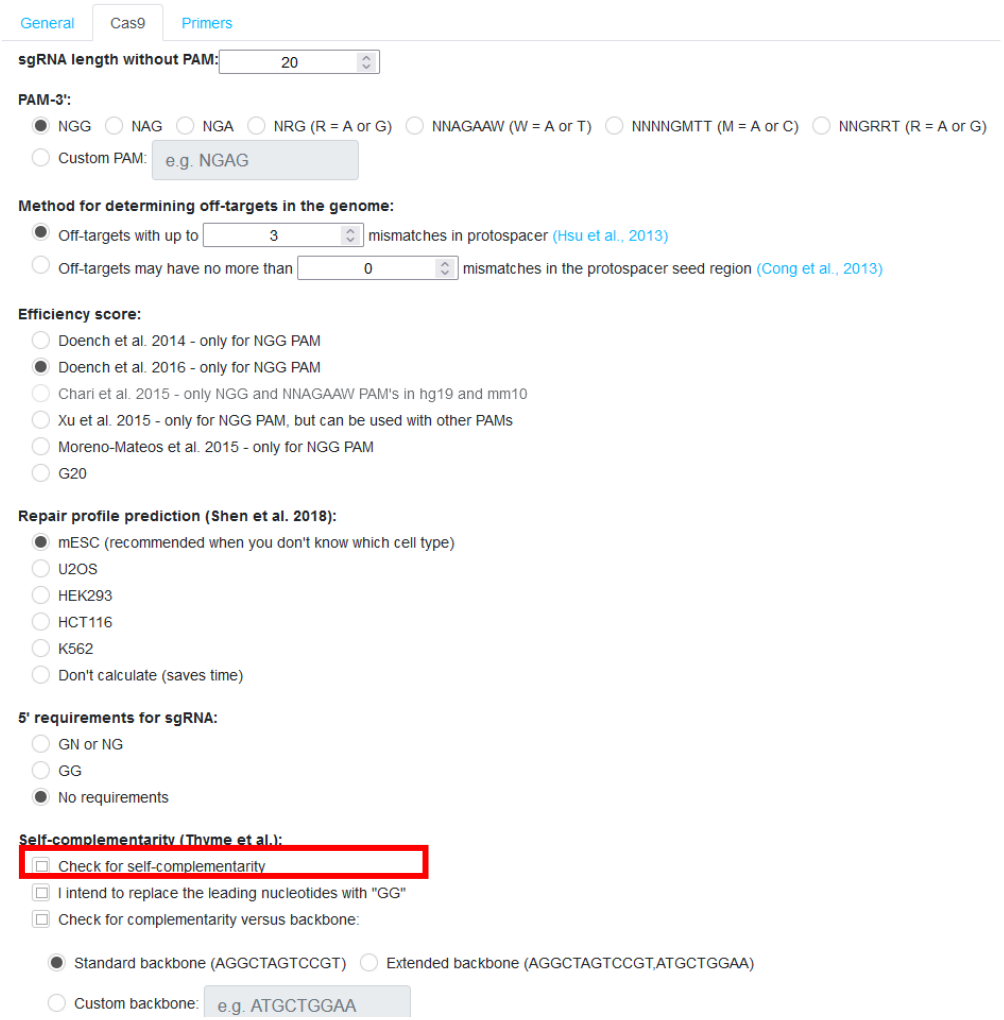
General
Cas9
Primers
sgRNA length without PAM: 20
PAM-3':
NGG NAG NGA NRG (R = A or G) NNAGAAW (W = A or T) NNNNGMTT (M = A or C) NNGRRT (R = A or G)
Custom PAM: e.g. NGAG
Method for determining off-targets in the genome:
Off-targets with up to 3 mismatches in protospacer (Hsu et al., 2013)
Off-targets may have no more than 0 mismatches in the protospacer seed region (Cong et al., 2013)
Efficiency score:
Doench et al. 2014 - only for NGG PAM
Doench et al. 2016 - only for NGG PAM
Chari et al. 2015 - only NGG and NNAGAAW PAM's in hg19 and mm10
Xu et al. 2015 - only for NGG PAM, but can be used with other PAMs
Moreno-Mateos et al. 2015 - only for NGG PAM
G20
Repair profile prediction (Shen et al. 2018):
mESC (recommended when you don't know which cell type)
U2OS
HEK293
HCT116
K562
Don't calculate (saves time)
5' requirements for sgRNA:
GN or NG
GG
No requirements
Self-complementarity (Thyme et al.):
Check for self-complementarity
I intend to replace the leading nucleotides with "GG"
Check for complementarity versus backbone:
Standard backbone (AGGCTAGTCCGT) Extended backbone (AGGCTAGTCCGT,ATGCTGGAA)
Custom backbone: e.g. ATGCTGGAA

Aiii

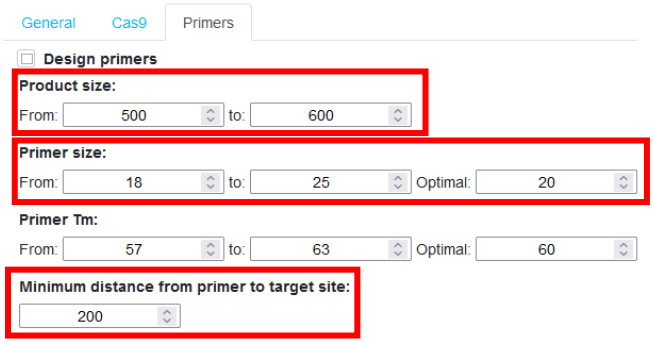
General
Cas9
Primers
Design primers
Product size:
From: 500 to: 600
Primer size:
From: 18 to: 25 Optimal: 20
Primer Tm:
From: 57 to: 63 Optimal: 60
Minimum distance from primer to target site:
200

B LLOJ001495

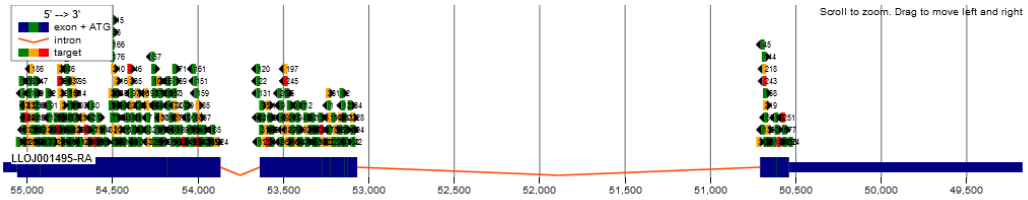

Download results: Please select one

View in UCSC genome browser

Rank	Target sequence	Genomic location	Strand	GC content (%)	Self-complementarity	MM0	MM1	MM2	MM3	Efficiency
1	CAAGACATGCCAGTGCAAGGGGG	Scaffold130:53219	+	55	0	0	0	0	0	75.68
2	TGGATCGACGTATGTCACAGAGG	Scaffold130:54571	-	50	0	0	0	0	0	75.21
3	TTAGGGTATTGCCATAACAGCGG	Scaffold130:53618	-	40	0	0	0	0	0	74.90
4	CGAAGTTATGCTCCTCACAGAGG	Scaffold130:54249	-	50	0	0	0	0	0	74.35
5	GAAGCTGTATTGATCCAACACGG	Scaffold130:50640	+	40	0	0	0	0	0	71.20
6	CCGCTGGATTGTAATTATCGGGG	Scaffold130:54159	+	45	0	0	0	0	0	68.75
7	ATTGAAAAGAGTTCACTGGAGGG	Scaffold130:54278	+	35	1	0	0	0	0	67.64
8	CCTGTCGTGCGAGATCCTGGAGG	Scaffold130:54330	+	65	0	0	0	0	0	66.55
9	TCGAGAGGACTGAGTACATGGGG	Scaffold130:53501	+	50	2	0	0	0	0	68.46
10	GAAGTTATGCTCCTCACAGAGGG	Scaffold130:54248	-	45	1	0	0	0	0	66.84
11	CAATACCCTAATGTCGATTGCGG	Scaffold130:53630	+	40	0	0	0	0	0	65.77
12	CCGATGCACATGAAGATGAGTGG	Scaffold130:53365	+	50	0	0	0	0	0	65.60
13	CTCCCGGATAAGTGGCCAGGAGG	Scaffold130:54123	+	65	2	0	0	0	0	67.49
14	AAGCTACCCGTCCCTCTGTGAGG	Scaffold130:54237	+	60	0	0	0	0	0	65.35
15	TGAGATTCACCATAAAAGTGAGG	Scaffold130:54597	+	35	0	0	0	0	0	65.17
16	ACGTATGTCACAGAGGGACAAGG	Scaffold130:54564	-	50	2	0	0	0	0	66.77
17	TGGCGTGCAGGGAGGCACCGGGG	Scaffold130:54739	-	75	1	0	0	0	0	65.71

C

Target: **LLOJ001495**
Rank: **1**
Target sequence: **CAAGACATGCCAGTGCAAGGGGG**

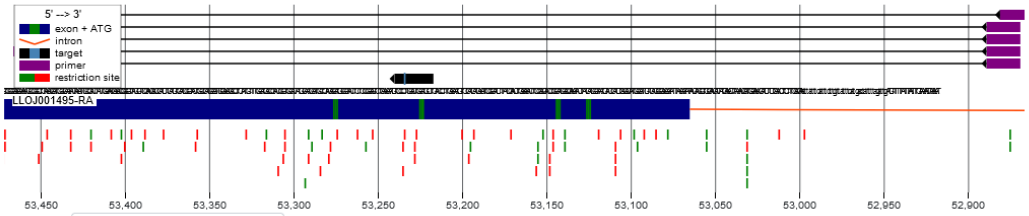

Download: Please select one

Pair	Left primer coordinates	Left primer	Left primer Tm	Left primer off-targets	Right primer coordinates	Right primer	Right primer Tm	Right primer off-targets
1	Scaffold130:53445-53465	AAAAGTCCGGCCTCTACAGC	60.8	0	Scaffold130:52870-52890	CCCCTGATTCGCAAAATATC	59.4	0
2	Scaffold130:53447-53467	GAAAAAGTCCGGCCTCTACA	59.3	0	Scaffold130:52870-52890	CCCCTGATTCGCAAAATATC	59.4	0
3	Scaffold130:53443-53463	AAGTCCGGCCTCTACAGCAT	61.2	0	Scaffold130:52870-52890	CCCCTGATTCGCAAAATATC	59.4	0
4	Scaffold130:53443-53462	AGTCCGGCCTCTACAGCAT	59.8	0	Scaffold130:52870-52890	CCCCTGATTCGCAAAATATC	59.4	0
5	Scaffold130:53443-53462	AGTCCGGCCTCTACAGCAT	59.8	0	Scaffold130:52862-52882	TTACTTAGCCCCTGATTCGC	59.3	0

Off-targets		
Location	Number of mismatches	Sequence (including mismatches)
There are no off-targets.		

Shen et al. 2018 predictions of repair profile - statistics	
Reference sequence	ATAAAGATGCCGGATGTCATCATGAGAACATTGTCAAAGGGTACAAGACATGCCAGTGCA<>AGGGGGACATTGTTGAAGACTGCCGAGAAGAAGTAGCCACATGCTGTAG
Frameshift frequency	70.89
Precision score	0.44
Frame +0 frequency	29.11
Frame +1 frequency	35.34
Frame +2 frequency	35.55
1-bp ins frequency	14.93
Highest del frequency	13.46
Highest ins frequency	13.34
Highest outcome frequency	13.46

Appendix 2. PCR primers used for CRISPR-Cas9 genome editing in phlebotomine sand flies.

Name of primer pair	Target gene	Function	Direction	Sequence
Caspar1	*caspar*	gRNA/CRISPR-Cas9 mutation confirmation of gRNA 1	Forward	CGAGGTCAAATCGGATGTCT
			Reverse	GATAGAATTCCGGATGGGGT
Caspar2	*caspar*	gRNA/CRISPR-Cas9 mutation confirmation of gRNA 2	Forward	AGAACCAATGGCAGGAACAC
			Reverse	CTTGATGCCTCACAGCGATA
Caspar3	*caspar*	gRNA/CRISPR-Cas9 mutation confirmation of gRNAs 3 & 4	Forward	CAGAGAATCGCGAAGAGACC
			Reverse	TTGTCTCTCGCCACATTGAG
Cinnabar_con	*cinnabar*	gRNA/CRISPR-Cas9 mutation confirmation	Forward	ATGTGGACGGTTCATTGACA
			Reverse	GTACTGCCCGAAGAAACCAA
Ebony_con	*ebony*	gRNA/CRISPR-Cas9 mutation confirmation of *L. longipalpis* gRNA	Forward	TTTCTTCAAAGCTCTGGGTCTT
			Reverse	TTGAAGGAGGGAGGCAATAA
Ebony1	*ebony*	gRNA/CRISPR-Cas9 mutation confirmation of *P. papatasi* gRNA 1	Forward	TCAAGGATGTGGCAACAAAA
			Reverse	TTTAGTTTCGATTCCGCCAC
Ebony2	*ebony*	gRNA/CRISPR-Cas9 mutation confirmation of *P. papatasi* gRNA 2, 3, & 4	Forward	TGTGGCAACAAAACAGCAAT
			Reverse	TTTAGTTTCGATTCCGCCAC
Eyeless_con	*eyeless*	gRNA/CRISPR-Cas9 mutation confirmation of *L. longipalpis* gRNA	Forward	CGGGGTTGTGGCTATCTTT
			Reverse	ATGCACTTCCCATCCCAAT
Rudimentary_con 1	*Rudimentary*	gRNA/CRISPR-Cas9 mutation confirmation of gRNA 1	Forward	AATCAAATTCCCATCGAACG
			Reverse	GAAACGGCAACAAAGGTGAT
Rudimentary_con 2	*Rudimentary*	gRNA/CRISPR-Cas9 mutation confirmation of gRNA 2	Forward	AACGCGGAAAAGGGAGTATT
			Reverse	GTTGCATGCTTTGGGGATAA
	Rudimentary		Forward	GCACAATACGCCCTGAATTT

Rudimentary_con 3		gRNA/CRISPR-Cas9 mutation confirmation of gRNA 3	Reverse	AAGCTAAAGAAATGCCCGTG
Scarlet_con5’	*scarlet*	gRNA/CRISPR-Cas9 mutation confirmation of 5’ gRNA	Forward	GCTTTGGGAGTGAGGGTGTA
			Reverse	CAGTGCCATCAATGTTCCAG
Scarlet_con3’	*scarlet*	gRNA/CRISPR-Cas9 mutation confirmation of 3’ gRNA	Forward	GTCACGACAAGAGTGCCTCA
			Reverse	TGGAGGTGAAACACCAACAA
Scarlet_con_cent	*scarlet*	gRNA/CRISPR-Cas9 mutation confirmation of central gRNA	Forward	AAAAGTCCGGCCTCTACAGC
			Reverse	CCCCTGATTCGCAAAATATC
Vestigial_con	*vestigial*	gRNA/CRISPR-Cas9 mutation confirmation of *L. longipalpis* gRNA 1	Forward	GTTGGTCGTGATGCAATCTG
			Reverse	AAATTTTAGCCCGGGAAATG
Vestigial_con	*vestigial*	gRNA/CRISPR-Cas9 mutation confirmation of *L. longipalpis* gRNA 2	Forward	TTACCACGCGAGATGAAAGG
			Reverse	TATCAAAAGGGCCGAACAAG
Vestigial_con	*vestigial*	gRNA/CRISPR-Cas9 mutation confirmation of *L. longipalpis* gRNA 3	Forward	CAAGGAGGCACACAATTGAA
			Reverse	TCGCCAAACCTTAGATAACAA
Vestigial1	*vestigial*	gRNA/CRISPR-Cas9 mutation confirmation of *P. papatasi* gRNA 1, 2 & 3	Forward	TGATCCATAACACAACCGGA
			Reverse	GCCATTGTGGGGTAGCTAGA
Vestigial2	*vestigial*	gRNA/CRISPR-Cas9 mutation confirmation of *P. papatasi* gRNA 4	Forward	CGGATTTGTATTCCGCAGAT
			Reverse	TTTGTAACTTTGCATCCACCA
White_con	*white*	gRNA/CRISPR-Cas9 mutation confirmation of gRNA	Forward	TTGCCCTTTATATCCCTTGC
			Reverse	CTCGAAACCGATGGTCATTT
Yellow_con1	*yellow*	gRNA/CRISPR-Cas9 mutation confirmation of *L. longipalpis* gRNA 1, 2 & 3	Forward	AAAATTCATACACGGGTGGG
			Reverse	ATCAAAATGCACTGCTCACG

Yellow1	*yellow*	gRNA/CRISPR-Cas9 mutation confirmation of *P. papatasi* gRNA 1, 2 & 4	Forward	CTCCCCATTGGAAGTTCAGA
			Reverse	CATCTCCAGGGACACTCCAT
Yellow2	*yellow*	gRNA/CRISPR-Cas9 mutation confirmation of *P. papatasi* gRNA 3	Forward	ACGAAATGGTCAGTCCCTTG
			Reverse	ATCGGACATGTAGGCGTAGG
Llon1_U6_insert	*L. longipalpis genome*	Amplification of the U6 promoter from the *L. longipalpis* genome for insertion into the pDCC6 plasmid	Forward	GGCAACTCGTGAAAGGTAGGC GGATCAGCGATTGAAGTGACAA TTGAATATCCAACGGTT
			Reverse	TAGCTCTAAAACAGGTCTTCTCG AAGACCCAATTCCATGGCAAAT CTATTTTCCTTATAA
Llon1_U6_vector	*L. longipalpis genome*	Amplification of pDCC6 vector for insertion of *L. longipalpis* U6 promoter.	Forward	TTATAAGGAAAATAGATTTGCC ATGGAATTGGGTCTTCGAGAAG ACCTGTTTTAGAGCTA
			Reverse	AACCGTTGGATATTCAATTGTCA CTTCAATCGCTGATCCGCCTACC TTTCACGAGTTGCC
Ppap1_U6_insert	*P. papatasi genome*	Amplification of the U6 promoter from the *P. papatasi* genome for insertion into the pDCC6 plasmid	Forward	GGCAACTCGTGAAAGGTAGGC GGATCAGCGTGTGATATCCCGT GGGCCAAATTTGAAATG
			Reverse	TAGCTCTAAAACAGGTCTTCTCG AAGACCCAAATGCATAGAAATC GAATTGATATATGAA
Ppap1_U6_vector	*P. Papatasi genome*	Amplification of pDCC6 vector for insertion of *P. papatasi* U6 promoter.	Forward	TTCATATATCAATTCGATTTCTAT GCATTTGGGTCTTCGAGAAGAC CTGTTTTAGAGCTA
			Reverse	CATTTCAAATTTGGCCCACGGG ATATCACACGCTGATCCGCCTAC CTTTCACGAGTTGCC
U6_con	*pDCC6 plasmid*	Confirmation of endogenous promoter/gRNA insertion into the pDCC6 plasmid	Forward	CCGAGCGCAGCGAGTCAGTG
			Reverse	AAACAAAAAAGCACCGACTC
St_LHA_I	*scarlet*	Amplification of the left homology arm for incorporation into	Forward	ACCTTTGAGTTCTCTCAGTTGGG GGCGTAGCTTGCATAACCCACTT CACTCCAAGATACT

		pDsRed-*Ubi63e*-attP for the HUTR approach	Reverse	CTTCGTATAGCATACATTATACG AAGTTATGTTGAGACTGAGCAC CACGAGACGACATTG
St_LHA_V	*scarlet*	Amplification of the vector for incorporation of the left homology arm for the HUTR approach	Reverse	AGTATCTTGGAGTGAAGTGG GTTATGCAAGCTACGCCCCC AACTGAGAGAACTCAAAGGT
St_RHA_I	*scarlet*	Amplification of the right homology arm for incorporation into pDsRed-*Ubi63e*-attP for the HUTR approach	Forward	CTTCGTATAATGTATGCTATACG AAGTTATGCTTTAATGGTGCGAT ATAGTGTGTGCCTG
			Reverse	ATGCATGGAGATCTTTACTAGT GCTCTTCTATATATATTTTTTCCA GTGCATTCAAATGT
St_RHA_V	*scarlet*	Amplification of the vector for incorporation of the right homology arm for the HUTR approach	Forward	ACATTTGAATGCACTGGAAA AAATATATATAGAAGAGCAC TAGTAAAGATCTCCATGCAT
SC_LHA_I	*scarlet*	Amplification of the left homology arm for incorporation into pDsRed-*Ubi63e*-attP for the HSC approach	Forward	ACCTTTGAGTTCTCTCAGTTGGG GGCGTAGTGGTGAACCTTGAAT ACCATATGGCCGAGA
			Reverse	CTTCGTATAGCATACATTATACG AAGTTATACATTGTTGAAGACT GCCGAGAAGAAGTAG
SC_LHA_V	*scarlet*	Amplification of the vector for incorporation of the left homology arm the HSC approach	Reverse	TCTCGGCCATATGGTATTCAA GGTTCACCACTACGCCCCCA ACTGAGAGAACTCAAAGGT
SC_RHA_I	*scarlet*	Amplification of the right homology arm for incorporation into pDsRed-*Ubi63e*-attP the HSC approach	Forward	CTTCGTATAATGTATGCTATACG AAGTTATTACCCTTTGACAATGT TCTCATGATGACAT
			Reverse	ATGCATGGAGATCTTTACTAGT GCTCTTCTTTAAGAGTTCATATA TTAAGCCCAAAATAA
SC_RHA_V	*scarlet*	Amplification of the vector for incorporation of the right homology arm the HSC approach	Forward	TTATTTTGGGCTTAATATATG AACTCTTAAAGAAGAGCACT AGTAAAGATCTCCATGCAT

St_HDR_con	*scarlet*	Confirmation of HDR insertion universal primer	Forward	CGCGACTCTAGATCATAATC
St_RHA_R	*scarlet*	Confirmation of HDR insertion for HUTR approach	Reverse	TATTTATTATGCATTTAGAA
SC_HC	*scarlet*	Confirmation of HDR insertion for HSC approach	Reverse	ACATGTAGAAGACTTATTTA

Appendix 3. Densitometric analysis results showing mutations in the *vestigial* gRNA1 region of *L. longipalpis* insects transfected with CRISPR-Cas9 plasmids.

Sample ID	Band No.	Band Volume	% of Lane	% Modification
V1A*	1	10195259	15.68	N/A
V1A	1	47635951	78.73	N/A
V1B*	1	22080219	21.65	N/A
V1B	1	69835173	81.21	N/A
V1C*	1	22959437	21.95	N/A
V1C	1	58899169	67.31	N/A
V1D*	1	17260922	25.94	N/A
	2	8512520	4.96	
V1D	1	43281751	72.69	N/A
V1E	1	65243734	74.12	N/A
V1F*	1	25287577	35.02	N/A
V1F	1	53337947	60.89	N/A
V1G	1	59195585	79.59	N/A
V1H*	1	37120086	48.69	5.72
	2	15853477	6.02	
	3	8723622	0.07	
V1H	1	91932443	77.09	N/A
V1I*	1	21126130	25.75	9.87
	2	10864555	5.39	
	3	5385579	0.56	
V1I	1	51745065	68.46	N/A
V1K*	1	9759603	6.59	N/A
	2	7555422	1.46	
	3	7619378	1.04	
	4	49420583	70.18	
V1L*	1	19497848	42.75	N/A

V1L	1	48651990	71.70	N/A
V1M*	1	11052480	57.10	N/A
	2	6044006	5.46	
	3	5326430	3.65	
V1M	1	35664548	74.68	N/A
V1N*	1	4825368	12.09	N/A
	2	5164088	5.37	
	3	6723766	19.33	
V1N	1	6122712	0.86	N/A
	2	60976618	94.35	
	3	6046848	0.51	
V1O*	1	8241626	30.42	N/A
	2	6188484	7.71	
	3	5927542	3.32	
V1O	1	43211508	84.42	N/A
V1P*	1	12604560	45.56	19.21
	2	5650534	3.89	
	3	9449882	20.91	
	4	5986006	3.32	
V1P	1	4731234	0.57	N/A
	2	5888914	0.39	
	3	55917858	93.94	
	4	5934618	0.47	
V1Q*	1	5599146	10.15	N/A
	2	6073180	9.68	
V1Q	1	4046428	0.06	N/A
	2	4838592	0.31	
	3	63050118	91.07	
	4	6010366	1.77	
V1R*	1	13916288	53.64	16.89
	2	5302418	1.13	
	3	6158324	3.52	
	4	11030382	21.96	
	5	5421318	2.06	
V1R	1	6345374	0.57	N/A
	2	67356328	96.18	
	3	5011258	0.31	
V1S*	1	15348888	64.61	N/A

	2	5985890	2.36	
	3	5192450	1.54	
V1S	1	7683550	1.01	N/A
	2	58253576	83.66	
V1T*	1	13617298	58.88	4.12
	2	7006110	3.87	
	3	6670638	3.77	
	4	5302476	1.39	
V1T	1	5341916	1.36	N/A
	2	42750698	79.76	
V1U*	1	14112270	51.98	N/A
	2	9324080	12.92	
V1U	1	3843254	0.02	N/A
	2	4276572	0.58	
	3	58495320	95.45	
	4	6242540	0.57	
V1V*	1	7863466	26.31	14.96
	2	5838802	12.60	
	3	5877952	7.48	
	4	5223538	2.59	
V1V	1	4749852	0.52	N/A
	2	50140130	83.91	
V1W*	1	15231032	65.23	1.67
	2	4013600	1.26	
	3	4563440	0.98	
V1W	1	46544014	84.44	N/A
V1X*	1	23972661	35.90	1.75
	2	7278729	1.17	
	3	7524171	1.21	
	4	4507503	0.08	
V1X	1	79643712	71.36	N/A
V1Y*	1	23961574	29.31	9.29
	2	5641442	0.73	
	3	12554566	5.82	
	4	5469950	0.49	
	5	4386004	0.09	
V1Y	1	6888944	1.38	N/A
	2	60009180	63.52	

	3	7302670	2.30	
V1Z*	1	31433380	42.10	2.56
	2	5922426	1.07	
	3	7959746	1.01	
	4	8935564	1.22	
	5	5773936	0.59	
V1Z	1	69679196	70.30	N/A
	2	5044196	1.41	

Appendix 4. Densitometric analysis results showing mutations in the *vestigial* gRNA2 region of *L. longipalpis* insects transfected with CRISPR-Cas9 plasmids.

Sample ID	Band No.	Band Volume	% of Lane	% Modification
V2A*	1	10218564	11.74	N/A
V2A	1	60075423	74.07	N/A
	2	6568968	0.96	
V2B*	1	26411597	45.32	N/A
	2	10204507	2.22	
	3	7273457	1.05	
V2B	1	61567361	72.85	N/A
	2	2977166	0.72	
	3	5620662	1.02	
	4	8532314	1.83	
V2C*	1	24368341	42.79	N/A
	2	12492983	5.02	
	3	6972483	0.83	
V2C	1	59606760	74.69	N/A
	2	6454410	1.15	
	3	7720892	1.21	
V2D*	1	20259259	30.63	N/A
	2	12293513	14.75	
V2D	1	84941036	84.35	N/A
	2	6236396	0.99	
	3	3786697	0.04	
V2E*	1	27221433	54.52	N/A
V2E	1	52074602	81.75	N/A
	2	5326215	0.79	
	3	6773867	2.25	

	4	3917176	0.97	
V2F*	1	23609501	54.09	N/A
V2F	1	27389427	58.98	N/A
V2G*	1	23000206	55.95	18.77
	2	16980790	24.72	
	3	7716669	4.13	
V2G	1	56255556	84.44	N/A
	2	2805568	0.54	
	3	6934565	0.36	
	4	6540504	1.26	
V2H*	1	14169853	44.86	17.71
	2	13569351	17.87	
	3	6242141	3.53	
	4	4102506	1.42	
V2H	1	53050499	85.58	N/A
	2	5044382	0.30	
	3	4621175	0.91	
V2I*	1	16881906	57.70	12.62
	2	10961964	11.23	
	3	9083935	6.64	
	4	5325340	1.30	
V2I	1	62024694	85.88	N/A
	2	4685780	0.72	
	3	5317021	0.55	
	4	4843251	0.94	
V2K*	1	16377043	55.37	11.27
	2	8569396	8.98	
	3	7818149	5.98	
V2K	1	40189089	80.72	N/A
	2	5740405	0.34	
	3	4496213	0.83	
V2M*	1	12237662	55.82	N/A
	2	6726354	6.81	
V2M	1	62743373	88.40	N/A
	2	6560623	0.41	
	3	7752954	1.24	
	4	7001648	1.85	
V2N*	1	20982937	66.02	6.43

	2	5750612	4.23	
	3	6882527	4.26	
	4	3903322	0.89	
	5	4335261	1.87	
V2N	1	56199801	86.02	N/A
	2	3897894	0.49	N/A
	3	3731042	0.38	N/A
	4	2564435	0.43	N/A
V2O*	1	12965368	46.74	17.30
	2	9565198	10.63	
	3	9713819	10.96	
V2O	1	46679502	76.94	N/A
	2	5155420	1.95	N/A
V2P*	1	12092935	62.05	N/A
V2P	1	29465367	83.42	N/A
V2Q*	1	12390472	52.27	15.15
	2	8287553	10.07	
	3	8706571	10.26	
V2Q	1	40422257	92.46	N/A
	2	4338565	0.31	
	3	4936943	0.41	
V2Q*	1	28422660	14.61	10.20
	2	12969098	1.99	
	3	13739076	1.51	
V2Q	1	74588170	51.14	N/A
V2R*	1	28939678	13.84	11.70
	2	17224530	2.08	
	3	14329750	1.83	
V2R	1	95716158	59.43	N/A
	2	8437890	1.22	
	3	11444022	0.96	
V2S*	1	42829662	26.39	N/A
V2S	1	97101052	60.95	N/A
	2	13443894	1.66	
	3	7191566	0.33	
V2T*	1	38963094	23.31	N/A
	2	15102828	2.84	
V2T	1	86791878	54.34	N/A

	2	12925946	2.17	
V2U*	1	45787124	24.83	15.24
	2	23882834	7.67	
	3	15698586	2.06	
V2U	1	106574342	67.89	N/A
V2V*	1	64274842	43.18	N/A
V2V	1	105832946	66.99	N/A
V2W*	1	45810374	28.33	N/A
V2W	1	84605696	66.51	N/A
V2X*	1	37135458	19.56	N/A
V2X	1	91289978	58.90	N/A
V2Y*	1	37126716	18.77	N/A
	2	21608550	6.60	
V2Y	1	85880106	60.64	N/A
V2Z*	1	25587648	13.06	N/A
V2Z	1	76175494	55.79	N/A

Appendix 5. Potential delayed development following transfection of *Rhodnius prolixus* embryos with piggyBac based plasmids.
A= a wild-type embryo B= an embryo transfected with the pHome-T plasmid. Both embryos are 10 days post oviposition. These images were taken using an Olympus SZ51 microscope at 30x magnification. The scale bars represent 1mm.

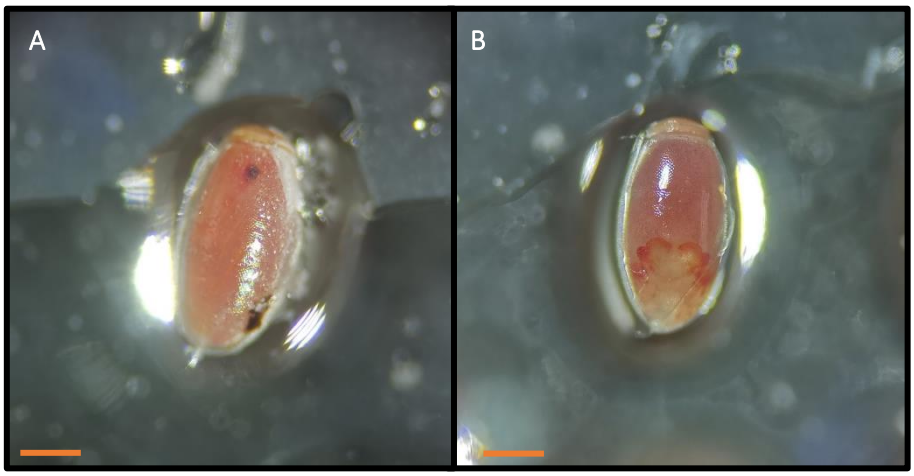

Appendix 6. PCR primers used for CRISPR-Cas9 genome editing in *R. prolixus*.

Name of primer pair	Target gene	Function	Direction	Sequence
white_con	*white*	gRNA/CRISPR-Cas9 mutation confirmation	Forward	TGAGTTGTGAATTCTTTGACGC
			Reverse	ATCAGCAATTGTGGTCTTCAA
eyeless_con	*eyeless*	gRNA/CRISPR-Cas9 mutation confirmation	Forward	GCTATTTCCTCAAAAATGGCA
			Reverse	ACCCGGCTCCTTCATACTTT
*krüppel*_con	*krüppel*	gRNA/CRISPR-Cas9 mutation confirmation	Forward	AGAAAAGCACTTTGACCGGA
			Reverse	GTCTTGCATTCGTGGAGGAT
*aaNAT*_con	*aaNAT*	gRNA/CRISPR-Cas9 mutation confirmation	Forward	TCAATCCCACTAACACACACG
			Reverse	CTGGATTCAGGGAATCACAAA
yellow_con	*yellow*	gRNA/CRISPR-Cas9 mutation confirmation	Forward	TTGTCCATATGCACTTCATGC
			Reverse	TGGTACCTTGCATCGTATGG
Rpro1_U6_insert	*R. prolixus* genome	Amplification of the U6 promoter from the *R. prolixus* genome for insertion into the pDCC6 plasmid	Forward	GGCAACTCGTGAAAGGTAGGC GGATCAGCGGTTGTTCTTACTG TGGGAAAATCCATTGTG
			Reverse	TAGCTCTAAAACAGGTCTTCTC GAAGACCCAGCTAGAAGAGAT TTTTTCTGGCTTATATA
Rpro1_U6_vector	*R. prolixus* genome	Amplification of pDCC6 vector for insertion of *R. prolixus* U6 promoter.	Forward	TATATAAGCCAGAAAAAATCTC TTCTAGCTGGGTCTTCGAGAAG ACCTGTTTTAGAGCTA
			Reverse	CACAATGGATTTTCCCACAGTA AGAACAACCGCTGATCCGCCTA CCTTTCACGAGTTGCC
U6_con	pDCC6 plasmid	Confirmation of endogenous promoter/gRNA insertion into the pDCC6 plasmid	Forward	CCGAGCGCAGCGAGTCAGTG
			Reverse	AAACAAAAAAGCACCGACTC
LHA_V_uni	Universal for DsRed-*ubi63e*-attP	Amplification of the vector for incorporation of the left homology arm	Forward	ATAATGTATGCTATACGAAGTT ATCGTACGCGCGCAGATCGCCG ATGGGCGTGGCGCCGG
ey_LHA_I	*eyeless*	Amplification of the left homology arm for incorporation into pDsRed-*Ubi63e*-attP	Forward	ACCTTTGAGTTCTCTCAGTTGG GGGCGTAGATGCAGAGCAAGC CTAACAGCTGGTAGTAT
			Reverse	CTTCGTATAGCATACATTATACG AAGTTATGTGACCTGCACCAAA TCACAAACAGTCCAT
ey_LHA_V	*eyeless*	Amplification of pDsRed-*Ubi63e*-attP for incorporation of the left homology arm	Reverse	ATACTACCAGCTGTTAGGCTTG CTCTGCATCTACGCCCCCAACT GAGAGAACTCAAAGGT
k_LHA_I	*krüppel*	Amplification of the left homology arm for incorporation into pDsRed-*Ubi63e*-attP	Forward	ACCTTTGAGTTCTCTCAGTTGG GGGCGTAGTAATTTTTTATAAC TTTGTTTCGGTCGGTT

			Reverse	CTTCGTATAGCATACATTATACGAAGTTATTCGTAAATTTGCGACTTGTACGAAATTTCT
k_LHA_V	*krüppel*	Amplification of pDsRed-*Ubi63e*-attP for incorporation of the left homology arm	Reverse	AACCGACCGAAACAAAGTTATAAAAAATTACTACGCCCCCAACTGAGAGAACTCAAAGGT
p_LHA_I	*aaNAT*	Amplification of the left homology arm for incorporation into pDsRed-*Ubi63e*-attP	Forward	ACCTTTGAGTTCTCTCAGTTGGGGGCGTAGGAGAATTGAAAATAATGTGAAAGCAAAGAA
			Reverse	CTTCGTATAGCATACATTATACGAAGTTATAAGAAAAACTTTCTTAAAAAAGCAATTACA
p_LHA_V	*aaNAT*	Amplification of pDsRed-*Ubi63e*-attP for incorporation of the left homology arm	Reverse	TTCTTTGCTTTCACATTATTTTCAATTCTCCTACGCCCCCAACTGAGAGAACTCAAAGGT
y_LHA_I	*yellow*	Amplification of the left homology arm for incorporation into pDsRed-*Ubi63e*-attP	Forward	ACCTTTGAGTTCTCTCAGTTGGGGGCGTAGTTCGGAAATATTTTACCCTTGATCTCAACC
			Reverse	CTTCGTATAGCATACATTATACGAAGTTATGGATCAGGATGAAAGAAACCATGTTCAAAT
y_LHA_V	*yellow*	Amplification of pDsRed-*Ubi63e*-attP for incorporation of the left homology arm	Reverse	ATTTGAACATGGTTTCTTTCATCCTGATCCCTACGCCCCCAACTGAGAGAACTCAAAGGT
RHA_V_uni	Universal for DsRed-*ubi63e*-attP	Amplification of the vector for incorporation of the right homology arm	Reverse	ATAGCATACATTATACGAAGTTATACCGGTTAAGATACATTGATGAGTTTGGACAAACCA
ey_RHA_I	*eyeless*	Amplification of the right homology arm for incorporation into pDsRed-*Ubi63e*-attP	Forward	CTTCGTATAATGTATGCTATACGAAGTTATTGTATTTGTCAGTGGGCGACCTTTGCCTGA
			Reverse	ATGCATGGAGATCTTTACTAGTGCTCTTCTTGTTAGGCAAGAGGTTTATTAAGATAGTCT
ey_RHA_V	*eyeless*	Amplification of pDsRed-*Ubi63e*-attP for incorporation of the right homology arm	Forward	GTGTTTATAAACATATAATTTTACAACTTTAGAAGAGCACTAGTAAAGATCTCCATGCAT
k_RHA_I	*krüppel*	Amplification of the right homology arm for incorporation into pDsRed-*Ubi63e*-attP	Forward	CTTCGTATAATGTATGCTATACGAAGTTATAGAACGGCCCTACGCTTGCACCCAGTGTAC
			Reverse	ATGCATGGAGATCTTTACTAGTGCTCTTCTATTTTGCAATTTTTTTATTACTTTTTTTTA
k_RHA_V	*krüppel*	Amplification of pDsRed-*Ubi63e*-attP for incorporation of the right homology arm	Forward	TAAAAAAAAGTAATAAAAAAATTGCAAAATAGAAGAGCACTAGTAAAGATCTCCATGCAT

p_RHA_I	*aaNAT*	Amplification of the right homology arm for incorporation into pDsRed-*Ubi63e*-attP	Forward	CTTCGTATAATGTATGCTATACGAAGTTATGTGTAGGACTGCTAGATGAGCCTGGATCTA
			Reverse	ATGCATGGAGATCTTTACTAGTGCTCTTCTAAAGTTGTAAAATTATATGTTTATAAACAC
p_RHA_V	*aaNAT*	Amplification of pDsRed-*Ubi63e*-attP for incorporation of the right homology arm	Forward	GTGTTTATAAACATATAATTTTACAACTTTAGAAGAGCACTAGTAAAGATCTCCATGCAT
y_RHA_I	*yellow*	Amplification of the right homology arm for incorporation into pDsRed-*Ubi63e*-attP	Forward	CTTCGTATAATGTATGCTATACGAAGTTATCCGGACTAAATTTCCAATGGGAAGCTGAAG
			Reverse	ATGCATGGAGATCTTTACTAGTGCTCTTCTTCTGTTTTAAGCTCCTTTAATTGGAAATAT
y_RHA_V	*yellow*	Amplification of pDsRed-*Ubi63e*-attP for incorporation of the right homology arm	Forward	ATATTTCCAATTAAAGGAGCTTAAAACAGAAGAAGAGCACTAGTAAAGATCTCCATGCAT
St_HDR_con	scarlet	Confirmation of HDR insertion universal primer	Forward	CGCGACTCTAGATCATAATC
HDR_ey	*eyeless*	Confirmation of HDR insertion via amplification of gRNA/HA region	Forward	TCAATCCTAGCTAGACCCTT
			Reverse	GATTGTACAGGAGTCACTGAATCAG
HDR_k	*krüppel*	Confirmation of HDR insertion via amplification of gRNA/HA region	Forward	GGCCATTCGTCGGACTTGGA
			Reverse	TTTCGGTTCAAAAATACCCG
HDR_p	*aaNAT*	Confirmation of HDR insertion via amplification of gRNA/HA region	Forward	AAAAGTACGCCTTTGATAAC
			Reverse	TATGCTTCCACACACCCTTG
HDR_y	*yellow*	Confirmation of HDR insertion via amplification of gRNA/HA region	Forward	CATTATGTCCGTTGCAATCA
			Reverse	ACTTAATGGAGCAATATTCT

Appendix 7. Reference images for the mean grey scale analysis of *aaNAT* targeted *R. prolixus* nymphs.
A) wild-type nymphs imaged in session 1. B) *aaNAT* targeted nymphs imaged in session 1. C) wild-type nymphs imaged in session 2. D) *aaNAT* targeted nymphs imaged in session 2. The associated graphs for these images are found in Figure 46, and the data is found in Appendix 8.

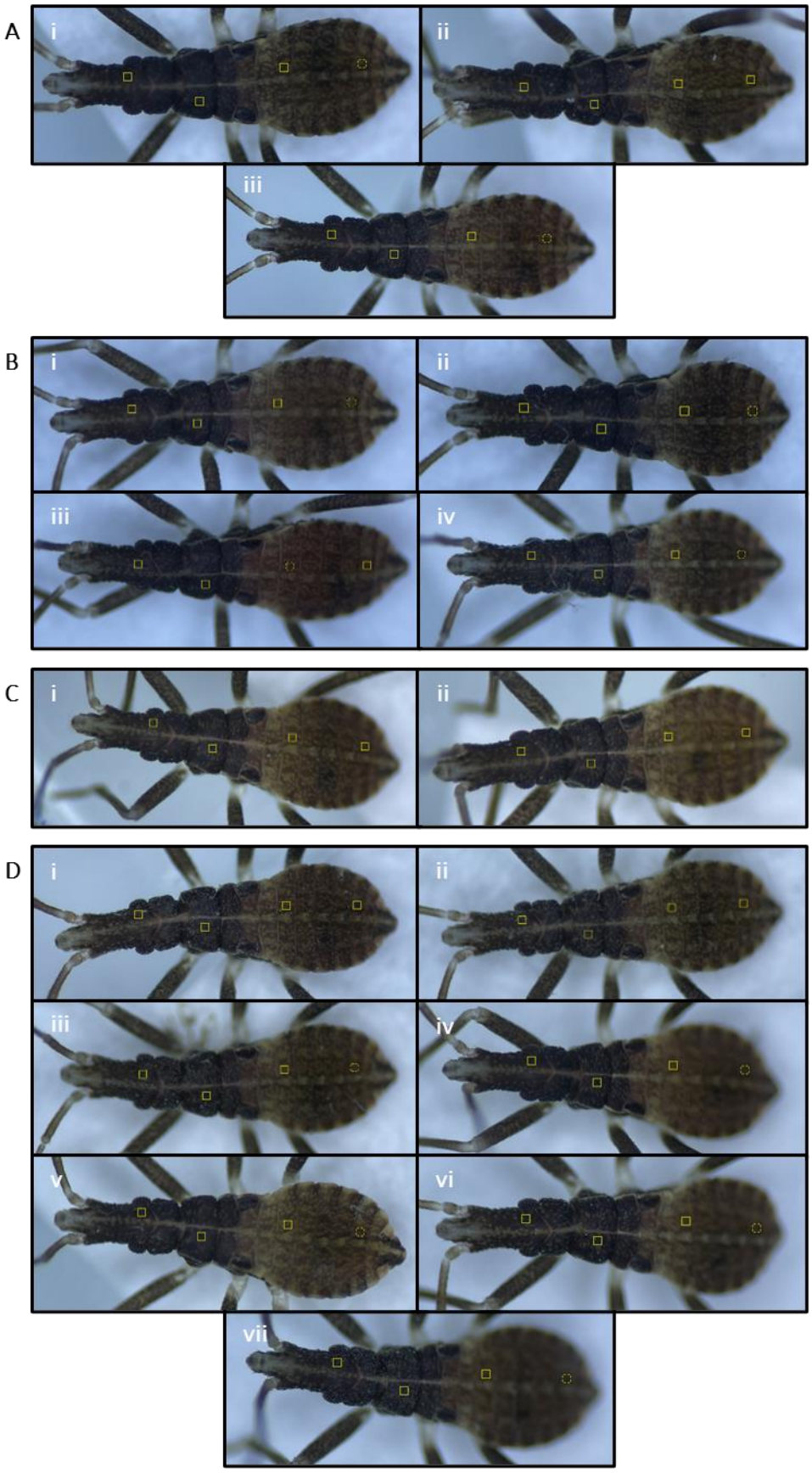

Appendix 8. Data output for mean grey scale analysis of *aaNAT* targeted *R. prolixus* nymphs.

Session	Nymph target	Nymph number	ROI	Mean (a. u.)	Minimum grey value (a. u.)	Maximum grey value (a. u.)	Mean of ROIs (a. u.)
1	WILDTYPE	1	Head	32.143	24	40	35.44225
			Thorax	33.205	24	43	
			Tergite 3	37.278	28	65	
			Tergite 7	39.143	27	59	
		2	Head	40.35	26	74	38.9645
			Thorax	34.346	19	68	
			Tergite 3	43.861	31	88	
			Tergite 7	37.301	24	51	
		3	Head	36.504	26	55	42.92675
			Thorax	39.604	27	72	
			Tergite 3	55.62	38	78	
			Tergite 7	39.979	31	55	
	aaNAT	1	Head	38.952	28	51	42.585
			Thorax	39.36	29	59	
			Tergite 3	47.682	40	63	
			Tergite 7	44.346	31	64	
		2	Head	32.101	22	56	33.13075
			Thorax	31.424	19	52	
			Tergite 3	34.275	23	71	
			Tergite 7	34.723	26	60	
		3	Head	38.865	20	80	36.41475
			Thorax	31.167	16	68	
			Tergite 3	38.751	24	68	
			Tergite 7	36.876	29	47	
		4	Head	38.287	24	74	42.20925
			Thorax	44.595	25	88	
			Tergite 3	50.059	37	75	
			Tergite 7	35.896	30	43	
2	WILDTYPE	1	Head	44.832	30	80	46.6935
			Thorax	47.235	32	80	
			Tergite 3	53.206	38	74	
			Tergite 7	41.501	34	49	

		2	Head	41.905	32	51	49.1205
			Thorax	44.913	32	71	
			Tergite 3	62.205	49	86	
			Tergite 7	47.459	40	66	
	aaNAT	1	Head	47.261	26	103	42.873
			Thorax	44.37	26	69	
			Tergite 3	45.326	29	77	
			Tergite 7	34.535	26	52	
		2	Head	43.96	28	84	41.89325
			Thorax	40.171	24	73	
			Tergite 3	43.496	29	68	
			Tergite 7	39.946	27	53	
		3	Head	37.845	21	82	38.929
			Thorax	32.167	20	64	
			Tergite 3	45.389	34	57	
			Tergite 7	40.315	29	47	
		4	Head	35.44	24	50	38.638
			Thorax	32.282	17	79	
			Tergite 3	48.618	37	59	
			Tergite 7	38.212	34	43	
		5	Head	37.243	28	55	42.61625
			Thorax	39.417	32	53	
			Tergite 3	51.552	39	72	
			Tergite 7	42.253	29	79	
		6	Head	38.275	25	72	41.38625
			Thorax	36.059	19	71	
			Tergite 3	49.546	39	60	
			Tergite 7	41.665	34	51	
		7	Head	37.779	23	72	41.36075
			Thorax	40.437	19	77	
			Tergite 3	45.257	31	55	
			Tergite 7	41.97	35	52	

Appendix 9. Reference images for the mean grey scale analysis of *yellow* targeted *R. prolixus* nymphs.
A) wild-type nymphs imaged in session 1. B) *yellow* targeted nymphs imaged in session 1. C) wild-type nymphs imaged in session 2. D) *yellow* targeted nymphs imaged in session 2. The * symbol signifies this insect was excluded from analysis due to light distortion. The associated graphs for these images are found in Figure 47, and the data is found in Appendix 10.

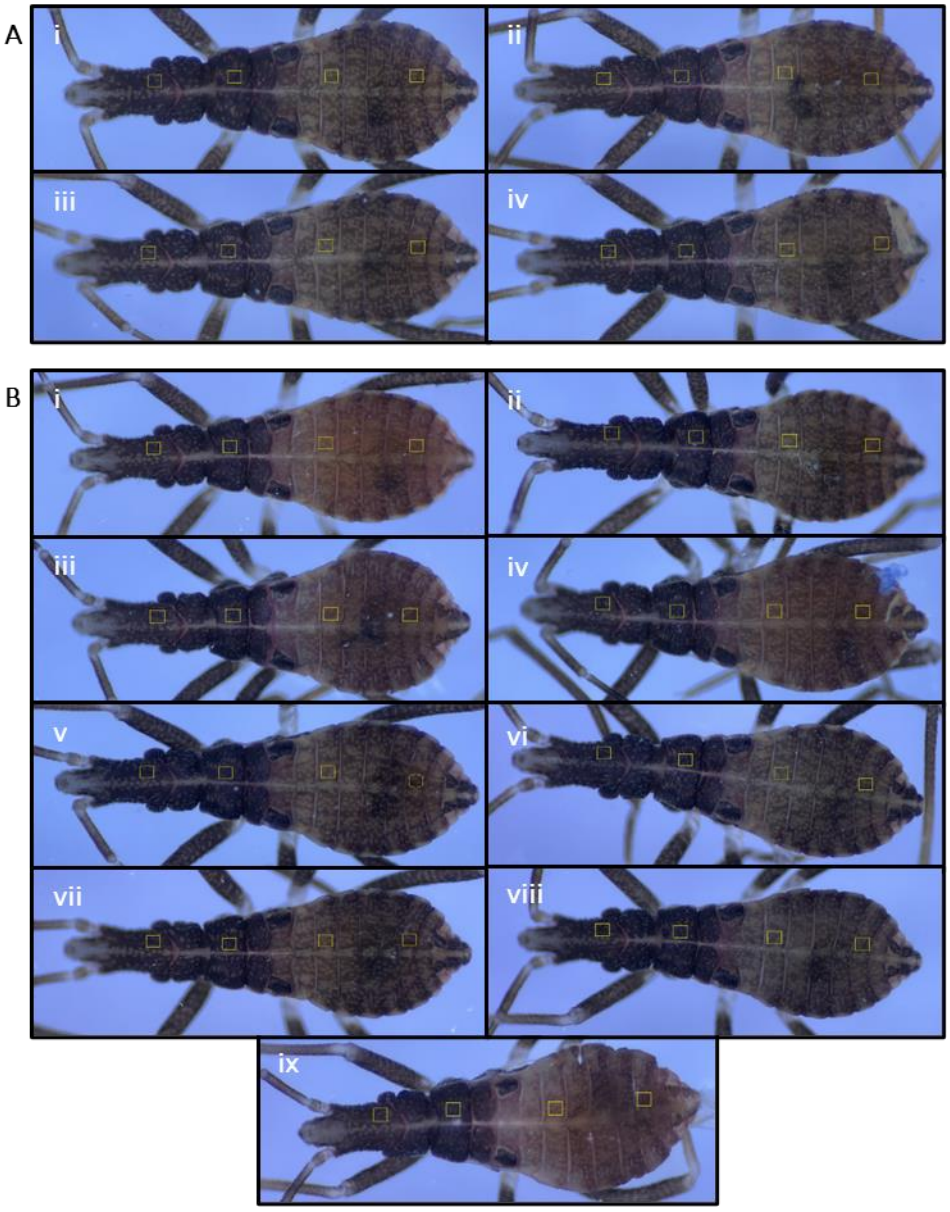

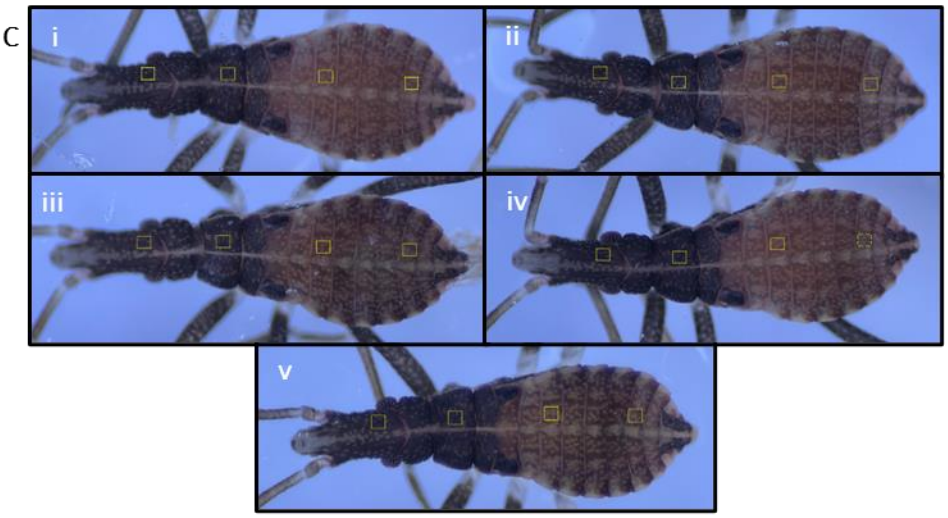
C
i
ii
iii
iv
v

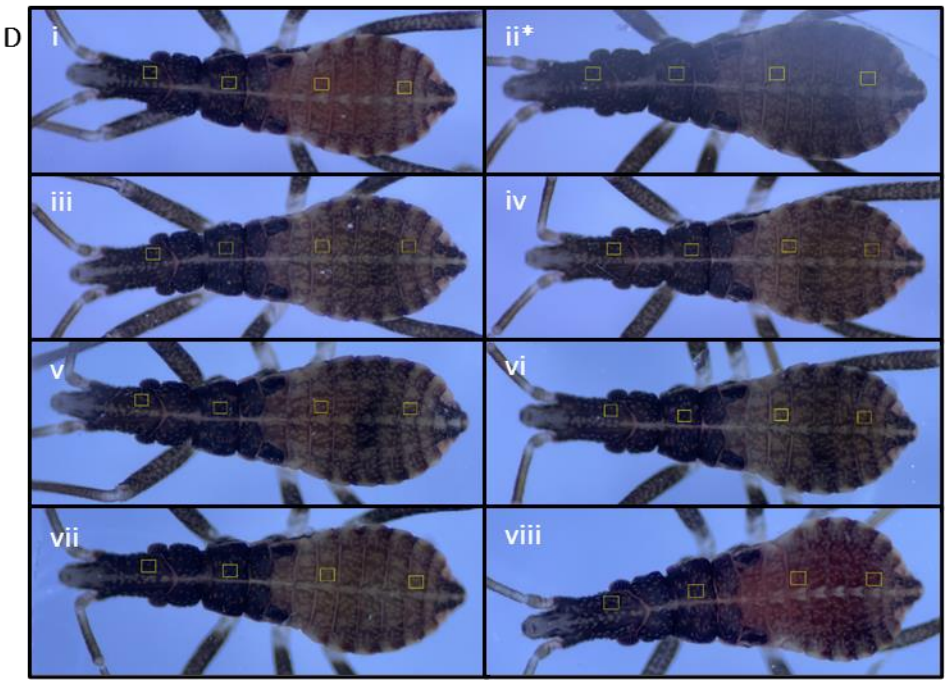
D
i
ii*
iii
iv
v
vi
vii
viii

Appendix 10. Data output for mean grey scale analysis of *yellow* targeted *R. prolixus* nymphs.

Session	Nymph target	Nymph number	ROI	Mean (a. u.)	Minimum grey value (a. u.)	Maximum grey value (a. u.)	Mean of ROIs (a. u.)
1	WILDTYPE	1	Head	49.988	33	90	57.801
			Thorax	45.381	33	68	
			Tergite 3	74.144	51	121	
			Tergite 7	61.691	37	120	
		2	Head	56.039	30	138	62.12625
			Thorax	55.987	37	97	
			Tergite 3	84.68	57	131	
			Tergite 7	51.799	37	101	
		3	Head	57.156	34	115	61.5355
			Thorax	52.631	29	124	
			Tergite 3	80.918	64	112	
			Tergite 7	55.437	33	116	
		5	Head	51.184	27	108	58.06
			Thorax	50.203	30	101	
			Tergite 3	72.311	52	100	
			Tergite 7	58.542	39	86	
	YELLOW	1	Head	47.182	24	81	58.99325
			Thorax	47.703	25	101	
			Tergite 3	77.394	50	107	
			Tergite 7	63.694	46	113	
		2	Head	39.022	19	88	51.29925
			Thorax	40.852	18	89	
			Tergite 3	74.48	43	116	
			Tergite 7	50.843	27	76	
		3	Head	51.169	27	103	55.81125
			Thorax	49.223	25	106	
			Tergite 3	69.125	46	111	
			Tergite 7	53.728	32	116	
		4	Head	43.656	17	119	51.24025
			Thorax	45.009	20	107	
			Tergite 3	68.135	46	121	
			Tergite 7	48.161	34	74	

		5	Head	38.152	12	85	47.40875
			Thorax	41.476	20	77	
			Tergite 3	67.817	43	116	
			Tergite 7	42.19	22	89	
		6	Head	39.496	10	104	50.27925
			Thorax	41.259	17	100	
			Tergite 3	68.924	38	111	
			Tergite 7	51.438	29	82	
		7	Head	42.759	19	77	46.813
			Thorax	38.444	14	114	
			Tergite 3	62.421	34	110	
			Tergite 7	43.628	21	92	
		8	Head	37.075	12	80	47.83
			Thorax	40.51	14	128	
			Tergite 3	63.844	43	95	
			Tergite 7	49.891	25	98	
		9	Head	49.807	27	79	58.6255
			Thorax	50.39	34	72	
			Tergite 3	79.372	65	110	
			Tergite 7	54.933	35	107	
2	WILDTYPE	1	Head	45.625	28	137	60.446
			Thorax	46.73	26	102	
			Tergite 3	77.462	57	112	
			Tergite 7	71.967	50	106	
		2	Head	41.61	22	92	60.06875
			Thorax	49.721	23	145	
			Tergite 3	71.869	51	115	
			Tergite 7	77.075	54	131	
		3	Head	54.216	33	92	57.69525
			Thorax	48.817	27	113	
			Tergite 3	63.587	38	115	
			Tergite 7	64.161	44	93	
		4	Head	39.212	23	85	57.0745
			Thorax	41.52	24	84	
			Tergite 3	75.872	55	141	

			Tergite 7	71.694	58	111	
		5	Head	44.61	26	98	58.0375
			Thorax	44.283	30	80	
			Tergite 3	73.214	44	111	
			Tergite 7	70.043	44	122	
	YELLOW	1	Head	32.11	12	74	51.03125
			Thorax	39.178	19	68	
			Tergite 3	60.968	40	121	
			Tergite 7	71.869	42	102	
		2	Head	65.832	51	89	78.70225
			Thorax	68.475	54	92	
			Tergite 3	87.383	75	111	
			Tergite 7	93.119	80	109	
		3	Head	40.415	10	99	51.2425
			Thorax	39.649	20	103	
			Tergite 3	65.581	37	111	
			Tergite 7	59.325	39	88	
		4	Head	39.208	17	85	50.114
			Thorax	42.571	19	97	
			Tergite 3	64.536	38	112	
			Tergite 7	54.141	25	130	
		5	Head	35.895	10	94	42.93025
			Thorax	29.7	13	70	
			Tergite 3	50.045	22	90	
			Tergite 7	56.081	23	111	
		6	Head	36.565	11	85	41.0765
			Thorax	28.251	9	73	
			Tergite 3	58.754	26	104	
			Tergite 7	40.736	11	95	
		7	Head	25.324	8	71	43.48675
			Thorax	28.19	10	74	
			Tergite 3	59.251	32	111	
			Tergite 7	61.182	38	95	
		8	Head	33.004	10	81	43.11
			Thorax	37.881	13	85	
			Tergite 3	55.247	32	113	
			Tergite 7	46.308	24	98	

Appendix 11. Reference images for the mean grey scale analysis of the *yellow 1 R. prolixus* nymph.
A) wild-type nymphs. B) the *yellow 1* nymph. The * symbol highlights that the ROI highlighted was excluded from data analysis.

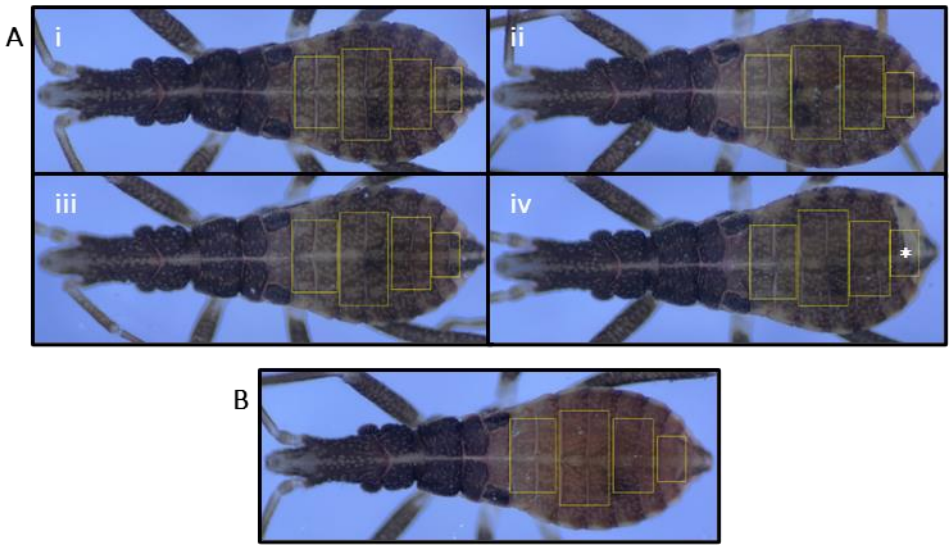

Appendix 12. Data output for mean grey scale analysis of *yellow 1 R. prolixus* nymph.

Nymph target	Nymph number	ROI	Mean grey value (a. u.)	Minimum grey value (a. u.)	Maximum grey value (a. u.)	Mean of ROIs (a. u.)
WILDTYPE	1	1	77.191	39	148	67.4645
		2	59.822	20	136	
		3	59.726	28	129	
		4	73.119	30	145	
	2	1	87.394	38	143	68.069
		2	60.767	24	142	
		3	57.697	34	117	
		4	66.418	37	115	
	3	1	81.521	46	151	67.506
		2	63.072	25	126	
		3	58.054	31	131	
		4	67.377	30	124	
	5	1	76.477	40	146	65.9597
		2	61.111	25	139	
		3	60.291	30	140	
		4	N/A	35	136	
YELLOW	1	1	84.74	44	160	72.07025
		2	67.189	26	164	
		3	59.835	22	141	
		4	76.517	40	125	